CORSO DI DOTTORATO DI RICERCA IN ELETTRONICA APPLICATA

XXXII CICLO DEL CORSO DI DOTTORATO

Study of motor coordination for functional assessment in clinical and neurophysiological applications

PhD Student: Martina Rinaldi

Tutors:

Prof.ssa Silvia Conforto

Prof. Maurizio Schmid

Coordinator: Prof. Enrico Silva

Table of Contents

Keywords

Neurological disorders

Gait Analysis

Kinematics

Kinetics

Surface electromyography (sEMG)

Muscle co-activation

Publications

International Journal Papers

1. **M. Rinaldi**, M. Petrarca, A. Romano, G. Vasco, C. D'Anna, M. Schmid E. Castelli, S. Conforto. Progression of muscular co-activation and gait variability in children with Duchenne Muscular Dystrophy: a 2-year follow-up study. Clinical Biomechanics, 2019 Submitted.
2. T. Varrecchia, M. Serrao, **M. Rinaldi**, A. Ranavolo, S. Conforto, C. De Marchis, A. Simonetti, I. Poni, S. Castellano, A. Silvetti, A. Tatarelli, L. Fiori, C. Conte, F. Draicchio. Common and specific gait patterns in people with varying anatomical levels of lower limb amputation and different prosthetic components.. Human Movement Sciences, 2019.
3. **M. Rinaldi**, C. D' Anna, M. Schmid, S. Conforto. Assessing the influence of SNR and pre-processing filter bandwidth on the extraction of different muscle co-activation indexes from surface EMG data. Journal of Electromyography and Kinesiology, 2018.
4. **M. Rinaldi**, Y. Nasr, G. Atef, F. Bini, T. Varrecchia, C. Conte, G. Chini, A. Ranavolo, F. Draicchio, F. Pierelli, M. Amin, F. Marinozzi, M. Serrao. Biomechanical characterization of the Junzuki karate punch: indexes of performance. European Journal of Sport Science, 2018.
5. T. Varrecchia, **M. Rinaldi**, M. Serrao, F. Draicchio, C. Conte, S. Conforto, M. Schmid, A. Ranavolo. Global lower limb muscle coactivation during walking at different speeds: relationship between spatio-temporal, kinematic, kinetic and energetic parameters. Journal of Electromyography and Kinesiology, 2018.
6. A. Ranavolo, T. Varrecchia, S. Iavicoli, A. Marchesi, **M. Rinaldi**, M. Serrao, S. Conforto, M. Cesarelli, F. Draicchio. Surface electromyography for risk assessment in work activities designed using the "revised NIOSH lifting equation". International Journal of Industrial Ergonomics, 2018.
7. T. Varrecchia, C. De Marchis, **M. Rinaldi**, F. Draicchio, M. Serrao, M. Schmid, S. Conforto, A. Ranavolo. Lifting activity assessment using surface electromyographic features and neural networks. International Journal of Industrial Ergonomics, 2018.
8. G. Martino, Y. Ivanenk, M. Serra, A. Ranavolo, F. Draicchio, **M. Rinaldi**, C. Casali, F. Lacquaniti. Differential changes in the spinal segmental locomotor output in Hereditary Spastic Paraplegia. Clinical Neurophysiology, 2018.
9. M. Serrao, G. Chini, M. Bergantino, D. Sarnari, C. Casali, C. Conte, A. Ranavol, C. Marcotulli, **M. Rinaldi**, G. Coppola, F. Bini, F. Pierelli, F. Marinozzi. Identification of specific gait patterns in patients with cerebellar ataxia,spastic paraplegia, and Parkinson's disease: A non-hierarchical cluster analysis. Human Movement Sciences, 2018.
10. **M. Rinaldi**, A. Ranavolo, S. Conforto, G. Martino, F. Draicchio, C. Conte, T. Varrecchia, F. Bini, C. Casali, F. Pierelli, M. Serrao. Increased lower limb muscle coactivation reduces gait performance and increases metabolic cost in patients with hereditary spastic paraparesis. Clinical Biomechanics, 2017.
11. A. Ranavolo, T. Varrecchia, **M. Rinaldi**, A. Silvetti, M. Serrao, S. Conforto, F. Draicchio. Mechanical lifting energy consumption in work activities designed by means of the "revised NIOSH lifting equation". Industrial Health, 2017
12. M. Serrao, G. Chini, C. Casali, C. Conte, **M. Rinaldi**, A. Ranavolo, C. Marcotulli, L. Leonardi, G. Fragiotta, F. Bini, G. Coppola, F. Pierelli. Progression of Gait Ataxia in

Patients with Degenerative Cerebellar Disorders: a 4-Year Follow-UpStudy. Cerebellum, 2017.

13. M. Serrao, **M. Rinaldi**, A. Ranavolo, F. Lacquaniti, G. Martino, L. Leonardi, C. Conte, T. Varrecchia, F. Draicchio, G. Coppola, C. Casali, F. Pierelli. Gait Patterns inPatients with Hereditary Spastic Paraparesis. PLoS One, 2016.

International Conference Papers

1. **M. Rinaldi**, M. Petrarca, A. Romano, G. Vasco, C. D'Anna, M. Schmid E. Castelli, S. Conforto. EMG-based indicators of muscular co-activation during gait in children with Duchenne Muscular Dystrophy. EMBC 2019, Biomedical Engineering arranging from wellness to intensive care medicine, Berlin, Germany, 23-27 July.
2. S. Ranaldi, C. De Marchis, **M. Rinaldi** , S. Conforto. "The effect of Non-Negative Matrix Factorization initialization on the accurate identification of muscle synergies with correlated activation signals". MeMea 2018, Rome, Italy, 11-13 June.
3. S. Conforto, M. Serrao, T. Varrecchia, **M. Rinaldi.** "Kinetic and kinematic patterns for prosthetic gait analysis". ISEK International Society of Electrophysiology and Kinesiology 2018, University College Dublin, 29 June-02 July
4. A. Silvetti, A, Ranavolo, T. Varrecchia, **M. Rinaldi**, G. Chini, A. Marchesi, F. Draicchio. Comparison of two post office workstation layouts by means of an optoelectronic motion analysis system. AHFE 2017, California, USA, 17-21 July.

National Conference Papers

1. **M. Rinaldi,** T. Varrecchia, A. Ranavolo, F. Draicchio, SF. Castiglia, F. Pierelli, M. Serrao.The role of trunk on human locomotion: damper, generator or perturbator? SIAMOC 2019, Bologna, Italy, 9-12 October.
2. T. Varrecchia**,** A. Ranavolo, **M. Rinaldi**, F. Draicchio, SF. Castiglia, F. Pierelli, C. Conte M. Serrao. Artificial neural networks for staging the gait deficit in Parkinson disease. SIAMOC 2019, Bologna, italy, 9-12 October.
3. **M. Rinaldi,** M. Serrao, T. Varrecchia, C. Conte, A. Ranavolo, F. Draicchio, C. Casali, F. Pierelli. The role of trunk in neurological gait disorders: damper,generator or perturbator? SIN 2018, Rome, Italy, 27-30 October.
4. T. Varrecchia, M. Serrao, L. Fiori, **M. Rinaldi**, A. Ranavolo, C. Conte, F. Draicchio, C. Casali, F. Pierelli. Global lower limb co-activation in patients with cerebellar ataxia SIN 2018, Rome, Italy, 27-30 October.
5. T. Varrecchia, M. Serrao, A. tatarelli, **M. Rinaldi,** C. Conte, A. Ranavolo, F. Draicchio, C. Casali, F. Pierelli. Gait harmonic structure of walking in patients with neurological gait disorders. SIN 2018, Rome, Italy, 27-30 October.
6. **M. Rinaldi**, C. D'Anna, M. Schmid, S. Conforto. The effect of pre-processing settings on muscle co-activation assessment with synthetic and experimental signals.Congress of the National Group of Bioengineering, GNB 2018, Milan, Italy, 25-27 June.
7. **M. Rinaldi**, M. Serrao, A. Ranavolo, C. Conte, T. Varrecchia, G. Chini, C. Casali, F. Pierelli. Increased lower limb muscle coactivation and its relationship with gait performance and metabolic cost in patients with hereditary spastic paraparesis SIN 2017, Naples, Italy, 14-17 October.

8. T. Varrecchia, A. Ranavolo, C. Casali, A. Filla, A. Silvetti, F. Pierelli, **M. Rinaldi,** C. Conte, G. Chini, A. Roca, C. Marcotulli, F. Draicchio, M. Serrao. The working life of people with degenerative cerebellar ataxia. SIN 2017, Naples, Italy, 14-17 October.
9. G. Chini, M. Serrao, G. Caramanico, **M. Rinaldi,** T. Varrecchia, C. Conte, E. Sinibaldi, G. Monari, F. Pierelli. Predictors of gait improvement in patients with Parkinson's disease after rehabilitation. SIN 2017, Naples, Italy, 14-17 October.
10. C. Conte, P. Caliandro, C. Iacovelli, C. Casali, A. Ranavolo, G. Chini, **M. Rinaldi,** T. Varrecchia, L. Padua, F. Pierelli, M. Serrao. Trunk-lower limb coordination pattern during gait in patients with ataxia; autori. SIN 2017, Naples, Italy, 14-17 October.
11. M. Guaitolini, C. De Marchis, **M. Rinaldi**, T. Varrecchia, G. Chini, A. Silvetti, M. Serrao, A. Ranavolo, M. Schmid, F. Draicchio, S. Conforto. Analisi Cinematica del Cammino in Amputati per la Valutazione Funzionale della Stabilità Dinamica. SIAMOC 2017, Turin, Italy, 4-7 October.
12. S. Ranaldi, C. De Marchis, **M. Rinaldi**, T. Varrecchia, A. Marchesi, A. Silvetti, M. Serrao, A. Ranavolo, M. Schmid, S. Conforto, F. Draicchio. Controllo motorio modulare dell'arto controlaterale nel cammino di amputati trans-femorali. SIAMOC 2017, Turin, Italy, 4-7 October.
13. A. Silvetti, A, Ranavolo, T. Varrecchia, **M. Rinaldi**, G. Chini, A. Marchesi, F. Draicchio. Analisi Cinematica di una postazione di interfaccia cliente/operatore. SIE 2016, Naples, Italy, 16-18 November.

ABSTRACT

This PhD project was focused on the study of motor coordination for the purposes of functional evaluation in the clinical and neurophysiological fields.

Neurological diseases, as well as being a personal problem, are also a social issue because of their high incidence, in terms of cost, on the national health system and on the employment sphere.

The study of postural and motor alteration in patients with pathologies associated with movement alterations allows to know the level of functional limitation consequent to the pathology and its evolution through time, and can provide useful elements to define an appropriate rehabilitative strategy.

Since walking disorders are one of the first symptoms of these patients, gait analysis, which allows evaluating kinematics, dynamics and muscle activity, provides very important information in this context.

It has been shown that the breakdown of the functional balance between the various circuits is the cause of extrapyramidal motor disorders. Furthermore. a progressive loss of muscle coordination has been found in diseases affected by a deficit in the cerebellum, which therefore makes it difficult to perform voluntary movements. Injuries at the level of the pyramidal system, on the other hand, result in a progressive spasticity in the lower limbs.

In this scenario, a complete characterization of the locomotion of subjects affected by several neurological diseases could be a useful tool for identifying the motor strategies put in place in order to guarantee stability and ensure progression.

Among the different aspects which are the object of debate in the scientific community on gait analysis in pathologic conditions, two main questions were deepened within this PhD:

- the assessment of gait patterns in patients with several neurological gait disorders (Hereditary spastic paraparesis, Parkinson's disease, cerebellar Atassia and Duchenne Muscular Dystrophy) and lower limb amputations. Some specific biomechanical features, that may not emerge because they are hidden within the global walking strategy, were highlighted by subgroups or cluster analysis.
- the assessements of the role of muscle coactivation mechanisms during walking in pathologic conditions and its relstionship with gait performance. The influence of several factors in the sEMG measurement and pre-processing on the linear envelope profiles extraction, and therefore on the outcome of muscle co-activation were taken into account.

Firstly, starting from a review of literature, I addressed my attention to a kinematic, kinetic, energetic and electromyographic characterization of the path of the aforementioned subjects with the aim of identifying the motor strategies to ensure stability and coordination during movement.

As regard patients with Hereditary Spastic Paraparesis (HSP), several previous studies highlighted the clinical variability and heterogeneity of the pathology. In addition to general biomechanical characteristics of gait, one would expect some differential characteristics in distinct subgroups of patients according to clinical involvement of the pyramidal tract, given that patients with HSP exhibit different degrees of severity both within and between families. The analysis of limb joint kinematics revealed that, when subgrouping patients according to the hip, knee and ankle joint kinematic behavior, three clear gait patterns emerged HPS patients. Thus, the identification of several walking strategies among HSP patients provide useful elements to define an appropriate rehabilitative strategy.

The progression of gait impairment in a group of patients with primary degenerative cerebellar ataxias (CA) over a period of 4 years revealed a progressive increase in gait variability which may directly reflect gait function deterioration. Interestingly, the increase in trunk rotation may represent a compensatory mechanism aimed at maintaining an adequate gait speed.

As regard patients affected by Duchenne Muscular Dystrophy (DMD), the progressive increase in gait variability observed at the 2-year follow-up may thus directly reflect a deterioration of the gait function, which leads to greater instability. Taking this into consideration, gait variability seems to anticipate the future loss of walking autonomy.

The analysis of the trunk movement suggested that the abnormal trunk movement in neurological patients reflect either a primary deficit or a compensatory mechanism. Particularly, the trunk may be used as generator of movement to improve gait performance in some patients (e.g. in HSP) but not in other (e.g. in Parkinson's disease). Patients with whole body deficits may use trunk movement either as a perturbator, increasing its range of motion, either as a damper, decreasing its range of motion.

Finally, in spite of common gait characteristics in subjects with lower limb prostheses, both the anatomical level of amputation and type of prostheses determine a specific gait pattern that should be taken into account when developing new and ergonomic prosthetic devices and when planning the rehabilitation programs aimed at improving the physiology of gait and reducing the gait asymmetries.

Afterwards, I followed a methodological approach with the aim of identifying robust indices to characterize pathologic conditions. Specifically, the mechanism of muscle co-activation, which is important for providing adequate spine and joint stability, energy efficiency and for adapting to environmental demands, was investigated focusing on the influence of sEMG processing technique (such as the extraction of linear envelopes or signal to noise condition) on the outcome of muscle co-activation. The analysis of the results shows that the performance of the methodologies used to assess muscle co-activation are influenced by the choice of the low pass cut-off frequency, as well as by the level of signal to noise ratio. Thus, since the relevance of the analysis of muscle co-activation to several fields is well known, it is important to correctly process myoelectric signals in order to extract this parameter by avoiding estimation bias.

During walking, muscle joint coactivation varies within the gait cycle according to the functional role of the lower limb joints. Our results show that muscle coactivation in healthy subjects is speed dependent and positively correlated with both energy consumption and balance-related gait parameters. The investigation of the lower limb muscle coactivation in patients with HSP showed that the abnormal coactivation pattern may reflect both or either abnormal descending motor commands and/or plastic rearrangement of the spinal circuitries which, in turn, lead to a lack of selectivity of the descending motor drives to motoneuronal pools. In addition, these abnormalities influence the mechanisms of both energetic consumption and recovery during walking. Furthermore, in patients with DMD, since gait speed remained approximately unchanged over time, increased muscle co-activation at proximal level represents the most important strategy to compensate for a deterioration in both functional ability and increase in gait instability.

The results highlight the importance of a methodological approach for testing the role of muscle co-activation mechanism during the execution of motor tasks avoiding possible bias due to sEMG processing techniques. Muscle coactivation in patients could be a useful measure of the motor control strategy, limb stiffness, postural stability, energy efficiency optimization, and several aspects in pathological conditions.

In conclusion, the results obtained in this PhD project may provide important support to extend the knowledge about functional assessment in clinical and neurophysiological fields.

In particular, these results suggested that both the characteristics of the pathology and the technique used for data elaboration are two important aspects to be considered in the design of tools for training and rehabilitation.

CHAPTER 1

1. INTRODUCTION AND PURPOSE OF THE STUDY

The research activity was focused on the study of motor coordination for the purposes of functional evaluation in the clinical and neurophysiological fields. Neurological diseases, as well as being a personal problem, are also a social issue because of their high incidence, in terms of cost, on the national health system and on the employment sphere.

The study of postural and motor alteration in patients with pathologies associated with movement alterations allows to know the level of functional limitation consequent to the pathology and its evolution through time, and can provide useful elements to define an appropriate rehabilitative strategy.

Since walking disorders are one of the first symptoms of these patients, gait analysis, which allows evaluating kinematics, dynamics and muscle activity, provides very important information in this context.

It has been shown that the breakdown of the functional balance between the various circuits is the cause of extrapyramidal motor disorders [1]. Futhermore. a progressive loss of muscle coordination has been found in diseases affected by a deficit in the cerebellum, which therefore makes it difficult to perform voluntary movements [2]. Injuries at the level of the pyramidal system, on the other hand, result in a progressive spasticity in the lower limbs [3-5].

In this scenario, a complete characterization of the locomotion of subjects affected by several neurological diseases could be a useful tool for identifying the motor strategies put in place in order to guarantee stability and ensure progression. The activities of the project are aimed at a deep characterization of the gait patterns of subjects suffering from disorders such as Hereditary spastic paraparesis, Parkinson's disease, cerebellar Atassia and Duchenne Muscular Dystrophy (DMD), as

well as amputees. Furtehrmore, the relationship between gait parameters abnormalities and the related muscle activity is provided.

Firstly, starting from a review of literature, I addressed my attention to a kinematic, kinetic, energetic and electromyographic characterization of the path of the aforementioned subjects with the aim of identifying the motor strategies to ensure stability and coordination during movement.

Afterwards, I followed a methodological approach with the aim of identifying robust indices to characterize pathologic conditions. Specifically, the mechanism of muscle co-activation, which is important for providing adequate spine and joint stability, energy efficiency and for adapting to environmental demands, was investigated focusing on the influence of sEMG processing technique (such as the extraction of linear envelopes or signal to noise condition) on the outcome of muscle co-activation. The results highlight the importance of a methodological approach for testing the role of muscle co-activation mechanism during the execution of motor tasks avoiding possible bias due to sEMG processing techniques.

The mechanism of muscle co-activation was investigated in patients affected by Hereditary Spastic Parapareis, (HSP), Cerebellar ataxia (CA), Parkinson disease (PD) and Duchenne Muscular Dystrophy (DMD). This approach may be useful for a better interpretation of the pathologic mechanisms, in terms of muscle behavior, to address rehabilitation treatment.

1.1 Thesis outline

Chapter 2: describes the basis of gait analysis technique.

Chapter 3: describes the kinematic, kinetic and electromyographic methods used to study motor patterns.

Chapter 4: describes the types of neurological disorders investigated, such as Hereditary Spastic Paraparesis, Cerebellar Ataxia, Parkinson, Duchenne Muscular Dystrophy and the the major results obtained in term of gait patterns.

Chapter 5: describes the major results obtained from the characterization of gait patterns in subjects with lower limb amputation at several anatomical levels.

Chapter 6,7,8,9,10: this chapter group represents the core of my thesis, describing the mechanisms of muscle co-activation in human locomotion. Muscle behaviour in patients affected by neurological disorders and in healthy subjects are presented in the *Chapters 6,7,8,* and a new approach for the muscle co-activation estimation is proposed. A comparison among algoritmhs performance are assessed in the *Chapter 9*. Algorithms for muscle synergy extraction are investigated in the *Chapter 10*.

Chapter 11: this chapter reports the general discussions and the conclusion of the thesis, highlighting the most important contribution of this work in both clinical and neurophysiological field, especially in terms of muscular characterization during human locomotion.

Appendix: describes secondary activities carried out during my PhD research activities, such as biomechanical characterization of both work-related disorders and sport activities.

Bibliography

[1] Morris ME, et al. 2001. The biomechanics and motor control of gait in Parkinson disease. Clinical Biomechanics, 10:459-470.
[2] Martino G, Ivanenko YP, Serrao M, Ranavolo A, d'Avella A, Draicchio F, Conte C, Casali C, Lacquaniti F. 2014. Locomotor patterns in cerebellar ataxia. Journal of Neurophysiology, 112:2810-2821.
[3] Klebe S, Stolze H, Kopper F, Lorenz D, Wenzelburger R, Volkmann J, Porschke H, Deuschl G. 2004. Gait analysis of sporadic and hereditary spastic paraplegia. Journal of Neurology, 251(5): 571-578.
[4] Fink JK. Hereditary spastic paraplegia. 2006. Current Neurology and Neuroscience Reports, 6(1): 65-76.
[5] Marsden J, Ramdharry G, Stevenson V, Thompson A. 2012. Muscle paresis and passive stiffness: key determinants in limiting function in Hereditary and Sporadic Spastic Paraparesis. Gait Posture, 35(2): 266- 271.

CHAPTER 2

2. GAIT ANALYSIS

2.1 Fields of application

Gait is characterized by a cyclic pattern of motor activity of the lower limbs and trunk that allows to transfer the weight on the limb support and advance against the limb-side forward [1]. Gait analysis provides very important information especially when it concerns the analysis of the step of pathological subjects. In fact, the study of the postural and motor alteration in patients with pathologies associated with alterations of the movement allows to know the level of functional limitation resulting from the disease and its evolvution over time, and may provide useful elements to define an appropriate rehabilitation strategy [2-3].

Gait analysis is a suitable discipline for the characterization of human movements and can be a very useful tool in a clinical and therapeutic context in order to optimize the rehabilitative strategies aimed at recovering motor skills. Gait is the most common type of movement performed by humans and the autonomy and safety during gait in several contexts represent for the individual an important aspect of daily life. For this reason, a deep characterization of gait is crucial to define motor ability.

It represents a valid tool in the clinical field for diagnostics, rehabilitation and injury prevention as well as in the sports field as a support element for athletes and coaches for improving performance.

The use of motion analysis begins in the nineteenth century, but the technological development has further automated measurement techniques. The development in the fields of electronics, information technology and computer combined with engineering efforts continue to provide solutions that continuously improve measurement techniques [4].

Today motion analysis is based on count on vanguard detection systems, efficient sensors (of force, pressure, electromyography, inertia) and on modern computers that allow the integration of various types of information. Currently there are numerous systems of motion analysis that differ mostly on the type of sensor used. Motion analysis can be based on the use of stereo-photogrammetric techniques, or wearable inertial sensors or other sensors. In this thesis, stereo-photogrammetric techniques are described.

Bibliography

[1] M.W. Whittle, Gait analysis, pp. 187-199, 1993.

[2] J.B. Saunders, V.T. Inman, H.D. Eberhart, “The major determinants in normal and pathological gait.” The Journal of Bone and Joint Surgery, American vol. 35-A, pp. 543– 558, 1953.

[3] M.W. Whittle, “Clinical gait analysis: A review,” Human Movement Science, vol. 15, no. 3, pp. 369-387, 1996.

[4] M. Akhtaruzzaman, A.A. Shafie, M.R. Khan, “Gait Analysis: Systems, Technologies, and Importance,” Journal of Mechanics in Medicine and Biology, vol. 16, no. 7, 1630003, 2016.

CHAPTER 3

3. INSTRUMENTATION

3.1 Biomechanical characterization

Motion analysis tools are usually based on the study of kinematic, kinetic and electromyographic parameters.

Kinematics focuses on the variation in space of anatomical references and body segments involved in the execution of motor activities and describes human movement through the positions, angles and velocities of the various body segments. The reconstruction of the position of a point or set of points need the definition of the space. [1-3]

The points of which the trajectory is to be reconstructed are typically the markers positioned on the body of the subject under examination [4]. The choice of the plan refers to standardized definitions built on the human body: three fundamental planes are defined, namely frontal or coronal, sagittal and transverse plane. The axes with origin are defined anteroposterior, mediolateral and longitudinal (or craniocaudal) (Fig. 3.1).

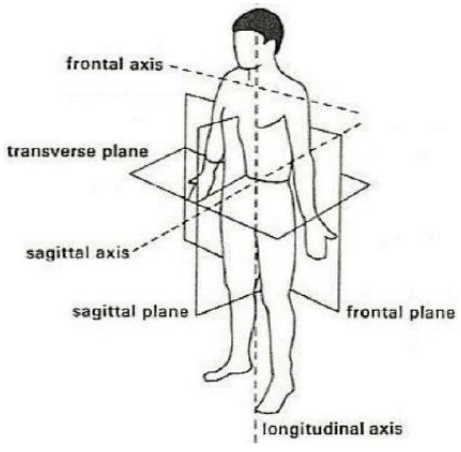

Figure 3.1. Anatomical planes

The analysis of the kinematics in a three-dimensional space provides a complete observation of the joint movement. However, three-dimensional analysis with stereo-photogrammetric technique requires at least two cameras to reconstruct the position of a point in the space, thus it will be necessary to use an appropriate number of cameras positioned in the space such that each observed point is visible in every moment from at least two cameras. The positioning of the cameras is therefore strictly related to the task to be studied. Each camera captures a two-dimensional image (the projection of the acquired space on the image plane) and two images acquired from cameras are required to reconstruct three-dimensional space.

The body is represented as a set of body segments, considered rigid segments for simplicity. This obviously represents an approximation with respect to the real nature of the body segments composed of bone (hypothesized as a rigid body) and soft tissues that can cause artifact [5]). The identification of a rigid body in space is possible from the position of three non-aligned points, while the geometric parameters are obtained through anthropometry and kinematics, while the mass of the segment is concentrated in the center of mass. The lengths of the anatomical segments ere reported in literature [6-7] and the figure represents the lengths of the various segments expressed as percentages of the height of the body, as defined by Drillis et al. [1,22] (Fig. 3.2)

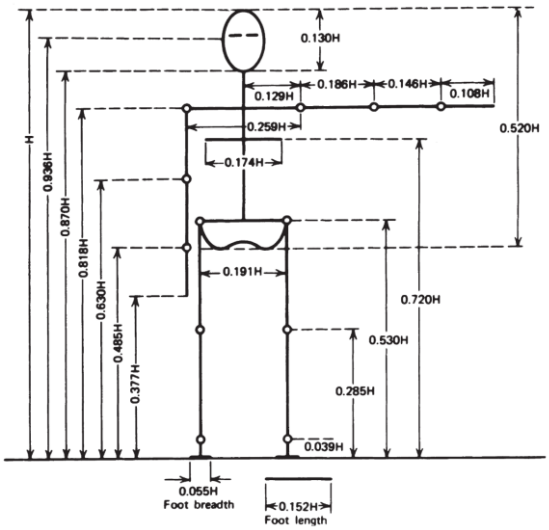

Figure 3.2. Body segments length as a function of height H

Kinetics describes the role of forces in generating movement by studying the forces and angular moments at the base of motor acts, [9]. Kinetics can be used to study the principles of segments interaction. The forces studied can be internal and external to the body and both types play a role in motor performance.

For the study of kinetics, force transducers can be used. These instruments provide an electrical signal proportional to the applied force. The transducers can be piezoelectric, piezoresistive, capacitive or extensometric. These sensors are based on the deformation of the sensitive element following the application of a certain stress, with consequent variation of voltage or electric charge in output.

The most common tool in the study of kinetics is represented by the force platform. It is equipped with piezoelectric or extensometric sensors capable of recording the forces acting on it following the interaction with the subject under examination. The force platforms are often integrated in the floor of the laboratory and the recorded signals provide information on how the weight of the body is distributed on the entire platform. The force platforms can be used for the study of posture [1,9], for diagnostics and rehabilitation. Furthermore, they represent a useful tool for the recognition of events and for the reconstruction of motor patterns [1].

The balance and body posture can be studied through the center of pressure (Center of Pressure, CoP), by the projection on the plane of the platform of the center of gravity of the body in static pose. The position of the CoP if related to that of the center of mass (Center of Mass, CoM) can provide very useful data in relation to the posture and balance of the subject, which is also very useful in the diagnostic field [2,10] .

The dynamometric platforms can be used to integrate the kinematic information with the GRF (Ground Reaction Force) for the definition of the heel strike and toe-off events during gait. The observation of CoP oscillations can also be useful to obtain information on subject.

The use of surface electromyography (surface Electromyography, sEMG) is widespread due to the non-invasive characteristics and the potentialities offered by modern techniques for the electromyographic signal analysis.

Although neurophysiopathology is the clinical field that historically has made the most use of for diagnostic purposes, recently surface electromyography has been used in clinical and research fields for the evaluation of muscular activity, performance of isometric tests, study of muscle fatigue, pain, movement control and performance analysis in sports medicine [3]. EMS is also used in the study of muscle tremors, biofeedback of muscle contraction, and muscle spasticity.

Surface electromyography studies the electrical signals associated with muscle contraction. Muscles produce bursts of electrical potential associated with the activation of motor units. This signal propagates through the tissues and can be recorded on the surface through appropriate electrodes. To obtain a properly intelligible signal it is necessary to position the electrodes oriented according to the direction of the muscle fibers, ie along the direction of propagation of the electromyographic signal. It is also necessary to prepare the skin for the positioning of the electrodes, cleaning the affected surface in order to reduce its low-pass effect. The acquisition can be performed in a monopolar way (an active electrode and a reference one, positioned on a neutral point) or bipolar (two active electrodes both placed on the muscle) [1]. With technological progress small and wireless electromyographic sensors were developed, facilitating the study of muscular activity without influencing the naturalness of the movements.

The use of multiple electromyographic probes and the simultaneous acquisition of different muscles can provide important information on the activity of the different muscle groups.

In this sense, sEMG is a particularly useful tool for the study of muscular activity during gait analysis, since it provides the activation phases of the different muscle groups during the different phases of the gait and the role of muscles in stabilizing the body [2,3,9].

3.2 Data recording and processing

3.2.1 Stereo-photogrammetric systems

3.2.1.1 Kinematics

A stereo-photogrammetric system acquires kinematic data through video cameras used to record the movements that take place in the two- or three-dimensional acquisition space. The cameras can be based on different types of technology and consequently may require different types of experimental setup. Typically, markers are used for the reconstruction of the kinematics [1,4]. The position of the markers is recorded by the cameras and thy are recognized clear spots on a homogeneous background. The position of the markers in the space allows to reconstruct the position of the body, obtaining the so-called stick diagram.

The most used type of marker is represented by reflective passive markers that combine simplicity and low cost with good operational reliability. Active markers, which emit light, may also be used.

Stereo-photogrammetry is a type of analysis that is especially suited to indoor applications because the greater amount of light in outdoor environments makes it more difficult to recognize markers (both active and passive)

The positioning of the markers must follow specific protocols in order to guarantee a standardized description of the motor activity; the number and position of the markers strictly depend on the type of movement studied. For a correct reconstruction, the mass and height of the subject and the length of the leg are used.

In optical systems data is presented in an absolute spatial reference containing the cameras. Each camera records the movements on the basis of its own reference system. The data obtained from the cameras are reported in the global reference system by knowing the position of the cameras in the space and applying the appropriate roto-translation matrices.

The cameras record the movements that occurs in the space through images (frames) sampled over time. The sequence of images will allow us to reconstruct the trajectory of each marker and therefore of the body segments. For the acquisition of the movement in a three-dimensional space, multiple cameras are needed and typically in a motion analysis laboratory 6-12 cameras are used for the complete capture of the movements. Currently most of the stereo-photogrammetry systems consist of a set of optoelectronic cameras, suitable for operating in combination with reflective passive markers. The cameras are equipped with an infrared illuminator, typically composed of a series of LEDs, and with the camera sensor, typically CCD sensor. The capture volume is then illuminated with infrared light which is reflected by the markers and captured by the cameras [1]. The active infrared lights form a ring around the lens of the chamber and are pulsed at 120 Hz for a period of less than a millisecond. Since the light sent is pulsed, the images of the markers are captured in very precise moments of time.

Before each acquisition, the space is firstly calibrated using special reference wands on which markers are placed at known distances along the three axes, which are positioned in the capture space and acquired for a few seconds. Then a capture volume calibration using a wand moved by an operator are performed. Once the entire procedure is finished, it is extremely important that the cameras do not undergo further movement, which would require a new calibration, Since calibration is a procedure that can be performed in few minutes, it is advisable to repeat it before each acquisition session.

Thus, as the definition of the reference systems as well as the marker positioning is fundamental, for a correct and complete description of the kinematics. A specific protocol for the type of task investigated should be chosen. Specifically, as regards the gait analysis one of the most importante protocol are there are Davis protocol [8].

Davis protocol was developed in 1991 at the NCH (Newington Children 's Hospital, USA) [9]. In this protocol the number of markers used, 22, represents the minimum set-up for the 3D description

of the path. In the Davis protocol the markers are used to define the kinematics of the trunk and legs. First of all, the protocol requires the measurement of some anthropometric values such as height and body weight of the subject under examination and the measurement of the parameters related to the bone segments necessary for the estimation of joint centers (the distance between the anterior right and left iliac spines or the distance in the sagittal plane of the iliac spines anterior and the great trochanter).

At the beginning of an experimental session the protocol provides for a static acquisition: the subject remains upright and stable within the capture volume for some seconds during which the data are acquired marker positions. These measures, integrated with the anthropometric ones, allow to build reference systems associated with bone segments and the position of the articular centers of the lower limbs. This protocol has the advantages of the marker being an essential and non-invasive device, and the consequent rapidity with which the subject can be prepared.

In this work all the recording sessions were performed through SMART D Motion Capture system, BTS, Milan (Fig. 3.3), in particular through SMART Capture, the application of the system that allows you to capture images (static or dynamic) in order to be analyzed. With this system, synchronized and integrated kinematic, kinetic, sEMG and video signal acquisition was possible.

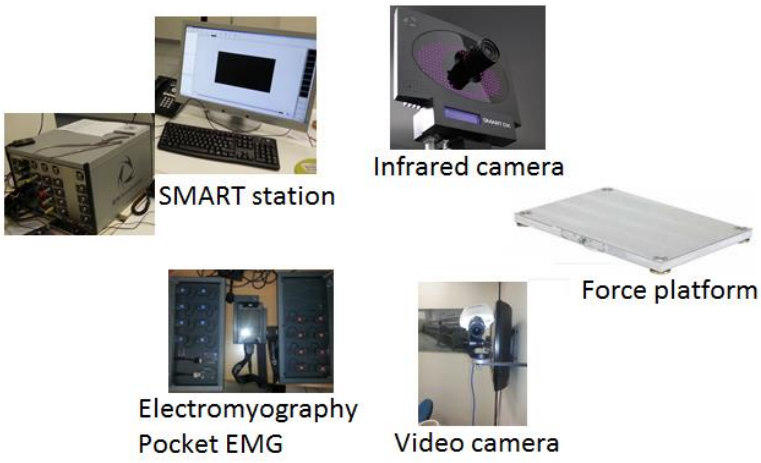

Figure 3.3. Components of SMART system.

In most recordings for the experiments described in this thesis, kinematic data were recorded bilaterally at 300 Hz using an optoelectronic motion analysis system (*SMART-D System; BTS, Milan, Italy*) consisting of eight infrared cameras spaced around the walkway that detect the motion of passive reflective markers (Fig.3.4). The marker-set (summarized in Table 3.1) consisted of twenty-two retro-reflective spherical markers (15 mm in diameter) attached on anatomical landmarks (Fig. 3.5), according to *Davis et al.* [8].

Figure 3.4. Twenty-two retro-reflective spherical markers (left) and additional wands (right).

In addition to markers directly applied to the skin, sticks, or wand, varying in length from 7 to 10 cm, placed at 1/3 of the length of the body segment were used. In particular, a wand on the femur and on a leg was used, so that the plane containing the three points was parallel to the frontal plane.
The requirements of easy identification and visibility of the markers were respected, as they were all identifiable by the cameras: the markers, spherical or semi-spherical, were placed on the subject under examination and the infrared reflected by these were seen by the cameras as a bright spot on the scene.
Anthropometric measurements were collected for each subject in order to determine the joints offset angles; these included the mass and height of the subject and the length of the main segments of the body according to Winter [1]: height, weight, length of the shank of the subject, diameter of knee, diameter of ankle, distance between the anterior iliac crests and the thickness of the pelvis.
A calibration procedure was executed before the first task, to define the volume in which the acquisition took place (the physical space in which the movements were made to acquire, in our case, the space necessary for the patient to take certain steps).

Body segment	Marker acronym	Marker name
Trunk	r should	Right Acromion
	l should	Left Acromion
	c7	Spinous process c7
Pelvis	r asis	Right anterior superior iliac spine
	l asis	Left anterior superior iliac spine
	sacrum	Sacrum
Femur	r thigh	Right greater trochanter
	l thigh	Left greater trochanter
	r bar 1	Right femur wand
	l bar 1	Left femur wand
	r knee 1	Right lateral femoral epicondyle
	l knee 1	Left lateral femoral epicondyle
Leg	r knee 2	Right head of the fibula
	l knee 2	Left head of the fibula
	r bar 2	Right tibia wand
	l bar 2	Left tibia wand
	r mall	Right lateral malleolus
	l mall	Left lateral malleolus
Foot	r met	Right fifth metatarsal head
	l met	Left fifth metatarsal head
	r heel	Right heel
	l heel	Left heel

Table 3.1. Marker-set.

The analysis was based on the recognition and three-dimensional reconstruction of passive markers positioned on the anatomical landmarks.

A

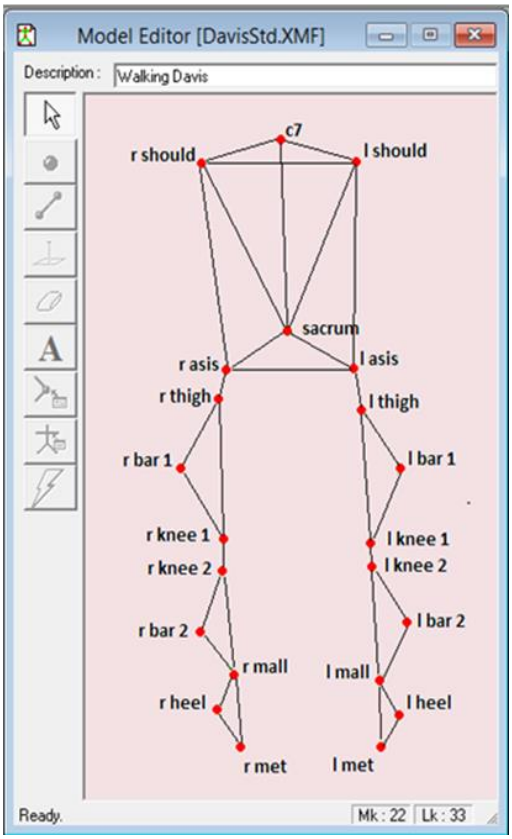

B

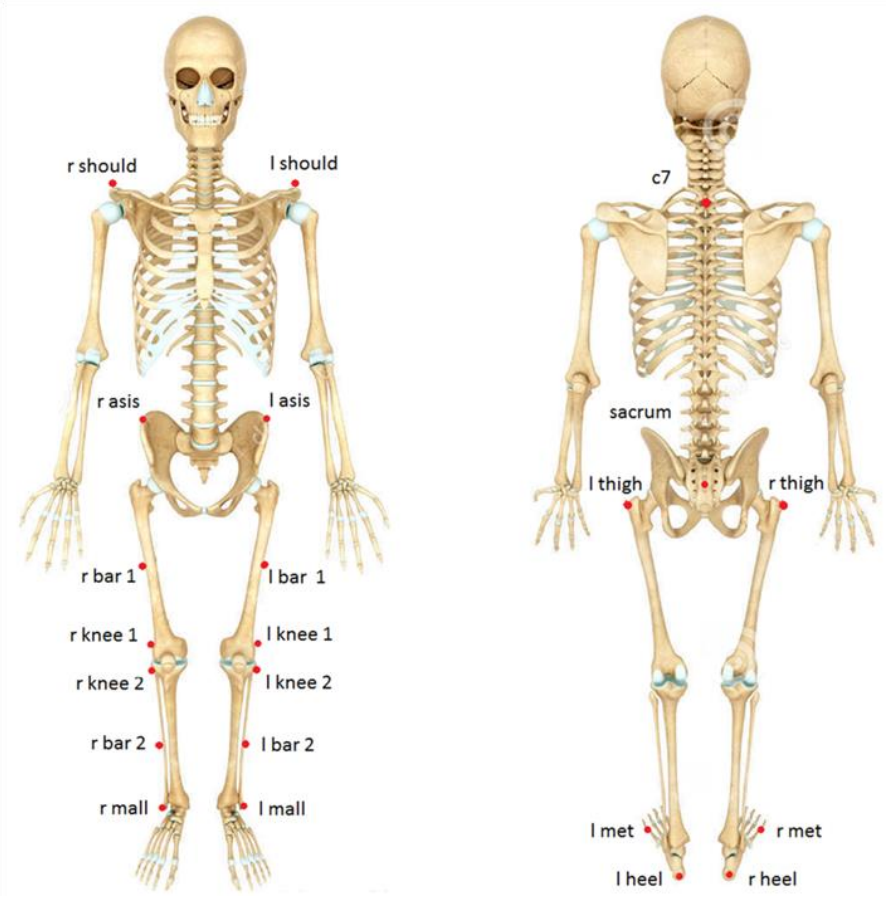

Figure 3.5.. Kinematic Davis model (A) and arrangement of markers according to Davis protocol (B).

Two different types of acquisitions, static and dynamic must be carried out: the first, the individual recordings of the twenty two reference points required for the construction of the protocol are recorded, while dynamics acquisitions are needed to record some samples of the subjects gait.

3.2.1.2 Dynamometric platforms

For most of the sessions acquired in this thesis, Ground reaction forces (GRFs) were recorded at 1200 Hz by means of two force platforms (0.6 x 0.4 m; *Kistler 9286B, Winterthur, Switzerland*), placed at the center of the walkway, attached to each other in the longitudinal direction but displaced by 0.2 m in the lateral direction (Fig. 3.6). The use of force platforms allowed the analysis of reaction forces to the soil.

The force platforms consisted of four load cells, each of which was placed in one of the four angles of the platform. They were constituted by three force transducers, each of which is idealized and designed to be able to detect only one of the three components of force or moment. The force transducers, also known as load cells, employing sensors that converted applied force in a deformation which, in turn, produced an electrical signal of output. The force platforms measured the resultant of the reaction of the soil at the time of the impact of the subject. The forces were analyzed in the three fundamental levels, decomposed in the vertical, anterior-posterior and medial-lateral components (Fy, Fx, Fz). The measured forces in combination with the kinematic analysis allowed to study the moments at the level of hip, knee and ankle articulation.

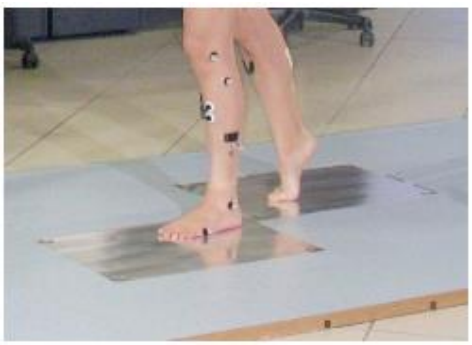

Figure 3.6. Force platforms.

Video recording of the subject, through 2 video cameras, is usually complementary to kinematic and kinetics analysis and provides qualitative information that support clinical investigation.

3.2.1.3 Surface electromyography (sEMG)

The electromyographic analysis is the electrical manifestation of muscle contraction: the muscle fibers, excited by the impulse of the nervous system through the motor neuron, contract.

Figure 3.7. Bipolar Ag-AgCl surface electrodes.

In most recordings for the experiments described in this thesis, sEMG data were recorded at 1000 Hz using a 16-channel wireless system (*FreeEMG300 System; BTS, Milan, Italy*) and with band-pass filtering between 10 and 400 Hz (Hamming filter) for the attenuation of the motion artifacts and high frequency noise. Bipolar Ag-AgCl surface electrodes (*H124SG, Kendall ARBO, Donau, Germany*) (Fig.3.7), prepared with electro-conductive gel (diameter 1 cm, distance between the electrodes 2 cm) and placed over the muscle belly in the direction of the muscle fibers were used to record EMG activity from body muscles

A variation of the potential distribution during muscle contraction can be observed through bipolar electrodes: registering this variation, an indicative signal of muscle according to the movement performed is obtained. The use of surface electrodes greatly simplifies the sampling operations of the signal and, together with the non- invasiveness, makes possible the recordings in both conditions of isometric contraction and dynamic effort.

The correct placement of the electrodes is a critical point of the surface electromyography technique. sEMG signal makes possible the extraction of information related to skeletal muscle activity, but this information may be incorrect if electrodes are placed near the innervation zone (IZ), or tendon regions, strongly influencing sEMG amplitude and frequency. According to SENIAM guidelines (European Recommendations for Surface Electromyography) [11,12] we were able to locate innervation zone improving therefore the correct placement of sEMG electrodes and the quality of the electromyographic signal acquired.

This allowed us to get information about the status of muscle activation during the movement; to record muscle interventions defining the sequence, the time intervention, duration, and intensity within certain limits without any invasive. Particularly suitable in gait analysis, also provides useful information on strategies to control the movement of the upper part of the central nervous system.

Acquisition of the EMGs, kinematic, and kinetic data was synchronized

3.2.2 Pre-processing

Data acquisition from the integrated surface EMG system and from the optoelectronic cameras and force platforms were integrated and synchronized.

A reconstruction of the tridimensional position of each marker, from the images of each camera, was necessary to process data (Fig. 3.8). This procedure was carried out through the SMART Software Tracker (*BTS, Milan, Italy*), which allowed you to apply the anatomical model (in our case the Davis model) and match the individual points of this scheme to the marker represented in the file acquisition, by assigning a label to each marker (labeling). Kinematic and electromyographic data were then normalized to the duration of the gait cycle. After rebuilding the 3D position of each marker at each instant of time, next step was to calculate their trajectory (tracking), from which it was possible to estimate the joint kinematics and, consequently, the relative position and orientation of the reference systems in agreement with the bone segment under examination. The operation of

tracking was the first stage of data processing: represents the logical connection of two successive frames, so as to identify the time curve of each single marker. Thus from the trajectories of the markers, the kinematic speed and acceleration were obtained by derivation. In this step, you could also assign a label to force signals from the platform, displayed as a vector with the origin in the center of pressure and magnitude and direction equal to the vector sum of the three components of force.

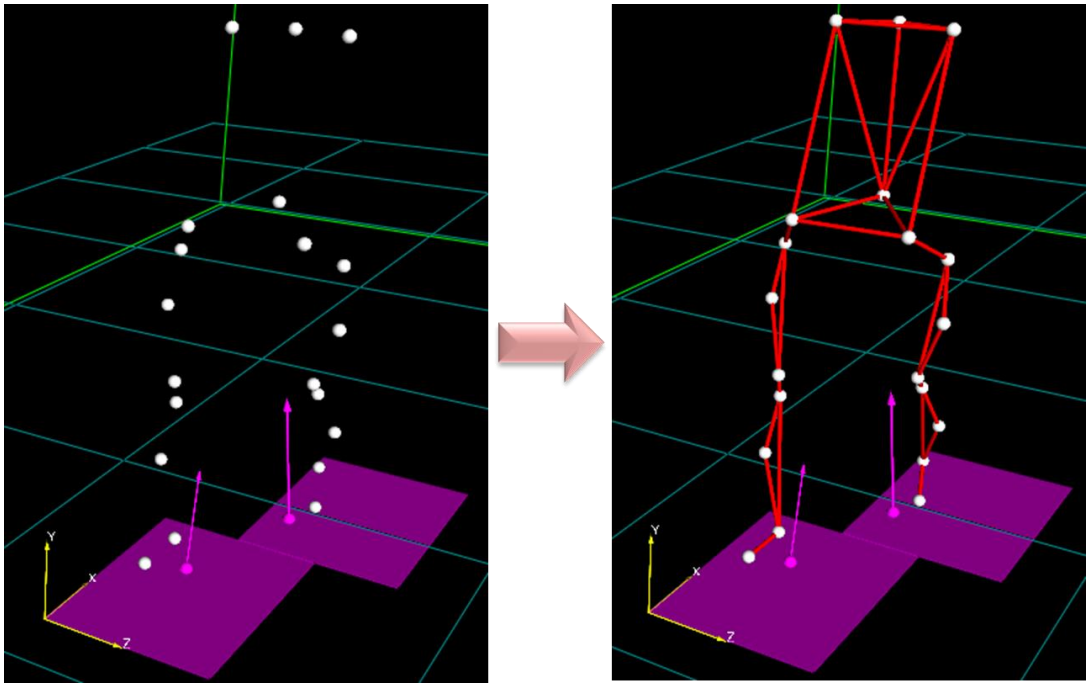

Figure 3.8. Reconstruction of the 3D position of each marker according to Davis model (left) and tracking procedure (right).

3.2.3 Data analysis

After the procedure of tracking, data were processed using 3D reconstruction software (*SMART Analyzer, BTS, Milan, Italy*) and an algorithm written in MATLAB software (*MATLAB R2014a, MathWorks, Natick, MA, USA*) which calculated all biomechanical and electromyographic parameters of interest, such as the relative angles between two segments body, speeds, distances, forces and moments acting on the joints. In particular, during this phase a temporal analysis of the signals was carried out to define manually events in the gait cycle. To correctly identify the instants

of support and toe-off, the user used the information from the signals of the force platforms (where possible), and the reconstruction of temporal trends of joint kinematics of lower limbs.

3.2.3.1 Gait event estimation

Gait is characterized by a cyclic pattern of motor activity of the lower limbs and trunk that allows to transfer the weight on the limb support and advance against the limb-side forward. Gait analysis provides very important information especially when it concerns the analysis of the step of pathological subjects. In fact, the study of the postural and motor alteration in patients with pathologies associated with alterations of the movement allows to know the level of functional limitation resulting from the disease and its evolution over time, and may provide useful elements to define an appropriate rehabilitation strategy. The gait cycle is the functional unit of reference for gait analysis and is defined as the time between two successive foot contacts of the same leg.

In the studies described in this thesis, heel strike (HS) and toe-off (TO) events were determined by maximum and minimum excursions of the limb angle, defined as the angle between the vertical axis and the limb segment (from the greater trochanter to the lateral malleolus) projected on the sagittal plane (Fig. 3.9). When subjects step on the force platforms, these kinematic criteria can be verified using the information from the signals of the force platforms.

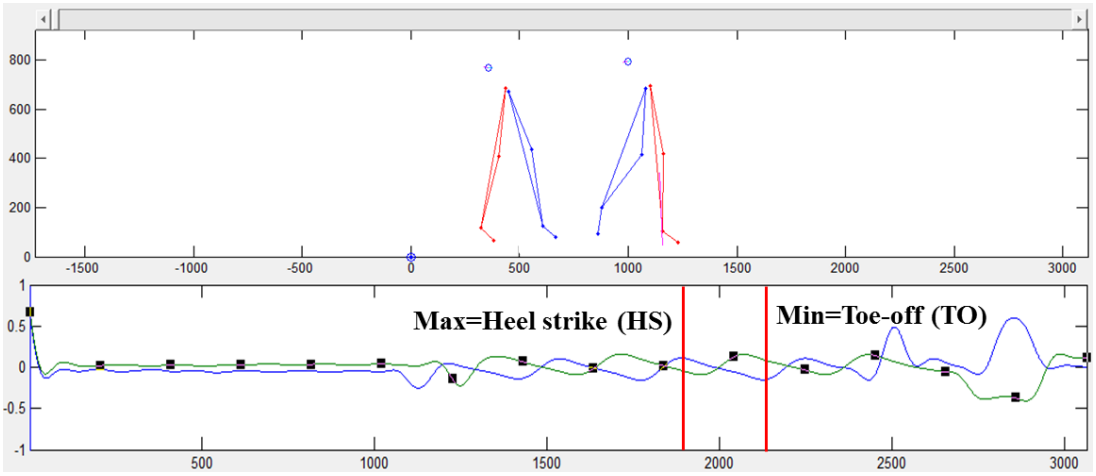

Figure 3.9. Definition of the instants of heel strike and toe-off: the reconstruction of lower limbs segments and force platforms (top); the trends of lower limbs angles (bottom).

Gait cycle is normally divided into eight steps (*Perry 1992*): initial contact (0%); loading response (0-10%); midstance (10-30%); terminal stance (30-50%); preswing (50-60%); initial swing (60-70%); midswing (70-85%); terminal swing (85-100%) (Fig. 3.10)

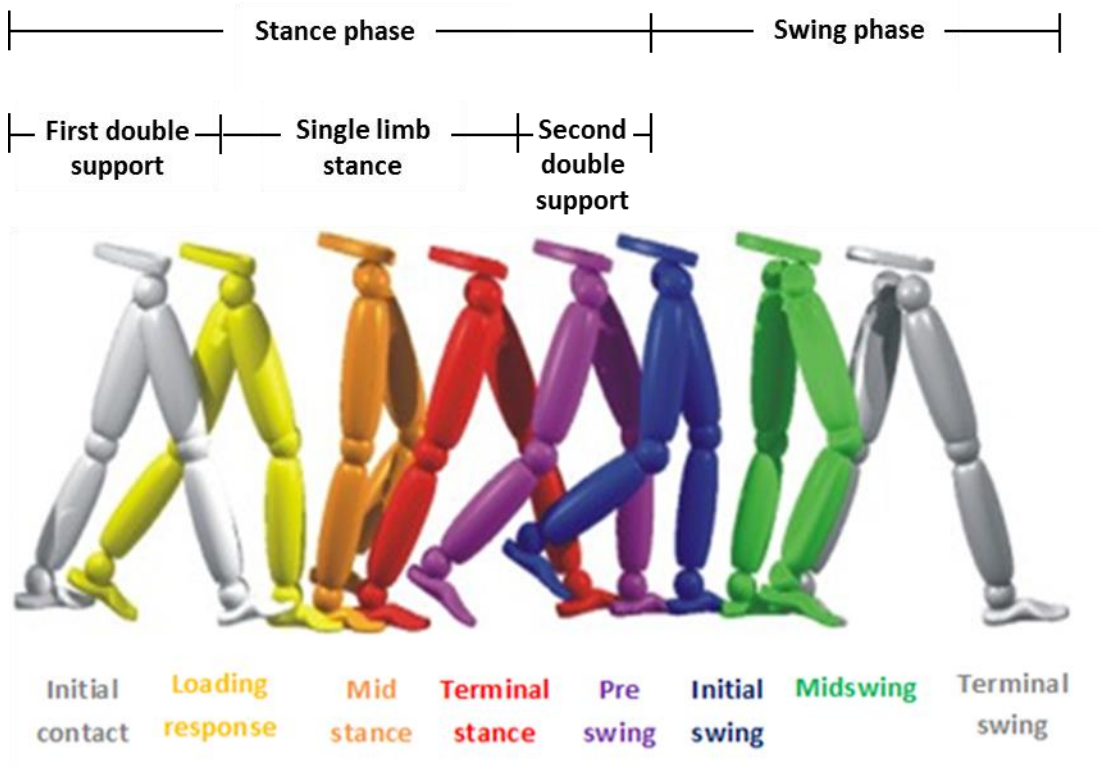

Figure 3.10. Normal gait cycle.

Globally, the gait cycle can be divided into two phases: the stance phase (from the current initial contact to foot-off) and the swing phase (from foot-off to the successive initial contact). Finally, within the stance phase, the following three subphases were considered:

- initial double support (first double support): both feet are in contact with the ground;
- single support: during which the reference foot is in contact with the soil and the counter-side is swinging;
- terminal double support (second double support): in which both feet are again contact with the ground.

3.2.3.2 Gait parameters

The most important time-distance gait parameters are: walking speed (km/h), cycle and step duration (s), relative stance duration (s), stride and step length (m), first and second double support duration (s), cadence (step/min) and step width (m). The stride and step length and the step width were normalized to the limb length of each subject (Table 3.2).

Time-distance parameters
Walking speed
Cycle duration: time interval between two successive initial contact of the same foot
Step duration: time interval between the initial contact of a foot and the initial contact of the contralateral foot
Stance duration: the entire period during which the foot is in contact with the ground
Cycle length: distance between two successive supports of the same foot
Step length: distance between the heel of one foot and the heel of the contralateral foot
1st double support duration: time in which both feet are in contact with the ground after the initial contact
2nd double support duration: time in which both feet are in contact with the ground after single standby
Cadence: number of steps in the time unit
Step width: mediolateral distance between the feet

Table 3.2 . Summary of the general time-distance and kinematics evaluated parameters.

Additional quantification of gait can be obtained by extracting the Coefficient of Variation (CV), which corresponds to the ratio of standard deviation of the parameter over its mean value (CV = 100* SD/mean, where SD is the standard deviation). It is a measure of variability.

The anatomical joint angles for hip, knee and ankle (sagittal plane), trunk and pelvis (frontal, sagittal and transverse plane) are useful to derive the joint range of motion (RoM), defined as the differences between the maximum and minimum values during the gait cycles.

Kinetic data in combination with the kinematic analysis allow the study of the hip, knee and ankle internal moments as well as the support moment.

sEMG data are useful to study muscular parameters, such as muscle activation and co-activation, or center of muscular activity.

3.2.3.3 Muscle coactivation

Muscle co-activation is the mechanism that regulates simultaneous activity of agonist and antagonist muscles crossing the same joint [13]. It has been demonstrated to be important for providing adequate spine and joint stability, movement accuracy (such as in precision tasks) and energy efficiency [14,15] and for adapting to environmental demands [16] When substantial antagonist activations counteract the agonist actions, thus producing moments that do not contribute to the required net joint moments, co-activation may become functionally unfavourable, or even detrimental. It may, in fact, represents a factor that contributes to the inefficiency of human movement by increasing the physiological and metabolic cost, thereby reducing the net moment and power development. Furthermore, excessive muscle co-activation increases compressive loading across the joint, which may in turn lead to cartilage loss. [16-19].

Robust measurement techniques are required for an accurate determination of the muscle co-activation during functional movements [20].

Surface electromyography (sEMG) is able to give insights on muscular contractions in agonist and antagonist muscles and to monitor the relative modifications through time [21,22]; it thus represents one of the elective means to monitor co-activation, also in the case of functional movements, when robustness in the determination of muscle co-activation is necessary [23].

Muscle co-activation has been measured by means of surface electromyography (sEMG) through the analysis of the relative variations in agonist and antagonist muscles contraction through time [21].

Several computational approaches have been used to quantify muscle co-activation: ratio, overlapping or cross-sectional areas of simultaneous activation of opposite muscles [21]. These mathematical tools derive from an agonist–antagonist approach on EMG signals recorded from two

antagonist muscles or between two antagonist muscles of the same joint. Outcomes of these tools are expressed in term of both the time of overlapping between the linear envelopes of two opposite muscles and the magnitude of muscle co-activation [24-23].

Moreover, another approach, proposed by Ranavolo et al. 2015 [27], is based on the time-varying multi-muscle co- activation function (TMCf), allowing the characterization of the simultaneous work on multiple muscles or muscle groups. A global characterization of it may be helpful to understand the general strategy adopted by CNS to control the lower limb.

More recently, an approach based on a Vector Coding Technique (VCT) has been proposed [28] to quantify co-activation and coordination: with this method, in addition to the analysis of each muscle activation phase, users are able to continuously monitor over time the co-activation between muscles.

All measurement techniques may be liable to error that can reduce validity and reliability and confound the interpretation of the findings. Various factors in the sEMG measurement process, such as signal acquisition and signal analysis procedures, might influence the establishment of representative envelope profiles, and therefore the outcome of co-activation evaluated from the signal envelope. An important aspect is related to the variations of the signal to noise ratio (SNR) level: sensitivity of the algorithm performances may change with respect to SNR variations [29]. A further aspect that does not guarantee the estimation of stable and repeatable information from the algorithms is the arbitrary choice of the lowpass cut-off frequency used to obtain the classical envelope: the frequency used in the sEMG ranges from 3 Hz to 25 Hz [30].

High levels of muscle coactivation in knee and in ankle joints during gait have been reported in elderly people [31], individuals who have undergone knee arthroplasty[32], patients with several central nervous system lesions including Parkinson’s disease [33], cerebellar ataxia [34] and multiple sclerosis [15]. Increased muscle coactivation in these neurological disorders seems to reflect different abnormalities of the motor control. On the one hand, muscle coactivation may be the result of balance-related adaptive compensatory mechanism aimed at reducing instability in the

lower limbs such as in cerebellar ataxia [34,35]. On the other hand, it is an expression of primary deficits reflecting either abnormal descending motor commands or lack of reciprocal inhibition of the neural circuits of the spinal cord such as in Parkinson's disease [35].

During ground surface linear walking, muscle joint coactivation varies within the gait cycle, according to the functional role of the lower limb joints along gait phases, reaching higher values during weight acceptance and transition from stance to swing subphases [16] and lower values during mid-stance [37]. In addition to gait phases, several other factors influence the rate of the muscle coactivation during locomotion, including age [38], speed and motor context, i.e., stable vs. unstable conditions [39].

3.2.3.4 Muscle synergies

The fundamental task of the nervous system is to interpret and interact with a highly complex, multidimensional environment. Both aspects of this task potentially involve monitoring the state of many thousands of variables, considering either the many individual sensory receptors or individual motor units. The multiarticular nature of the limb and its large number of muscles together imply many available degrees of freedom to accomplish motor tasks [40]. While this redundancy provides flexibility, it appears that generally the CNS utilizes preferred ways to achieve a given task [41]. One strategy for the nervous system to overcome this complexity might be to identify statistical regularities within the environment and then operate using these regularities rather than the individual variables of either sensation or action. One common hypothesis is that these regularities in the motor system might be represented as "muscle synergies," each of which draws a specific balance of muscle activations. As a result of producing movements through a linear combination of muscle synergies, the number of degrees of freedom needed to be coordinated is substantially reduced. A muscle synergy consists in the activation of coordinated muscle groups characterized by a specific time profile [42]; each synergy is scaled in amplitude and shifted in time, independently

of each other, and the activation of the muscles comes from a number of different synergies combined with each other linearly.

Evidence in favor of such a hypothesis has come from several studies, each examining the muscle activation patterns observed in a particular behavior: many behaviors can be well described in terms of combinations of a small number of muscle synergies [43]. While observed electromyographic patterns, muscles although not controlled individually, can be grouped in a flexible fashion by the CNS to accomplish the same general task.

Throughout most of the last century, the scientific community believed that movement production and control were attributable to central brain structures, such as the cortex, basal ganglia and cerebellum. A passive role was attributed to the spinal cord, which was believed to receive commands from supraspinal systems. Furthermore, the coordination of motion was a unknown issue that aroused wonder given how the Central Nervous System (CNS) manages the high number of degrees of freedom of the musculoskeletal system to produce movements [40]. However, a vast pioneering literature in last two decades has led to a consensus on the active role of the spinal motor system, which is actively involved in various mechanisms that produce movement, ranging from basic reflexes to complex voluntary movements. These findings confirmed the hypothesis of the existence of spinal building blocks, discrete generators whose combinations produce movement. This modular organization of the spinal cord circuitry is based on functional units (called muscle synergy) that generate a specific motor output by imposing a specific pattern of muscle activations specified together. The first corroborative evidence supporting this modular architecture of the spinal cord came from examinations conducted by microstimulation of the spinal cord gray matter, N-methyl-d-aspartate ionophoresis or skin stimulation in animals [41,43,44]. To gain an insight into this discrete organization process, the outputs of modules were usually characterized as force fields or in terms of electromyographic muscle responses. It has thus been possible to understand how the CNS produces a wide range of complex movements using only a few functional units within the spinal cord combining them linearly.

When the field of forces recorded following co-stimulation were compared with those obtained by vector summation of the two individual fields, co-stimulation fields and the summation fields were equivalent in most cases .

This principle of summation, which allows a wide range of motor responses in the computationally simplest manner, might also subserve the motor responses produced by supraspinal systems [45].

The force fields generated by the activation of supraspinal structures, such as the vestibular nerve, result from combinations of a small number of spinal modules.

Further studies conducted on spinalized or intact and freely moving animals [42] are consistent with this hypothesis of a low-dimensional controller capable of simplifying control without degrading performance. In the last few years, this small alphabet of control signals and motor modules has also been directly investigated in humans. The first evidence of low-dimensional representation of motor output comes studies performed by d'Avella and colleagues [42,46]. The authors showed that the spatiotemporal characteristics of the phasic and tonic muscles patterns during upper limb goal directed reaching movements, in different directions, loads, postures and velocities, are determined by linear combinations of a small number of muscle synergies.

A series of papers written by Ivanenko and colleagues [47-50] instead highlighted the spinal functional modular architecture during human locomotion in healthy subjects. The ability of spinal systems to contribute to the production and adaptation of movement has more recently led several neuroscientists to investigate of how nervous system diseases alter the organization of motor modules. This was done in stroke patients during walking and upper limb movement [51-54]. Finally, in recent times a study about the adjustments of the locomotor modules related to unstable walking conditions was carried out by Martino and colleagues [55]: comparing three different conditions, i.e. locomotion of healthy subjects on slippery ground and on narrow beam and of cerebellar ataxic patients on normal ground they assessed that the overall variation of EMG waveforms was accounted for by few motor modules. This suggests that nervous system adopts a

specific strategy to cope with unstable conditions resulting from either slippery ground, reduced support surface or pathology.

Understanding the reorganization underlying neuronal drives of synergies might allow motor function to be recovered by means of specific rehabilitation strategies.

Mathematically, every profile of muscle activation m_j was assumed to be the linear combination of a small number of muscular synergies each of which is composed of two positive components: a fixed component w_{ji} (vector of muscular synergies), which represents the relative weight of each muscle within each synergy, and a time-varying component c_{ik} (vector of coefficients of activation of the synergy), which represents the relative contribution of the synergy of muscle activation patterns, and since the muscle activation is not negative the two components must have both values always positive:

$$m_{kj} = \sum_{i=1}^{N} c_{ki}\, w_{ij} \quad c_{ki}, w_{ij} \geq 0$$

Thus the vector of muscle activation for each j-th muscle is hypothesized have the form:

$$m_j = C_1 w_{1j} + C_2 w_{2j} + \ldots + C_N w_{Nj}$$

where w_{1j} is the j-th element of the synergy W_1 and so on, for N synergies.

Similarly muscle activation in each time instant can be expressed as a vector in which each element is the level of activation resulting in every muscle:

$$m_k = c_{k1} W_1 + c_{k2} W_2 + \ldots + c_{kN} W_N$$

where c_{k1} represents the k-th element of the corresponding coefficient C_1; at the time instant k. The equations above may be represented in matrix notation:

$$M = CW$$

where each row of the matrix M is a muscle, and each column represents a time instant (Fig. 3.11).

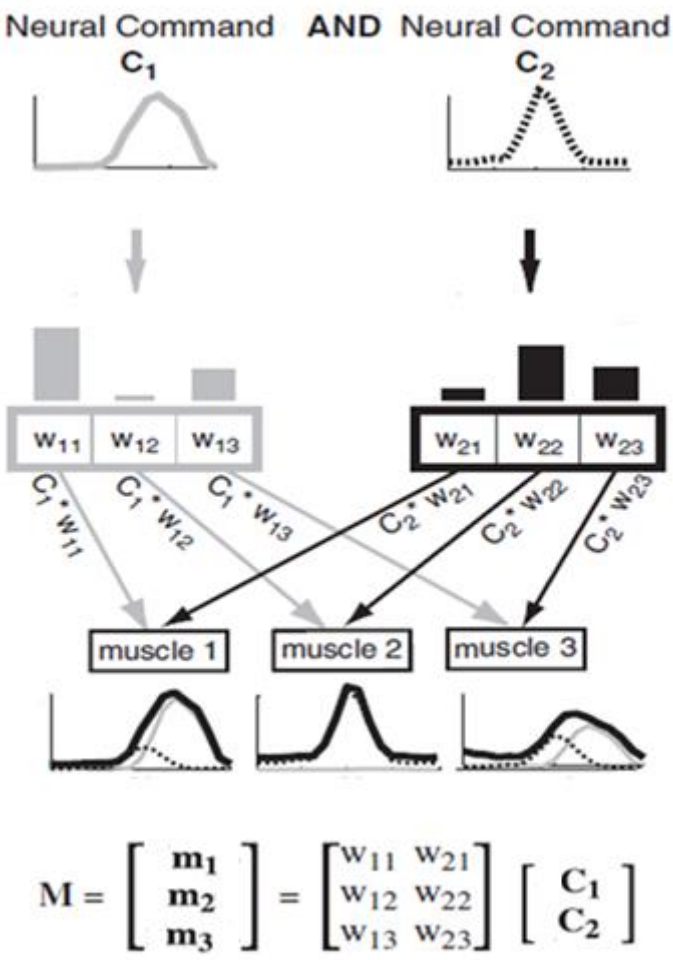

Figure 3.11. Generation model of muscle patterns as a linear combination of muscle synergies.

Each element of W takes a value between 0 and 1 (after normalization with respect to the maximum value) representing the relative contribution of each muscle in the muscle synergy and muscle synergy can be seen as modulated by a set of independent neural commands C for each synergy and in each task:

$$\begin{bmatrix} m_{11} & \dots & m_{1j} \\ \dots & \dots & \dots \\ m_{k1} & \dots & m_{kj} \end{bmatrix} = \begin{bmatrix} c_{11} & \dots & c_{1i} \\ \dots & \dots & \dots \\ c_{k1} & \dots & c_{kN} \end{bmatrix} \begin{bmatrix} w_{11} & \dots & w_{1j} \\ \dots & \dots & \dots \\ w_{i1} & \dots & w_{Nj} \end{bmatrix}$$

Non-negative matrix factorization

Different statistical methods have been developed to obtain a linear decomposition of the original set of data and extract synergies from muscle activation patterns based on different assumptions. In

general, factorization algorithms are used, for example ‘Principal Component Analysis (PCA)’, ‘Factor Analysis (FA)’, ‘Indipendent Component Analysis (ICA)’, ‘Nonnegative Matrix Factorization (NMF)’. Based on several studies in literature, we chose to adopt the NMF algorithm. Nonnegative matrix factorization was implemented using the matrix multiplication update rules based on the Euclidean distance objective function described by Lee and Seung (2001) which it has been shown to be a good compromise between speed and ease of implementation. There are no explicit assumptions about the distributions of activation coefficients for NMF, other than that all the elements of the matrix of initial data and the factors that break it down must be greater than or equal to zero. It is likely that the robust performance of NMF is to a large extent explained by the strong constraints imposed by its assumption of nonnegativity [43].

Given a nonnegative matrix M, the problem is to find two nonnegative matrices W and C, such that:

$$M \sim CW$$

where W and C are a compressed version of the original matrix. Thus, each element of M is estimated by the linear combination of the columns of C weighted for the components of W (Fig. 3.12).

Thus, the problem is to minimize $||\mathrm{M} - \mathrm{CW}||^2$ compared to C and W, with the constraint C,W≥0. It is unrealistic to think that the algorithm can solve the problem finding a global minimum of the cost function, however, there are numerical techniques that allow to find a local minimum.

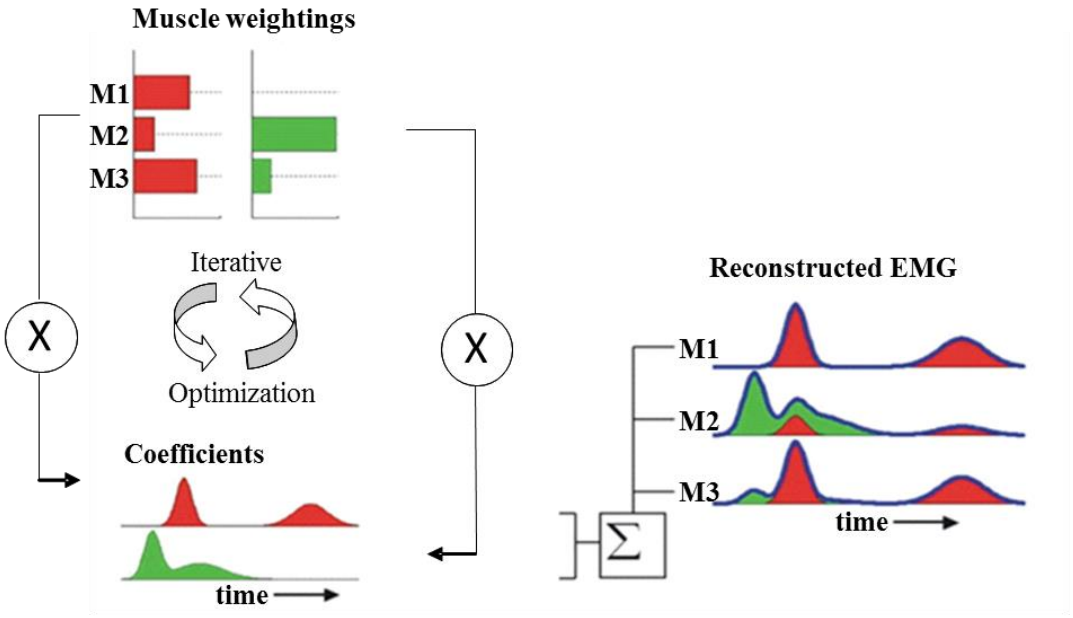

Figure 3.12. From the sEMG processed, the figure shows a diagram of the iteration procedure of the NMF algorithm for the extraction of muscle synergies, and reconstruction made from this estimate (Cheung et al. 2009).

As convergence criterion in our study it was decided to apply the multiplicative rule proposed by Lee and Seung (2001) [56], which have shown that the Euclidean distance $||M - CW||$ does not increase under particular update rules:

$$c_{nk} = c_{nk} \frac{(W^T M)_{nk}}{(W^T WC)_{nk}} \qquad w_{jn} = w_{jn} \frac{(MC^T)_{jn}}{(WCC^T)_{jn}}$$

The algorithm is then initialized with non-negative random values (between 0 and 1) for the matrix W and C and proceeds in the minimization of the total reconstruction error by alternating the rules described before until a convergence condition is satisfied (defined as the reaching a threshold in the total reconstruction error $< 10^{-4}$).

In order to minimize the probability to find a local minimum, the algorithm was repeated for 100 times on each set of data, choosing the factorization that produced the lower mistake of total reconstruction.

The NMF algorithm requires that the number N of synergies that make up the set of data was determined a priori. In order to determine this number, we adopted a procedure based on the analysis of the amount of total variation explained (R^2). This value R^2 is the result of the relationship between two variances, defined as:

$$R^2 = 1 - \frac{SSE}{SST} = 1 - \frac{\sum_{i=1}^{n}(y_i - \hat{y}_i)^2}{\sum_{i=1}^{n}(y_i - \bar{y}_i)^2}$$

where SSE is the sum of the quadratic residues, SST is the total variance, y is the observed data, $\hat{y}$ is the estimate data and $\bar{y}$ is the mean value. Therefore, R^2 is the fraction of total variation explained by the reconstruction of the synergies and can take on values between 0 and 1 (1 in the case where the variance is fully explained and the reconstruction error is null, 0 in the opposite case). Thus, we repeated the extraction with a range of synergies from 1 to 8 and selected the minimum number of N synergies by examining the characteristic of R^2 as a function of N.

Then we adopted a procedure based on linear regression in order to identify the value of N after which the curve R^2 remains essentially straight. A series of linear regressions was conducted, starting from a regression whole curve (with N from 1 to 8 synergies) of R^2 and progressively removing the smallest value of N from the range of regression. The optimal number of synergies N was selected as the first value corresponding to a regression line from N to N^{max} with a mean square error (MSE) <10-4.

This procedure has been shown to be a good compromise between speed and ease of implementation.

After identifying the number of synergies for each subject, a specific script was designed to identify and average the similar synergies across subjects, based on the best-matching scalar product of weighting coefficients normalized to the Euclidean norm. After assuming a threshold of 0.6 on this criterion, synergies were grouped in inter-individual sets and the correlation between the identified synergies was calculated.

3.2.3.5 MATLAB

Matlab is a high-level language for scientific and engineering computing, a tool for matrix manipulations, signal processing, data classification and graphical visualization, and many other functionalities.

In many processing sections of the studies described in this thesis, it was used for algorithm implementation (including all the methods for gait events and parameter estimation), graphical visualization and data classification.

Bibliography

[1] D. A. Winter, Biomechanics and motor control of human movement, Fourth Edition, John Wiley & Sons, 2009.
[2] E. Ceseracciu, Z. Sawacha e C. Cobelli, Comparison of Markerless and Marker-Based Motion Capture Technologies through Simultaneous Data Collection during Gait: Proof of Concept, PLoS One, 2014.
[3] A. Leardini, L. Chiari, U. Della Croce e A. Cappozzo, Human movement analsysis using stereophotogrammetry Part 3. Sofrt tissue artifact assessment and compensation, Elsevier, 2005.
[4] U. Della Croce, A. Leardini, L. Chiari e A. Cappozzo, Human movement analysis using stereophotogrammetry part 4: assessment of anatomical landmark misplacement and its effects on joint kinematics, Elsevier, 2005.
[5] A. Leardini, U. Della Croce, L. Chiari e A. Cappozzo, Human Movement analysis using stereophotogrammetry Part 1: theoretical background, Elsevier, 2004.
[6] W. T. Dempster, W. C. Cabel e W. J. L. Felts, The Anthropometry of Manual Work Space for Seated Subjects, Am J. Phys. Anthrop., 1959.
[7] R. Drillis e R. Contini, Body Segment Parameters, Office of Vocational Rehabilitation, Department of Health, Education and Welfare, New York, 1966.
[8] R. B. Davis, S. Ounpuu,, D. Tyburski e J. R. Gage, A gait analysis data collection and reduction technique, Human movement Science, 1991.
[9] M. W. Whittle, Gait Analisys An Introduction, Fourth Edition, Elsevier, 2007.
[10] A. D. Koelewijn e A. J. Van den Bogert, Joint contact forces can be reduced by improving joint moment symmetry in below-knee amputee gait simulations, Elsevier, 2016.
[11] Barbero M, Merletti R, Rainoldi A. 2012. Atlas of Muscle Innervation Zones: Understanding Surface Electromyography and Its Applications. New York: Springer.
[12] Hermens HJ, Freriks B, Disselhorst-Klug C, Rau G. 2000. Development of recommendations for SEMG sensors and sensor placement procedures, 10(5):361-74.
[13] Busse ME, Wiles CM, et al. ‘‘Muscle co-activation in neurological conditions’’. Phys Ther Rev 2005;7(4):247–53.
[14] Darainy M, Ostry DJ. Muscle cocontraction following dynamics learning. Exp Brain Res 2008;190:153–63.
[15] Boudarham, J., Hameau, S., Zory, R., Hardy, A., Bensmail, D., Roche, N., 2016. Coactivation of Lower Limb Muscles during Gait in Patients with Multiple Sclerosis. PLoS One 11 (6).
[16] Higginson JS, Zajac FE, et al. Muscle contributions to support during gait in an individual with post-stroke hemiparesis. J Biomech 2006;39(10):1769–77.
[17] Falconer, K., Winter, D.A., 1985. Quantitative assessment of co-contraction at the ankle joint in walking. Electromyography and clinical neurophysiology 25, 135–149.
[18] Lewek, M.D., Rudolph, K.S., Snyder-Mackler, L., 2004. Control of Frontal Plane Knee Laxity During Gait in Patients with Medial Compartment Knee Osteoarthritis. Osteoarthritis Cartilage 12 (9), 745–751.
[19] Childs, J.D., Sparto, P.J., Fitzgerald, G.K., Bizzini, M., Irrgang, J.J., 2004. Alterations in Lower Extremity Movement and Muscle Activation Patterns in Individuals with Knee Osteoarthritis. Clinical Biomechanics (Bristol, Avon) 19 (1), 44–49.
[20] Den Otter A, Geurts A, et al. Speed related changes in muscle activity from normal to very slow walking speeds. Gait Posture 2004;19(3):270– 8.
[21] Fonseca ST, Silva PLP ST, Ocarino JM, Ursine PGS. Analysis of an EMG method for quantification of muscular co-contraction. Rev Bras Ciên e Mov 2001;9(3):23-30.
[22] Fonseca ST, Silva PLP, Ocarino JM, Guimaràes RB, Oliveira MTC, Lage CA. Analyses of dynamic co-contraction level in individuals with anterior cruciate ligament injury. J Electromyogr Kinesiol 2004;14:239-47.
[23] Den Otter A, Geurts A, Mulder T, Duysens J. Gait recovery is not associated with changes in the temporal patterning of muscle activity during treadmill walking in patients with post-stroke hemiparesis. Clin Neurophysiol: Off J Int Fed Clin Neurophysiol 2006;117(1):4–15.
[24] Unnithan VB, Dowling JJ, Frost G, Volpe Ayub B, et al. Cocontraction and phasic activity during GAIT in children with cerebral palsy. Electromyogr Clin Neurophysiol 1996;36(8):487–94.
[25] Rudolph KS, Axe MJ, Snyder-Mackler L. Dynamic stability after ACL injury: who can hop? Knee Surg Sports Traumatol Arthrosc. 2000;8(5):262-9.
[26] Kellis E, Arabatzi F, Papadopoulos C. Muscle co-activation around the knee in drop jumping using the co-contraction index. J Electromyogr Kinesiol. 2003 Jun;13(3):229-38.

[27] Ranavolo A, Mari S, Conte C, Serrao M, Silvetti A, Iavicoli S, Draicchio F. A new muscle co-activation index for biomechanical load evaluation in work activities. Ergonomics. 2015;58(6):966-79.
[28] Yoo HJ, Sim T, Choi A, Park HJ, Yang H, Heo HM, Park KS, Mun JH. Quantifying coordination between agonist and antagonist muscles during a gait. Journal of Mechanical Science and Technology 2016;30(11)5321-28.
[29] Bonato P, D'Alessio T, Knaflitz M. A statistical method for the measurement of muscle activation intervals from surface myoelectric signal during gait. IEEE Trans Biomed Eng. 1998 Mar;45(3):287-299.
[30] Rosa MC, Marques A, Demain S, Metcalf CD, Rodrigues J. Methodologies to assess muscle co-contraction during gait in people with neurological impairment – a systematic literature review. J Electromyogr Kinesiol. 2014 Apr;24(2):179-91.
[31] Peterson, D.S., Martin, P.E., 2010. Effects of age and walking speed on coactivation and cost of walking in healthy adults. Gait & Posture 31, 355–359.
[32] Dietz, V., Zijlstra, W., Prokop, T., Berger, W., 1995. Leg muscle activation during gait in Parkinson's disease: adaptation and interlimb coordination. Electroencephalography and Clinical Neurophysiology 97, 408–415.
[33] Fallah-Yakhdani, H.R., Abbasi-Bafghi, H., Meijer, O.G., Bruijn, S.M., van den Dikkenberg, N., Benedetti, M.G., van Dieën, J.H., 2012. Determinants of cocontraction during walking before and after arthroplasty for knee osteoarthritis. Clinical biomechanics (Bristol, Avon) 27, 485–494.
[34] Mari, S., Serrao, M., Casali, C., Conte, C., Martino, G., Ranavolo, A., Coppola, G., Draicchio, F., Padua, L., Sandrini, G., Pierelli, F., 2014. Lower limb antagonist muscle co-activation and its relationship with gait parameters in cerebellar ataxia. Cerebellum 13, 226–236.
[35] Martino, G., Ivanenko, Y.P., Serrao, M., Ranavolo, A., d'Avella, A., Draicchio, F., Conte, C., Casali, C., Lacquaniti, F., 2014. Locomotor patterns in cerebellar ataxia. Journal of Neurophysiology 112, 2810-2821.
[36] Meunier, S., Pol, S., Houeto, J.L., Vidailhet, M., 2000. Abnormal reciprocal inhibition between antagonist muscles in Parkinson's disease. Brain Journal of Neurology 123 (5), 1017–1026.
[37] Olney SJ. Quantitative evaluation of cocontraction of knee and ankle muscles in normal walking. Champaign: Human Kinetics Publishers, 1985.
[38] Franz JR, Kram R. How does age affect leg muscle activity/coactivity during uphill and downhill walking? Gait Posture 2013;37:378–84.
[39] Martino G, Ivanenko YP, d'Avella A, Serrao M, Ranavolo A, Draicchio F, Cappellini G, Casali C, Lacquaniti F. Neuromuscular adjustments of gait associated with unstable conditions. J Neurophysiol. 2015;114(5):2867-82.
[40] Bernstein NA. 1967. The Coordination and Regulation of Movements. Pergamon Press.
[41] Saltiel P, et al. 2001. Muscle synergies encoded within the spinal cord: evidence from focal intraspinal NMDA iontophoresis in the frog. Journal of Neurophysiology, 85(2), p. 605-19
[42] D'Avella A, Saltiel P, Bizzi E. 2003. Combinations of muscle synergies in the construction of a natural motor behavior. Nature Neuroscience, p. 6(3): p. 300-8.
[43] Tresch MC, Cheung V, d'Avella A. 2006. Matrix Factorization Algorithms for the Identification of Muscle Synergies: Evaluation on Simulated and Experimental Data Sets. Journal of Neurophysiology: 95:2199-2212.
[44] Bizzi E, et al. 1995. Modular organization of motor behavior in the frog's spinal cord. Trends in Neuroscience, 18(10), p. 442-6.
[45] D'Avella A, Bizzi E. 1998. Low dimensionality of supraspinally induced force fields. Proceedings of the National Academy of Sciences of the United States of America, 95(13):7711-4.
[46] Berger DJ, Gentner R, Edmunds T, Pai DK, d'Avella A. 2013. Differences in adaptation rates after virtual surgeries provide direct evidence for modularity. Journal of Neuroscience, 33(30):12384-94.
[47] Ivanenko YP, Grasso R, Zago M, Molinari M, Scivoletto G, Castellano V, Macellari V, Lacquaniti F. 2003. Temporal components of the motor patterns expressed by the human spinal cord reflect foot kinematics. Journal of Neurophysiology, 90: 3555-3565.
[48] Ivanenko YP, Poppele RE e Lacquaniti F. 2004. Five basic muscle activation patterns account for muscle activity during human locomotion. Journal of Physiology, 556 (Pt 1), p. 267-82.
[49] Ivanenko YP, et al. 2005. Coordination of locomotion with voluntary movements in humans. Journal of Neuroscience, 25(31), p. 7238-53.
[50] Ivanenko YP, Poppele RE, Lacquaniti, F. 2006. Spinal cord maps of spatiotemporal alpha-motoneuron activation in humans walking at different speeds. Journal of Neurophysiology, 95(2), p. 602-18.
[51] Ivanenko YP, et al. 2008. Spatiotemporal organization of alpha-motoneuron activity in the human spinal cord during different gaits and gait transitions. European Journal of Neuroscience, 27(12), p. 3351-68.

[52] Kautz SA, Bowden MG, Clark DJ, Neptune RR. 2011. Comparison of motor control deficits during treadmill and overground walking poststroke. Neurorehabilitation and Neural Repair, 25(8):756-65.

[53] Cheung VC, et al. 2009. Stability of muscle synergies for voluntary actions after cortical stroke in humans. Proceedings of the National Academy of Sciences of the United States of America, 106(46), p. 195638.

[54] Clark DJ, Ting LH, Zajac FE, Neptune RR, Kautz SA. 2010. Merging of healthy motor modules predicts reduced locomotor performance and muscle coordination complexity post-stroke. Journal of Neurophysiology, 103(2):844-57.

[55] Martino G, Ivanenko YP, Serrao M, Ranavolo A, d'Avella A, Draicchio F, Conte C, Casali C, Lacquaniti F. 2014. Locomotor patterns in cerebellar ataxia. Journal of Neurophysiology, 112:2810-2821.

[56] Lee DD, Seung HS. 2001. Algorithms for non-negative matrix factorization. Neural Information Processing Systems, 13, p. 556-562.

CHAPTER 4

4. GAIT ANALYSIS IN NEUROLOGICAL DISORDERS

4.1 Characterization of investigated pathologies

Gait analysis, which allows evaluating kinematic variables, dynamics or muscle activity, provides very important information especially when it is applied to individuals with pathologies. In fact, the study of postural and motor alteration in patients with pathologies associated with movement alterations allows to know the level of functional limitation consequent to the pathology and its evolution over time and can provide useful elements to define an appropriate rehabilitative strategy.

The characterization of motor activity in the pathological population is important in order to identify effective rehabilitative programs. In particular, walking disorders are one of the first symptoms for these patients. It has been shown that the breakdown of the functional balance between the various circuits is the cause of extrapyramidal motor disorders. It follows, for example, that the first symptoms of patients suffering from Parkinson's disease are shown by a shorter and more crawled locomotion, with a decrease in the angular movements of the joints [1]. A progressive loss of muscle coordination has been found in diseases affected by a deficit in the cerebellum, such as cerebellar ataxia, which therefore makes it difficult to perform voluntary movements [2]. Injuries at the level of the pyramidal system, on the other hand, result in a progressive spasticity in the lower limbs, as occurs in hereditary spastic paraparesis [3-5]. For all these reasons, a complete characterization of the locomotion of such patients could be a useful tool for identifying the motor strategies put in place in order to guarantee stability and ensure progression.

4.1.1 Hereditary Spastic Paraparesis

Hereditary spastic paraparesis is a heterogeneous group of inherited neurodegenerative disorders characterized by retrograde degeneration of the corticospinal axonal fibers [6]. Lower limb spasticity, usually more prominent than muscle weakness, is the key clinical feature in patients with hereditary spastic paraparesis [7] and impairs walking ability, autonomy, and quality of life [8,9]. No treatment is known to reduce disease progression, but antispastic drugs and physiotherapy [10–13] may help reduce the functional impairment of gait. Quantifying and typifying the specific gait disorder in hereditary spastic paraparesis is crucial to designing individual pharmacological and rehabilitative treatments. Most descriptions of paraparetic gait are based on qualitative clinical observations [6,7,10]. Some studies have quantitatively evaluated gait impairment in hereditary spastic paraparesis patients, revealing several gait abnormalities of reduced step length, increased step width, reduced range of motion (RoM) at the knee joint [3,4,14], impaired knee torque and stiffness [4,14], and decreased activity of the rectus femoris muscle [4]. Despite the great relevance of such quantitative assessments, they remain generic without reflecting the wide clinical heterogeneity of gait disorders in hereditary spastic paraparesis patients.

Furthermore, clinical experience suggests that spasticity may differentially affect distal and proximal muscles, which in turn can be related to impairments of specific motor pools. Spasticity is a complex feature involving several mechanisms. Central motor lesions lead to alterations in the excitability of spinal reflexes and changes of supraspinal drive [15,16]. Consequently, gradual lesion- and activity-dependent adaptive changes within the higher centres, the spinal cord, and the musculo-tendinous tissues occur, leading to spastic movement disorder. Furthermore, corrupting or removing descending input severely disrupts the functioning of spinal pattern generation circuits and contributes to motor dysfunction in conditions such as cerebral palsy, spinal cord injury and other movement disorders. Since degeneration of corticospinal fibers in HSP affects the state and excitability of the lumbosacral segments innervating lower limb muscles [14], it is important to

consider the impairments in the spinal locomotor output. The locomotor motoneuron activity is the end-product of the interaction between complex supraspinal and spinal circuitries under the influence of sensory feedback [17]. The output of this process can be evaluated by mapping the simultaneous activity from a large number of muscles during walking onto the anatomical rostrocaudal location of the motorneuron pools in the human spinal cord derived from published literature [18]. Thus, a comprehensive treatment of Hereditary Spastic Paraplegia should consider the specific pathophysiological changes in the spinal cord.

In the study *"Gait patterns in patients with hereditary spastic paraparesis"(*M. Rinaldi et al. 2016), which was published on PLoS One, a description of the gait patterns in hereditary spastic paraparesis and with the identification of subgroups of patients according to specific kinematic features of walking was carried out.

Furthermore, in the study *"Differential changes in the spinal segmental locomotor output in Hereditary Spastic Paraplegia"* (2018), which was published by Clinical Neurophysiology, a detailed characterization of the spinal motoneuronal output in HSP during locomotion was reported in order to investigate whether gait impairments in HSP patients are related to changes in the spinal activity.

Patients' subgroups classification

Patients were classified on kinematic behavior during walking. In particular, we chose a z-score equal to the mean ± 1.5 SD of the range of motion (RoM) at the lower limb joints of the control group as the threshold for clustering HSP patients in subgroups. According to this criterion, the joint RoM of each patient could be either reduced (below threshold), increased (above threshold), or not significantly different from the corresponding value of the healthy controls. Thus, three subgroups of patients were identified. Subgroup one consisted of patients with hip joint RoM significantly increased, but ankle and knee joint RoMs not significantly different from the control values. Subgroup two included patients with knee and ankle joint RoMs significantly reduced, but

hip joint RoM not significantly different from the control value. Subgroup three included patients with a statistically significant reduction of RoM at hip, knee, and ankle joints.

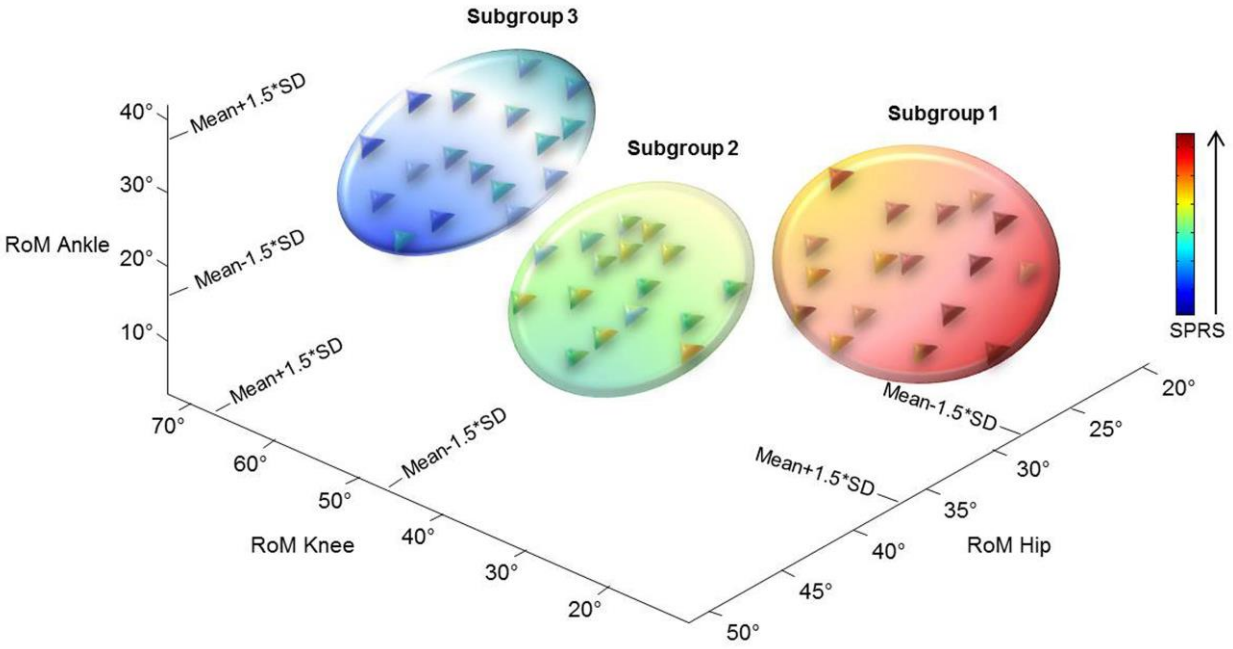

*Figure 4.1. Patients' subgroups classification according to lower limb joint kinematic behavior. The threshold of mean±1.5*SD of the joint RoMs of the control group is reported. Each patient joint RoM could be either reduced (below the threshold), increased (above the threshold) or close to the values of healthy controls. It is possible to note that the subgroups' division corresponds also to the severity of the disease scored by SPRS scale (higher values of SPRS correspond to higher disease's severity). Each triangle represents a patient with different colors according to the SPRS scores. Each circle represents a qualitative characterization of subgroup of patients with different color shades corresponding, in the three spatial dimensions, to the SPRS scores.*

Time-distance parameters

When comparing the whole sample of patients with the healthy participants, no significant differences were found in any time-distance parameters, except for step width and step length, whose values were significantly increased and reduced, respectively, in patients compared with controls. A significant effect of patients' subgroup was found, using one-way ANOVA, on most of the time-distance parameters. Post-hoc analysis revealed significantly higher values of walking speed in subgroup three than in subgroup one, lower stance duration in subgroup three than in subgroup one, higher swing duration in both subgroups two and three than in subgroup one, lower second double support duration in subgroup three than in subgroup one and higher step length in

subgroup three than in both subgroups one and two and in subgroup two than in subgroup one (Fig. 4.1,4.2).

Kinematic parameters

Significant lower values in knee and ankle RoMs and significant higher values in trunk lateral bending, flexion-extension, and rotation RoMs and pelvis rotation RoM were found in patients than in controls. A significant main effect of the subgroup was found, using one-way ANOVA, on hip, knee, ankle, and pelvis tilt RoMs. Post-hoc analysis revealed significant higher values in hip RoM in both subgroups two and three than in subgroup one, higher values of knee RoM in both subgroups two and three than in subgroup one and in subgroup three than in subgroup two, higher values of ankle RoM in subgroup three than in both subgroups one and two, and lower values of pelvis tilt RoM in both subgroups two and three than in subgroup one (Fig. 4.1,4.2).

Kinetic parameters

Significant differences were found only for knee first extensor angular impulse (AI_{1st_Knee}) whose value was higher in patients than controls. A significant effect of the subgroup was found, using one-way ANOVA, on hip flexor angular impulse during the second double support subphase (AI_{1stDS_Hip}). Post-hoc analysis showed lower values of this parameter in subgroup three than subgroup one (Fig. 4.3). No significant difference emerged for hip flexor angular impulse during the second double support subphase (AI_{2ndDS_Hip}); knee first and second extensor angular impulse (AI_{1st_Knee} and AI_{2nd_Knee} respectively) during the stance phase; ankle dorsiflexor angular impulse during the first double support subphase (AI_{1stDS_Ankle}); ankle plantar flexor angular impulse during the mid-stance subphase ($AI_{MidStance\_Ankle}$); ankle plantar flexor angular impulse during the second double support subphase (AI_{2ndDS_Ankle}), and moment of support (MS).

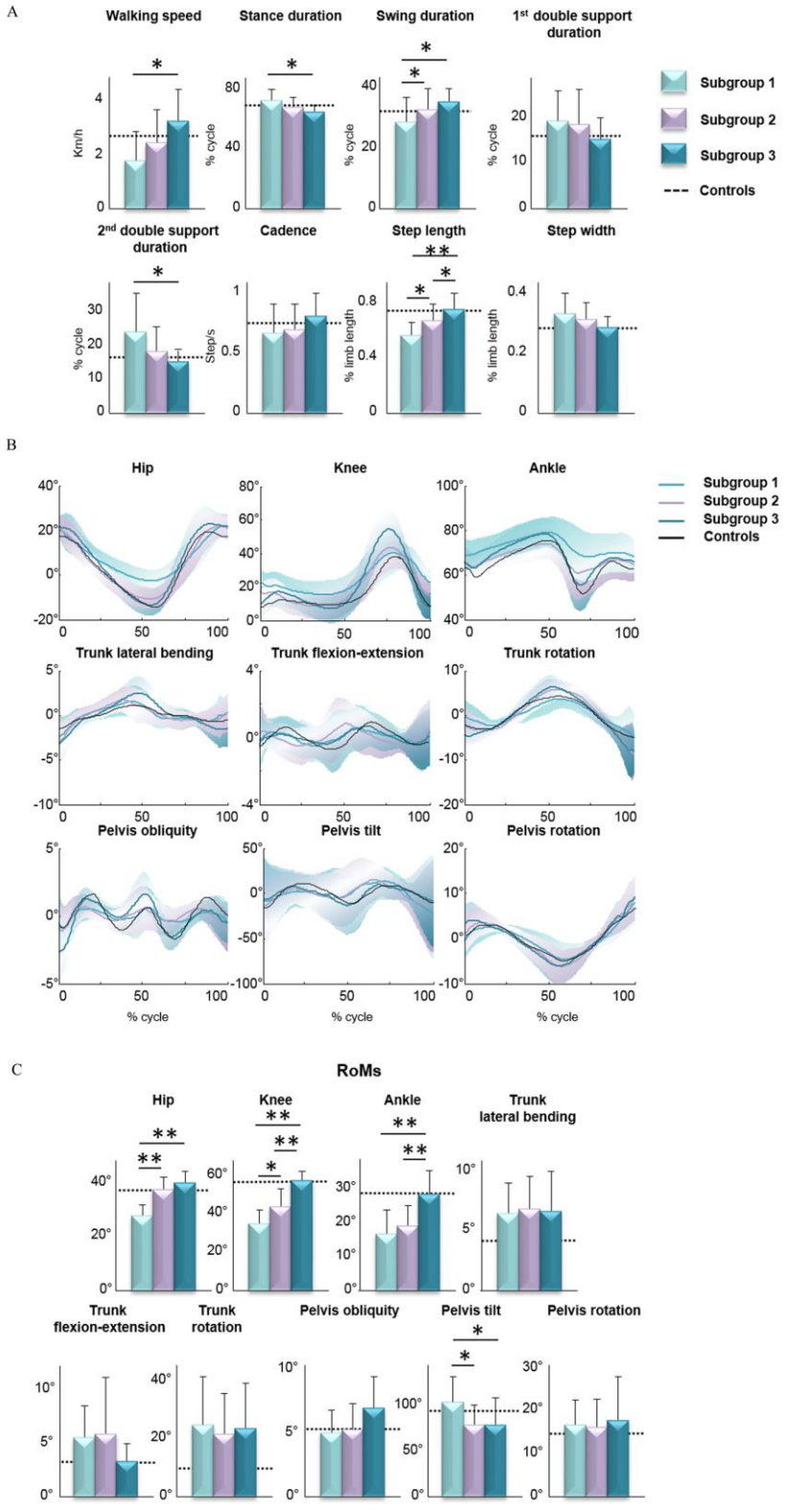

Figure 4.2. Time-distance and joint and trunk kinematic parameters in HSP subgroups.
(A) Mean values (±SD) of time distance parameters. (B) Mean (with SDs in light colors) kinematic plot of joint angular displacements during the gait cycle. (C) Mean values (±SD) of range of angular motion (RoM). Mean values of healthy controls for both time-distance and kinematic parameters, are reported in each bar graph (dotted line) and plot (black line). Asterisks indicate significant differences among the three subgroups at post hoc analysis (* $p<0.05$, ** $p<0.001$).

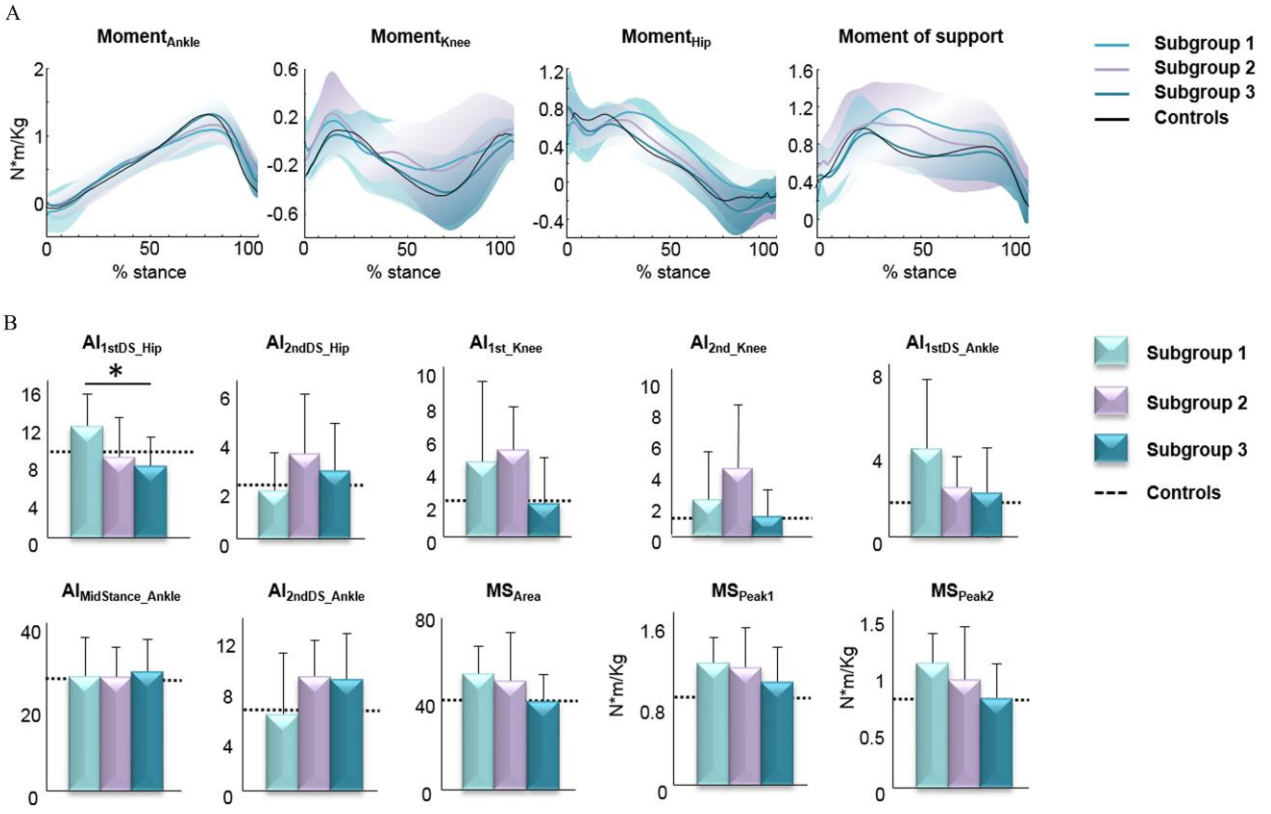

Figure 4.3: Joint kinetic and muscles parameters in HSP subgroups.
(A) Mean (with SDs in light colors) kinetic plot of joint moments (hip, knee and ankle) and support moment. The patterns are normalized to body weight and plotted vs. normalized stance. (B) Mean values (±SD) of kinetic parameters. Mean values of healthy controls for kinetic parameters are reported in each bar graph (dotted line) and plot (black line). Asterisks indicate significant differences among the three subgroups at post hoc analysis ($p<0.05$).*

Intersegmental Coordination.

From the elevation angles, we derived the RoM and the covariation between thigh, shank, and foot segments [19]. Briefly, when these angles are plotted in three dimensions (3D), they describe a path that can be least-squares fitted to a plane over each gait cycle [19] A principal component analysis was applied to the group of three segment elevation angle trajectories to determine covariance loop planarity, width, and orientation. To this end, we computed the covariance matrix of the ensemble of time-varying elevation angles over each gait cycle. The three eigenvectors u_1–u_3, rank-ordered on the basis of the corresponding eigen values, correspond to the orthogonal directions of maximum variance in the sample scatter. The first two eigenvectors u_1 and u_2 lie on the best-fitting plane of

angular covariation, and the third eigenvector (u_3) is the normal to the plane and thus defines the plane orientation. Covariance loop shape was determined using the percent variance (PV_1 and PV_2) explained by the first and second eigenvector u_1 *and* u_2, the greater the value of PV_1 relative to PV_2, the more eccentric (closer to a line segment) is the elliptic loop. The planarity of the trajectories was quantified by the percentage of total variation (PV_3) accounted for by the third eigenvector of the data covariance matrix (for ideal planarity PV_3 = 0%). To quantify the rotation of the plane, we analyzed the u_{3t} parameter (the direction cosine of the normal to the plane with the axis of thigh elevation). For each participant, the parameters of planar covariation (PV_1, PV_2, PV_3 and u_{3t}) were averaged across strides.

Motor output of the spinal segments

To characterize the spatiotemporal organization of the total motor output, the recorded averaged profiles of EMG-activity were mapped onto the rostrocaudal location of MN-pools in the human spinal cord derived from published literature. This approach provides an interpretation of the motor pool activation at a segmental level rather than at the individual muscle level [20] It can be used to characterize the spinal locomotor output by considering relative intensities, spatial extent, and temporal structure of the spinal motor output. Briefly, each muscle is innervated by several spinal segments, and each segment supplies several muscles. To reconstruct the motor-pool output pattern of any given spinal segment of the lumbosacral segments (L2-S2) most active during locomotion, we subdivided each segment into six slices, according to the anatomical data, resulting in 36 subsegments S_j.

In order to compare the general spatiotemporal features of the lumbosacral enlargement activation in different groups of participants, and the relative activation of each segment, we computed the timing of the maximal activation and the $FWHM$ throughout the gait cycle. Even though we recorded a limited set of muscles, we have previously shown that the muscles recorded here are those that contribute mostly to the overall spinal maps [21]. Furthermore, the recorded muscles contribute a large part of the total cross-sectional area of leg muscles [22].

Spinal maps of MN activation

Mapping the EMG activity profiles onto the rostrocaudal location of the MN pools in the lumbosacral enlargement allowed us to reconstruct the spinal maps of MN activation.

Figure 4.4A shows the average segmental MN output over the step cycle and figures 1B and C illustrate the mean timing of max activation and the mean FWHM of the spatiotemporal activation of MNs for each spinal segment in each group.

The prominent feature of these maps in control participants consisted of a distinct activation of lumbar and sacral segments during early and late stance, respectively, as previously seen in other studies. In contrast, despite inter-individual variability (see individual spinal maps, Fig. 4.5), in HSP patients the activity timings in lumbar and sacral segments tend to be quasi-synchronous because of a progressive widening of the activity involving the sacral segments (already present in subgroup 1) and, in more severe subgroups, the lumbar segments (Fig. 4.4C). As a result, the timing of maximum activity of sacral segments was significantly different in subgroup 3 with respect to controls in S2, and in subgroup 2 and 3 with respect to controls and subgroup 1 in S1, while the timing of lumbar segments did not show any significant difference between groups (Fig. 4.4B).

Overall, the spinal maps were characterized by a spread of the loci of activation in HSP, involving initially the sacral segments and, at more severe stages, the lumbar segments (Fig. 4.4).

Correlations between gait parameters, spinal segment characteristics and clinical scores in HSP

Figure 16A illustrates significant correlations between clinical SPRS measures and gait parameters. The following parameters correlated significantly with the SPRS score: walking speed, stride length, ankle RoM, knee RoM. We observed significant relationships between the SPRS score and the FWHM of spinal activation of lumbar segments L2, L3 and L4 (Fig. 4.6B). However, correlating the FWHM of spinal activation with the knee RoM, that was the most sensitive kinematic parameter among those used in the subgroups classification criterion (see Patients' subgroups classification), we found significant values for all segments (Fig. 4.6C).

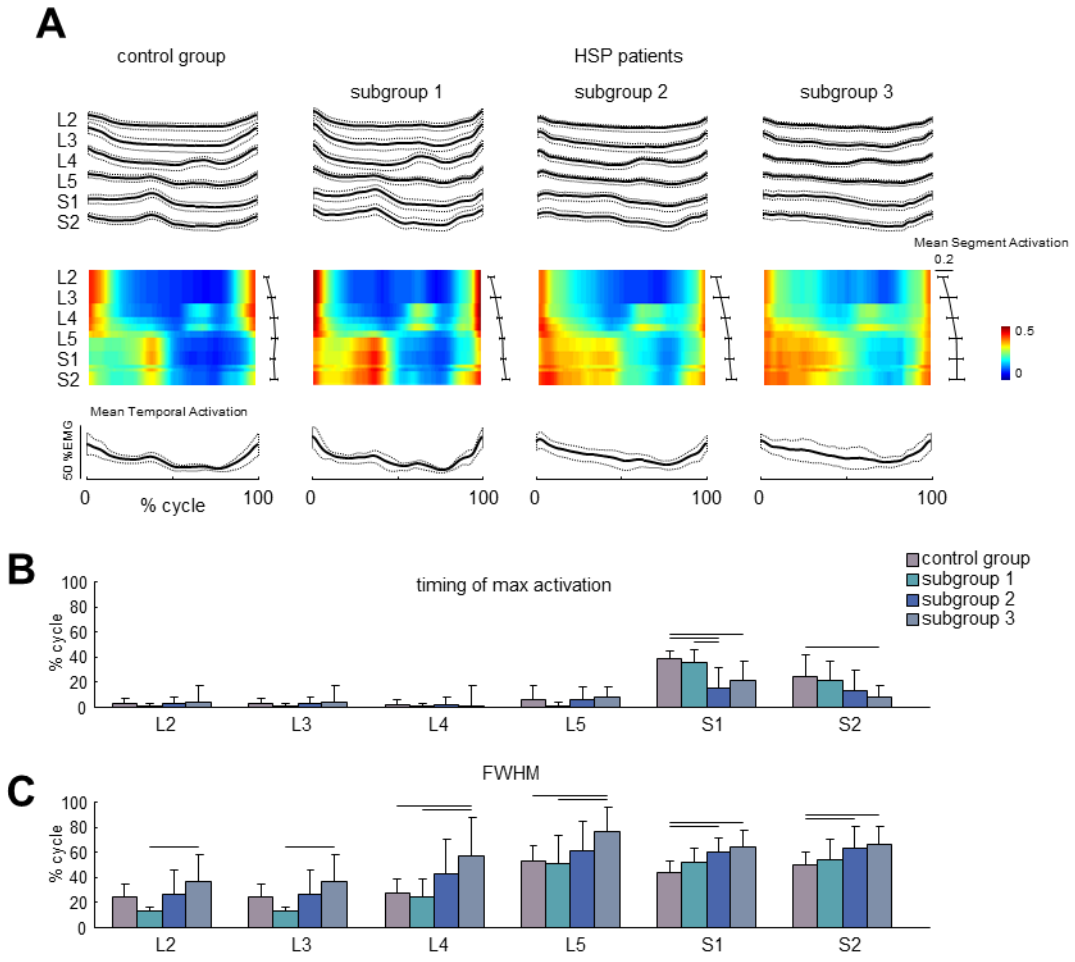

Figure 4.4. Spatiotemporal maps of motoneuron activity of the lumbosacral enlargement in controls and HSP subgroups. A: Output pattern of each segment is shown in the top panels (mean ± SD), while the same pattern is plotted in a color scale at the bottom. Motor output (averaged across participants in each group, reported in percent of maximum segment activation) is plotted as a function of gait cycle and spinal segment level (L2 − S2). Mean temporal activation across all segments (mean ± SD) at the bottom of each spinal map. B: Timing of maximum activation of each segment for each group. The values represent the mean + SD. C: Depicted are mean (+ SD) FWHM of each segment activity. Lines over bars denote significant differences.

Spinal maps revealed a tendency for spreading the main loci of activation, involving initially the sacral segments and, at more severe stages, the lumbar segments. The degeneration of the corticospinal tract in HSP is associated with a widening of spinal locomotor output spreading from caudal to rostral segments. The findings highlight pathophysiologically relevant differential changes in the spinal locomotor output in HSP related to the specific innervation of muscles in the spinal cord, and might be helpful for developing future therapeutic strategies and identifying physiological markers of the disease.

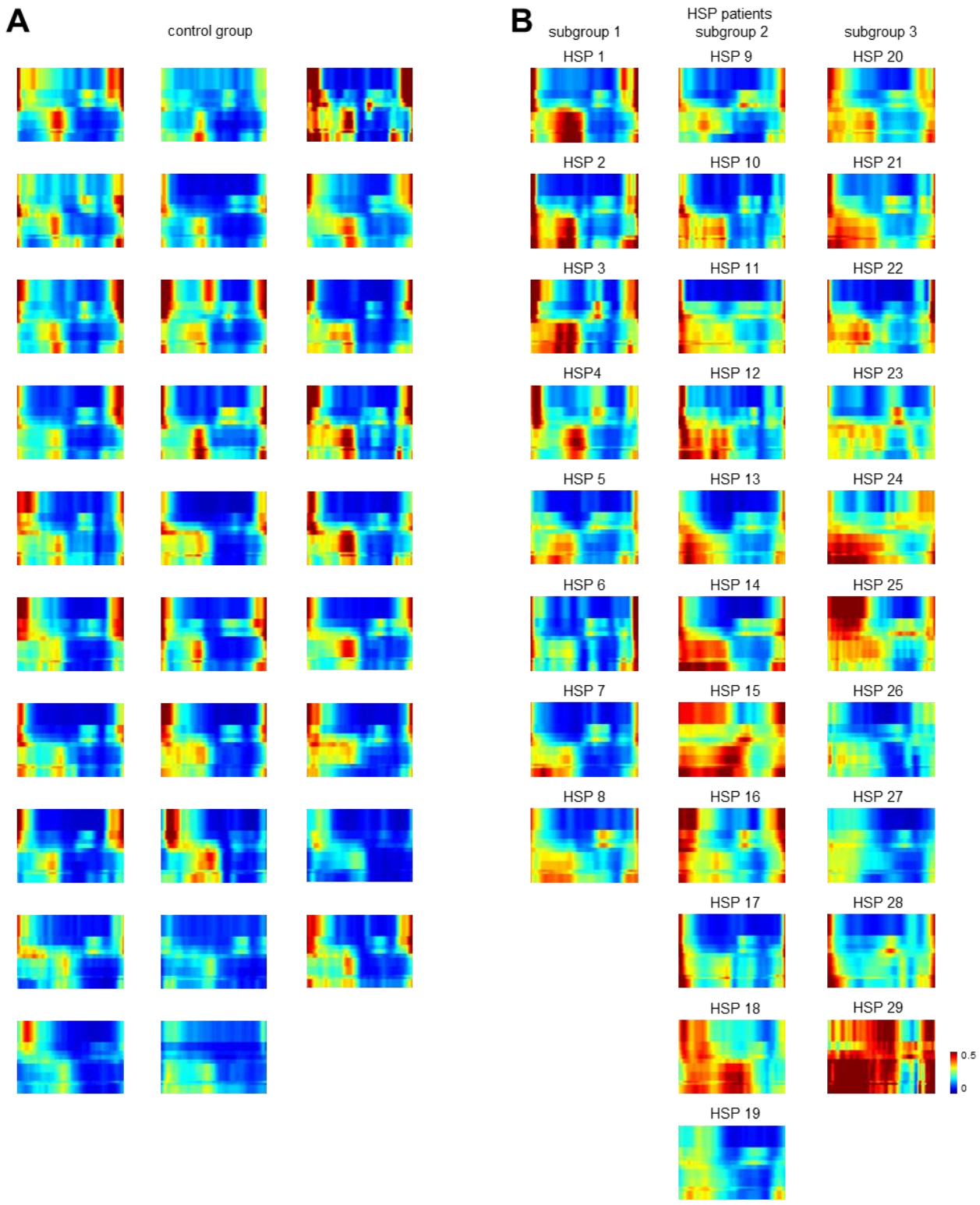

Figure 4.5. Individual spatiotemporal maps of motoneuron activity of the lumbosacral enlargement in HSP patients (ordered by SPRS score). The pattern is plotted in a color scale. Motor output (averaged across strides, reported in units of % of maximum of EMG activity) is plotted as a function of gait cycle and spinal segment level (L2-S2).

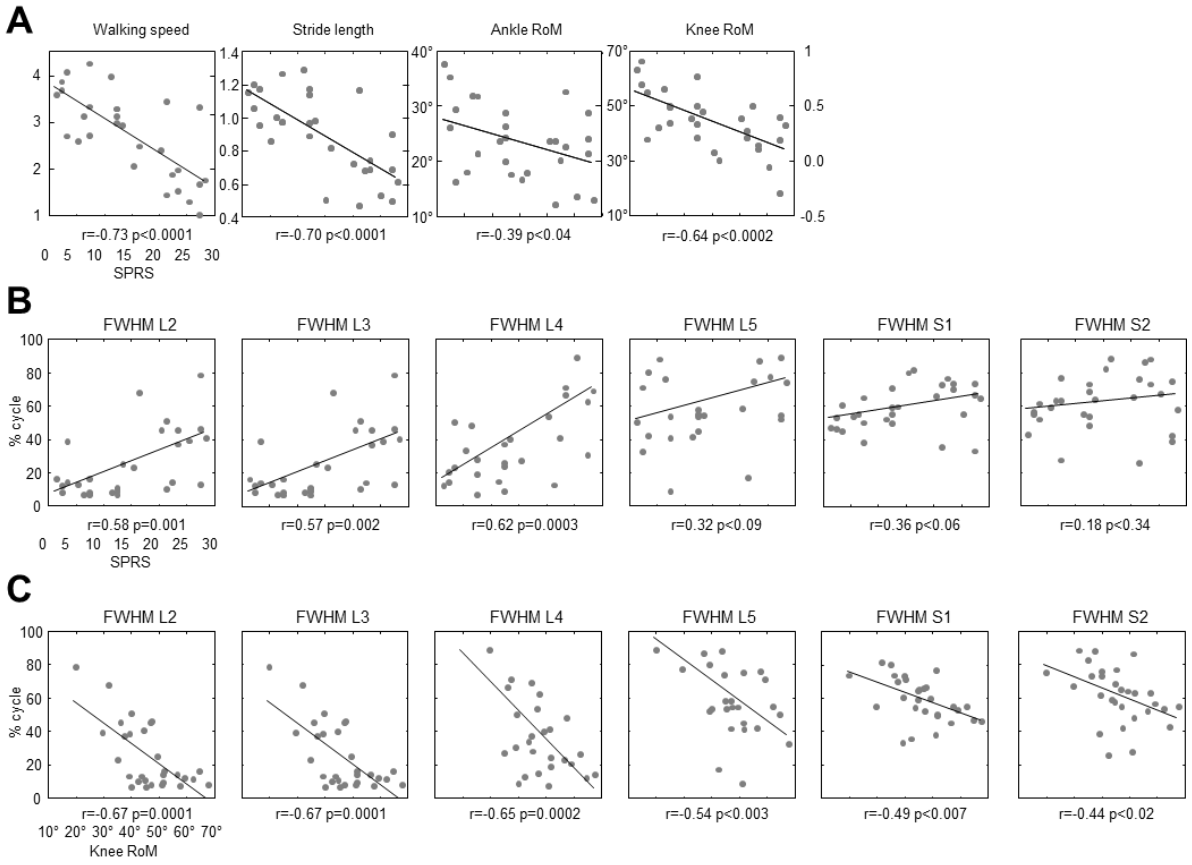

Figure 4.6. Correlations between gait parameters, widening of spinal segment activations and clinical scores. Each point represents the stride-averaged value for the individual patient. Linear regression lines with corresponding r and p values are reported. A: Relationships between walking speed, stride length, ankle and knee RoMs, and SPRS scores. B: mean FWHM of each spinal segment activation vs. SPRS scores. C: mean FWHM of each spinal segment activation vs. knee RoM.

4.1.2 Cerebellar Ataxia

Gait ataxia is a key characteristic of cerebellar disorders and is described as an unstable stumbling walk, with the need for an increased base of support [23,24]. Gait impairment greatly impacts a person's autonomy and daily life activities and significantly increases the risk of falls [25,26]. Recently, modern motion analysis systems have been used to quantitatively characterize the nature and degree of walking dysfunction in patients affected by cerebellar ataxias. Several abnormalities in spatio-temporal parameters, joint kinematics and kinetics, muscle activation patterns, and upper body control together with increased variability in global and segmental gait parameters have been observed [27,28]. Almost all the previous studies on ataxic patients were transversal studies, and

therefore little information is available on the progression of gait impairment in these patients. It is well-known that patients with degenerative cerebellar ataxias, e.g., spinocerebellar ataxias, show a progressive course [29-30]. Consequently, the patient's walking ability is expected to gradually decline over time. As walking is an essential function in everyday life, the longitudinal assessment of gait is critical to measure the actual progression of gait impairment, to determine if differences in the progression of gait impairment exist for different ataxic disorders and to identify which gait parameters are more sensitive to gait decline.

The assessment of the extent and progression of gait impairment at the 2- and 4-year follow-up evaluations in a group of patients with degenerative cerebellar ataxias were performed in the study published on Cerebellum *"Progression of Gait Ataxia in Patients with Degenerative Cerebellar Disorders: a 4-Year Follow-Up Study"* (2016) in order to compare the obtained data with disease severity, and to compare gait decline among subgroups of patients with different clinical forms of cerebellar ataxia.

We carried out a prospective longitudinal gait analysis study With 12 patients with degenerative cerebellar ataxias; recordings were done in our Motion Analysis LAB (Policlinico Italia, Rome, Italy). Gait analysis was performed with the use of an optoelectronic motion analysis system (SMART-DX 500 System, BTS, Milan, Italy). The scale for the assessment and rating of ataxia (SARA) was used to rate disease severity [31].

Time was found to have a significant effect on the SARA Scores. Post hoc analysis revealed significantly higher values at 2 and 4 years than at the baseline (Fig. 4.7). In particular, the SARA total score increased by 3.65 ± 1.92 points at the 2-year and 5.29 ± 3.23 points at the 4-year follow-up as compared to the baseline. No significant effect of group and time × group interaction were found on the SARA scores. Fisher's test showed significant differences in frequency distribution between groups across the time evaluations. Particularly, independent patients were 10 out of 12 (83.3%) at the baseline, 8 out of 12 (66.6%) at the 2-year follow-up, and 5 out of 12 (41.6%) at the

4-year follow-up, whereas dependent patients were 2 out of 12 (17.7%) at the baseline, 4 out of 12 (33.4%) at the 2- year follow-up, and 7 out of 12 (58.4%) at the 4-year follow-up. Changes in gait variables over the 2- and 4-year follow-up evaluations are reported in Fig. 4.7. Time was found to have a significant effect on step length; hip, knee, ankle joint, and trunk rotation RoM; and on the stride-to-stride duration and step length CV values.

Post hoc analysis revealed significantly lower step length and hip joint RoM values at the 4-year follow-up than at the baseline and 2-year follow-up, lower knee joint RoM values at the 4-year follow-up than at the 2-year follow-up, and lesser ankle joint RoM at the 4-year follow-up than at the baseline (Fig. 4.7). Figure 4.7 shows hip, knee, and ankle joint angles at the baseline, 2-year follow-up, and 4-year follow-up. Significantly higher CV values for left step length and left hip flexion–extension were found at the 4-year follow-up than at the 2-year follow-up (Fig. 4.7,4.8).

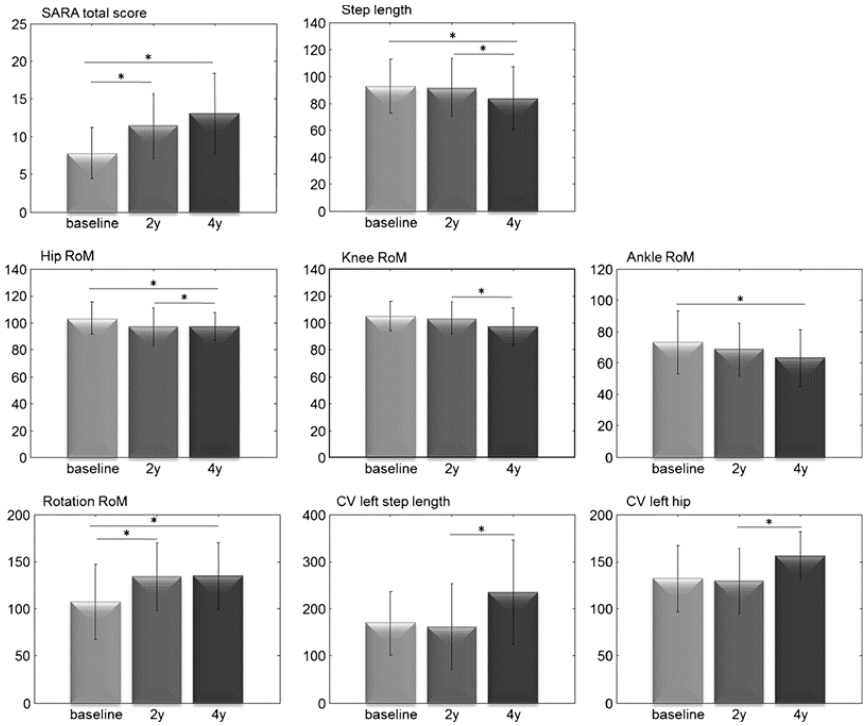

Figure 4.7. The time–distance parameters, trunk and lower limb joint kinematics, and coefficients of variation at the baseline and at the 2- and 4-year follow-up evaluations. The mean and standard deviation values of 12 patients are presented. All the values are expressed as a percentage of the mean values recorded for the group of healthy subjects. The asterisks denote significant differences

A significant effect of group was found on the ankle joint RoM. Post hoc analysis revealed reduced ankle joint RoM in SCA patients as compared to SAOA patients. Time × group interaction was not found to have a significant effect on gait parameters.

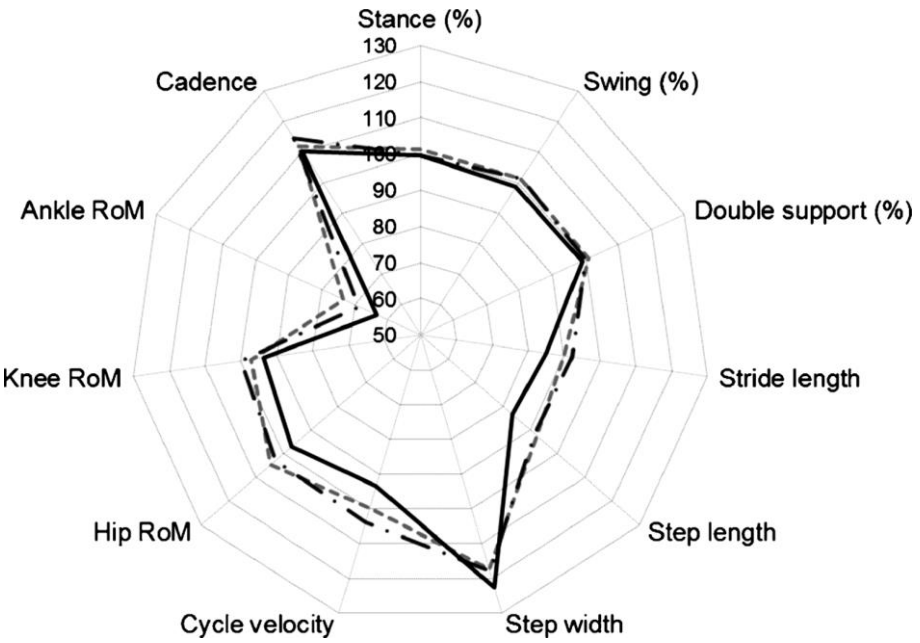

Figure 4.8. Radar plot illustrating the pattern of the time–distance parameters at the baseline (dotted light grey line), at 2-year follow-up (middle grey line), and at 4-year follow-up (continuous, darkest grey line). The mean and standard deviation values of the 12 patients are presented. All the values are expressed as a percentage of the mean values recorded for the group of healthy subjects

4.1.3 Parkinson's disease

Patients with Parkinson's disease show a gait disturbance which is considered as one of the most disabling aspect of the disease that strongly impacts on patients' autonomy and quality of life. The mechanism underlying gait impairment is multi-factorial, reflects the global motor impairment of patients with PD and is mainly related to a neurotransmitter deficiency inducing bradykinesia, rigidity, abnormal trunk control and postural instability. For this reason, and considering the impact of social and economic costs, one of the main foci of intervention in patients with PD should be

treating gait abnormalities. This need is further reinforced by the knowledge that gait outcomes are correlated with longevity, cognitive decline and adverse events.

Besides the shorten-step gait clinical description of the gait disorder in PD, in the last years, studies using modern 3D motion analysis systems have further detailed the gait pattern in PD disclosing abnormalities in cadence, stance duration, swing duration, double support duration, leg length, step length, velocity, hip, knee and ankle ROMs. Such abnormal gait parameters seem to correlate with the clinical outcomes of UPDRS score, H-Y stage and milliequivalents of levodopa taken. Importantly, gait parameters can either normalize or improve after several rehabilitative treatment strategies including physiotherapy, assistive equipment, sensory cueing, treadmill training, physical activity, home base exercises. However, none of the previous studies specifically investigated which biomechanical factor can be modified after rehabilitation and which clinical characteristic can predict the rehabilitation-induced gait improvement. This would be extremely important to typifying, grouping and selecting patients, optimizing the rehabilitative strategies and cost management.

The aims of the study *"Predictors of gait improvement in patients with Parkinson's disease after rehabilitation"* presented at 48° CONGRESSO SIN 2017 were to evaluate in a sample of patients with PD: i) which gait parameters can be modified after a short-term rehabilitation program; ii) which, if any, clinical variable can predict the improvement of the gait function after rehabilitation.

Furthermore, in the work *"Artificial neural networks for staging the gait deficit in Parkinson disease"* presented at SIAMOC 2019, I developed a diagnostic algorithm based on machine-learning technique (i.e. Artificial Neural Networks (ANNs)) able to automatically classify the gait deficit according to the disease severity staging.

Seventy-six patients with PD were enrolled for the study (age, 69.68±8.92 years). The severity of PD was evaluated using the Hoehn and Yahr (H&Y) staging system [32] (H&Y=1: 20; H&Y=2: 17;

H&Y=3:27; H&Y=4:12). Patients were asked to walk barefoot at comfortable self-selected speeds along a walkway with twenty-two reflective spherical markers attached on the anatomical landmarks, in accordance with a validated biomechanical model [33]. Time-distance, joint and trunk kinematics (range of motion, RoM) were recorded using an optoelectronic motion analysis system. An ANNs approach based on Levenberg-Marquardt back-propagation algorithm [34], was used to estimate staging of the gait deficit in Parkinson disease in terms of H&Y scale starting with time-distance and kinematic features used in different combinations (see Fig. 4.9). Different topologies of networks with different numbers of hidden layers and different numbers of neurons (Fig. 1) were trained. For each trained network, a confusion matrix was calculated based on the real H&Y value and the one estimated on the randomly extracted testing set. The mean 4 × 4 confusion matrix was then obtained by averaging the confusion matrixes of the trained ANNs. A performance parameter (P) was calculated as the mean (%) of the elements on the diagonal of the mean confusion matrix, where 100% indicates the absence of misclassifications.

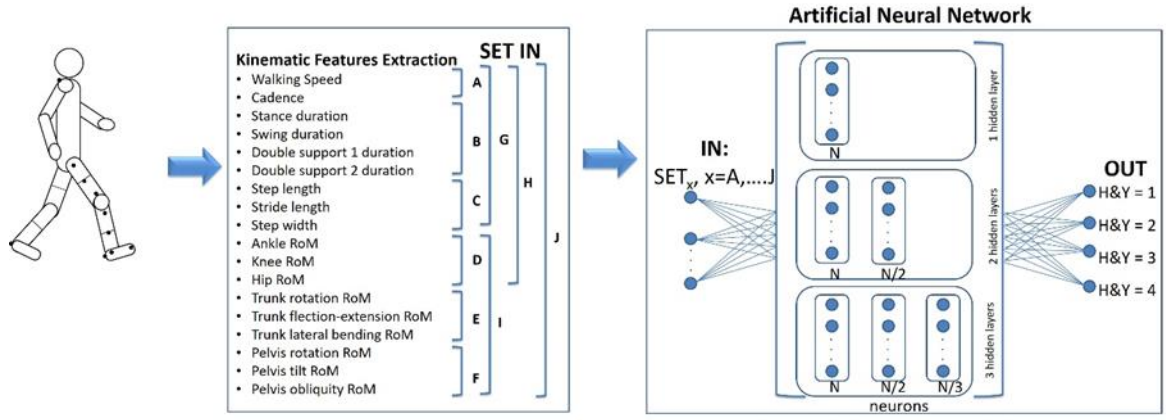

Figure 4.9. A schematic description of experimental set-up and methodological approach based on ANNs method used to map time-distance and kinematic features on the H&Y levels.

Three-way ANOVA showed significant effects of multiple factors on the performances considering training set, numbers of hidden layers and numbers of neurons.

The best performance was obtained with SETG, 3 hidden layers and 20 neurons on first layer (P = 88.82% ± 5.58%), while the worst performance was obtained with SETB, 2 hidden layers and 20 neurons on first layer (P = 55.02% ± 27.31%).

ANNs, that recently have been used as diagnostic tool in several clinical conditions, could be used with gait analysis to identify the severity of gait deficit in PD. Indeed, a diagnostic algorithm based on ANNs technique can automatically classify the gait deficit according to the disease progression.

4.1.4 Duchenne Muscular Dystrophy

Duchenne muscular dystrophy (DMD) is an X-linked muscle disease caused by a deficiency of a protein, dystrophin, which is responsible for supporting muscle fiber strength. DMD has an inherited origin in two thirds of cases while for the remaining one it is linked to a genetic mutation. It is characterised by a progressive muscular weakness that can compromise ambulatory status and cardiopulmonary function. The prevalence rate for DMD is around 63 per million and it affects children in the first years of life. It is generally diagnosed between the age of 3/4 years by physician observations, and it is confirmed through genetic tests [35,36]. Muscle weakness is more proximal than distal, it usually affects lower limbs more often than upper limbs, and it shows up more often on extensor muscles than in flexor ones [37].

When DMD strikes very young individuals, motor, cognitive and language functions result poorer as compared to age-matched unaffected children. Furthermore, boys with DMD have clear difficulties in running and climbing and descending stairs [38]. Muscle weakness is a major determinant of the gait impairments in patients with DMD, followed by muscle and tendon retractions and joint deformities. The compensatory movements to maintain the motor function are needed through the selection of possible synergic movements at the hip, knee and ankle levels [39]. Biomechanical adaptations explain how children with DMD can walk for some period despite limited muscle strength [40,41].

Nowadays the only accessible cure involves the use of cortical-steroids, which are capable to slow down the course of the disease, and to prolong the walking autonomy time. The goal in children with DMD is to keep them ambulant as long as possible, aiming to postpone spinal deformities and muscle contractures [42]. One important aspect, in this scenario, is thus to delineate the mechanisms associated with abnormal gait patterns. Walking ability in DMD is generally evaluated by means of the six-minute walking test (6MWT) [43], which is usually able to assess walking endurance and aerobic capacity. Being an overall measure of functional capacity, it does not directly allow for a detailed analysis of neuromuscular and biomechanical determinants of walking function.

Kinematics and kinetics extracted from gait data on convenience samples of children with DMD report that they usually modify their trunk and lower limb position during the stance phase; higher hip flexion is evidenced, as the result of a reduced muscular strength for hip and knee muscle extensors (i.e. gluteus maximus and quadriceps). Furthermore, to maintain the pelvic stability and alignment, DMD patients exploit hip flexion and abduction to compensate for an increased ankle plantar-flexion [40]. The observed shortening of the plantar flexor muscles (i.e. Soleus and Gastrocnemius) then leads to a more prominent lumbar curve during the years [44].

The progression of the disease causes a decrease on walking parameters, such as gait cadence and speed, a reduction of the step length, and a concurrent increase of the base of support (step width) to maintain balance. Despite these compensating mechanisms, further disease progression makes most children become wheelchair-dependent when they are about 12 years old [40].

4.2 Comparison of gait features among patients

4.2.1 Gait patterns

Patients with degenerative neurological diseases such as cerebellar ataxia, spastic paraplegia, and Parkinson’s disease often display progressive gait function decline that inexorably impacts their

autonomy and quality of life. Therefore, considering the related social and economic costs, one of the most important areas of intervention in neurorehabilitation should be the treatment of gait abnormalities. Patients affected by three different types of primary degenerative neurological diseases were studied in the work *"Identification of specific gait patterns in patients with Cerebellar Ataxia, Spastic Paraplegia, and Parkinson's disease: a non-hierarchical cluster analysis"*, published from Human Movement Sciences (2017) with the aim to determine whether an entire dataset of gait parameters recorded in patients with degenerative neurological diseases can be clustered into homogeneous groups distinct from each other and from healthy subjects. These diseases were: i) cerebellar ataxia (28 patients), ii) hereditary spastic paraplegia (31 patients), and iii) Parkinson's disease (70 patients). Sixty-five gender-age-matched healthy subjects were enrolled as a control group. An optoelectronic motion analysis system was used to measure time-distance parameters and lower limb joint kinematics during gait in both patients and healthy controls.

When clustering single parameters, step width and ankle joint range of motion (RoM) in the sagittal plane differentiated cerebellar ataxia group from the other groups. When clustering sets of two, three, or four parameters, several pairs, triples, and quadruples of clusters differentiated the cerebellar ataxia group from the other groups. Interestingly, the ankle joint RoM parameter was present in 100% of the clusters and the step width in approximately 50% of clusters. In addition, in almost all clusters, patients with cerebellar ataxia showed the lowest ankle joint RoM and the largest step width values compared to healthy controls, patients with hereditary spastic paraplegia, and Parkinson's disease subjects.

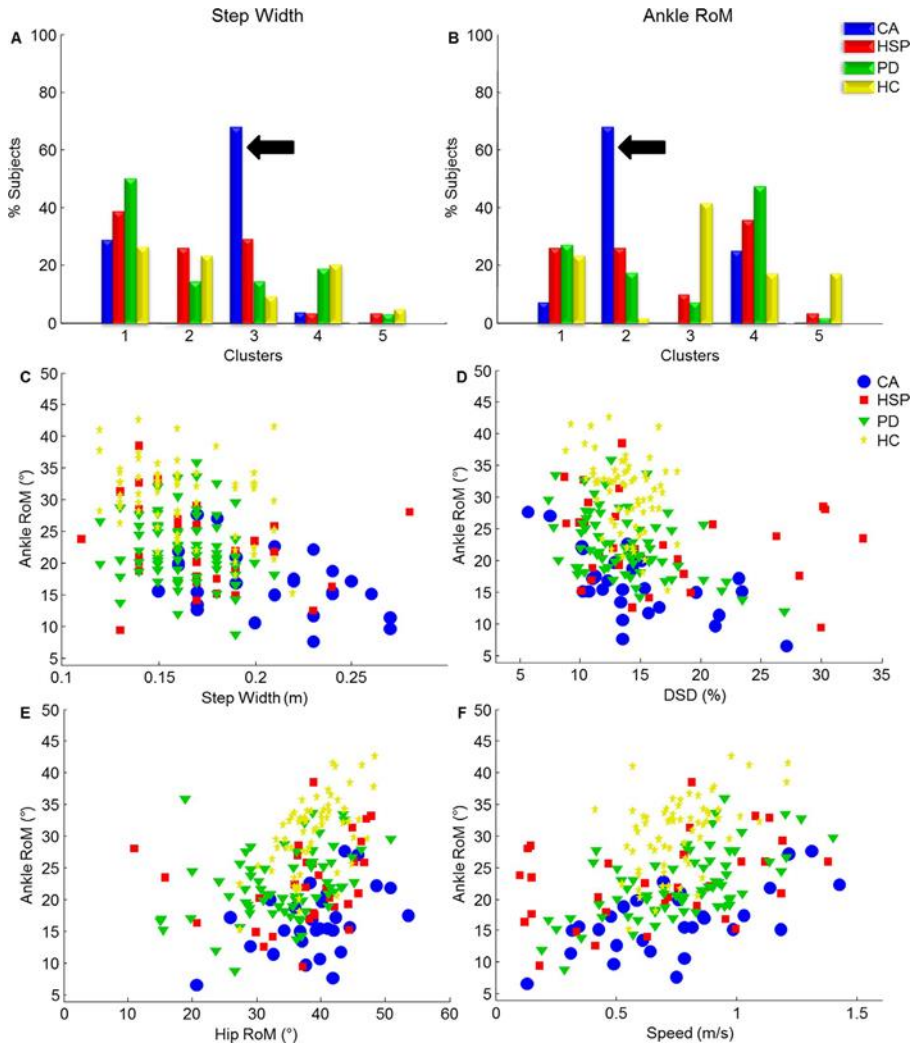

Figure 4.10. Bar heights in panel A and B represent the percentage of CA, HSP, PD patients and control subjects clustered by step width and ankle joint RoM, respectively.The horizontal black arrows point towards the bar relative to CA patients who show the highest rate compared to both HSP and PD in clusters 3 and 2, respectively. Panels C, D, E and F. In these panels, the ankle joint RoM values respect to step width (m), double support duration (DSD,%), hip joint RoM (°) and speed (m/s) values of the CA (dots), HSP (rectangles), PD (triangles) patients and healthy controls (asterisks), inside each of these clusters, are represented.

This study identified several clusters reflecting specific gait patterns in patients with degenerative neurological diseases. In particular, the specific gait pattern formed by the increased step width, reduced ankle joint RoM, and increased gait variability, can differentiate patients with cerebellar ataxia from healthy subjects and patients with spastic paraplegia or Parkinson's disease. These abnormal parameters may be adopted as sensitive tools for evaluating the effect of pharmacological and rehabilitative treatments.

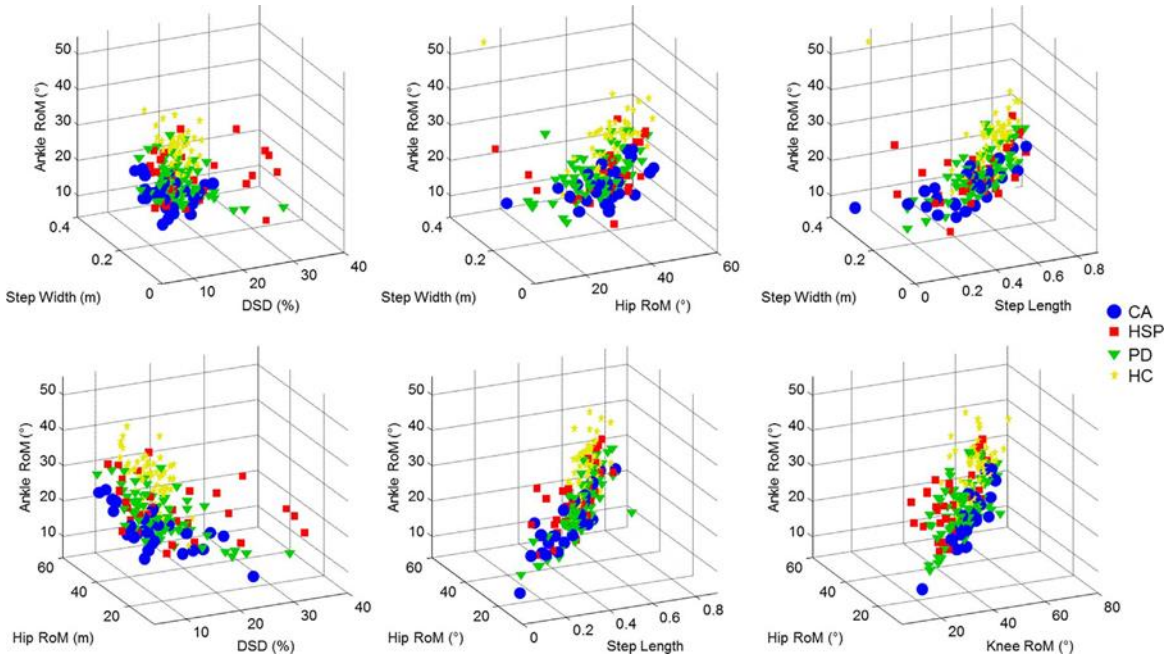

Figure 4.11. Panel A: in this 3D plot, the ankle joint RoM values respect to step width (m) and double support duration (DSD, %) values of the CA (dots), HSP (rectangles), PD (triangles) patients and healthy controls (asterisks), inside the cluster, are reported. Panel B: this 3D plot represents the ankle joint RoM values respect to step width (m) and hip joint RoM (°) values of the CA (dots), HSP (rectangles), PD (triangles) patients and healthy controls (asterisks) inside the cluster. Panel C: this 3D plot illustrates the ankle joint RoM values respect to step width (m) and normalized step length values of the of the CA (dots), HSP (rectangles), PD (triangles) patients and healthy controls (asterisks) inside the cluster. Panel D: in this 3D plot the ankle joint RoM values respect to the hip joint RoM (°) and double support duration (DSD, %) of the CA (dots), HSP (rectangles), PD (triangles) patients and healthy controls (asterisks) inside the cluster are reported. Panel E: in this 3D graph, the ankle joint RoM (°) values respect to the hip joint RoM and normalized step length values of the CA (dots), HSP (rectangles), PD (triangles) patients and healthy controls (asterisks) inside the cluster are represented. Panel F: this 3D plot illustrates the ankle joint RoM values (°) with respect to the hip joint RoM (°) and knee joint RoM (°) values of the CA (dots), HSP (rectangles), PD (triangles) patients and healthy controls (asterisks) inside the cluster.

<u>*Clustering findings and group comparisons*</u>

Figs. 4.10-4.12 represent clusters as either single parameters or a set of parameters (couples, triples, and quadruples).

Single parameters

Among the gait parameters, step width and ankle joint RoM partitioned in cluster 3 and 2, respectively, showed both a good accuracy in detecting CA patients, who showed the highest rate compared to both HSP and PD (Fig. 20, panels A and B). In cluster 3, a significant group was found on step width, while in cluster 2 no significant effect was found on ankle joint RoM. Post-hoc

analysis revealed highest values of step width in CA compared to both PD and HC. We found significant higher SARA scores in patients inside the cluster 2 than those outside the cluster 2.

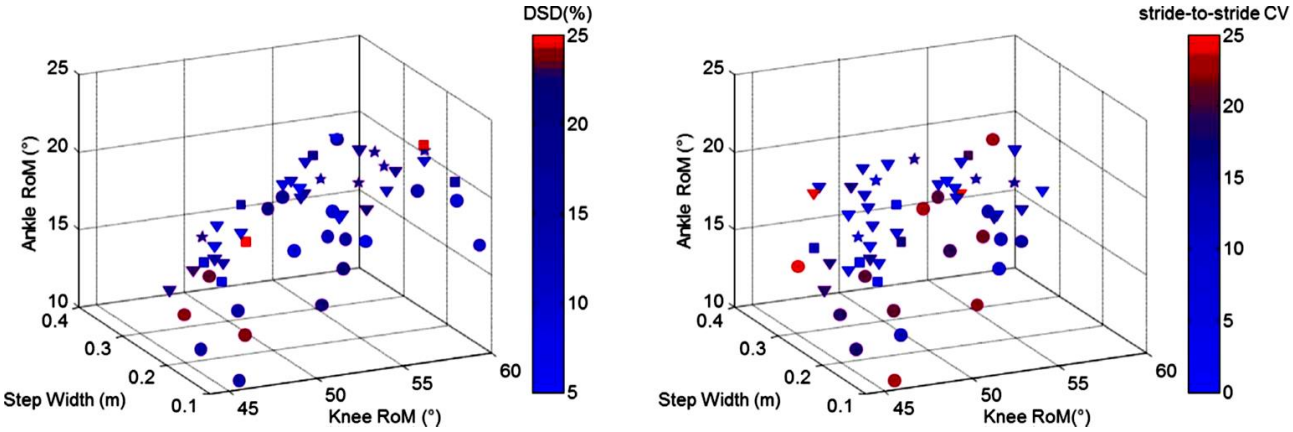

Figure 4.12. Panel A: this figure illustrates the ankle joint RoM values (°) with respect to step width (m) and knee joint RoM (°) values of the CA (dots), HSP (rectangles), PD (triangles) patients and healthy controls (asterisks) inside the cluster. Each symbols color shade (from blue to red for higher values) is proportional to the corresponding subject's double support duration (DSD, %). Panel B: this figure illustrates the ankle joint RoM values (°) respect to step width (m) and knee joint RoM (°) values of the CA (dots), HSP (rectangles), PD (triangles) patients and healthy controls (asterisks) inside the cluster. Each symbols color shade (from blue to red for higher values) is proportional to the corresponding subject's stride-to-stride CV value.

Pairs of parameters

The following pairs, step width/ankle RoM, DSD/ankle RoM, hip RoM/ankle RoM, and gait speed/ankle RoM, partitioned in clusters 2,5,4, and 1, respectively, had good accuracy in detecting CA, which showed the highest rate compared to both HSP and PD (Fig. 4.10, panels C-F). In each of the four clusters, a significant effect of group was found on step width (cluster 2), ankle joint RoM (clusters 4 and 5), and hip RoM (cluster 4), while no significant differences were observed for the other variables. Post-hoc analysis revealed significantly high values of step width (cluster 2) and hip RoM (cluster 4) compared to PD, and the lowest values of ankle RoM in CA compared to both PD and HC (clusters 4) or PD (cluster 5). Significantly higher SARA scores were found for patients inside clusters 2 and 1 than for those outside these clusters.

Triples of parameters

The following triples, step width/ankle RoM/DSD, ankle RoM/step width/step length, DSD/hip RoM/ankle RoM, hip RoM/ankle RoM/step length, hip RoM/ankle RoM/step width, and hip RoM/knee RoM/ankle RoM partitioned in clusters 5a, 3, 4, 5b, 1, and 2, respectively, had good accuracy in detecting CA patients, who showed the highest rate compared to both HSP and PD (Fig. 4.11). In each of the six clusters, a significant effect of group was found on step width (clusters 1 and 5a), ankle RoM (clusters 1, 2, 4, 5a and 5b), and hip RoM (cluster 4). Post-hoc analysis revealed the highest values of step width compared to both PD and HC (cluster 1) or to PD (cluster 5a). It revealed the lowest values of ankle RoM occurred in patients with CA compared to HSP, PD, and HC (cluster 2) or both PD and HC (clusters 4 and 5b) or PD (clusters 1 and 5a). The analysis also revealed higher values of hip RoM compared to PD (cluster 4). SARA scores were found to be significantly higher for patients inside clusters 5a and 3, than for those outside.

Quadruples of parameters

The following quadruples, step width/ankle RoM/Knee RoM/stride-to-stride CV and step width/stride-to-stride CV/ankle RoM/Knee RoM, partitioned in clusters 4 and 3, respectively, had good accuracy in detecting CA patients who showed the highest rate compared to both HSP and PD (Fig. 4.12). In each of the two clusters, a significant effect of group was found on step width (clusters 3 and 4), ankle joint RoM (clusters 3 and 4), stride-to-stride-CV (cluster 3), and DSD (cluster 4). Post-hoc analysis revealed the highest values of step width in CA compared to either HSP, PD, and HC (cluster 3) or HSP and PD (cluster 4), the lowest values of ankle joint RoM compared to HSP, PD, and HC (clusters 3 and 4), the highest values of stride-to-stride CV (cluster 3) compared to PD. No significant differences in SARA scores were found between patients inside the clusters and those outside.

4.2.2 Gait harmony

Harmony is an important feature of physiological human gait warranting for efficient and smoothed movements during walking. Indeed, a recent study discovered an intrinsic fractal frame that is hidden below the orchestrated repetitive structure of physiological gait[45]. Particularly, if a straight line is drawn (the stride), the golden ratio represents the proportion of the whole to the longer part (stride/stance), which is the same as the proportion of the longer part to the shorter one (stance/swing) and it is the same as the proportion of this shorter part to the even shorter one (swing/double support)

In the work *"Gait harmonic structure of walking in patients with neurological gait disorders"* presented at 49° CONGRESSO SIN 2018, gait harmonic structure of walking in patients with neurological gait disorders was investigated with the aim of determining if and how this harmonic structure is altered in these subjects. A total of 192 patients affected by different types neurological diseases (28 with cerebellar ataxia (CA); 49 with hereditary spastic paraparesis, HSP; 23 with hemiparesis, H; 12 with Charcot-Marie-Tooth, CMT; 80 with Parkinson's disease, PD) and 67 healthy controls were included.

The three golden ratios, stride/stance, stance/swing and swing/double support, were evaluated. All the gait ratios of patients were compared with those of the respective control group, matched for gait speed. Higher values of gait ratios are found for subject respect to control groups. Significantly higher values of the three gait ratios are found in CA, HSP and PD; while in CMT second ratio (stance/swing) is significantly higher. While in H the first and third ratios are significantly higher.

Data revealed that patients with neurological gait disorders show abnormal gait ratios which are impaired in a different way depending to the specific disease and the consequent involvement of the biomechanical determinants.

The harmony of the human gait is not limited to an aesthetical and qualitative aspect of walking but seems to reflect the complex relationships among several biomechanical determinants (e.g. energy

consumption, gait speed, and balance control) which are altered in patients with neurological gait disorders [46]. In this light the gait ratio may represent a biomarker of the gait neurological disorders and thus a target to improve gait rehabilitation and management strategies.

4.2.3 Trunk involvement

Despite neurological pathologies have been investigated in literature and significant results have been obtained about lower limb kinematic, the evidence about the role of the trunk during walking has never been investigated.

The trunk comprises over 50% of total body mass and significantly affects whole body dynamics. Although the relevance of spine movements in walking is widely recognised [47], most of the studies on human locomotion almost exclusively deal with kinematics and kinetics of the lower limb joints. Nevertheless, several authors have emphasized the importance of trunk movements in human gait [48, 49]. According to Gracovetsky et al, lumbar spine is a key structure in land locomotion, the pelvis being driven by the spine. This theory of locomotion requires the central nervous system to control the torque at intervertebral joints and suggests that a breakdown of the control system would result in torsional failure of the spine [47].

It is well known that upper body segment minimising the magnitude of linear and angular displacement of the head and trunk has a great functional importance, ensuring clear vision, facilitating the integration of vestibular information, contributing to the maintenance of balance and creating a more energy-efficient gait pattern, driving forces for locomotion [50]. In this light, a biomechanical involvement of the spine might result in an ineffective and energy-consuming locomotion. However, previous studies have reported that trunk and neck play an important role in damping gait-related oscillations to ensure head control is maintained, and they are believed to play an important role in dissipating the transmission of forces from the ground to the head. When the neck and/or trunk were singularly braced, an overall decrease in the ability of the trunk to attenuate

gait-related oscillations was observed, which led to increases in the amplitude of vertical acceleration for all segments. [51].

Several studies have demonstrated that trunk motor control is important during distal limb movement and unpredictable perturbations and is related to functional movements5, balance and performance of motor tasks [52].

Trunk impairment was found to be correlated with balance, and gait; therefore, any intervention that improves trunk performance will facilitate improvement in balance and gait in pathology.

Improved trunk control helps to improve balancing abilities required for standing and walking in stroke patients and it was essential for coordinated limb movements and symmetrical trunk movement during gait in stroke patients [52].

Interestingly, young and highly active people with lower limb amputation appear to maintain a similar trunk and upper body stability during walking as able-bodied individuals [53].

The purpose of the study *"The role of trunk in neurological gait disorders: damper,generator or perturbator?"*, presented at 49° CONGRESSO SIN, 2018 and 49° CONGRESSO SIN and SIAMOC 2019 was to investigate the role of the trunk during gait in healthy subject and thus in patients with pathology. The hypothesis is that trunk movement, especially trunk rotation, is strictly linked to gait performance leading to an active role of the trunk as movement generator. In detail, patients with neurological deficits which not directly involve trunk motion maintain the active role of the trunk as movement generator together with the involvement of pelvis motion. Conversely, patients with whole body deficits may use trunk movement either as a perturbator, increasing its range of motion, either as a damper, decreasing its range of motion.

A total of 192 patients affected by different types neurological diseases (28 with cerebellar ataxia, CA; 49 with hereditary spastic paraparesis, HSP; 23 with hemiparesis, H; 12 with Charcot-Marie-Tooth, CMT; 80 with Parkinson's disease, PD) and 67 healthy controls (HS) were included in the study.

Time-distance, joint and trunk kinematics (range of motion, RoM) and energetic data were recorded using an optoelectronic motion analysis system. All the gait parameters of patients were compared with those of the respective control group, matched for gait speed.

Significantly higher values of the trunk RoM were found in one, two or all the three spatial planes in CA, H, HSP and CMT patients, conversely, significantly lower values were found in PD patients (Fig. 4.13). No significant differences in energetic parameters were found. Significant correlations between trunk rotation and both time distance parameters and RoMs were observed in all patients.

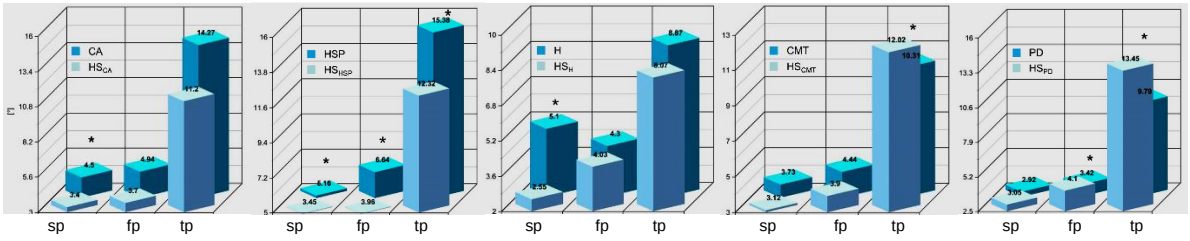

*Figure 4.13. Trunk RoMs in the sagittal (sp), frontal (fp) and transverse (tp) plane for each group of patients. *Significant differences between patients and healthy subjects ($p<0.05$).*

Abnormal trunk movements were present in all patients irrespective to the trunk involvement due to the specific neurological disease. Furthermore, in all patients the trunk movement, i.e. the trunk rotation, was positively correlated with the gait performance parameters (e.g. gait speed, step length, joint RoMs). Overall, our findings suggest that the abnormal trunk movement in neurological patients reflect either a primary deficit or a compensatory mechanism. Particularly, beyond its role as damper, the trunk may be used as generator of movement to improve gait performance in some patients (e.g. in HSP, H and CMT) but not in other (e.g. in PD). Conversely, in CA patients, despite of their efforts to maintain stability, there is a sort of vicious circle that transforms the upper body into a generator of perturbations.

The abnormal trunk control in patients with neurological gait disorders unveils the function of the trunk in human locomotion as damper, generator or perturbator. These findings may help the clinicians to optimize the rehabilitation and management strategies for improving gait function neurological diseases.

Bibliography

[1] Morris ME, et al. 2001. The biomechanics and motor control of gait in Parkinson disease. Clinical Biomechanics, 10:459-470.

[2] Martino G, Ivanenko YP, Serrao M, Ranavolo A, d'Avella A, Draicchio F, Conte C, Casali C, Lacquaniti F. 2014. Locomotor patterns in cerebellar ataxia. Journal of Neurophysiology, 112:2810-2821.

[3] Klebe S, Stolze H, Kopper F, Lorenz D, Wenzelburger R, Volkmann J, Porschke H, Deuschl G. 2004. Gait analysis of sporadic and hereditary spastic paraplegia. Journal of Neurology, 251(5): 571-578.

[4] Marsden J, Ramdharry G, Stevenson V, Thompson A. 2012. Muscle paresis and passive stiffness: key determinants in limiting function in Hereditary and Sporadic Spastic Paraparesis. Gait Posture, 35(2): 266- 271.

[5] Isakov E, Burger H, Krajnik J, Gregoric M, Marincek C. et al. 2001. Knee muscle activity during ambulation of trans- tibial amputee. Journal of Rehabilitation Medicine,33(5):196-199.

[6] Lo Giudice T, Lombardi F, Santorelli FM, Kawarai T, Orlacchio A. Hereditary spastic paraplegia: clinical-genetic characteristics and evolving molecular mechanisms. Exp Neurol. 2014; 261: 518±539. doi:10.1016/j.expneurol.2014.06.011 PMID: 24954637

[7] Faber I, Servelhere KR, Martinez AR, D'Abreu A, Lopes-Cendes I, FrancËa MC Jr. Clinical features andmanagement of hereditary spastic paraplegia. Arq Neuropsiquiatr. 2014; 72(3): 219±226. PMID:24676440

[8] Klimpe S, SchuÈ le R, Kassubek J, Otto S, Kohl Z, Klebe S, et al. Disease severity affects quality of lifeof hereditary spastic paraplegia patients. Eur J Neurol. 2012; 19(1): 168±171. doi: 10.1111/j.1468-1331.2011.03443.x PMID: 21631647

[9] Orsucci D, Petrucci L, Ienco EC, Chico L, Simi P, Fogli A, et al. Hereditary spastic paraparesis in adults. A clinical and genetic perspective from Tuscany. Clin Neurol Neurosurg. 2014; 120: 14±19.doi: 10.1016/j.clineuro.2014.02.002 PMID: 24731568

[10] Fink JK. Hereditary spastic paraplegia. Curr Neurol Neurosci Rep. 2006; 6(1): 65±76. PMID:16469273

[11] Zhang Y, Roxburgh R, Huang L, Parsons J, Davies TC. The effect of hydrotherapy treatment on gait characteristics of hereditary spastic paraparesis patients. Gait Posture. 2014; 39(4): 1074±1079. doi:10.1016/j.gaitpost.2014.01.010 PMID: 24556467

[12] Heetla HW, Halbertsma JP, Dekker R, Staal MJ, van Laar T. Improved gait performance in a patient with hereditary spastic paraplegia after a continuous intrathecal baclofen test infusion and subsequent pump implantation: a case report. Arch Phys Med Rehabil. 2015; 96(6): 1166±1169. doi: 10.1016/j.apmr.2015.01.012 PMID: 25626112

[13] Bertolucci F, Di Martino S, Orsucci D, Ienco EC, Siciliano G, Rossi B, et al. Robotic gait training improves motor skills and quality of life in hereditary spastic paraplegia. NeuroRehabilitation. 2015; 36 (1): 93±99. doi: 10.3233/NRE-141196 PMID: 25547770

[14] Piccinini L, Cimolin V, D'Angelo MG, Turconi AC, Crivellini M, Galli M. 3D gait analysis in patients with hereditary spastic paraparesis and spastic diplegia: a kinematic, kinetic and EMG comparison. Eur J Paediatr Neurol. 2011; 15(2): 138±145. doi: 10.1016/j.ejpn.2010.07.009 PMID: 20829081

[15] Dietz V, Sinkjaer T. Spastic movement disorder: impaired reflex function and altered muscle mechanics. Lancet Neurol. 2007 Aug;6(8):725–33.

[16] Gracies J-M. Pathophysiology of spastic paresis. II: Emergence of muscle overactivity. Muscle Nerve. 2005 May;31(5):552–71.

[17] Lacquaniti F, Ivanenko YP, Zago M. Patterned control of human locomotion. J Physiol (Lond). 2012 May 1;590(Pt 10):2189–99.

[18] Ivanenko YP, Dominici N, Cappellini G, Paolo AD, Giannini C, Poppele RE, et al. Changes in the Spinal Segmental Motor Output for Stepping during Development from Infant to Adult. J Neurosci. 2013 Feb 13;33(7):3025–36.

[19] Borghese, N.A., Bianchi, L., Lacquaniti, F., 1996. Kinematic determinants of human locomotion. Journal of Physiology 494, 863–879.

[20] Yakovenko S, Mushahwar V, VanderHorst V, Holstege G, Prochazka A. Spatiotemporal activation of lumbosacral motoneurons in the locomotor step cycle. J Neurophysiol. 2002 Mar;87(3):1542–53.

[21] La Scaleia V, Ivanenko YP, Zelik KE, Lacquaniti F. Spinal motor outputs during step-to-step transitions of diverse human gaits. Front Hum Neurosci. 2014;8:305.

[22] Ward SR, Eng CM, Smallwood LH, Lieber RL. Are current measurements of lower extremity muscle architecture accurate? Clin Orthop Relat Res. 2009 Apr;467(4):1074–82.
[23] Holmes G. The cerebellum of man. Brain. 1939;62:1–30.
[24] Manto M. The cerebellum, cerebellar disorders, and cerebellar research-two centuries of discoveries. Cerebellum. 2008;7(4): 505–16.
[25] Fonteyn EM, Schmitz-Hubsch T, Verstappen CC, Baliko L, Bloem R, Boesch S, et al. Prospective analysis of falls in dominant ataxias. Eur Neurol. 2013;69:53–7.
[26] Schniepp R,Wuehr M, Schlick C, Huth S, Pradhan C, Dieterich M, et al. Increased gait variability is associated with the history of falls in patients with cerebellar ataxia. J Neurol. 2014;261:213–23.
[27] Serrao M, Pierelli F, Ranavolo A, Draicchio F, Conte C, Don R, et al. Gait pattern in inherited cerebellar ataxias. Cerebellum. 2012;11:194–211.
[28] Bodranghien F, Bastian A, Casali C, Hallett M, Louis ED, Manto M, et al. Consensus paper: revisiting the symptoms and signs of cerebellar syndrome. Cerebellum. 2015;15 (3):369–91.
[29] Pulst SM. Spinocerebellar ataxia type 2. 1998 Oct 23 [updated 2015Nov 12]. In: Pagon RA, Adam MP, Ardinger HH, Wallace SE, Amemiya A, Bean LJH, Bird TD, Fong CT, Mefford HC, Smith RJH, Stephens K, editors. Seattle (WA): University ofWashington, Seattle; 1993–2016
[30] Chini G, Ranavolo A, Draicchio F, Casali C, Conte C, Martino G, et al. Local stability of the trunk in patients with degenerative cerebellar ataxia during walking. Cerebellum. 2016
[31].Schmitz-Hübsch T, du Montcel ST, Baliko L, Berciano J, Boesch S, Depondt C, et al. Scale for the assessment and rating of ataxia: development of a new clinical scale. Neurology. 2006;66:1717–20.
[32] Hoehn MM and M. D. Yahr, Parkinsonism onset, progression, and mortality, Neurology, 1967, vol. 17 (5), pp. 427-427.
[33] Davis III RB et al. A gait analysis data collection and reduction technique. Human Movement Science, 1991, vol. 10, pp. 575–587.
[34] Rumelhart DE et al., Learning internal representations by error propagation. In: Parallel Distributed Processing, 1986, vol. 1. MIT Press, Cambridge, MA, pp. 318-362.
[35] Armand S, Mercier M, Watelain E, Patte K, Pelissier J, Rivier F. Gait & Posture, A comparison of gait in spinal muscular atrophy, type II and Duchenne muscular dystrophy; 2005, 21: 369–378.
[36] Chakkalakal JV, Thompson J, Parks RJ, Asmin BJ. The FASEB Journal, Molecular, cellular, and pharmacological therapies for Duchenne/Becker Muscular Dystrophies, 2005; 19: 880–891.
[37] McDonald CM, Abresch RT, Carter GT, Fowler Jr WM, Johnson ER, Kilmer DD, Sigford BJ. Am J Phys Med Rehabil, Profiles of neuromuscular diseases. Duchenne muscular dystrophy. 1995, 74:S70–92.
[38] Bakker JP, De Groot IJ, Beelen A, Lankhorst GJ. American Journal of Physical Medicine and Rehabilitation, Predictive factors of cessation of ambulation in patients with Duchenne muscular dystrophy, 2002; 81: 906–912.
[39] Martini J, Voos MC, Hukuda ME, Resende MBD, Caromano FA. Arquivos de Neuro-Psiquiatria, Compensatory movements during functional activities in ambulatory children with Duchenne muscular dystrophy, 2014, 72: 5–11.
[40] Gaudreault N, Gravel D, Nadeau S, Desjardins P, Brière A. Clinical Orthopaedics and Related Research, A method to evaluate contractures effects during the gait of children with Duchenne dystrophy, 2007, 456: 51–57.
[41] D'Angelo MG, Berti M, Piccinini L, Romei M, Guglieri M, Bonato S, Degrate A, Turconi AC, Bresolin N. Gait & Posture, Gait pattern in Duchenne muscular dystrophy, 2009, 29: 36–41.
[42] Goudriaan M, Van den Hauwe M, Dekeerle J, Verhelst L, Molenaers G, Goemans N, Desloovere K. Gait & Posture. Gait deviations in Duchenne muscular dystrophy-Part 1. A systematic review, 2018,62:247-261.
[43] McDonald CM, Henricson EK, Han JJ, Abresch RT, Nicorici A, Atkinson L, Elfring GL, Reha A, Miller LL, Musc. Nerve,The 6-minute walk test in Duchenne/Becker muscular dystrophy: longitudinal observations, 2010,42:966–974.
[44]Carvalho EV, Hukuda ME, Escorcio R, Voos MC, Caromano FA. Physiotherapy Research International, Development and reliability of the functional evaluation scale for Duchenne muscular dystrophy, gait domain: a pilot study, 2015: 135-146.
[45] Iosa M, Fusco A, Marchetti F, Morone G, Caltagirone C, Paolucci S, et al. The golden ratio of gait harmony: repetitive proportions of repetitive gait phases. Biomed Res Int 2013; 2013: 918642.
[46] Lurija AR. The working brain: an introduction to neuropsychology. London: Allen Lane The Penguin Press 1973.

[47] Gracovetsky S. An hypothesis for the role of the spine in human locomotion: a challenge to current thinking. J Biomed Eng. 1985 Jul;7(3):205-16. PubMed PMID: 4033096.
[48] Lamoth CJ, Beek PJ, Meijer OG. Pelvis-thorax coordination in the transverse plane during gait. Gait Posture. 2002 Oct;16(2):101-14. PubMed PMID: 12297252.
[49] Frigo C, Carabalona R, Dalla Mura M, Negrini S. The upper body segmental movements during walking by young females. Clin Biomech (Bristol, Avon). 2003 Jun;18(5):419-25. PubMed PMID: 12763438.
[50] Gracovetsky S. An hypothesis for the role of the spine in human locomotion: a challenge to current thinking. J Biomed Eng. 1985 Jul;7(3):205-16. PubMed PMID: 4033096.
[51] Morrison S, Russell DM, Kelleran K, Walker ML. Bracing of the trunk and neck has a differential effect on head control during gait. J Neurophysiol. 2015 Sep;114(3):1773-83. doi: 10.1152/jn.00059.2015. Epub 2015 Jul 15. PubMed PMID: 26180113; PubMed Central PMCID: PMC4571772.
[52] Kim JH, Lee SM, Jeon SH. Correlations among trunk impairment, functional performance, and muscle activity during forward reaching tasks in patients with chronic stroke. J Phys Ther Sci. 2015 Sep;27(9):2955-8.
[53] Beurskens R, Wilken JM, Dingwell JB. Dynamic stability of superior vs. inferior body segments in individuals with transtibial amputation walking in destabilizing environments. J Biomech. 2014 Sep 22;47(12):3072-9. doi: 10.1016/j.jbiomech.2014.06.041. Epub 2014 Jul 10. PubMed PMID: 25064425; PubMed Central PMCID: PMC4163077.

CHAPTER 5

5. GAIT ANALYSIS IN PATIENTS WITH LOWER LIMB AMPUTATION

In this chapter, text and figures have been taken from or adapted from the article "*Common and specific gait patterns in people with varying anatomical levels of lower limb amputation and different prosthetic components*" *[2017, Human Movement Science]*, which was co-authored by me and from Conference papers "*Analisi Cinematica del Cammino in Amputati per la Valutazione Funzionale della Stabilità Dinamica" [2017, SIAMOC]* and *"Controllo motorio modulare dell'arto controlaterale nel cammino di amputati trans-femorali*" *[2017, SIAMOC]*, which were co-authored by me.

5.1 Study N° 1: Common and specific gait patterns in people with varying anatomical levels of lower limb amputation and different prosthetic components.

Prosthesis use in persons with lower limb amputation at different anatomic levels requires complex adaptation strategies, both in the prosthesis and in the sound sides, during gait [1,2] and other daily life locomotor tasks [3,4]. Indeed, prosthetic gait reflects a mixture of deviations from normal gait and adaptive and compensatory motions dictated by residual limb function after amputation. For this reason, quantifying and characterizing the gait of persons with a prosthesis is an essential prerequisite to improve our ability to develop new and ergonomic prosthetic devices, as well as to optimize the rehabilitation programs [5].

Many previous studies have been performed on gait kinematics and kinetics of people with amputation in order to characterize their typical walking patterns.

It has been reported that the prosthetic limb shows a longer stride than the intact limb; however, the prosthetic limb's stance phase lasts less than that of the unaffected one [1,6,7]. In addition, a greater

hip flexion in early stance of the prosthetic limb and a higher than normal knee flexion in the early stance phase of the intact limb have been reported to probably improve the overall stability and energy expenditure, respectively [1,8].

Regarding the force interaction, when increasing walking speed, the vertical ground reaction force increases, particularly in the intact limb [9]. This tendency to load the intact limb more than the prosthetic limb has been also reported during gait initiation [10].

The two factors influencing the gait in people with amputation are the level of the amputation and the type of prostheses. Regarding the former factor, the gait in people with transfemoral amputation seems to be more asymmetric than that in people with transtibial amputation: they show wider steps of longer duration compared to people with transtibial amputation [11]. Concerning the latter factor, in recent years the prostheses have improved in design, materials, and technology [12] to be more effective in terms of efficiency of ambulation, minimization of the asymmetries, and reduction of compensatory movements, which, over time, may prove damaging to individuals. Actually, subjects with lower limb amputation wear different type of prostheses, such as the old concept mechanical prostheses or the most recent and technologically advanced prostheses (Microprocessor Controlled Knees (MPKs)), i.e. CLeg and Genium [13-15]. These differences are related to different aspects, including individuals' preference and adaptation, time from the amputation/prosthesis implantation, local insurance laws for the prosthesis reimbursement.

To date, no consistent study has evaluated the impact of the different types of prostheses on the gait function according to the anatomical level of amputation. Such analysis would allow better understanding of the advantages and disadvantages of the different types of prostheses. In addition, some limitations are present in many studies, since most of them included a small sample of subjects [16-18], had no control group [11,18,19] and did not match controls for the gait speed [20, 21]. Since many kinematic and kinetic variables are speed-dependent [22, 23], not controlling for the speed (by not including a control group walking at matched gait speed) may create uncertainty in the interpretation of the pathologic gait pattern and may not allow detection of a reliable and

specific gait pattern in order to distinguish what is unique from what is common. Furthermore, the lack of a matched speed comparison between people with amputations and healthy subjects do not allow discriminating the primary deficits from compensatory mechanisms.

The aim of the study *"Common and specific gait patterns in people with varying anatomical levels of lower limb amputation and different prosthetic components"* published from Human Movement Science, 2017, was to identify the kinematic and kinetic gait patterns and to measure the energy consumption in a large sample of people with amputations according to both the anatomical level of amputation and the type of prosthetic components in comparison with a control group matched for the gait speed.

5.1.1 Materials and methods

Subjects

Fifty-five subjects with lower-limb amputation from the prosthetics center of Italian Workers' Compensation Authority (INAIL) of Rome were enrolled in this study between September 2015 and September 2018. All patients had a unilateral transtibial or transfemoral amputation as a consequence of a workplace traumatic accident. Among subjects with transfemoral amputation, mechanical prosthesis [2, 15], and two types of MPKs prosthesis: CLeg and Genium (Ottobock, Duderstadt, Germany) [14]) were used. INAIL provided the same type prosthetic foot (Ossur Variflex foot), as well as the same sockets and suspensions for all participants (Ossur, Reykjavík, Iceland). All patients wore their prosthesis daily at least since 2 years, and were able to ambulate independently along level surfaces without mobility aids. None of the subjects had any chronic disease, cardiac complication, uncontrolled asthma or diabetes mellitus, severe osteoporosis, or cognitive disorder.

The study group included 15 subjects with transtibial amputation (TTA) (15 men; age, 52.81 ± 14.51 years; height, 176.44 ± 5.40 cm; mass, 87.44 ± 11.08 kg) and 40 subjects with transfemoral amputation (TFA) (37 men; age, 54.94 ± 12.31 years; height, 172.85 ± 7.95 cm; mass, 83.47 ±

15.69 kg). Among the 40 subjects with TFA, 9 wore a mechanical prosthesis (TFA_M), 17 a CLeg prosthesis (TFA_C), and 14 a Genium prosthesis (TFA_G).

Forty healthy subjects were recruited as the control group (C) and were age-sex-speed matched with subjects with TFA (C_{mTFA}). A subgroup of 15 healthy subjects was age-sex-speed matched with subjects with TTA (C_{mTTA}) and a subgroup of 13 age-sex-speed matched subjects with TFA (TFA_m) was age-sex-speed matched with 13 subjects with TTA (TTA_m) to analyze the effect of different anatomical levels of amputation.

Gait analysis

Gait was analyzed by using an optoelectronic motion analysis system (SMART-DX 6000 System, BTS, Milan, Italy), consisting of six infra-red cameras (sample frequency, 340 Hz) used to detect the movement of twenty-seven passive spherical markers placed over prominent bony landmarks [24, 25]. In detail, the markers were placed over the head, the cutaneous projections of the spinous processes of the seventh cervical vertebra and sacrum, and bilaterally over the acromion, olecranon, ulnar styloid process, anterior superior iliac spine, and greater trochanter for all the subjects with TTA and TFA and C. In addition, markers were placed, bilaterally in C and unilaterally on the amputated side of subjects with amputation, over the lateral femoral condyle, fibula head, lateral malleoli, fifth metatarsal head, and heel (for these last two points the markers were placed on the shoes). In subjects with TTA and TFA, amputated limb markers were placed over symmetrical points (no anatomical landmarks) with respect to the homologous marker's position on the non-amputated limb. Furthermore, wand markers were placed bilaterally on femurs and legs (Davis et al., 1991). Two dynamometric platforms (Kistler 9286AA, Winterthur, Switzerland), adjacent to each other in the longitudinal direction, but displaced by 0.2 m in the lateral direction, were used to acquire ground reaction forces (sampling rate, 680 Hz). Data acquisition from the optoelectronic cameras and dynamometric platforms was integrated and synchronized.

Experimental procedure

Individuals in C and subjects with TTA and TFA underwent an initial training session to become familiar with the assessment procedures. Patients were asked to walk with their shoes at comfortable self-selected speeds along a walkway while looking forward. Because we were interested in natural locomotion, only qualitative instructions were provided, and each subject was free to choose his own cadence. On the other hand, subjects in C were requested to walk with their shoes at their preferred speed and at a lower speed to match the speed between groups. At least ten trials were recorded for each subject and for each speed. To avoid fatigue, groups of three trials were separated by 1-min rest periods in subjects with amputation.

Data analysis

After each acquisition performed by Smart Capture (BTS, Milan, Italy), data were processed using SMART Tracker and Analyzer software (BTS, Milan, Italy) and Matlab software (version 7.10.0, MathWorks, Natick, MA, USA). The gait cycle was defined as the interval between two successive foot contacts of the same leg. Kinematic and kinetic data were time-normalized to the duration of the gait cycle and interpolated to 101 samples using a polynomial procedure. In this study, heel strike and toe off instants were calculated from kinematic data. After this preprocessing procedure, time-distance, kinematic, and kinetic parameters were calculated. For people with amputations, each parameter was calculated for the amputated (A) and non-amputated (NA) side, while for C the parameters were evaluated without distinguishing between sides.

Speed matching procedure

Walking speed was matched between groups as follows: only the walking trials of C (preferred speed or at a lower speed) whose speed was near to a corresponding subject with amputation were considered. Furthermore, only a subgroup of subjects with TFA (TFA_m) was age-sex matched with subjects with TTA. To have the speed match between the groups of TFA_m and TTA, 2 subjects with TTA were excluded, leaving only 13 subjects (TTA_m), because their speeds were far from those of

the age-sex matched subjects with TFA_m. Paired two-sample t-test was used to investigate the differences in walking speed between patients and controls, both TTA vs. C_{mTTA} and TFA vs. $C_{mTFA,}$ and between TTA_m and TFA_m. In this way, the mean speed values were not statistically different (the p value for statistical significance was set at 0.05) between groups (TTA 1.08 ± 0.16 m/s, C_{mTTA} 0.97 ± 0.20 m/s, p = 0.116; TFA 0.92 ± 0.20 m/s, C_{mTFA} 0.93 ± 0.25 m/s, p = 0.813; TTA_m 1.05 ± 0.15 m/s, TFA_m 0.94 ± 0.16 m/s, p = 0.084).

Time-distance parameters

The following time-distance gait parameters were calculated for each subject: walking speed (m/s); cadence (step/s); step width (m); step length (m) (from the heel strike of a limb and the subsequent heel strike of the other limb); stance, swing, and double support phases durations (expressed as percentages of the gait cycle duration). Step length and the step width were normalized to the limb length of each subject.

Kinematic data

The anatomical and prosthetic joint angles for the hip, knee, ankle, trunk, and pelvis (frontal, sagittal, and transverse plane) were computed. Based on these variables, the joint range of motion (RoM) was calculated as the difference between the maximum and minimum values during the gait cycle.

Kinetic data

The vertical component of the ground reaction forces (Vertical Force, VF) provided by the dynamometric platforms, was normalized to the subject's body weight [26].

For each subject and gait speed, the values of the 2 peaks of VF ($Peak1_{VF}$ and $Peak2_{VF}$) were computed. Furthermore, the full width at half maximum (FWHM) and the center of activity (CoA) of VF ($FWHM_{VF}$ and CoA_{FV}) were computed [27]. FWHM was calculated as the sum of the time

durations during which the VF curves were higher than their half maximum. The CoA was calculated using circular statistics as follow:

$$A = \sum_{i=1}^{200}(\cos\theta_t \times VF_i)$$
$$B = \sum_{i=1}^{200}(\sin\theta_t \times VF_i)$$
$$CoA = \tan^{-1}\left({}^{B}/_{A}\right)$$

where θ_t is the angle that varies from 0° to 360° to plot in polar coordinates (polar direction denoted the phase of the gait cycle).

Energy consumption measurement

The mechanical behavior was measured in terms of energy recovery and energy consumption in relation to the whole-body center of mass (CoM). This methodology has been validated both in normal [28, 29] and abnormal gait patterns [30, 31], and gives information on the mechanical energy expenditure involving the whole skeletal muscle system during walking.

The whole-body CoM was calculated as the centroid of a set of elements composed by 13 body segments (head, trunk, arms, forearms, pelvis, thigh, shanks, and feet). The computation was performed by considering kinematic and anthropometric data together with the body segment parameters [32, 33] according to the weighted average of the individual body segments' center of mass [34]:

$$CoM_x = \frac{1}{m}\sum_{i=1}^{n} x_i \times m_i$$

$$CoM_y = \frac{1}{m}\sum_{i=1}^{n} y_i \times m_i$$

$$CoM_z = \frac{1}{m}\sum_{i=1}^{n} z_i \times m_i$$

where CoM_x, CoM_y and CoM_z are, respectively, the instantaneous x, y, and z components of the CoM position, m is the whole-body mass of the subject, $n = 13$ is the number of parts being considered, x_i, y_i, and z_i are the components of the CoM position of the i_{th} part, and m_i is the mass of the i_{th} segment or residuum or prosthesis components.

The kinetic energy (E_k) associated with CoM displacements during the gait cycle was calculated as the sum of the kinetic energy on the x (E_{kx}), y (E_{ky}), and z (E_{kz}) axes as follows:

$$E_k = E_{kx} + E_{ky} + E_{kz} = \frac{1}{2} m\left(v_x^2 + v_y^2 + v_z^2\right)$$

where m and v_x, v_y, and v_z are, respectively, the mass and the three velocity components of the CoM evaluated starting from its components ($CoM_x, CoM_y \; and \; CoM_z$). Furthermore, the potential energy (E_p) associated with CoM was calculated as follows:

$$E_p = mgh$$

where h is the vertical (y) CoM component and g is the gravity acceleration.

The total mechanical energy (E_{tot}) associated with CoM was computed as the sum of E_k and E_p.

The fraction of mechanical energy recovered during each walking step (R-step) [29] was calculated as follows:

$$R - step = \frac{W_p^+ + W_{kf}^+ - W_{tot}^+}{W_p^+ + W_{kf}^+} = \left(1 - \frac{W_{tot}^+}{W_p^+ + W_{kf}^+}\right)$$

where $W_p^+, W_{kf}^+, W_{tot}^+$ represent the positive work (sum of the positive increments over one step) produced by the gravitational potential energy, by the kinetic energy of forward motion, and by the total mechanical energy, respectively. Additionally, the total energy consumption (TEC) was calculated as follows [28]:

$$TEC = \frac{W_{tot}^+}{0.21}$$

TEC was then normalized to the body weight and step length. For each subject, R-step and the normalized TEC values of all the steps were averaged.

Statistics

The Shapiro-Wilk test was used to analyze the normal distribution of the data. The dependent t-test or the Wilcoxon's signed-rank test were used to evaluate the differences between the A and NA sides of subjects with TTA and TFA for each time-distance, kinematic, kinetic, and energy consumption measurements. Furthermore, paired two-sample t-test or the Mann-Whitney test (two-tailed) was used for each parameter to test for between-group differences (TFA vs. C_{mTFA}, TTA vs.

C_{mTTA}, and TFA_m vs. TTA_m). To evaluate the effect of the gait speed on the CoA across the gait cycle, Watson-Williams test was used to test for circular data (Varrecchia et al., 2018).

Furthermore, one-way ANOVA was used also to evaluate the differences among the three subgroups of subjects with TFA for each evaluated parameter. Post hoc analyses (with Bonferroni's corrections) were performed when ANOVA showed significant differences.

Significance level was set at $p < 0.05$. All analyses were performed using SPSS 20.0 (*SPSS Inc., Chicago, IL, USA*) and Matlab (*version 8.3.0.532, MathWorks, Natick, MA, USA*) software.

5.1.2 Results

Time-distance parameters

The means, standard deviations, and statistical results for each time-distance parameter and for each group are presented in Table 5.1.

People with amputation vs. controls

Significantly increased step width, step length, and double support duration in both sides were found in both TTA and TFA groups compared to the C group (C_{mTTA} and C_{mTFA}). Stance duration was significantly increased in the NA side in both TTA and TFA groups, and significantly decreased in the A side in the TFA group. Conversely, the swing duration was significantly decreased in the NA side in both TTA and TFA groups, and significantly increased in the A side in TFA group (Table 5.1).

Significantly shorter stance duration and longer swing duration were found in the A side than in the NA side (Table 5.1, Figure 5.2) in TTA and TFA groups.

Type of prostheses (TFAM, TFAC and TFAG)

A significant effect of the type of prosthesis on the step length of the NA side was detected. Post hoc analysis revealed higher values for the Genium prosthesis compared to mechanical prosthesis (Table 5.1).

A significantly shorter step length in A side than in the NA one (Table 5.1) was found in TFA_G subgroup. Furthermore, significantly shorter stance duration and longer swing duration in the A side than in the NA one (Table 5.2) were found in all three TFA_M, TFA_C and TFA_G subgroups.

TTAm vs. TFAm

A significant effect of the type of amputation (TTA_m vs. TFA_m) on the stance and swing duration was found in both sides, with the stance significantly increased and the swing significantly decreased in the NA side in TFA_m group compared to TTA_m group, (Table 5.1). Conversely, the stance significantly decreased, and the swing significantly increased in the A side in TFA_m group compared to TTA_m group (Table 5.1).

Significantly shorter stance duration and longer swing duration in the A side than in the NA one (Table 5.1) were found both in TTA_m and TFA_m.

People with amputation vs controls

Significantly increased hip and knee RoMs in NA side were found in TFA compared to C_{mTFA} (Figure 5.1). Furthermore, significantly decreased ankle RoMs in A side were detected in both TTA and TFA compared to the speed-matched C group (C_{mTTA} and C_{mTFA}) (Figure 5.1).

Significantly increased pelvic obliquity, trunk lateral bending, and trunk rotation RoMs of both sides were found in both TTA and TFA groups compared to C (Figs. 5.1, 5.2). Moreover, pelvic tilt, pelvic rotation, and trunk flection-extension RoMs of both sides were significantly increased in TFA group compared to C_{mTFA} group (Figs. 5.1, 5.2). Figure 5.2 also shows that people with amputation walked with the pelvis and trunk ante-flexed (flexed in a forward direction) compared to controls. A significantly shorter hip and knee RoMs were found in the A side than in the NA side (Fig. 5.1) in TFA group. Furthermore, a significantly shorter ankle RoMs were found in the A side than in the NA side (Fig. 5.1) in both TTA and TFA groups.

Type of prostheses (TFAM, TFAC, and TFAG)

A significant effect of the type of prosthesis on the hip and knee RoMs in the A side and on the pelvic obliquity RoM was found in both sides. Post hoc analysis revealed higher values of the hip and knee RoMs in the A side of TFA_G subgroup compared to TFA_M subgroup (Fig. 5.1) and lower values of the pelvic obliquity RoMs for the Genium prosthesis (TFA_G) compared to mechanical prosthesis (TFA_M) in both sides (Fig. 5.1).

Significantly decreased knee and ankle RoMs in the A side than in NA side were found in TFA_M, TFA_C, and TFA_G subgroups (Fig. 5.1). Furthermore, a significantly decreased hip RoM in A side than in NA side (Fig. 5.1) was detected in TFA_G subgroup.

Kinematic data

The means, standard deviations and statistical results of RoM for the hip, knee, ankle, pelvic, and trunk for each group are shown in Fig. 5.1.

TTAm vs. TFAm

A significant effect of the type of amputation (TTA_m vs. TFA_m) on the knee, pelvic tilt, and trunk flexion-extension RoMs was found, with the knee RoM significantly decreased in the A side in TFA_m subgroup compared to TTA_m subgroup (Fig. 5.1) and the pelvic tilt and trunk flexion-extension RoMs significantly increased in both sides in TFA_m subgroup compared to TTA_m subgroup (Fig. 5.1).

A significantly shorter hip and knee RoMs were found in the A side than in the NA side (Fig. 5.1) in TFA_m subgroup. Furthermore, a significantly shorter ankle RoM was found in the A side than in the NA side (Fig. 5.1) in both TTA_m and TFA_m subgroups. Significantly shorter trunk lateral bending, trunk flexion-extension, and trunk rotation RoMs were found in the A side than in the NA side (Fig. 5.3) in both TTA_m and TFA_m subgroups.

		People with amputation vs controls						Type of prostheses				TTA_m vs TFA_m		
Time-distance parameters		**C_{mTTA}**	**TTA**	p group	**C_{mTFA}**	**TFA**	p group	**TFA_M**	**TFA_C**	**TFA_G**	p group	**TTA_m**	**TFA_m**	p group
Walking speed (m/s)		0.97±0.20	1.08±0.16	0.1163	0.93±0.25	0.92±0.20	0.813	0.82±0.20	0.91±0.23	1.01±0.12	0.064	1.05±0.15	0.94±0.16	0.084
Cadence (cycle/s)	A	0.84±0.07	0.83±0.07	0.52	0.81±0.12	0.78±0.08	0.289	0.75±0.07	0.79±0.09	0.80±0.06	0.309	0.82±0.10	0.77±0.07	0.077
	NA		0.82±0.07	0.481		0.78±0.08	0.397	0.74±0.07	0.79±0.09	0.80±0.06	0.16	0.81±0.07	0.77±0.07	0.11
	p side		0.083			0.439		0.269	0.158	0.619		0.114	0.973	
Step width (% limb length)		0.20±0.05	0.28±0.06	**<0.001**	0.19±0.06	0.30±0.09	**<0.001**	0.33±0.10	0.32±0.08	0.27±0.09	0.214	0.27±0.05	0.29±0.09	0.538
Step length (% limb length)	A	0.61±0.12	0.74±0.09	**0.002**	0.60±0.10	0.66±0.09	**0.014**	0.63±0.11	0.65±0.12	0.66±0.08	0.729	0.74±0.10	0.64±0.11	0.058
	NA		0.75±0.07	**0.001**		0.67±0.09	**0.003**	0.64±0.12	0.65±0.09	0.72±0.05	**0.048**	0.74±0.07	0.70±0.08	0.182
	p side		0.903			0.241		0.681	0.877	**0.046**		0.946	0.38	
Stance duration (% cycle)	A	61.78±1.78	61.89±1.79	0.871	62.38±2.88	59.63±2.57	**<0.001**	60.14±2.31	60.09±3.02	58.74±2.02	0.285	61.68±1.80	58.71±0.88	**<0.001**
	NA		64.17±3.44	**0.009**		67.99±3.31	**<0.001**	67.21±3.02	69.27±3.92	66.94±2.14	0.107	64.68±3.42	67.99±3.15	**0.017**
	p side		**0.014**			**<0.001**		**0.004**	**<0.001**	**<0.001**		**0.01**	**<0.01**	
Swing duration (% cycle)	A	38.85±3.29	38.09±1.80	0.648	38.30±2.99	39.88±2.98	**<0.001**	39.9±2.93	39.01±2.33	40.91±2.05	0.205	38.28±1.82	40.58±2.20	**0.002**
	NA		35.82±3.43	**0.009**		31.91±3.30	**<0.001**	31.6±2.53	31.11±4.24	33.08±2.04	0.25	35.3±3.4	31.64±3.18	**0.011**
	p side		**0.015**			**<0.001**		**0.004**	**<0.001**	**<0.001**		**<0.01**	**<0.01**	
Double support duration (% cycle)	A	23.17±3.15	26.07±4.46	**0.049**	23.54±5.76	27.72±5.01	**0.001**	28.54±3.73	28.97±6.36	25.66±3.12	0.161	26.38±4.74	27.08±3.54	0.677
	NA		26.08±4.50	**0.037**		27.44±6.58	**<0.001**	24.28±9.03	30.26±6.47	26.04±2.98	0.05	24.4±4.77	27.41±4.09	0.568
	p side		0.670			0.367 [b]		0.125	0.081	0.298		0.672	0.698	

Table 5.1. The means, standard deviations, and statistical results (p value) of walking speed, cadence, step width, step length, stance duration, swing duration, and double support duration. C_{mTTA}: healthy subjects age-sex-speed matched with TTA; TTA: subjects with transtibial amputation; C_{mTFA}: healthy subjects age-sex-speed matched with TFA; TFA: subjects with transfemoral amputation; TFA_M: subjects with transfemoral amputation with mechanical prosthesis; TFA_C: subjects with transfemoral amputation with CLeg prosthesis; TFA_G: subjects with transfemoral amputation with Genium prosthesis; TFA_m: a subgroup of 13 age-sex-speed matched subjects with a subgroup of TTA; TTA_m: a subgroup of 13 age-sex-speed matched subjects with a subgroup of TFA.

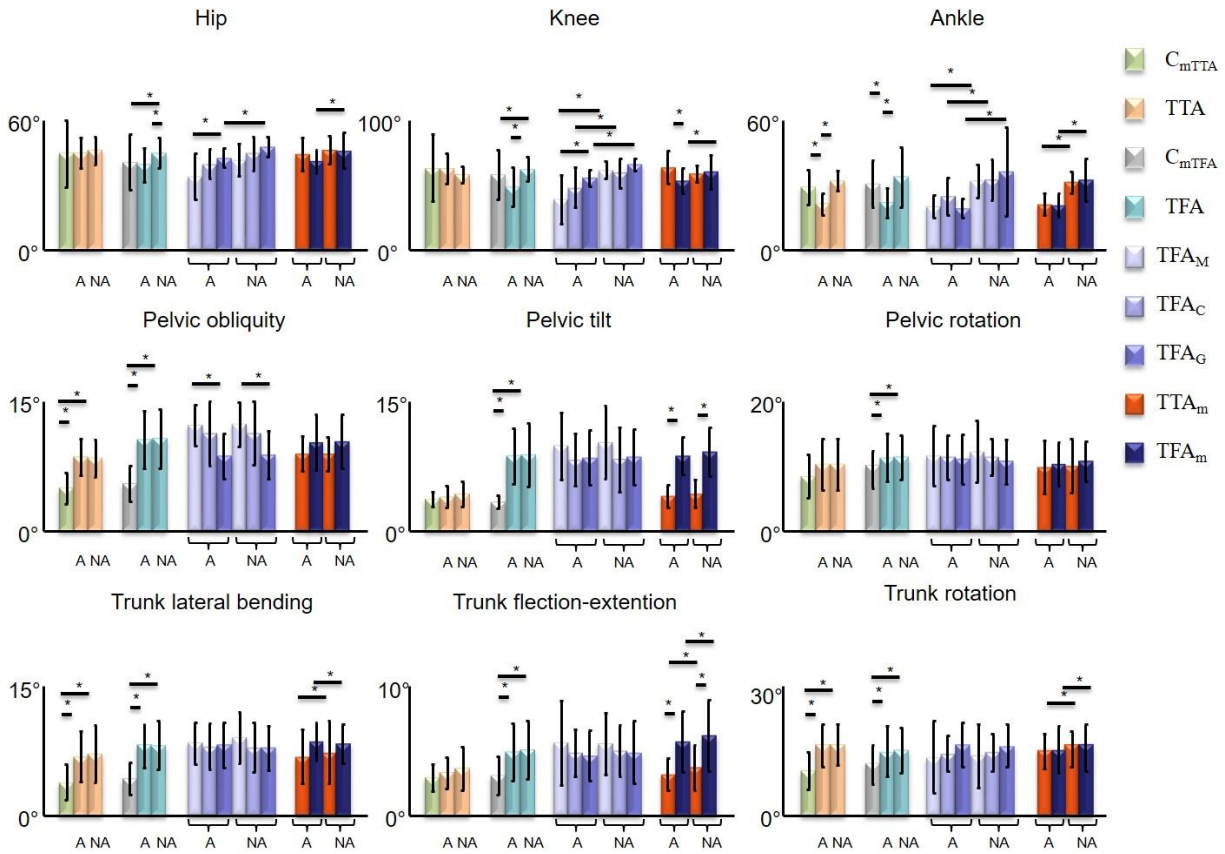

Figure 5.1. The means, standard deviations, and statistical results of range of motion for the hip, knee, ankle, pelvic, and trunk for each group. C_{mTTA}: healthy subjects age-sex-speed matched with TTA; TTA: subjects with transtibial amputation; C_{mTFA}: healthy subjects age-sex-speed matched with TFA; TFA: subjects with transfemoral amputation; TFA_M: subjects with transfemoral amputation with mechanical prosthesis; TFA_C: subjects with transfemoral amputation with CLeg prosthesis; TFA_G: subjects with transfemoral amputation with Genium prosthesis; TFA_m: a subgroup of 13 age-sex-speed matched subjects with a subgroup of TTA; TTA_m: a subgroup of 13 age-sex-speed matched subjects with a subgroup of TFA.

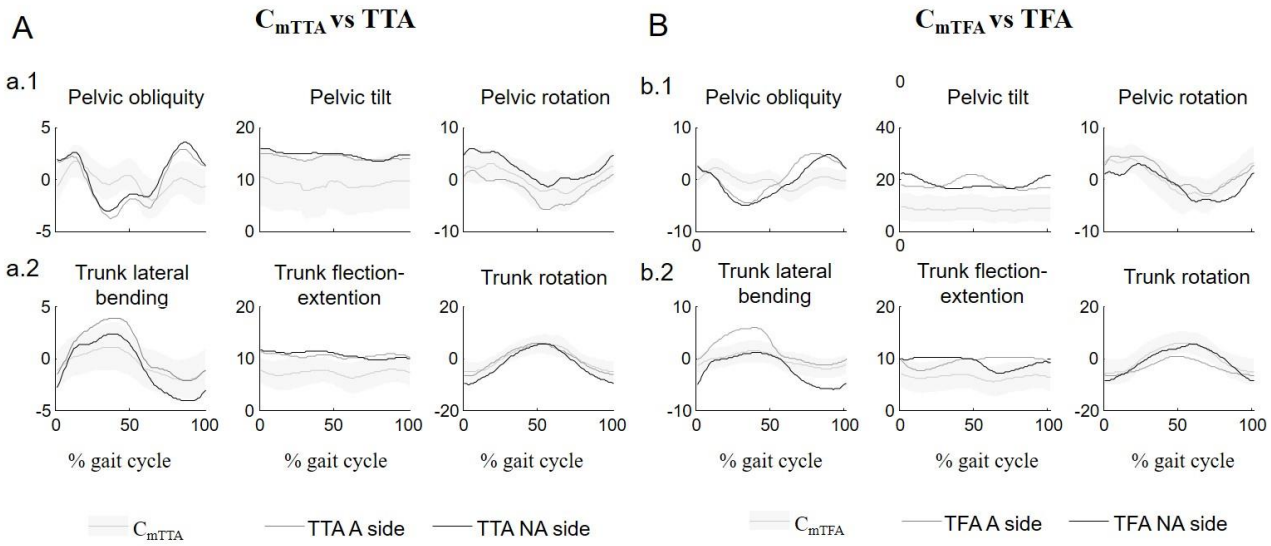

Figure 5.2.. Pelvic obliquity, pelvic tilt, pelvic rotation, trunk lateral bending, trunk flection-extension, and trunk rotation in both sides were found in both TTA and TFA groups compared to controls. C_{mTTA}: healthy subjects age-sex-speed matched with TTA; TTA: subjects with transtibial amputation; C_{mTFA}: healthy subjects age-sex-speed matched with TFA; TFA: subjects with transfemoral amputation.

Kinetic data

The curves of the vertical force for C_{mTTA} and TTA (Figure 5.3A) and for C_{mTFA} and TFA (Fig. 5.3B) are shown in Cartesian coordinates as mean curves (a.1 and b.1), and in polar coordinates as mean curve (a.2 and b.2), as well as single and mean CoA values (a.3 and b.3), all expressed as percentage of gait cycle.

The means, standard deviations, and statistical results of VF for each group are reported in Table 5.2.

People with amputation vs. controls

A significantly increased $Peak1_{VF}$ value in NA side and a significantly decreased $Peak2_{VF}$ value in A side were found in TTA group compared to C_{mTTA} group (Table 5.1). Significantly increased $Peak1_{VF}$, CoA_{VF}, and $FWHM_{VF}$ values in NA side were found in TFA compared to C_{mTFA}. Furthermore, significantly increased $Peak1_{VF}$ value and significantly decreased $FWHM_{VF}$ and CoA_{VF} values in A side were found in TFA compared to C_{mTFA} (Table 5.1).

$Peak1_{VF}$ was significantly lower in the A side than in the NA side (Table 5.1) in TTA group. A significantly lower $Peak2_{VF}$ value was found in the A side than in the NA side (Table 5.1) in both

TTA and TFA groups. Furthermore, significantly higher $Peak1_{VF}$ and lower $FWHM_{VF}$ and CoA_{VF} values were found in the A side than in the NA side (Table 5.1) in TFA.

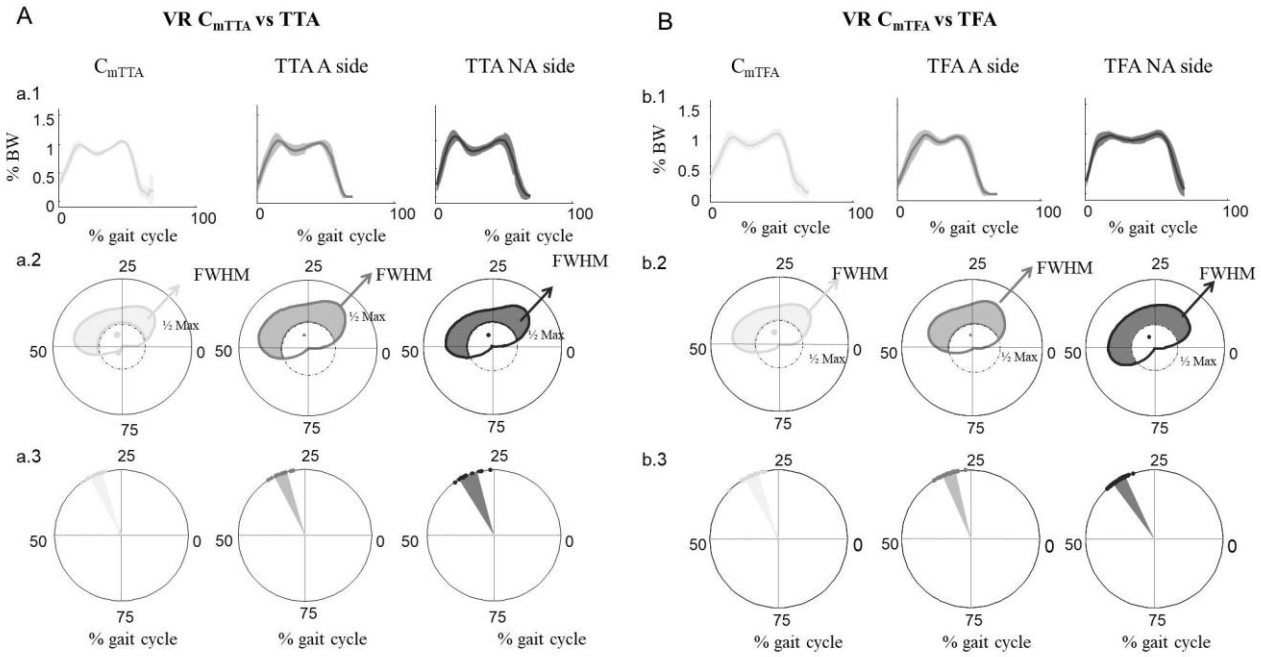

Figure 5.3. Curves of the vertical force for C_{mTTA} and TTA and for C_{mTFA} and TFA shown in Cartesian coordinates as mean curves (a.1 and b.1), and in polar coordinates as mean curve (a.2 and b.2), as well as single and mean CoA values (a.3 and b.3), all expressed as percentage of gait cycle.
C_{mTTA}: healthy subjects age-sex-speed matched with TTA; TTA: subjects with transtibial amputation; C_{mTFA}: healthy subjects age-sex-speed matched with TFA; TFA: subjects with transfemoral amputation

Type of prostheses (TFAM, TFAC, and TFAG)

No significant effects of the type of prosthesis on the VF values were detected for both sides (Table 5.1). A significantly increased $Peak1_{VF}$ value was found in A side than in the NA side (Table 5.1) in TFA_C and significantly decreased ($p < 0.05$) $Peak2_{VF}$ values were found in A side than in the NA side (Table 5.1) in TFA_C and in TFA_G subgroups. Furthermore, significantly decreased $FWHM_{VF}$ and CoA_{VF} values were found in A side than in the NA side (Table 5.1) in all three TFA_M, TFA_C, and TFA_G subgroups.

TTAm vs. TFAm

A significant effect of the type of amputation (TTA_m vs. TFA_m) on the VF values was detected. $Peak1_{VF}$ was significantly decreased in the NA side in TFA_m group compared to TTA_m group (Table 5.1). $FWHM_{VF}$ was significantly increased in the NA side and significantly decreased in the A side in TFA_m group compared to TTA_m group (Table 5.1).

Significantly lower values were found in the A side than in the NA side for $Peak1_{VF}$ and $Peak2_{VF}$ in TTA_m, for $FWHM_{VF}$ in both TTA_m and TFA_m group, and for CoA_{VF} in TFA_m (Table 5.1)

Energy consumption measurement

Fig. 5.4 shows means, standard deviations, and statistical results of R-step and TEC values.

People with amputation vs controls

A significantly lower value of R-step in TFA subgroup compared to C_{mTFA} subgroup was found (Fig. 5.4). No significant differences of TEC values were detected.

Type of prostheses (TFAM, TFAC and TFAG)

No significant effects of the type of prosthesis were found on both R-step and TEC (Fig. 5.4).

TTAm vs. TFAm

A significant effect of the type of amputation on R-step was found, with R-step value of TTA_m subgroup being significantly higher than that of TFA_m. Instead, no significant effect of the type of amputation on TEC was detected (Fig. 5.4).

.

		People with amputation vs controls						Type of prostheses				TTA_m vs TFA_m		
Kinetic parameters		C_{mTTA}	TTA	p group	C_{mTFA}	TFA	p group	TFA_M	TFA_C	TFA_G	p group	TTA_m	TFA_m	p group
$Peak1_{VF}$	A)	1.014±0.061	1.049±0.083	0.125	0.973±0.114	1.04±0.064	**<0.001**	1.065±0.068	1.052±0.051	1.03±0.075	0.423	1.021±0.039	1.043±0.071	0.336
	NA)		1.109±0.10	**0.005**		1.016±0.062	**0.1**	1.002±0.056	1.008±0.043	1.03±0.083	0.421	1.094±0.103	1.001±0.07	**0.014**
	p side		**0.029**			**0.011**		0.098	**0.013**	0.883		**0.02**	0.1	
$Peak2_{VF}$	A)	1.054±0.051	0.985±0.032	**<0.001**	1.00±0.124	0.989±0.048	0.355	0.997±0.054	0.986±0.043	0.987±0.054	0.838	0.982±0.032	0.976±0.046	0.538
	NA)		1.063±0.079	0.733		0.992±0.071	0.379	0.999±0.075	1.042±0.066	1.011±0.074	0.288	1.0584±0.083	1.007±0.063	0.084
	p side		**<0.001**			**0.008**		0.82	**0.001**	**0.288**		**0.002**	0.168	
CoA_{VF} (% gait cicle)	A)	31.25±1.599	30.87±1.68	0.654	31.43±1.77	30.09±1.67	**<0.001**	29.98±1.62	30.38±1.99	29.84±1.31	0.666	30.81±1.78	29.60±1.56	0.091
	NA)		31.40±2.45	0.475		33.57±1.74	**<0.001**	33.73±1.86	34.08±1.72	32.85±1.56	0.142	31.86±2.28	33.57±1.62	0.095
	p side		0.281			**<0.001**		**<0.001**	**<0.001**	**<0.001**		0.07	**<0.001**	
$FWHM_{VF}$	A)	50±1.604	47.667±3.457	0.066	47.179±1.798	44.051±3.809	**<0.001**	43.222±3.961	43.941±4.322	44.712±3.148	0.659	47.153±3.412	43.231±3.678	**0.01**
	NA)		50.47±2.446	0.652		56.72±2.611	**<0.001**	57.11±2.315	56.18±3.005	57.12±2.318	0.542	50.85±2.267	57.46±2.696	**<0.001**
	p side		0.076			**<0.001**		**<0.001**	**<0.001**	**<0.001**		**0.03**	**<0.001**	

Table 5.2. The means, standard deviations, and statistical results (p value) of parameters evaluated on vertical force (VF) curves ($Peak1_{VF}$ and $Peak2_{VF}$: 2 peaks, CoA_{VF}: center of activity and $FWHM_{VF}$: full width at half maximum). C_{mTTA}: healthy subjects age-sex-speed matched with TTA; TTA: subjects with transtibial amputation; C_{mTFA}: healthy subjects age-sex-speed matched with TFA; TFA: subjects with transfemoral amputation; TFA_M: subjects with transfemoral amputation with mechanical prosthesis; TFA_C: subjects with transfemoral amputation with CLeg prosthesis; TFA_G: subjects with transfemoral amputation with Genium prosthesis; TFA_m: a subgroup of 13 age-sex-speed matched subjects with a subgroup of TTA; TTA_m: a subgroup of 13 age-sex-speed matched subjects with a subgroup of TFA.

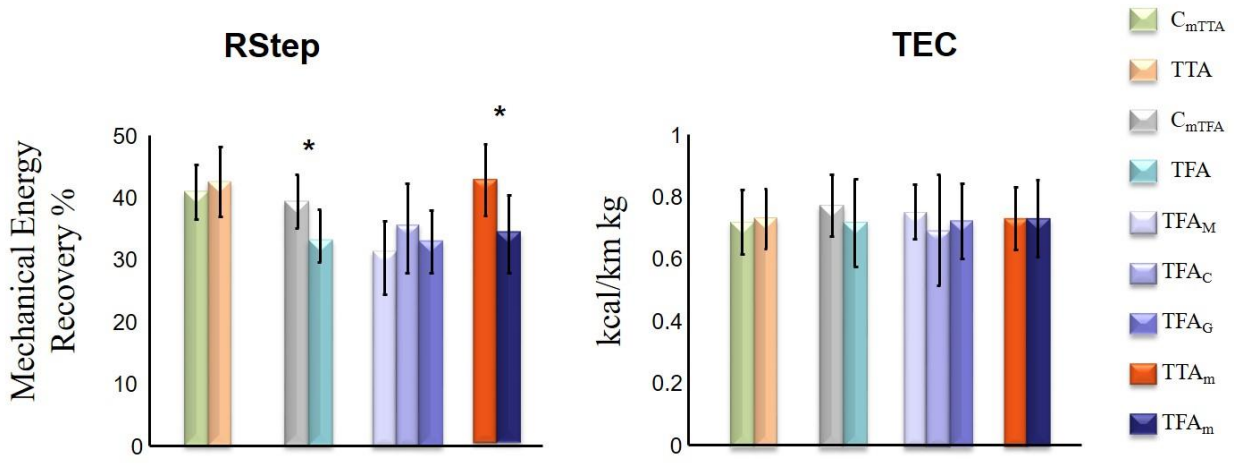

Figure 5.4. Means, standard deviations, and statistical results of fraction of mechanical energy recovered during each walking step (R-step) and total energy consumption (TEC) values for each group. C_{mTTA}: healthy subjects age-sex-speed matched with TTA; TTA: subjects with transtibial amputation; C_{mTFA}: healthy subjects age-sex-speed matched with TFA; TFA: subjects with transfemoral amputation; TFA_M: subjects with transfemoral amputation with mechanical prosthesis; TFA_C: subjects with transfemoral amputation with CLeg prosthesis; TFA_G: subjects with transfemoral amputation with Genium prosthesis; TFA_m: a subgroup of 13 age-sex-speed matched subjects with a subgroup of TTA; TTA_m: a subgroup of 13 age-sex-speed matched subjects with a subgroup of TFA.

5.1.3 Discussion and Conclusions

The study described in this section aimed to identify both common and specific gait patterns in people with amputation, either regardless of, or according to their level of amputation and the type of prosthetic component. Furthermore, this study was focused on the symmetric and asymmetric aspects of these patterns.

To have a global picture of all the gait deficits for both the common and the specific gait patterns, the data were summarized in Table 5.2.

In general, regardless of the level of amputation and type of prosthesis, subjects with TTA and with TFA showed a common gait pattern characterized by a symmetric increase of step length, step width, double support duration, pelvic obliquity, trunk lateral bending, and trunk rotation range of motions with increased pelvis and trunk ante-flexed (flexed in a forward direction) posture. Almost all these gait deficits reflect compensatory mechanisms adopted by people with amputation

presumably to increase their stability in the frontal plane (increased step width), to maintain the most stable configuration (increased double support duration), to assist the lift of the affected limb (increased trunk lateral bending), while increasing the time of the stance and the force production during weight acceptance in the unaffected limb. Conversely, the reduced ankle joint range of motion in the prosthetic limb, which is the common prosthetic joint in both subjects with TTA and with TFA, is directly linked to the use of the prosthesis.

The increased step length is likely related to a compensatory increased movement of the trunk and pelvis (Fig. 5.3), since both the knee and hip joint range of motions of the prosthetic limb were either not increased, in the TTA group, or even reduced, in TFA group. However, it is not possible to exclude that the lack of sensory feedback might have played a role in determining a hypermetric foot placement in the prosthetic limb, which, in turn, would have influenced the foot placement of the unaffected limb, as adaptive mechanism of the new support base schem [35, 36].

The subjects with TFA showed a specific gait pattern that differed from that of C and subjects with TTA in terms of kinematic, kinetic, and energetic behavior. The subjects with TFA reduced the duration of the stance and increased the duration of the swing in the prosthetic limb. Moreover, they increased the hip and knee joint range of motions in the unaffected limb. Interestingly, in the prosthetic limb of subjects with TFA, the Peak1 was increased, while the full width at half maximum was reduced. In general, the Peak and full width at half maximum parameters express two different spatio-temporal aspects of the force production. The first represents the maximal force produced in a given instant during the loading response subphase, while the second represents the amount of the force production (>50% of the maximum) maintained during the whole duration of the stance. In this view, the subjects with TFA seem to be unable to control the prosthetic limb during the heel strike, likely caused by a reduced deceleration of the prosthetic limb from the late swing to the initial contact, leading to an increase in the Peak1. At the same time, they are unable to produce and maintain an adequate force during the whole stance phase, leading to a decrease of the full width at half maximum. Such behavior is reflected by the shift of the center of activity toward

the initial contact event (initial part of the stance). Conversely, the full width at half maximum was increased in the unaffected limb, which compensated by producing a stronger force maintained for a longer time, determining, in this case, a shift of the center of activity toward the toe off event (final part of the stance). Altogether these findings deeply reflect the essence of the asymmetric gait revealing the greater effort achieved by subjects with TFA to compensate for the reduced motor performance by increasing both motion and force production in the unaffected limb. As a final result, this specific gait pattern makes the subjects with TFA unable to recover energy during the stance phase.

People with amputation with Genium prosthesis (TFA_G) showed a longer step length in NA side and increased hip and knee range of motions in the prosthetic side compared to subjects with mechanical prosthesis, who, conversely, showed a symmetric increased pelvic obliquity. These findings indicate that the type of prosthesis influences the gait pattern of people with amputation both in terms of gait performance and adaptation [14]. In this view, the increased step length and hip and knee ranges of motion, together with the trend of gait speed (Table 5.1), might reflect a better gait performance for the Genium vs mechanical prostheses. Conversely, the increased pelvic obliquity seems to reflect a greater compensatory effort in subjects with mechanical prostheses, likely aimed to lift the limbs during the gait progression.

In conclusion, in spite of common gait pattern in subjects with lower limb prostheses, both the anatomical level of amputation and type of prostheses determine a specific gait pattern that should be taken into account when developing new and ergonomic prosthetic devices and when planning the rehabilitation programs aimed at improving the physiology of gait and reducing the gait asymmetries.

Gait parameters	Common gait pattern* TTA and TFA compared to controls			Specific gait pattern (amputation level) TFA compared to both control and TTA groups			Specific gait pattern (type of prosthesis) TFA_G vs TFA_M		
	Symmetric	Asymmetric		Symmetric	Asymmetric		Symmetric	Asymmetric	
		A side	NA side		A side	NA side		A side	NA side
Time-distance	Increased step width Increased step length Increased double support duration		Increased stance duration Reduced swing duration		Decreased stance duration Increased swing duration				Increased step length in TFA_G compared to TFA_M
Kinematics	Increased pelvic obliquity Increased trunk lateral bending and rotation Increased ante-flexion of the pelvis and trunk	Decreased ankle RoM				Increased hip and knee RoM	Increased pelvic obliquity in TFA_M compared to TFA_G	Increased hip e knee RoMs in TFA_G compared to TFA_M	
Kinetics			Increased Peak1		Increased Peak1 Decreased CoA, FWHM	Increased CoA and FWHM			
Energetic				Reduced Rstep					

Table 5.3 . Common and specific gait patterns in people with amputation.
**irrespective of the amputation level*

5.2 Study N. 2: Kinematic analysis during gait in amputees for functional evaluation of dymanic stability

Stability and balance keeping are extremely important aspects of gait, for functional, safety and psychological reasons. In the field of rehabilitation medicine, the assessment of stability and the evaluation of the risk of fall could be of extreme importance. The study *"Analisi Cinematica del Cammino in Amputati per la Valutazione Funzionale della Stabilità Dinamica"* presented at SIAMOC 2017, aimed at finding an eligible analysis method for gait functional evaluation in lower limb amputees, able to provide an overall reliable information on stability and risk of fall also in short duration evaluation sessions, more adequate for amputees.

5.2.1 Materials and methods

Data were collected in a Gait Analysis Laboratory of CTO Hospital of Rome. The experimental setup consisted of 6 cameras (BTS Bioengineering, Smart DX) and passive markers positioned on participants' bodies according to Davis protocol guidelines. Each participant performed walking trials at self-selected speed along a 9m straight path. Data were recorded from 19 trans-femoral amputees (TF, 29-74 years), 9 trans-tibial amputees (TT, 34-80 years) and 12 healthy controls (H, 29-77 years). Kinematics were used to calculate the centre of mass (CoM) as the centroid of the pelvis triangle. Obtained CoM's traectories were used to calculate the Margin of Stability (MoS), together with gait symmetry and regularity, calculated from CoM acceleration signals along the Antero-Posterior (AP), Medial-Lateral (ML) and Cranial-Caudal (CC) directions as in [2].

5.2.2 Results

Amputees present a wider margin of stability than controls, both along AP and ML directions. Furthermore, amputees are characterized by a more asymmetric and irregular gait than controls (Fig. 5.5).

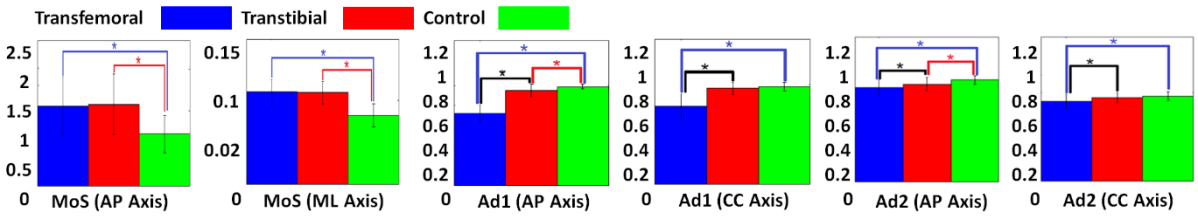

Figure 5.5: Means for populations of margin of stability and simmetry index (Ad1) and regularity (Ad2)

5.2.3 Discussion and Conclusions

MoS analysis might indicate differences in motor control strategies between amputees and healthy subjects: specifically, a wider MoS (resulting from a wider base of support and a lower gait speed) could compensate the lower balance control abilities in such patients.

Furthermore, the higher gait asymmetry and irregularity in amputees showhow such patients have a reduced motor control, resulting in a noisier gait pattern (more irregular and more asymmetric). The studied parameters, although don't represent effective estimator of the risk of fall, could give an overall functional characterization of gait, and could be used in clinical environment to improve therapies and design of prosthetic devices, starting from basic information such as stability and motor control.

5.3 Study N. 3: Modular motor control of the contralateral limb in trans-femoral amputees' gait

Muscular activity during walking is produced by the activation of a small set of motor modules (synergies) [37]. The analysis of the composition and time activation profiles of muscle synergies can help with the characterization of pathological gait. During the rehabilitation process, trans-femoral amputees (TFA) adapt their walking pattern to their new physical conditions. Studies in this field have shown that the most significant differences in muscular activity are found during the swing phase of the prosthetic limb [38]. In the study *"Controllo motorio modulare dell'arto controlaterale nel cammino di amputati trans-femorali"* presented at SIAMOC 2017, modular motor control in trans-femoral amputees' gait is investigated for the characterization of differences between TFA and healthy subject control strategies.

5.3.1 Materials and methods

8 healthy subjects (58.5 ± 12 years old) and 16 trans-femoral amputees (52.5 ± 15 years old) participated in the study. sEMG data were recorded from 12 muscles of the sound limb. Kinematic data was recorded with a stereophotogrammetric system and was used for the segmentation of stance and swing phases. The experiment consisted of 12 repetitions of walking along a 6m walkway. Muscle synergies were extracted by means of a non-negative matrix factorization algorithm (NNMF) applied on the matrix containing the envelope of the sEMG signal, as to obtain synergy vectors W and synergy activation coefficients H.

5.3.2 Results

Four modules accounted for more than 90% of the variability in muscle activation for each subject. All four mean synergy vectors W have been found to be similar between the two populations (average normalized scalar product = 0.8). Modules 1 and 2 showed significant differences in shape

of the time activation profiles H between populations, while all four modules showed a significantly delayed activation in amputees (Fig. 5.6).

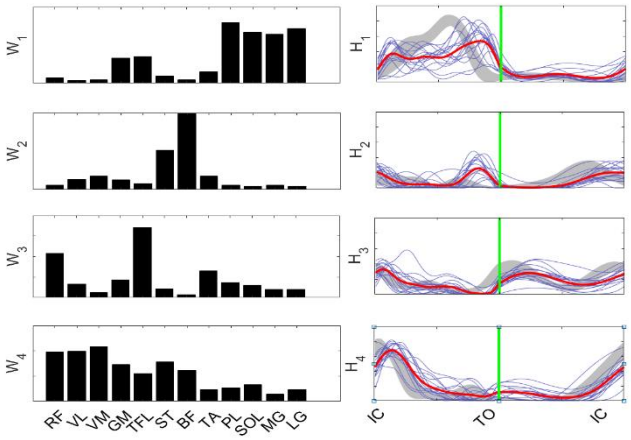

Figure 5.6. W and H, in arbitrary units. In grey data from control subject, in blue from TFA. In red the mean activation profiles for TFA. The vertical line represents the instant of toe off.

5.3.3 Discussion and Conclusions

Results suggest that both populations share the same set of synergies. The difference in the activation of the second module can be the result of a compensation, by means of an increased hip extension moment, of the decrease in the propulsion force during the swing of the prosthetic leg. The prolonged activation of the first module might reflect a stabilization mechanism of the ankle during the swing phase of the prosthetic leg. Further investigation is needed to differentiate the effect of different types of prostheses and different elapsed time from the first prosthesis implant, in order to provide a quantitative indication for a proper choice of the prosthetic device and for the most adequate treatment.

Bibliography

[1] Bateni, H., & Olney, S. J. (2002). Kinematic and Kinetic Variations of Below-Knee Amputee Gait. JPO Journal of Prosthetics and Orthotics, 14(1), 2–10. https://doi.org/10.1097/00008526-200203000-00003

[2] Tura, A., Rocchi, L., Raggi, M., Cutti, A. G., & Chiari, L. (2012). Recommended number of strides for automatic assessment of gait symmetry and regularity in above-knee amputees by means of accelerometry and autocorrelation analysis. Journal of NeuroEngineering and Rehabilitation, 9(1), 11. https://doi.org/10.1186/1743-0003-9-11

[3] Ventura, J. D., Segal, A. D., Klute, G. K., & Neptune, R. R. (2011). Compensatory mechanisms of transtibial amputees during circular turning. Gait & Posture, 34(3), 307–312. https://doi.org/10.1016/j.gaitpost.2011.05.014

[4] Vrieling, A. H., van Keeken, H. G., Schoppen, T., Otten, E., Halbertsma, J. P. K., Hof, A. L., & Postema, K. (2008). Gait initiation in lower limb amputees. Gait & Posture, 27(3), 423–430. https://doi.org/10.1016/j.gaitpost.2007.05.013

[5] Schafer, Z. A., Perry, J. L., & Vanicek, N. (2018). A personalised exercise programme for individuals with lower limb amputation reduces falls and improves gait biomechanics: A block randomised controlled trial. Gait & Posture, 63, 282–289. https://doi.org/10.1016/j.gaitpost.2018.04.030

[6] Sanders, J. E., Bell, D. M., Okumura, R. M., & Dralle, A. J. (1998). Effects of alignment changes on stance phase pressures and shear stresses on transtibial amputees: measurements from 13 transducer sites. IEEE Transactions on Rehabilitation Engineering : A Publication of the IEEE Engineering in Medicine and Biology Society, 6(1), 21–31. Retrieved from http://www.ncbi.nlm.nih.gov/pubmed/9535520

[7] Smidt GL. (1990). Gait in rehabilitation: Churchill Livingstone.

[8] Esquenazi, A. (2014). Gait analysis in lower-limb amputation and prosthetic rehabilitation. Physical Medicine and Rehabilitation Clinics of North America, 25(1), 153–167. https://doi.org/10.1016/j.pmr.2013.09.006

[9] Nolan, L., Wit, A., Dudziñski, K., Lees, A., Lake, M., & Wychowañski, M. (2003). Adjustments in gait symmetry with walking speed in trans-femoral and trans-tibial amputees. Gait & Posture, 17(2), 142–151. Retrieved from http://www.ncbi.nlm.nih.gov/pubmed/12633775

[10] Rossi, S. A., Doyle, W., & Skinner, H. B. (1995). Gait initiation of persons with below-knee amputation: the characterization and comparison of force profiles. Journal of Rehabilitation Research and Development, 32(2), 120–127. Retrieved from http://www.ncbi.nlm.nih.gov/pubmed/7562651

[11] Highsmith, M. J., Kahle, J. T., Carey, S. L., Lura, D. J., Dubey, R. V., Csavina, K. R., & Quillen, W. S. (2011). Kinetic asymmetry in transfemoral amputees while performing sit to stand and stand to sit movements. Gait & Posture, 34(1), 86–91. https://doi.org/10.1016/J.GAITPOST.2011.03.018

[12] Chitragari, G., Mahler, D. B., Sumpio, B. J., Blume, P. A., & Sumpio, B. E. (2014). Prosthetic options available for the diabetic lower limb amputee. Clinics in Podiatric Medicine and Surgery, 31(1), 173–185. https://doi.org/10.1016/j.cpm.2013.09.008

[13] Cutti, A. G., Lettieri, E., Del Maestro, M., Radaelli, G., Luchetti, M., Verni, G., & Masella, C. (2017). Stratified cost-utility analysis of C-Leg versus mechanical knees: Findings from an Italian sample of transfemoral amputees. Prosthetics and Orthotics International, 41(3), 227–236. https://doi.org/10.1177/0309364616637955

[14] Highsmith, M. J., Kahle, J. T., Miro, R. M., Cress, M. E., Lura, D. J., Quillen, W. S., … Mengelkoch, L. J. (2016). Functional performance differences between the Genium and C-Leg prosthetic knees and intact knees. Journal of Rehabilitation Research and Development, 53(6), 753–766. https://doi.org/10.1682/JRRD.2014.06.0149

[15] Kannenberg, A., Zacharias, B., Mileusnic, M., & Seyr, M. (2013). Activities of Daily Living. JPO Journal of Prosthetics and Orthotics, 25(3), 110–117. https://doi.org/10.1097/JPO.0b013e31829c221f

[16] Segal, A. D., Orendurff, M. S., Czerniecki, J. M., Schoen, J., & Klute, G. K. (2011b). Comparison of transtibial amputee and non-amputee biomechanics during a common turning task. Gait & Posture, 33(1), 41–47. https://doi.org/10.1016/J.GAITPOST.2010.09.021

[17] Shell, C. E., Segal, A. D., Klute, G. K., & Neptune, R. R. (2017). The effects of prosthetic foot stiffness on transtibial amputee walking mechanics and balance control during turning. Clinical Biomechanics, 49, 56–63. https://doi.org/10.1016/j.clinbiomech.2017.08.003

[18] Sturdy, J., Gates, D. H., Darter, B. J., & Wilken, J. M. (2014). Assessing preparative gait adaptations in persons with transtibial amputation in response to repeated medial-lateral perturbations. Gait & Posture, 39(3), 995–998. https://doi.org/10.1016/J.GAITPOST.2013.12.006

[19] Howcroft, J., Lemaire, E. D., Kofman, J., & Kendell, C. (2015). Understanding dynamic stability from pelvis accelerometer data and the relationship to balance and mobility in transtibial amputees. Gait & Posture, 41(3), 808–812. https://doi.org/10.1016/J.GAITPOST.2015.03.001
[20] Fradet, L., Alimusaj, M., Braatz, F., & Wolf, S. I. (2010). Biomechanical analysis of ramp ambulation of transtibial amputees with an adaptive ankle foot system. Gait & Posture, 32(2), 191–198. https://doi.org/10.1016/j.gaitpost.2010.04.011
[21] Sturk, J. A., Lemaire, E. D., Sinitski, E. H., Dudek, N. L., Besemann, M., Hebert, J. S., & Baddour, N. (2017). Maintaining stable transfemoral amputee gait on level, sloped and simulated uneven conditions in a virtual environment. Disability and Rehabilitation. Assistive Technology, 1–10. https://doi.org/10.1080/17483107.2017.1420250
[22] Kluge, F., Krinner, S., Lochmann, M., & Eskofier, B. M. (2017). Speed dependent effects of laterally wedged insoles on gait biomechanics in healthy subjects. Gait & Posture, 55, 145–149. https://doi.org/10.1016/j.gaitpost.2017.04.012
[23] Stoquart, G., Detrembleur, C., & Lejeune, T. (2008). Effect of speed on kinematic, kinetic, electromyographic and energetic reference values during treadmill walking. Neurophysiologie Clinique = Clinical Neurophysiology, 38(2), 105–116. https://doi.org/10.1016/j.neucli.2008.02.002
[24] Davis, R. B., Õunpuu, S., Tyburski, D., & Gage, J. R. (1991). A gait analysis data collection and reduction technique. Human Movement Science, 10(5), 575–587. https://doi.org/10.1016/0167-9457(91)90046-Z
[25] Wu, G., van der Helm, F. C. T., Veeger, H. E. J. D., Makhsous, M., Van Roy, P., Anglin, C., … International Society of Biomechanics. (2005). ISB recommendation on definitions of joint coordinate systems of various joints for the reporting of human joint motion--Part II: shoulder, elbow, wrist and hand. Journal of Biomechanics, 38(5), 981–992. Retrieved from http://www.ncbi.nlm.nih.gov/pubmed/15844264
[26] Serrao, M., Rinaldi, M., Ranavolo, A., Lacquaniti, F., Martino, G., Leonardi, L., … Pierelli, F. (2016). Gait patterns in patients with hereditary spastic paraparesis. PLoS ONE, 11(10). https://doi.org/10.1371/journal.pone.0164623
[27] Varrecchia, T., Rinaldi, M., Serrao, M., Draicchio, F., Conte, C., Conforto, S., … Ranavolo, A. (2018). Global lower limb muscle coactivation during walking at different speeds: Relationship between spatio-temporal, kinematic, kinetic, and energetic parameters. Journal of Electromyography and Kinesiology, 43, 148–157. https://doi.org/10.1016/j.jelekin.2018.09.012
[28] Cavagna, G. A., Thys, H., & Zamboni, A. (1976). The sources of external work in level walking and running. The Journal of Physiology, 262(3), 639–657. Retrieved from http://www.ncbi.nlm.nih.gov/pubmed/1011078
[29] Cavagna, G. A., Willems, P. A., Legramandi, M. A., & Heglund, N. C. (2002). Pendular energy transduction within the step in human walking. The Journal of Experimental Biology, 205(Pt 21), 3413–3422. Retrieved from
[30] Detrembleur, C., Dierick, F., Stoquart, G., Chantraine, F., & Lejeune, T. (2003). Energy cost, mechanical work, and efficiency of hemiparetic walking. Gait & Posture, 18(2), 47–55. Retrieved from http://www.ncbi.nlm.nih.gov/pubmed/14654207
[31] Don, R., Serrao, M., Vinci, P., Ranavolo, A., Cacchio, A., Ioppolo, F., … Santilli, V. (2007). Foot drop and plantar flexion failure determine different gait strategies in Charcot-Marie-Tooth patients. Clinical Biomechanics, 22(8), 905–916.
[32] de Leva, P. (1996). Adjustments to Zatsiorsky-Seluyanov's segment inertia parameters. Journal of Biomechanics, 29(9), 1223–1230. Retrieved from http://www.ncbi.nlm.nih.gov/pubmed/8872282
[33] Zatsiorsky, V., Seluyanov, V., & Chugunova, L. (1990). Methods of Determing Mass-Inertial Characteristics of Human Body Segments. Contemporasy Problems of Biomechnics.
[34] Ranavolo, A., Varrecchia, T., Rinaldi, M., Silvetti, A., Serrao, M., Conforto, S., & Draicchio, F. (2017). Mechanical lifting energy consumption in work activities designed by means of the "revised NIOSH lifting equation." Industrial Health, 55(5). https://doi.org/10.2486/indhealth.2017-0075
[35] Head, H., & Holmes, G. (1911). SENSORY DISTURBANCES FROM CEREBRAL LESIONS. Brain, 34(2–3), 102–254. https://doi.org/10.1093/brain/34.2-3.102
[36] Ivanenko, Y. P., Dominici, N., Daprati, E., Nico, D., Cappellini, G., & Lacquaniti, F. (2011). Locomotor body scheme. Human Movement Science, 30(2), 341–351. https://doi.org/10.1016/J.HUMOV.2010.04.001
[37] Neptune et al. Journal of Biomechanics 42.9 (2009): 1282-287.
[38] Wentink et al. Journal of NeuroEngineering and Rehabilitation 10.1 (2013): 87.

CHAPTER 6

6. LOWER LIMB MUSCLE COACTIVATION AND GAIT PERFORMANCE IN PATIENTS WITH HEREDITARY SPASTIC PARAPARESIS

In this chapter, text and figures have been taken from or adapted from the article "*Increased lower limb muscle coactivation reduces gait performance and increases metabolic cost in patients with hereditary spastic paraparesis*" *[2017, Clinical Biomechanics]* which was co-authored by me.

The presence of spasticity in these patients greatly impairs their walking ability and thus their autonomy and quality of life. Coactivation may be somehow linked to spasticity. For instance, a rearrangement of the interneuronal circuits may be the common neural mechanism at the bases of both features. Otherwise, coactivation may reflect the lack of selectivity by descending drive in tuning the motoneurons of agonist/antagonist muscles. In order to clarify the role of muscle coactivation on the gait performance of HSP patients, a sample of 23 HSP patients was investigated from a kinematic, kinetic, electromyographic, and energetic point of view in the work published from Clinical Biomechanics: *"Increased lower limb muscle coactivation reduces gait performance and increases metabolic cost in patients with hereditary spastic paraparesis",* which I drafted (M. Rinaldi et al., 2017).

The first aim of this study was to determine the level of coactivation of agonist-antagonist muscles at the knee and ankle joints during gait. The second aim was to evaluate the relationship between muscle coactivation during gait and limb spasticity, energy consumption, and gait performance.

Identifying the level of muscle coactivation may be helpful in individuating the rehabilitative treatments and designing specific orthosis that may provide a greater joint stability, thus restraining spasticity.

Patients	Gender	Heigth (cm)	Body Wt. (kg)	Age (yr)	Diagnosis	Onset (yr)	Duration (yr)	SPRS		
								Ashworth ankle	Ashworth knee	Total
P1	F	156	66	57	SPG5	36	21	2	2	20
P2	M	160	57	34	SPG4	1-2	33	4	3	25
P3	M	164	76	67	__AR	45	22	2	3	21
P4	M	170	73	58	SPG4	45	13	3	2	27
P5	M	177	104	24	SPG4	14	10	1	2	11
P6	M	170	88	48	__AR	10	38	2	2	13
P7	M	180	85	25	__AD	13	12	1	0	3
P8	M	182	109	49	SPG4	37	12	2	2	21
P9	F	158	69	72	SPG4	40	32	4	3	31
P10	F	162	58	43	SPG4	5	38	1	2	7
P11	F	142	56	78	SPG4	45	33	3	3	28
P12	F	159	73	56	__AR	35	21	2	3	20
P13	F	158	61	64	SPG31	15	49	1	0	12
P14	M	157	87	59	__AR	30	29	3	2	28
P15	M	164	76	32	__AR	14	18	3	4	26
P16	M	170	104	39	__AD	36	3	1	2	12
P17	M	181	81	28	SPG4	13	15	1	2	12
P18	M	161	78	58	SPG4	43	15	2	3	17
P19	M	177	103	70	SPG4	60	10	2	2	23
P20	M	165	69	28	__AD	20	8	2	3	16
P21	M	186	136	39	SPG3A	20	19	2	2	27
P22	M	161	84	62	SPG4	40	22	1	1	5
P23	M	183	78	38	SPG4	30	8	3	4	27

Table 6.1. Patients' characteristics. AD = autosomal dominant; AR = autosomal recessive; F = female; M = male; SPRS = Spastic Paraplegia Rating Scale; __ = molecular diagnosis still not available. The table lists the SPRS scores; higher scores indicate higher disease's severity.

	CI		
		r	**P**
Clinical variables			
Ankle spasticity	TA-SOL	0.542	**0.035**
Knee spasticity	VL-BF	0.491	**0.045**
Walking speed	VL-BF	-0.525	**0.010**
Other time-distance parameters*		NS	
Kinematic parameters*		NS	
Kinetic parameters			
A_{WA}*	TA-SOL (ST)	0.565	**0.006**
A_{PS}*	TA-SOL (ST)	0.517	**0.014**
Energetic parameters			
TEC* [kcal/km*kg]	VL-BF	0.429	**0.040**
	TA-SOL	0.549	**0.007**
R-step* [%]	VL-BF	-0.609	**0.002**
	TA-SOL	-0.434	**0.047**

*Table 6.2. Significant correlations (with P values) between both the coactivation indexes and clinical variables, time-distance, kinematic, kinetic and energetic parameters in HSP patients. * partial correlation. NS no significant correlation*

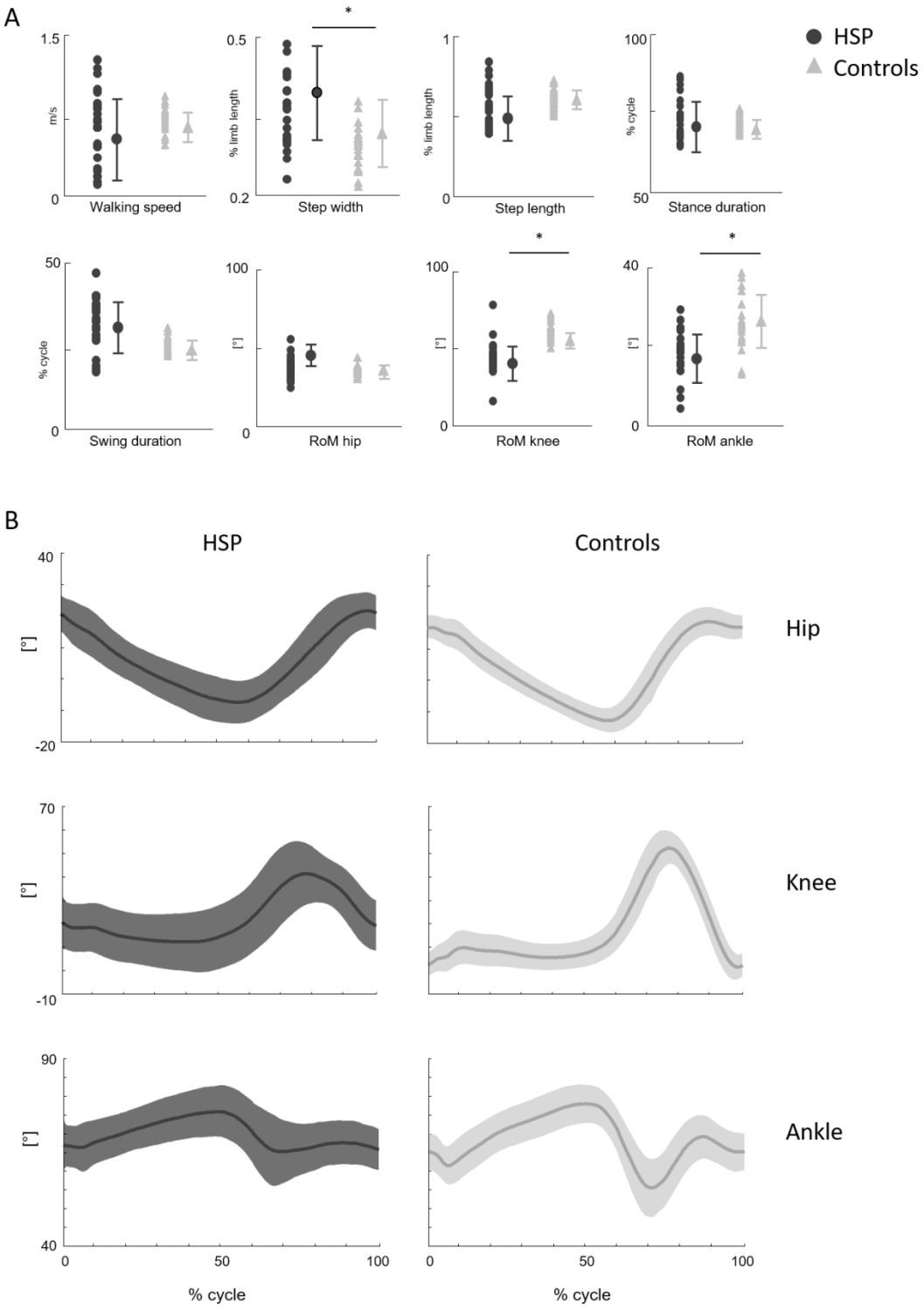

Figure 6.1. Time distance and joint kinematic parameters A: Values of each patient and control (small circles and triangles) and mean values (big circles and triangles) with SD of 23 patients and 23 controls for time distance and joint kinematic parameters. Asterisks indicate significant differences between patients and controls (P<0.05). B: Mean (with SDs in light colors) kinematic plot of lower limb joint angular displacements in the sagittal plane during the gait cycle of HSP patients (black curves) and controls (grey curves).

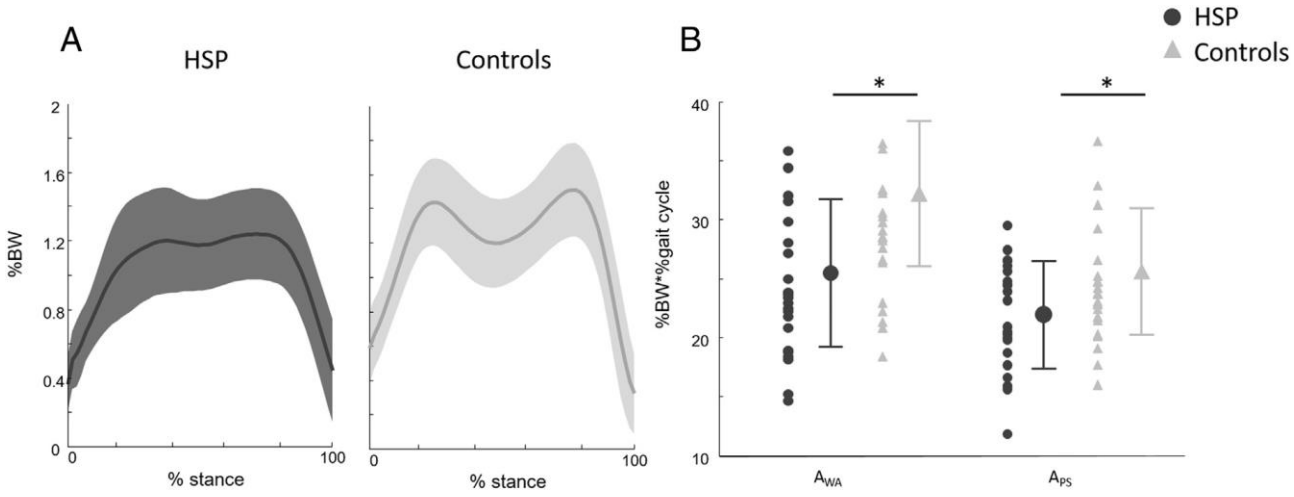

Figure 6.2. Kinetic parameters A: Mean (with SDs in light colors) kinetic plot of vertical ground reaction forces (GRF) of HSP patients (black curves) and controls (grey curves). The patterns are normalized to body weight and plotted vs. normalized stance. B: Values of each patient and control (small circles and triangles) and mean values (big circles and triangles) with SD of patients and controls for the area under GRF curves during weight acceptance (A_{WA}) and pre-swing (A_{PS}) subphases. Asterisks indicate significant differences between patients and controls ($P<0.05$). (incollare originale)

6.1 Materials and methods

Subjects

Twenty-three patients with HSP were recruited (6 women and 17 men, age: mean 49.04 (SD 16.31) years, height: mean 1.67 (SD 0.11) m, weight: mean 80.07 (SD 21.70) kg) (Table 6.1). All patients included in the study were able to walk without assistance or walking aids on a level surface. None of the patients showed any involvement of neurological systems other than the pyramidal one (e.g., cerebellar or sensory deficits). The severity of the disease was rated using the spastic paraplegia rating scale (SPRS). The spasticity of ankle and knee joint muscles was scored by the modified Ashworth scale included in the SPRS as a spasticity-related subscale [1]. Five of the twenty-three patients were taking oral antispastic drugs (baclofen or tizanidine) for 4 to 6 years. Their clinical assessment (SPRS) did not change over the last six months prior to the study. At the time of the evaluation, all patients were undergoing physical therapy, which included lower limb and stretching exercises, balance, and gait training. Twenty-three subjects were enrolled as a control group (HS):

(8 women and 15 men, age: mean 52.00 (SD 13.83) years, height: mean 1.67 (SD 0.06) m, weight: mean 71.53 (SD 11.90) kg).

All participants provided informed written consents before taking part in the study, which complied with the Helsinki Declaration and had local ethics committee approval.

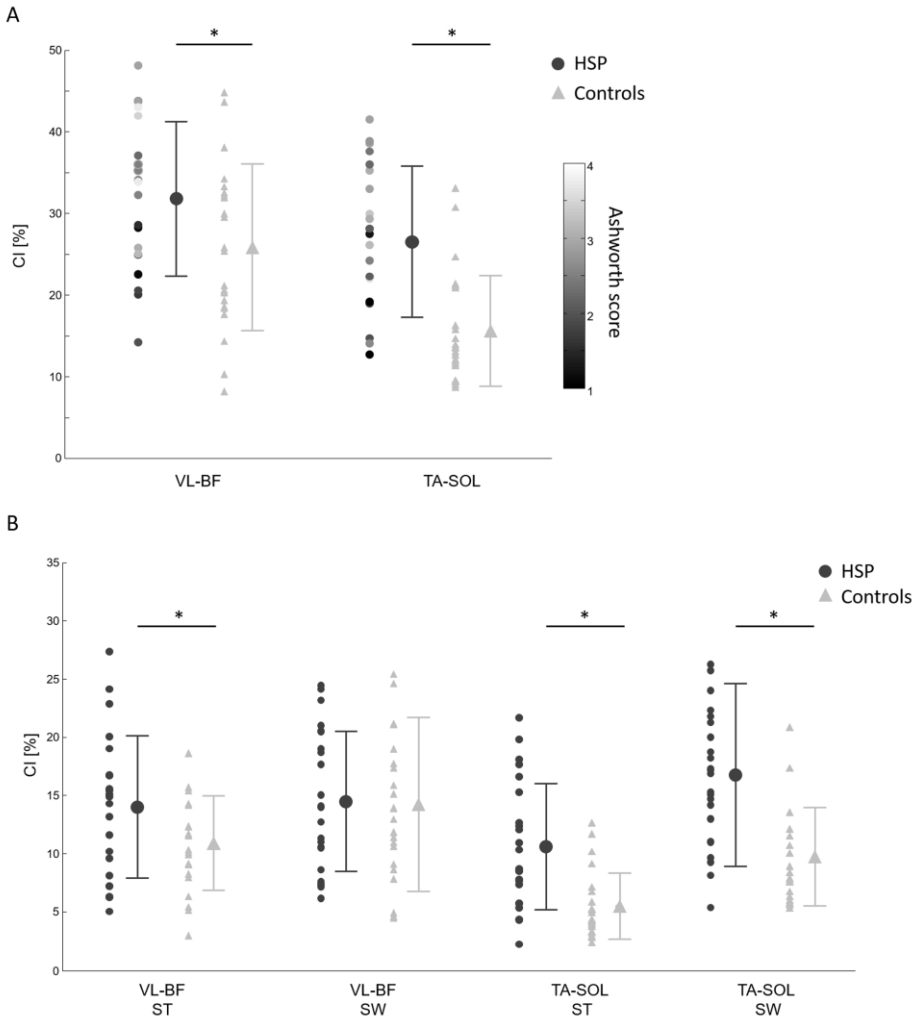

Figure 6.3. Coactivation index A: Values of each patient and control (small circles and triangles) and mean values (big circles and triangles) with SD of patients and controls for CI (area under the coactivation curve) of the ankle and knee antagonist muscles calculated in the entire gait cycle. Each circle is plotted in different shades of gray according to knee and ankle Ashworth scores on VL-BF and TA-SOL graphs, respectively. Asterisks indicate significant differences between patients and controls (P<0.05). B: Values of each patient and control (small circles and triangles) and mean values (big circles and triangles) with SD of patients and controls for CI (area under the coactivation curve) of the ankle and knee antagonist muscles calculated in the two subphases of the gait cycle (stance and swing). Asterisks indicate significant differences between patients and controls (P<0.05).

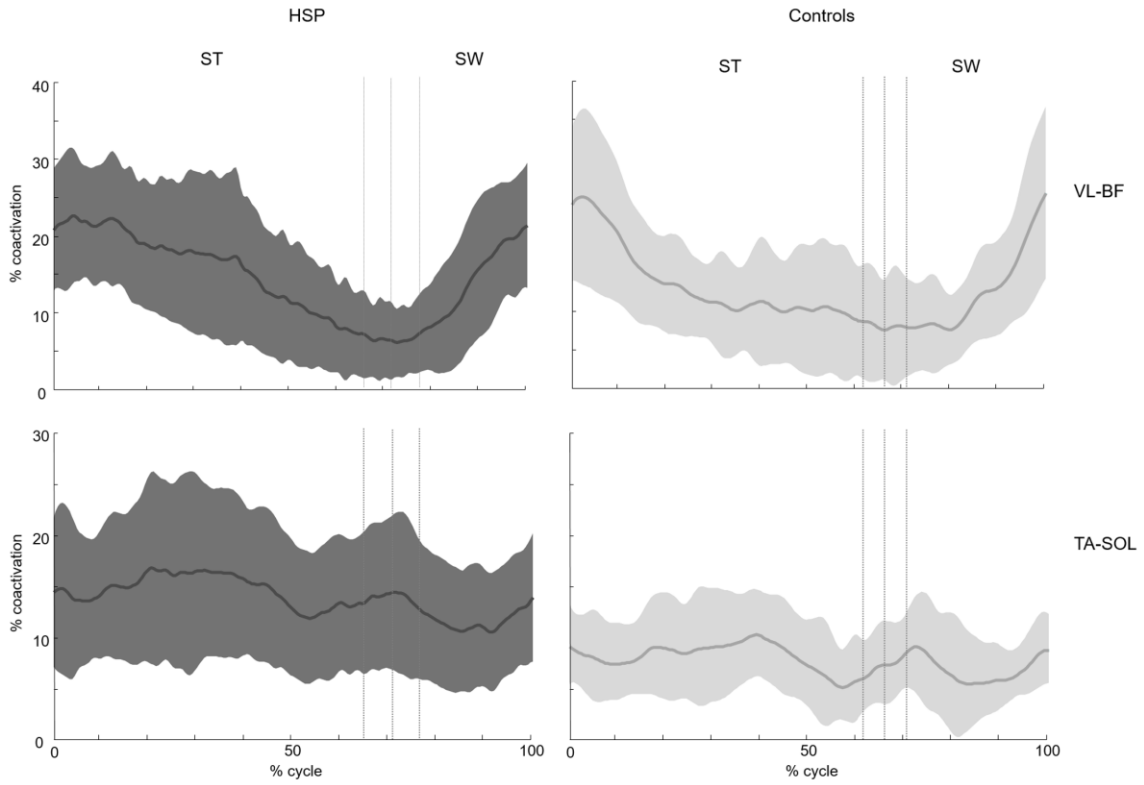

Figure 6.4. Coactivation of ankle and knee joint antagonist muscles
Mean (with SDs in light colors) plot of coactivation of ankle and knee joint antagonist muscles during the gait cycle of HSP patients (black curves) and controls (grey curves).

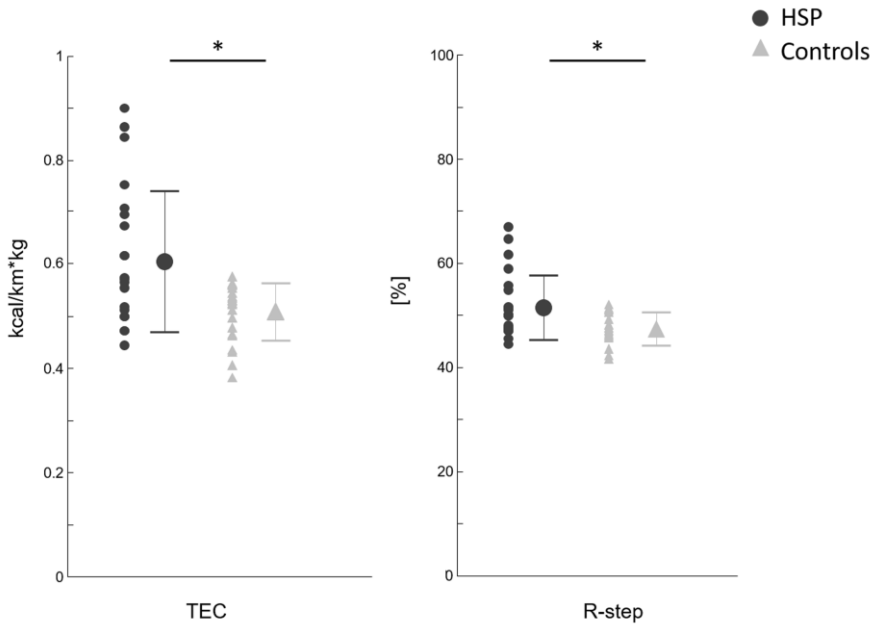

Figure 6.5. Energetic parameters. Values of each patient and control (small circles and triangles) and mean values (big circles and triangles) with SD of patients and controls for TEC and R-step during walking. Asterisks indicate significant differences between patients and controls ($P<0.05$).

Gait analysis

Kinematic data were recorded bilaterally at 300 Hz using an optoelectronic motion analysis system (SMART-D System, BTS, Milan, Italy) consisting of eight infrared cameras spaced around the walkway. Twenty-two reflective spherical markers were attached on the anatomical landmarks, in accordance with a validated biomechanical model [2]. In detail, the markers were placed over the cutaneous projections of the spinous processes of the seventh cervical vertebra and sacrum and bilaterally over acromion, anterior superior iliac spine, great trochanter, lateral femoral condyle, fibula head, lateral malleoli and metatarsal head. In addition to markers directly applied to the skin, sticks, or wand, varying in length from 7 to 10 cm, placed at 1/3 of the length of the body segment (femur and leg) were used. Anthropometric data were collected for each subject [3].

Ground reaction forces (GRFs) were acquired by two dynamometric platforms (Kistler 9286B, Winterthur, Switzerland), attached to each other in the longitudinal direction but displaced by 0.2 m in the lateral direction (sampling rate 1200 Hz).

Surface myoelectric signals were recorded at 1000 Hz using a 16-channel wireless system (FreeEMG300 System, BTS, Milan, Italy). After skin preparation, bipolar Ag/AgCl surface electrodes (2 cm diameter) were placed over the muscle belly in the direction of the muscle fibers according to the European recommendations for surface electromyography (SENIAM) and the atlas of muscle innervation zones [4,5]. Four bipolar electrodes were placed on the right side of the body on the tibialis anterior (TA); soleus (SOL); vastus lateralis (VL), and biceps femoris (BF). The acquisition of kinematic, kinetic, and surface electromyographic (sEMG) data was synchronized.

Experimental procedure

The patients and controls were asked to walk barefoot at comfortable self-selected speeds along a walkway approximately 10 m in length while looking forward. Because we were interested in natural locomotion, only general, qualitative instructions were provided. Before the recording session, the subjects practiced for a few minutes to familiarize themselves with the procedure.

Given that typical walking speeds were on the slow side in patients, we instructed the control subjects to also walk at low speeds and to compare the parameters between groups without the potential velocity bias (see speed matching procedure). Ten trials per patient and 15 trials per control (10 trials self-selected speed and 5 trials slow walking) were recorded. To avoid muscle fatigue, groups of three trials were separated by 1 min rest periods.

Speed matching procedure

The speed was matched between groups as follows: for each control group subject we considered only those trials in which their walking speed fell within the range identified by HSP patients' mean walking speed ± SD. On this basis, we selected two controls walking at self-selected speed and 21 controls walking at low speed. The Student's t-test was used to investigate differences in walking speeds between patients and controls; thus, the mean speed values were not statistically different between groups (HSP patients: mean 2.05 (SD 1.27) km/h; controls: mean 2.19 (SD 0.46) km/h; unpaired samples test, $P > 0.05$).

Data analysis

The data were processed using a 3D reconstruction software (SMART Tracker and SMART Analyzer, BTS, Milan, Italy) and MATLAB (version 8.3.0.532, MathWorks, Natick, MA, USA) software. Kinematic, kinetic, and electromyographic data were then normalized to the duration of the gait cycle and interpolated to 201 samples using a polynomial procedure.

The gait cycle was defined as the time between two successive foot contacts of the same leg. In this study, heel strike and toe-off events were determined by maximum and minimum excursions of the limb angle, defined as the angle between the vertical axis and the limb segment (from the greater trochanter to the lateral malleolus) projected on the sagittal plane [6]. When participants stepped on the force platforms, these kinematic criteria were verified by comparison with foot strike and lift-off estimated from the vertical ground reaction force, namely when this force exceeded a threshold of 7% of body weight. In general, the difference between the time events measured from kinematics

and kinetics was < 3%. Since spasticity and weakness in patients with HSP typically affect both lower limbs symmetrically , we focused our analyses on the right leg locomotor output.

Time–distance parameters

The walking speed (km/h), stance duration (% gait cycle), swing duration (% gait cycle), step length (% limb length), and step width (% limb length) were calculated for each subject.

Walking speed was calculated as the modulus of the mean over the strides durations of the first derivative malleolus markers' positions in the three spatial directions. The mean gait speed is the mean of the gait speeds among all the strides considered for each subject.

Kinematic parameters

We computed the anatomical angles of the hip, knee, and ankle joints in the sagittal plane. From these variables, we derived the RoM at each joint, defined as the difference between the maximum and minimum values during the gait cycles.

Kinetic parameters

The right vertical GRF was calculated and normalized to the body mass. We considered the values of the area under GRF curve during weight acceptance (A_{WA}) and pre-swing (A_{PS}) subphases of the gait cycle.

sEMG parameters

The raw EMG signals were band-pass filtered using a zero-lag third-order Butterworth filter (20–450 Hz), rectified, and low-pass filtered with a zero-lag fourth-order Butterworth filter (10 Hz). For each individual, the EMG signal from each muscle was normalized to its peak value across all trials. From the elaborated sEMG signals, we calculated, sample by sample, the VL–BF and TA–SOL coactivation values as follows [7]:

$$CA = [(EMG_H + EMG_L)/2] * (EMG_L/EMG_H)$$

where EMG_H and EMG_L represented the highest and the lowest activity between the antagonist muscle pairs. A coactivation index (CI) during the two subphases of gait was then obtained by

calculating the area under the coactivation curve in each cycle window: the stance and swing. In order to obtain a global measure of the coactivation level, the CI was evaluated as well during the entire gait cycle.

Energetic behavior

We measured the mechanical behavior in terms of energy recovery and energy consumption of the entire skeletal muscle system in relation to the whole body center of mass (CoM) during walking. This methodology has been validated in both normal [8, 9] and abnormal gait patterns [10, 11]. The whole body CoM was calculated by means of the "reconstructed pelvis method" [12, 13] considering the kinematic data. Adopting this method, the CoM coincides with the pelvic centre, which is the geometric centre of the triangle formed by the markers over the two anterior superior iliac spines and sacrum.

The kinetic energy (E_k) associated with CoM displacements during the gait cycle was calculated as the sum of the kinetic energy on the x (E_{kx}), y (E_{ky}), and z (E_{kz}) axes as follows:

$$E_k = E_{kx} + E_{ky} + E_{kz} = \frac{1}{2}m\left(v_x^2 + v_y^2 + v_z^2\right),$$

where m and v_x, v_y and v_z are the mass and velocity components of the CoM, respectively. Furthermore, the potential energy (E_p) associated with the CoM was calculated as

$$E_p = mgh$$

where h is the vertical (y) component of the CoM, and g is the acceleration of gravity (m/s^2).

The total mechanical energy (E_{tot}) associated with the CoM was computed as the sum of E_k and E_p. We calculated the fraction of mechanical energy (R-step) recovered during each walking step [9], as follows:

$$R - step = \frac{W_p^+ + W_{kf}^+ - W_{tot}^+}{W_p^+ + W_{kf}^+} x\ 100 = \left(1 - \frac{W_{tot}^+}{W_p^+ + W_{kf}^+}\right) x\ 100,$$

where W_p^+, W_{kf}^+, W_{tot}^+ represent the positive work (sum of the positive increments over one step) produced by the gravitational potential energy, kinetic energy of forward motion, and total

mechanical energy, respectively. We calculated as well the total energy consumption (TEC) as the sum of the negative (W_{tot}^{-}) and positive work (W_{tot}^{+}), each divided by their respective efficiencies[8], as follows:

$$TEC = \frac{W_{tot}^{+}}{1.20} + \frac{W_{tot}^{-}}{0.25}.$$

Given the cyclic nature of walking, the positive work done at each step is equal to the negative work, which thus changes the previous formula to

$$TEC = \frac{W_{tot}^{+}}{0.21}.$$

TEC was then normalized to the body weight and step length. For each subject, the R-step and normalized TEC values of all the steps were averaged.

Statistical analysis

The Kolmogorov–Smirnov and Shapiro–Wilk test were used to analyze the normal distribution of the data. Unpaired two-sample t-test or Mann–Whitney test were used to compare the kinematic, sEMG, and energetic data of HSP patients and controls. Cohen's d values were evaluated as well to estimate the effective size for comparison between the two means. The correlation between muscle coactivation patterns and clinical scores (knee and ankle-spasticity Ashworth score) was performed using Pearson's rank correlation coefficient.

Partial correlations were used to analyze correlations between muscle coactivation indexes and time–distance, kinematic, kinetic, and energetic parameters controlling the walking speed.

Descriptive statistics included means and SD, and significance level was set at $P < 0.05$. All the analyses were performed using SPSS 20.0 (SPSS Inc. Chicago, IL, USA) and MATLAB (version 8.3.0.532, MathWorks, Natick, MA, USA) software.

6.2 Results

Demographic characteristics

No significant differences were found between HSP patients and controls with respect to age, weight, and height values (P>0.05).

Time–distance parameters

Patients with HSP walked statistically slower than HS (HSP: mean 2.05 (SD 1.27) km/h, HS: mean 2.83 (SD 0.67), P=0.005). At matched speed, HSP patients showed no significant differences in almost all time–distance parameters (P>0.05) except for step width (P=0.002, d=0.939), significantly increased in patients (n=23) than controls (n=23) (Fig.6.1A).

Kinematic parameters

At matched speed, significantly lower values in knee (P<0.001, d=1.664) and ankle (P<0.001, d=1.474) RoMs were found in patients compared with controls (Fig. 6.1A). Fig. 6.1B shows the mean joint kinematic traces of HSP patients and controls.

Kinetic parameters

Analysis of the vertical GRF (Fig. 6.2A) showed significantly lower values of A_{WA} and A_{PS} (P=0.004, d=0.915 and P=0.042, d=0.630, respectively) in patients compared with controls at matched speed (Fig. 6.2B).

sEMG parameters

At matched speed, HSP patients showed significantly higher values of coactivation index throughout the gait cycle both for the VL–BF (P=0.04, d=0.625) and the TA–SOL (P<0.001, d=1.343) pairs of antagonist muscles (Fig. 6.3A). Analysis of the CI in different gait subphases showed significantly higher values in HSP patients, compared with controls, in the stance (P<0.001, d=1.175) and swing (P<0.001, d=1.132) phases for the TA–SOL muscles and in the stance (P=0.04,

d=0.603) phase for the VL–BF muscles (Fig. 6.3B). In Fig. 6.4, the coactivation of ankle and knee joint antagonist muscles is plotted during the gait cycle.

Energetic parameters

Both TEC (P=0.016 and d=0.968) and R-step (P=0.033 and d=0.844) values were significantly higher in HSP patients than in controls at matched speed (Fig. 6.5).

Correlations

Regarding the clinical variables, significant positive correlations were found between the Ashworth score for both the knee and ankle joints and CI for VL–BF and TA–SOL muscles, respectively. A significant negative correlation was found between the CI for VL–BF muscles and walking speed, while no significant partial correlations were found between the CI and other time–distance parameters and kinematic variables. Significant positive partial correlations were found between CI for TA–SOL muscles during the stance phase and both A_{WA} and A_{PS}. Significant positive partial correlations were observed between TEC and coactivation indexes for both VL–BF and TA–SOL muscles. Significant negative partial correlations were observed between R-step and coactivation indexes for both VL–BF and TA–SOL muscles.

6.3 Discussion and Conclusions

This study described the coactivation of the lower limb joint antagonist muscles and its relationship with biomechanics of locomotion in 23 patients affected by HSP.

The main findings of this study are: i) the knee and ankle joint muscle coactivation is higher in HSP patients compared with controls, in both the entire gait cycle and subphases of gait; ii) both knee and ankle coactivation patterns are positively correlated with knee and ankle joints spasticity; iii) both knee and ankle coactivation patterns are positively correlated with energy consumption and negatively correlated with energy recovery.

In our study, we found that patients with HSP showed a significantly higher level of lower limb coactivation of both knee and ankle antagonist muscles compared with controls (Fig. 6.3A). Abnormal coactivation patterns at both knee and ankle joints during gait have been demonstrated in patients with several central nervous system lesions including Parkinson's disease, cerebellar ataxia, and multiple sclerosis. In these diseases, muscle coactivation has been supposed, on one hand, to be the result of balance-related adaptive compensatory mechanisms aimed at reducing instability, such as in cerebellar ataxia. On the other hand, it reflects the expression of a primary deficit owing to either motor control impairment and joint rigidity such as in Parkinson's disease.

In our study, we found that higher values of Ashworth scores for both knee and ankle joint were associated with increased coactivation of knee and ankle antagonist muscles, respectively (Table 6.1). This finding suggests that lower limb coactivation in patients with HSP reflects a primary deficit linked to lower limb spasticity. In this regard, spasticity and coactivation may share common physiopathological mechanisms. In patients with spasticity, e.g., stroke and spinal injury, plastic rearrangements have been demonstrated at several levels throughout the central nervous system including the motor cortex and spinal cord [14]. In patients with HSP, the abnormal coactivation pattern may reflect both or either abnormal descending motor commands and/or plastic rearrangement of the spinal circuitries [15, 16] which, in turn, lead to a lack of selectivity of the descending motor drives to motoneuronal pools.

On analyzing the CI in the subphases of the gait cycle, we found that both the ankle and knee joint muscles were more coactivated in patients than in controls during the stance phase (Figs. 6.3B and 6.4). Conversely, during the swing phase we observed only an increased ankle joint coactivation (Figs. 6.3B and 6.4). These findings suggest that in corticospinal tract lesions, the abnormal coactivation pattern mainly involves the distal lower limb muscles (ankle joint), as also happens for the upper limbs [17], and that there is a distal-proximal gradient in the coactivation pattern, related to the mechanical effort, e.g., unloading (swing phase) or loading (stance phase) of the limb. A decreased cortical inhibition after lesion of corticospinal tract, which mainly controls distal muscles

in more selective movements, may be bypassed by brain stem extrapyramidal pathways such as vestibulospinal, reticulospinal, and tectospinal tracts, thereby inducing the abnormal patterns of muscle contraction [18]. according to the mechanical demands of the locomotor task (Dierick et al., 2002). In this regard, the increased lower limb joint coactivation reflects the inability of the neuromuscular system to modulate muscle activation according to the external requirements that differ depending on the gait phase [19].

Our results showed that HSP patients increase both energy recovery and consumption during gait compared with healthy subjects (Fig. 6.5). The increased energy consumption might be caused by a greater mechanical effort achieved by patients to walk against a constant mechanical constraint provided by the lower limb spasticity [17, 20]. In addition, the positive correlation between coactivation indexes and the energy consumption strongly suggests that the unselective recruitment of the agonist and antagonist muscles, resulting in nonfunctional abnormal muscle activations, determine an excessive energy expenditure. Although a higher energy recovery was observed in HSP patients compared with controls, a negative correlation was found with the muscle coactivation. This seems to suggest that the basic energy recovery mechanism, which is an efficient way to reduce the energetic cost of walking [21], is still exploited by HSP patients, as also observed in parkinsonian patients [22]. In this aspect, the abnormal muscle coactivation is an unfavorable factor for the energy recovery in these patients.

Furthermore, we investigated the relationships between lower limb muscle coactivation and kinetics during stance phase. We found that the increased ankle muscle coactivation during the stance phase was positively correlated with increased values of A_{WA} and A_{PS}. According to these results, the increased ankle muscle coactivation might influence weight acceptance and push-off mechanisms in patients with HSP. However, the positive correlation might suggest that HSP patients try to increase the joint torque production through an increased of motor recruitment which, in turn, results in an increased co-activation due to the inability of the CNS in tuning antagonist muscles activity.

In conclusion, in the present study, we have investigated the lower limb muscle coactivation and its relationship with limb spasticity, energetic mechanisms, and gait performance in patients with HSP. Our findings clearly suggest that abnormal lower limb muscle coactivation in these patients reflects a primary deficit linked to lower limb spasticity. In addition, these abnormalities influence the mechanisms of both energetic consumption and recovery during walking. A comprehensive treatment of HSP should take into account also the changes in muscle properties [23]. To achieve adequate treatment, it is crucial to address the mechanisms underlying the impaired function. These results may be useful for evaluating the pharmacological and rehabilitative treatments aimed at reducing the requirement for excessive antagonist muscle coactivation and restraining spasticity.

6.4 Bibliography

[1] Schüle, R., Holland-Letz, T., Klimpe, S., Kassubek, J., Klopstock, T., Mall, V., Otto, S.,Winner, B., Schöls, L., 2006. The Spastic Paraplegia Rating Scale (SPRS): a reliable and valid measure of disease severity. Neurology 67 (3), 430-434.

[2] Davis III, R.B., Õunpuu, S., Tyburski, D., Gage, J.R., 1991. A gait analysis data collection and reduction technique. Human Movement Science 10, 575–587.

[3] Winter, D.A., 1979. Biomechanics of Human Movement, 2nd ed. Wiley and Sons (Ed.). New York.

[4] Barbero, M., Merletti, R., Rainoldi, A., 2012. Atlas of Muscle Innervation Zones: Understanding Surface Electromyography and Its Applications. Springer, New York.

[5] Hermens, H.J., Freriks, B., Disselhorst-Klug, C., Rau, G., 2000. Development of recommendations for SEMG sensors and sensor placement procedures. Journal of Electromyography and Kinesiology 10 (5), 361-374.

[6] Borghese, N.A., Bianchi, L., Lacquaniti, F., 1996. Kinematic determinants of human locomotion. Journal of Physiology 494, 863–879.

[7] Rudolph, K.S., Axe, M.J., Snyder-Mackler, L., 2000. Dynamic stability after ACL injury: who can hop? Knee Surgery Sports Traumatology Arthroscopy 8, 262–269.

[8] Cavagna, G.A., Thys, H., Zamboni, A., 1976. The sources of external work in level walking and running. Journal of Physiology 262 (3), 639-657.

[9] Cavagna, G.A., Willems, P.A., Legramandi, M.A., Heglund, N.C., 2002. Pendular energy transduction within the step in human walking. Journal of Experimental Biology 205 (21), 3413-3422.

[10] Detrembleur, C., Dierick, F., Stoquart, G., Chantraine, F., Lejeune, T., 2003. Energy cost, mechanical work, and efficiency of hemiparetic walking. Gait & Posture 18 (2), 47-55.

[11] Don, R., Serrao, M., Vinci, P., Ranavolo, A., Cacchio, A., Ioppolo, F., Paoloni, M., Procaccianti, R., Frascarelli, F., De Santis, F., Pierelli, F., Frascarelli, M., Santilli, V., 2007. Foot drop and plantar flexion failure determine different gait strategies in Charcot-Marie-Tooth patients. Clinical Biomechanics 22 (8), 905-916.

[12] Whittle, M.W., 1997. Three-dimensional motion of the center of gravity of the body during walking. Human Movement Science 16 (2), 347-355.

[13] Ranavolo, A., Conte, C., Iavicoli, S., Serrao, M., Silvetti, A., Sandrini, G., Pierelli, F., Draicchio, F., 2011. Walking strategies of visually impaired people on trapezoidal- and sinusoidal- section tactile ground surface indicators. Ergonomics 54 (3), 246-256.

[14] Filli, L., Schwab, M.E., 2015. Structural and functional reorganization of propriospinal connections promotes functional recovery after spinal cord injury. Neural Regeneration Research 10 (4), 509-513. Review

[15] Nardone, R., Trinka, E., 2015. Reorganization of spinal neural circuitry and functional recovery after spinal cord injury. Neural Regeneration Research 10 (2), 201-202.

[16] Purves, D., Augustine, G.J., Fitzpatrick, D., Lawrence, C., LaMantia, A.S., McNamara, J.O., Williams, S.M., 2001. Neuroscience. Damage to Descending Motor Pathways: The Upper Motor Neuron Syndrome. Sinauer Associates, Sunderland.

[17] Ohn, S.H., Yoo, W.K., Kim, D.Y., Ahn, S., Jung, B., Choi, I., Lee, N.J., Jung, K.I., 2013. Measurement of synergy and spasticity during functional movement of the post-stoke hemiplegic upper limb. Journal of Electromyography and Kinesiology 23 (2), 501-517.

[18] Kamper, D.G., Rymer, W.Z., 2001. Impairment of voluntary control of finger motion following stroke: role of inappropriate muscle coactivation. Muscle Nerve 24 (5), 673–681.

[19] Mileva, K., Turner, D., 2003. Neuromuscular and biomechanical coupling in human cycling: adaptations to changes in crank length. Experimental Brain Research 152 (3), 393-403.

[20] Ropars, J., Lempereur, M., Vuillerot, C., Tiffreau, V., Peudenier, S., Cuisset, J.M., Pereon, Y., Leboeuf, F., Delporte, L., Delpierre, Y., Gross, R., Brochard, S., 2016. Muscle Activation during Gait in Children with Duchenne Muscular Dystrophy. PLoS One 11 (9).

[21] Neptune, R.R., Zajac, F.E., Kautz, S.A., 2004. Muscle mechanical work requirements during normal walking: The energetic cost of raising the body's center-of-mass is significant. Journal of Biomechanics 37 (6), 817–825.

[22] Dipaola, M., Pavan, E.E., Cattaneo, A., Frazzitta, G., Pezzoli, G., Cavallari, P., Frigo, C.A., Isaias, I.U., 2016. Mechanical Energy Recovery during Walking in Patients with Parkinson Disease. PLoS One 11 (6).

[23] Rösche J., 2002. Treatment of spasticity. Spinal Cord 40, 261–262.

CHAPTER 7

7. LOWER LIMB MUSCLE COACTIVATION DURING WALKING AT DIFFERENT SPEEDS

In this chapter, text and figures have been taken from or adapted from the article "*Global lower limb muscle coactivation during walking at different speeds: relationship between spatio-temporal, kinematic, kinetic and energetic parameters" [2018*, Journal of Electromyography and Kinesiology*]*, which was co-authored by me.

The motor system coordinates muscles, combines and hierarchically controls muscle synergies, regulates local spinal interneuronal reflexes, and synchronizes the neural systems, throughout the CNS, into an integrated and adaptive motor behavior. Thus, a global characterization of lower limb muscle coactivation during walking may be helpful to understand the general strategy adopted by the CNS to control the whole lower limb depending on the motor context i.e., gait phases, balance, speed, and metabolic cost. We hypothesized that the simultaneous activation of the lower limb muscles was modulated by gait speed and torque production and correlated with energy cost and gait stability. In the work published from Journal of Electromyography and Kinesiology, 2018: "*Global lower limb muscle coactivation during walking at different speeds: relationship between spatio-temporal, kinematic, kinetic and energetic parameters*", we used a time-varying multi-muscle coactivation function (TMCf) with the aim of investigating the relationship between global lower limb muscle coactivation and gait cycle, speed, ground reaction force (GRF), gait variability, and mechanical energy consumption in a sample of healthy subjects.

7.1 Materials and methods

Subjects

Twenty healthy subjects were recruited (8 women and 12 men, mean age: 40±13.81 years, BMI: 24.86±3.35 kg/m^2). None of the subjects had pathologies known to influence the normal gait pattern. All participants provided informed written consents, which complied with the Helsinki Declaration and had local ethics committee approval.

Experimental procedure

Surface myoelectric signals were recorded at 1000 Hz using a bipolar 16-channel wireless system (FreeEMG300 System, BTS). After skin preparation, Ag/AgCl surface electrodes (Kendall ARBO) were placed over the muscle belly in the direction of the muscle fibers according to the European Recommendations for Surface Electromyography [1]. A pre-processing filtering and denoising procedure was performed (Hamming filter between 10 and 400 Hz and common mode reaction ratio equal to 100 dB). Electrodes pairs (inter-electrodes distance 2 cm) were placed unilaterally on the dominant side of each participant on the gluteus medius, rectus femoris, vastus lateralis, vastus medialis, tensor fascia lata, semitendinosus, biceps femoris, tibialis anterior, gastrocnemius medialis, gastrocnemius lateralis, soleus and peroneus longus.

Ground reaction forces (GRFs) were acquired at the sampling rate of 680 Hz by eight dynamometric platforms (P6000, BTS).

Kinematic data were recorded by using an eight infrared cameras optoelectronic motion analysis system at a sampling frequency of 340 Hz (SMART-DX 6000 System, BTS). Twenty-two reflective spherical markers were attached on the anatomical landmarks [2]. Acquisition of sEMG, kinetic and kinematic data was synchronized.

Subjects were asked to walk barefoot at comfortable self-selected (SS), low (L) and fast (F) gait speeds along a walkway approximately 10 m in length. Because we were interested in natural locomotion, only general, qualitative, verbal instructions (no analog or digital metronomes were

used) were provided. Before the recording session, the subjects practiced for a few minutes to familiarize themselves with the procedure. Ten trials per subjects and per gait speeds (total 30 trials) were recorded.

Data analysis

The data were processed using a 3D reconstruction software (SMART Tracker and SMART Analyzer, BTS) and MATLAB (8.3.0.532, MathWorks). Electromyographic, kinetic and kinematic data were time-normalized to the duration of the gait cycle (time between two successive foot contacts of the same leg) and interpolated to 201 samples using a polynomial procedure. Heel strike and toe-off events were determined as in Serrao et al, 2016.

Global coactivation of lower limb muscles

The raw sEMG signals were band-pass filtered using a zero-lag third-order Butterworth filter (20–400 Hz), full wave rectified, and low-pass filtered with a zero-lag fourth-order Butterworth filter (10 Hz). For each individual, the sEMG signal from each muscle was normalized to its peak value across all trials [3]. From the processed sEMG signals, we calculated the simultaneous activation of the twelve lower limb muscles by considering the time-varying multi-muscle coactivation function (TMCf) [4]. This sigmoid-weighted, time-dependent function for the inclusion of multiple muscles during walking was designed to receive as input full wave rectified, low-pass filtered and 0-100 amplitude normalized sEMG signals. Sample values of these function are ranged between 0 and 100 and are calculated by the following equation:

$$TMCf(d(i),i) = \left(1 - \frac{1}{1+e^{-12(d(i)-0.5)}}\right).\frac{\left(\sum_{m=1}^{M} EMG_m(i)/M\right)^2}{max_{m=1\ldots M}[EMG_m(i)]}$$

where M is the number of muscles considered, $EMG_m(i)$ is the sEMG sample value of the m_{th} muscle at the instant i, d(i) is the mean of the differences between each pair among the twelve $EMG_m(i)$ samples at the instant i:

$$d(i) = \left(\frac{\sum_{m=1}^{M-1} \sum_{n=m+1}^{M} |EMG_m(i) - EMG_n(i)|}{(M!/(2!\,(M-2)!))} \right)$$

$M!/2!\,(M-2)!$ is the total number of possible differences between each pair of $EMG_m(i)$. The 201 samples $TMCf(d(i), i)$ has the following properties: inverse relationship with the mean of the differences d(i), values close to the mean activation of the m(i) muscle sample values considered when d(i) is close to 0, and values close to 0 when d(i) is close to 1. In particular, the smaller the differences in muscle samples activation are, the closer the d(i) values become to 0 and the closer the sigmoid-coefficient values become to 1, leaving the $TMCf(d(i), i)$ value close to the value of its mean. Vice versa, the greater the differences in muscle activations are, the more d(i) increases and the more the sigmoid-coefficient decreases, thereby reducing the TMCf (d(i),i) values. For each subject and for each gait speed, data over individual strides were calculated and then averaged across cycles.

Full width at half maximum and center of activity

For each subject and for each gait speed, we computed the full width at half maximum ($FWHM_{TMCf}$) and the center of activity (CoA_{TMCf}) to characterize in terms of time-amplitude the TMCf curves and to understand where most co-activation is concentrated within the gait cycle. $FWHM_{TMCf}$ was calculated as the sum of the time durations during which the TMCf curve is higher than its half maximum (see Fig. 7.1) and represent a measure of the width of the TMCf peak at the half height position. The CoA_{TMCf} was calculated using circular statistics as follow:

$$A = \sum_{i=1}^{200} (\cos\theta_t \times EMG_i)$$

$$B = \sum_{i=1}^{200} (\sin\theta_t \times EMG_i)$$

$$CoA = \tan^{-1}\left({}^{B}/_{A}\right)$$

and plotted in polar coordinates to understand if the distribution of coactivation remains unaltered across different speed conditions. For each subject and for each gait speed, data over individual strides were calculated and then averaged across cycles.

Coefficient of multiple correlation

We used the coefficient of multiple correlation (CMC) as a measure of the overall waveform similarity of a group of curves [5]. The closer to 1 the CMC is, the more similar the waveforms are: in the range 0-0.3 the correlation is weak, in 0.3-0.7 the correlation is moderate and 0.7-1 it is strong. In particular, for each gait speed (L, SS, F), we calculated the intra-subject similarity ($CMC_{\_IS}$) for TMCf (CMC_{TMCf_IS}) among all the TMCf curves of all strides for each subject. Then we computed the mean and standard deviation between the $CMC_{\_IS}$ of all subjects within each gait speed. Furthermore, we evaluated the between-subjects similarity on the mean TMCf curves (CMC_{TMCf_BS}) of all subjects to verify the repeatability between subjects within each gait speed. Finally, we calculated the similarity among the mean TMCf curves at the three gait speeds, evaluated among all the subjects (CMC_{TMCf_speed}) to verify the repeatability among the three gait speed.

Kinetic parameters

The vertical component of GRFs (Vertical Force, VF) provided by the dynamometric platforms, for each gait speed were normalized to the subject's body weight [4].

To characterize VF curves, we computed the full width at half maximum ($FWHM_{VF}$) and the center of activity (CoA_{VF}) during the gait cycle.

Cross-correlation analysis

In order to have information on the similarity of timing and shape of TMCf (relating to the stance phase) and VF curves at the three gait speeds (L, SS and F) we used the cross-correlation analysis [6].

A normalized cross-correlation function $R_{xy}(k)$ was calculated as in Nelson-Wong et al, 2009. $R_{xy}(k)$ revealed the shape similarity between the two signals as a scalar between 0 and 1.

Specifically, the $R_{xy}(k)$ curves were calculated between the mean TMCf curves and the mean VF curves (across the subjects) for each gait speed ($R_{L,}$ $R_{SS,}$ R_F).

The maximum value (R_{max}) of the cross-correlation curves for each gait speed ($R_{L\_max,}$ $R_{SS\_max,}$ R_{F_max}) was used as an index of TMCf and VF curves similarity in terms of shape.

The temporal shift, or phase delay (τ^*), indicates if similar events in the cross-correlated signals are either simultaneous ($\tau^* = 0$) or time delayed. It has units of time, and can vary between 0 and the total duration of the record in both positive and negative directions [7]. The value of τ^* where the maximal correlation occurs was used for determining similarities and differences in timing between the TMCf and VF curves at the three gait speeds ($\tau^*_{L,}$ $\tau^*_{SS,}$ τ^*_F).

Energetic cost parameters

In order to investigate the relationship between the TMCf and the mechanical energy behavior, we measured the energy recovery (R-step) during each walking step [8] and total energy consumption (TEC) of the entire skeletal muscle system in relation to the whole body center of mass during walking, calculated by means of the "reconstructed pelvis method". For each subject, the R-step and TEC (normalized to the body weight and step length) values of all the steps were averaged. The former is an index of storage capacity and reuse kinetic energy during walking, the latter is an index of energy expenditure per unit of distance traveled during walking.

Spatio–temporal and kinematic parameters

The walking speed, cadence, stride length, step width, stance duration, swing duration, first and second double support duration were calculated for each subject. We computed the anatomical angles of the hip, knee, and ankle joints in the sagittal plane and the anatomical angles of trunk and pelvis in the three planes of space. From these variables, the range of motion (RoM) were derived as the difference between the maximum and minimum values during the gait cycles.

Statistical analysis

The Shapiro–Wilk test were used to test the normal distribution of the data. To evaluate the presence of significant differences between each gait speed pair (L vs SS, L vs F and SS vs F) and the effect of the gait speed on the kinetic, kinematic, sEMG (FWHM and CMC_{TMCf_IS}) and energetic data, we performed a one-way ANOVA among the three walking speeds. Post-hoc analyses were performed using a paired *t* test with Bonferroni's corrections when significant differences were observed in the ANOVA. To evaluate the effect of the gait speed on the CoA across the gait cycle we used the Watson-Williams test for circular data [9].

To investigate the relationship between the TMCf and kinetic curves we evaluated the similarity between TMCf and VF waveforms, by using the cross-correlation analysis.

Correlation analysis was performed using Pearson's rank correlation coefficient between CoA (evaluated on TMCf) and both R-step and TEC to investigate the relationship between the TMCf and the mechanical energy behavior. Furthermore, the partial correlation analysis was performed between CoA_{TMCf} and gait parameters, controlling for the effect of gait speed. Descriptive statistics included means ± SD, and significance level was set at $p < 0.05$. All the analyses were performed using SPSS 20.0 (SPSS Inc. Chicago, IL, USA) and MATLAB (8.3.0.532, MathWorks, USA).

7.2 Results

The values were 0.887 ± 0.174 for L speed, 1.121±0.173 for SS speed and 1.563±0.267 for F speed. A significant effect of gait speed condition was found on walking speed (main effect, $F_{(2,57)}=81.761$, $p<0.001$. Post hoc analysis showed significant differences between L and SS, L and F and SS and F for walking speed ($p<0.001$).

Lower limb global co-activation findings

$FWHM_{TMCf}$ and CoA_{TMCf}

The global co-activation of the lower limb muscles, recorded at L, SS and F speeds, is shown in Cartesian coordinates as mean linear envelop (Fig. 7.2A) and, in polar coordinates, as mean circular envelop (Fig. 7.2B) and as single and mean CoA values (Fig. 7.2C), all expressed as percentage of gait cycle.

A significant effect of gait speed was found on $FWHM_{TMCf}$ (main effect, $F_{(2,57)}$=5.046, p=0.010). Post-hoc analysis revealed significant higher values at L than at SS (57.00 ± 24.28 vs 38.15 ± 20.24, p=0.016) and significant higher values at L than at F (57.00 ± 24.28 vs 40.30 ± 16.34, p=0.038). No differences were found between SS and F (57.00 ± 24.28 vs 40.30 ± 16.34, p>0.05) (Figure 8.2B). Significant differences were found in CoA_{TMCf} between L and SS (24.11 ± 6.64 % of gait cycle vs 17.91 ± 5.81 % of gait cycle; $F_{(1,38)}$=5.553; p=0.002) and L and F (24.11 ± 6.64 % of gait cycle vs 18.21 ± 6.48 % of gait cycle; $F_{(1,38)}$=8.827; p=0.005). No significant differences were found between SS and F (17.91 ± 5.81 % of gait cycle vs 18.21 ± 6.48 % of gait cycle; $F_{(1,38)}$=1.1013; p>0.05). (Fig. 7.2C).

CMC_{TMCf}

The CMC_{TMCf_IS} values were 0.844±0.061 for L speed, 0.867±0.065 for SS speed, 0.884±0.100 for F speed. No significant effect of gait speed on CMC_{TMCf_IS} was found at Anova test ($F_{(2,57)}$=0.490, p=0.614). Furthermore the CMC_{TMCf_BS} values were 0.734 for L speed, 0.725 for SS speed and 0.714 for F speed. Finally, the CMC_{TMCf_speed} value was 0.944.

Kinetic parameters

$FWHM_{VF}$ and CoA_{VF}

The curves of vertical forces, recorded at L, SS and F speeds, are shown in Cartesian coordinates as mean curves (Fig. 7.3A), and in polar coordinates, as mean curve (Fig. 7.3B) and single and mean CoA values (Fig. 7.3C), all expressed as percentage of gait cycle.

A significant effect of gait speed was found on $FWHM_{VF}$ (main effect, $F_{(2,57)}$=4.98, p=0.010). Post-hoc analysis revealed significant higher values at L than at F (100.89 ± 3.01 vs 95.42 ± 10.20, p=0.047) and significant higher values at SS than at F (101.78 ± 4.02 vs 95.42 ± 10.20, p=0.016). No differences were found between L than at SS (100.89 ± 3.01 vs 101.78 ± 4.02, p>0.05) (Fig. 7.3B).

Significant differences were found in CoA_{VF} between L and F (32.54 ± 1.65 % of gait cycle vs 28.42 ± 2.07 % of gait cycle; $F_{(1,38)}$=39.359; p<0.001), between SS and F (30.39 ± 1.52 % of gait cycle vs 28.42 ± 2.07 % of gait cycle; $F_{(1,38)}$=13.446; p<0.001) and between L and SS (32.54 ± 1.65 % of gait cycle vs 30.39 ± 1.52 % of gait cycle; $F_{(1,38)}$=14.301; p<0.001).

TMCf and VF Cross-correlation

Figure 39A shows the adimensional (normalized to the own maximum value) mean curves of TMCf and VF at L, SS and F, obtained from curves of subjects. In Fig. 7.4B are reported the curves of the strong cross-correlation between TMCf and VF at each gait speed. As regard the timing, the values of delay, in terms of samples between TMCf and VF curves, indicate that VF curves are delayed compared to TMCf waveforms at L (τ^*_L = 4.5% of the gait cycle), SS (τ^*_{SS} = 4.5% of the gait cycle) and F (τ^*_F = 3.5% of the gait cycle).

Energetic parameters

A significant effect of gait speed was found for R-step ($F_{(2,57)}$=4.449, p=0.016) and TEC ($F_{(2,57)}$=4.192, p=0.020). Mean (±SD) values and post hoc analysis results were shown in Table 8.1 (p<0.01).

TMCf and energetic cost parameters correlations

Significant moderate negative correlation was found between CoA_{TMCf} and R-step (r=-0.374, p=0.003), while significant moderate positive correlation was found between CoA_{TMCf} and TEC (r=0.315, p=0.014).

	Parameters	L	SS	F	p value of Post hoc analysis		
					L vs SS	L vs F	SS vs F
Energetic	**Rstep (%)**	47.79±8.99	55.24±6.99	48.47±9.98	**0.027**	p>0.05	**0.042**
	Tec (kcal/km*kg)	0.71±0.17	0.61±0.14	0.75±0.19	**0.023**	p>0.05	**0.042**
Spatio-temporal	**Walking speed (m/s)**	2.58±0.62	4.04±0.63	5.63±0.96	**p<0.001**	**p<0.001**	**p<0.001**
	Cadence (cycle/s)	0.67±0.08	0.88±0.07	1.05±0.10	**p<0.001**	**p<0.001**	**p<0.001**
	Stride length (% limb length)	1.35±0.18	1.61±0.17	1.86±0.25	**p<0.001**	**p<0.001**	**0.001**
	Step width (% limb length)	0.29±0.03	0.29±0.04	0.29±0.03	p>0.05	p>0.05	p>0.05
	Stance duration (% cycle)	67.35±2.43	63.80±1.19	62.37±1.36	**p<0.001**	**p<0.001**	**0.038**
	Swing duration (% cycle)	32.65±2.43	36.20±1.19	37.63±1.36	**p<0.001**	**p<0.001**	**0.038**
	1st Double support duration (% cycle)	16.98±2.20	13.88±1.38	12.61±1.41	**p<0.001**	**p<0.001**	p>0.05
	2nd Double support duration (% cycle)	17.34±2.58	13.65±1.03	12.07±1.29	**p<0.001**	**p<0.001**	**0.019**
Kinematic	**Hip RoM (°)**	35.02±4.32	39.42±4.29	44.04±6.00	**0.020**	**p<0.001**	**0.013**
	Knee RoM (°)	57.93±6.15	63.34±5.00	64.20±3.66	**0.004**	**0.001**	p>0.05
	Ankle RoM (°)	30.75±4.86	34.54±6.36	35.69±7.33	p>0.05	**0.047**	p>0.05
	Trunk lateral bending (°)	4.05±1.66	4.59±1.46	5.47±1.54	p>0.05	**0.049**	p>0.05
	Trunk flexion-extension (°)	2.92±0.76	2.95±0.92	3.03±0.72	p>0.05	p>0.05	p>0.05
	Trunk rotation (°)	14.13±13.68	16.78±5.43	21.74±7.38	p>0.05	**0.042**	p>0.05
	Pelvis obliquity (°)	5.13±1.42	6.44±1.63	8.53±2.62	p>0.05	**p<0.001**	**0.004**
	Pelvis tilt (°)	102.70±23.80	92.31±26.17	79.06±28.63	p>0.05	**0.018**	p>0.05
	Pelvis rotation (°)	14.79±5.01	17.15±5.38	23.43±8.87	p>0.05	**p<0.001**	**0.013**

Table 7.1. Mean ±SD of energetic, spatio-temporal and kinematic parameters in in subjects at L, SS and F. Post hoc analysis results test with Bonferroni's corrections for energetic, spatio-temporal and kinematic parameters. Bold type significant differences (p<0.05).

Spatio-temporal and kinematic parameters

A significant effect of gait speed was found on almost all spatio-temporal parameters: walking speed ($F_{(2,57)}$=81.761, p<0.001), cadence ($F_{(2,57)}$=103.088, p=<0.001), stride length ($F_{(2,57)}$=32.204, p=<0.001), stance duration ($F_{(2,57)}$=42.906, p<0.001), swing duration ($F_{(2,57)}$=42.906, p<0.001), first ($F_{(2,57)}$=34.710, p<0.001) and second ($F_{(2,57)}$=46.930, p<0.001) double support duration.

Table 8.1 shows mean (±SD) values and post hoc analysis results (p<0.01).

A significant effect of gait speed was found on all RoM values, except for trunk flexion-extension: hip RoM ($F_{(2,57)}$=16.725, p<0.001), knee RoM ($F_{(2,57)}$=9.064, p<0.001), ankle RoM ($F_{(2,57)}$=3.396, p=0.040), trunk lateral bending ($F_{(2,57)}$=3.304, p=0.044) and rotation ($F_{(2,57)}$=3.303, p=0.044), pelvis obliquity ($F_{(2,57)}$=15.265, p<0.001), tilt ($F_{(2,57)}$=4.069, p=0.022) and rotation ($F_{(2,57)}$=9.012, p<0.001). Furthermore, Table 8.1 shows mean (±SD) values and post hoc analysis results (p<0.05).

TMCf and gait parameters correlations

Partial correlation analysis showed positive correlation between CoA_{TMCf} and stance duration (r=0.600, p<0.001), 1st double support duration (r=0.466, p<0.001), 2st double support duration (r=0.594, p<0.001), RoMs of ankle (r=0.291, p=0.025), pelvis obliquity (r=0.401, p=0.002) and pelvis rotation (r=0.398, p=0.002). Furthermore, negative correlation was found between CoA_{TMCf} and both swing duration (r=-0.600, p<0.001) and cadence (r=-0.265, p=0.043).

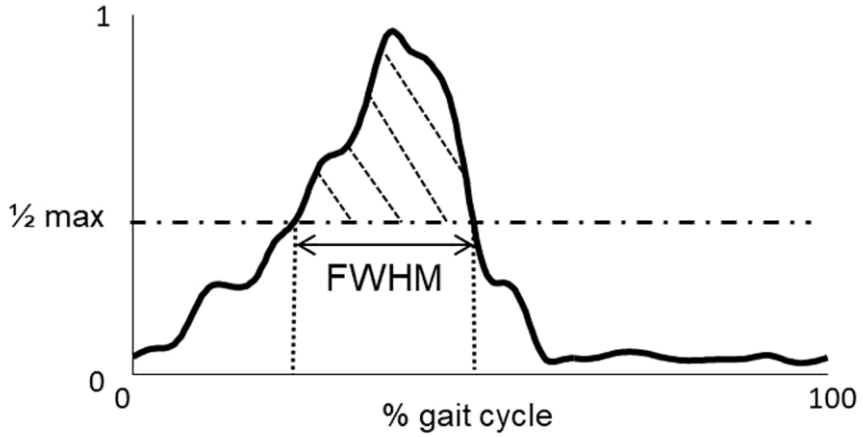

Figure 7.1. Example of Full Width at Half Maximum (FWHM): the sum of the time durations during which the curve is higher than its half maximum (dotted area).

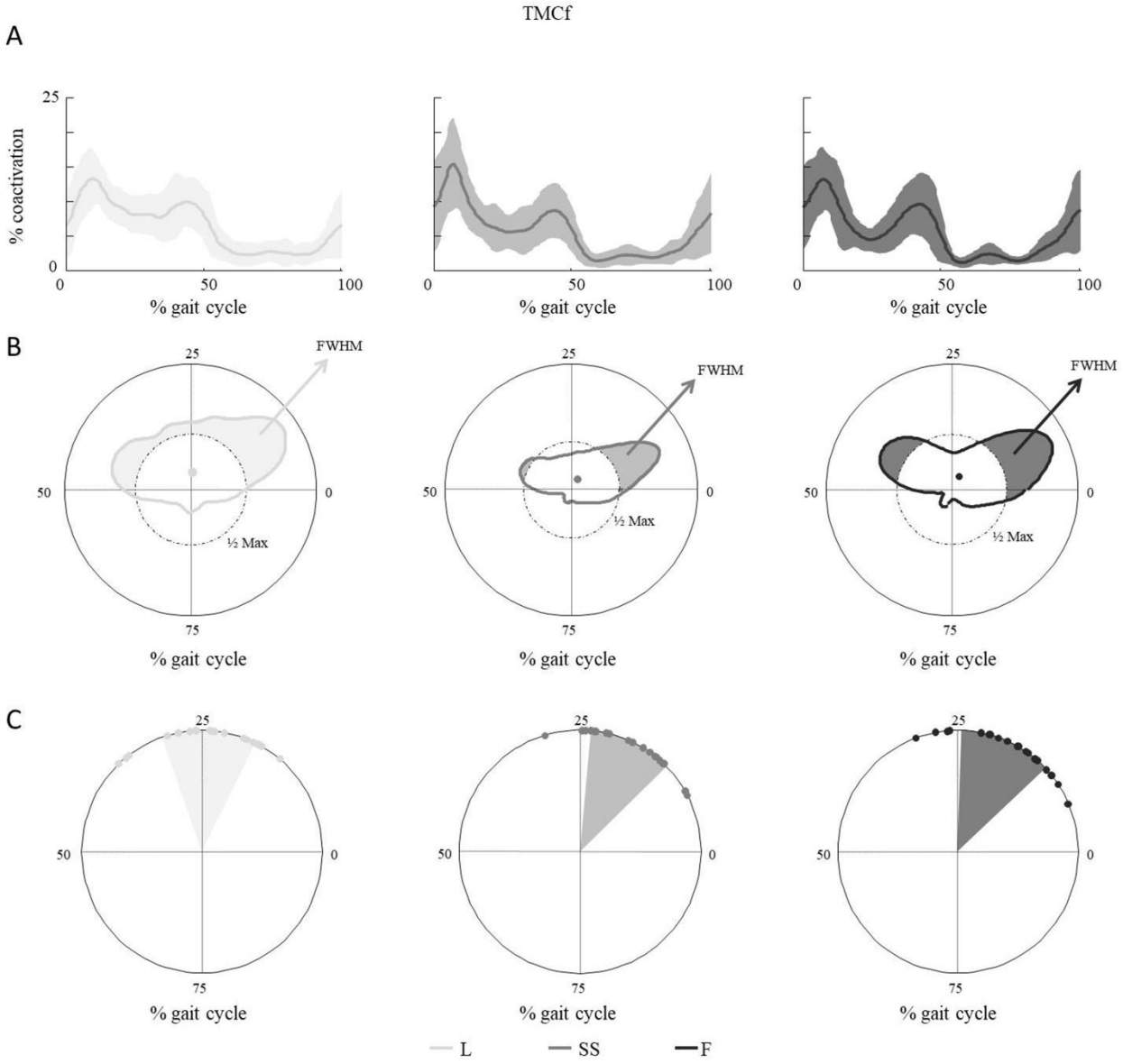

Figure 7.2. Lower limb global coactivation for subject at low (L), self-selected (SS) and fast (F) gait speeds. (A) Mean (with SDs in light colors) plot of coactivation of lower limb antagonist muscles during the gait cycle. (B) Time-varying multi-muscle coactivation function (TMCf) curves, center of activity (dot) and Full Width at Half Maximum (FWHM) (colored area of the curve) at the three gait speeds plotted in the polar coordinates. (C) TMCf centre of activity at three velocities. Each dot on the circle represents the subject's centre of activity expressed as a percentage of the normalized gait cycle, polar direction denotes the relative time over the gait cycle, while the width of the sector represents angular SD across subjects.

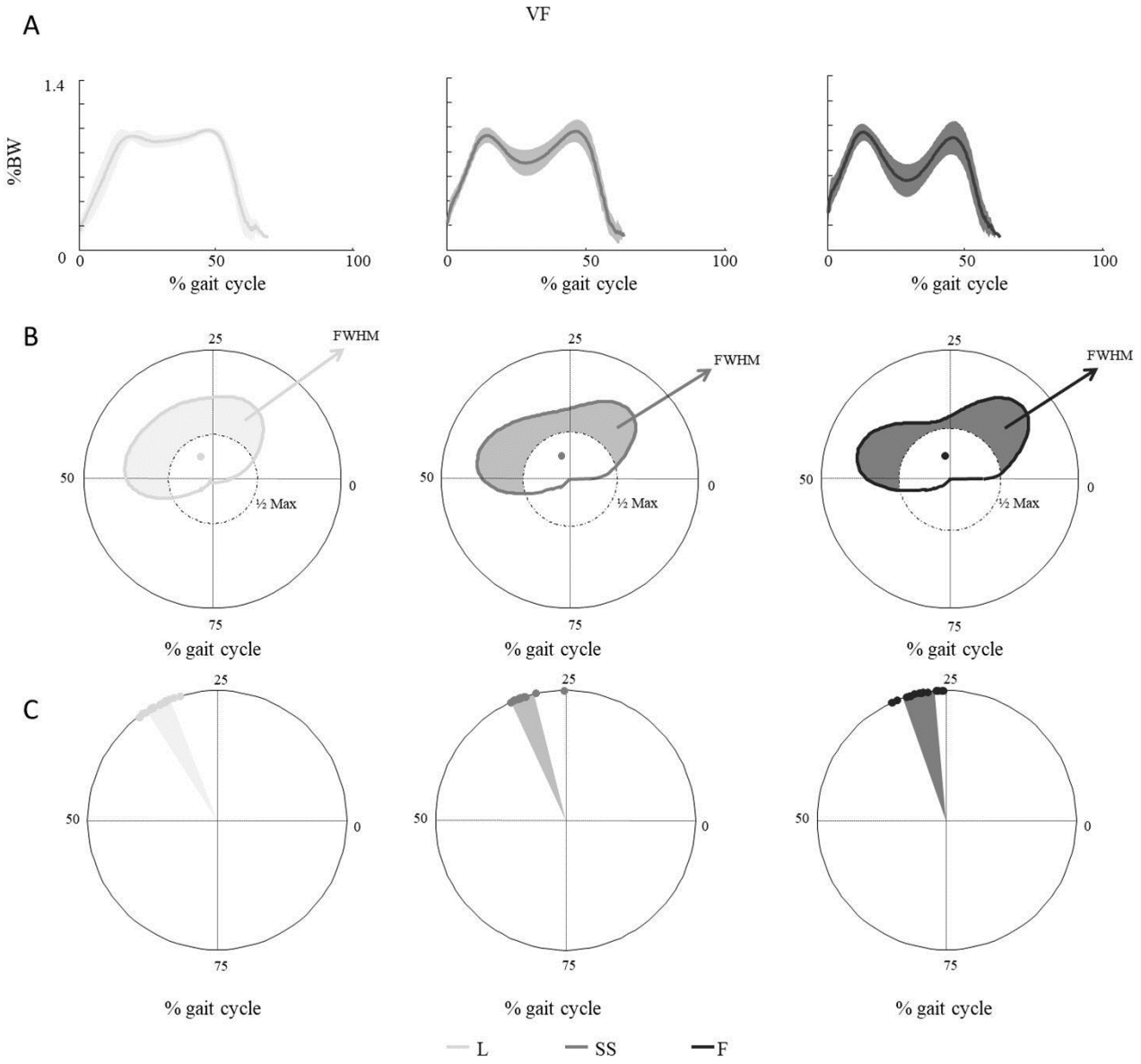

Figure 7.3. Vertical Force (VF) for subject at low (L), self-selected (SS) and fast (F) gait speeds. (A) Mean (with SDs in light colors) plot of VF during the gait cycle. (B) VF curves, center of activity (dot) and Full Width at Half Maximum (FWHM) (colored area of the curve) at the three gait speeds plotted in the polar coordinates. (C) VF centre of activity at three velocities. Each dot on the circle represents the subject's centre of activity expressed as a percentage of the normalised gait cycle, polar direction denotes the relative time over the gait cycle, while the width of the sector represents angular SD across subjects.

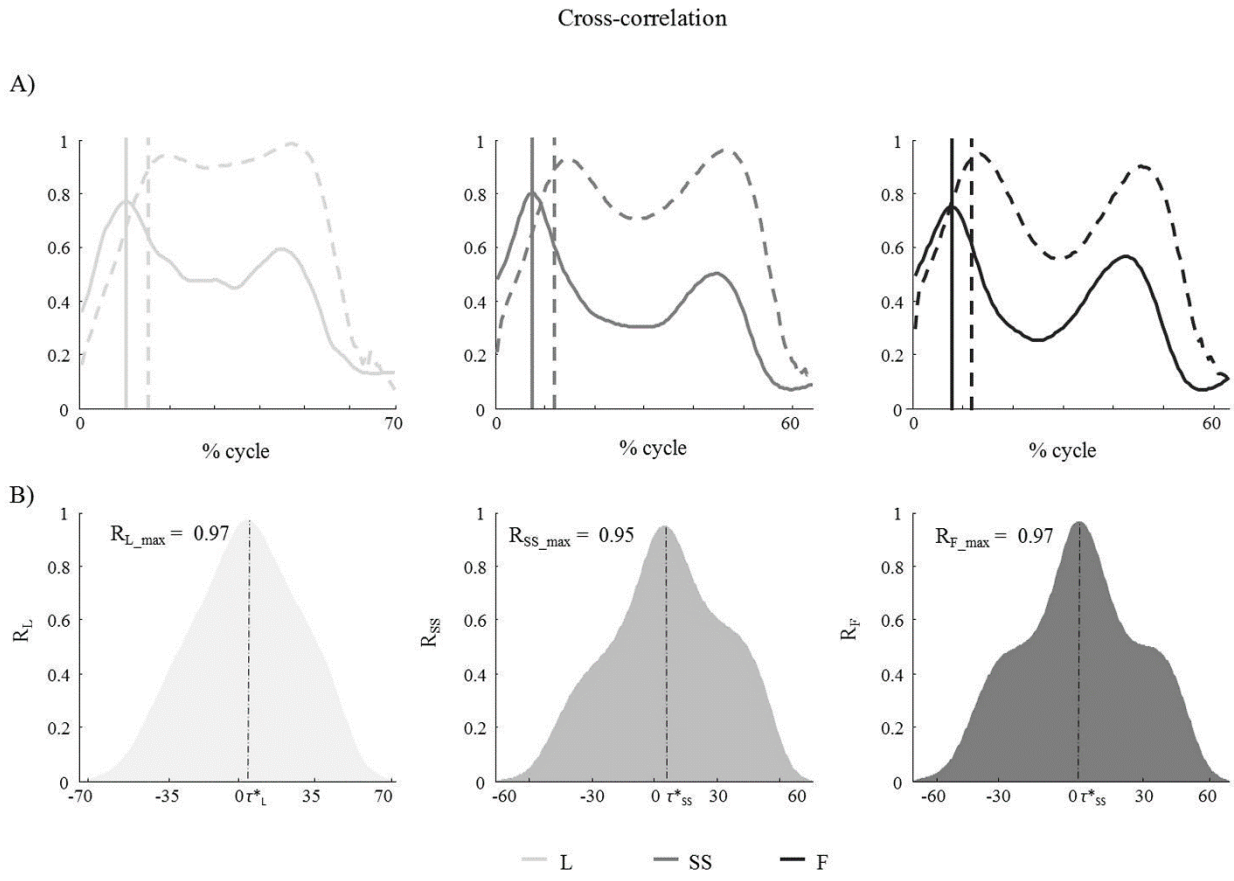

Figure 7.4. Cross-correlation. (A) Mean curves of Time-varying multi-muscle coactivation function (TMCf) (continuous line) and Vertical Force (VF) (dashed line) at low (L), self-selected (SS) and fast (F) gait speeds. (B) Cross-correlation curves between TMCf and VF curves and values of the maximum value (R_{max}) of the cross-correlation curves at L, SS and F (R_{L_max}, R_{SS_max}, R_{F_max}). The vertical dashed black lines show the temporal shift (τ^*), in term of samples, of one signal relative to the other.

7.3 Discussion and Conclusions

This study describes for the first time the global lower limb coactivation of twelve muscles involved within the gait cycle at low, self-selected and fast gait speeds, using a time-varying multi-muscle co-activation function [4]. This approach has some technical and clinical strengths if compared with other methods. The formers lie on the fact that the algorithm used for TMCf accept as input also a number $N \geq 2$ of muscles (in this case twelve) without requiring an a-priori sorting of the muscles depending on the moment generated at the ankle, knee and hip joints. Furthermore, it provides the possibility to analyze the global lower limb coactivation in each time point and sub-phase of the gait cycle (time-varying). Previous methods require as input only two muscles or muscle groups without

providing a time-varying analysis, with the exception of the original and modified methods proposed by Rudolph and collegues and Don and colleagues [10]. The latter lie on the fact that TMCf allows a global and simple description of a complex motor control mechanism providing useful information on how the CNS manage, for instance, the lower limb stiffness during walking. In summary, such a parameter lends itself to be used to evaluate the motor behavior differences between before and after any rehabilitative, pharmacological and surgical treatment.

The statistical differences between each gait speed pair (L vs SS, L vs F and SS vs F) imply that there isn't a confounding effect of gait speed on our results due to the fact that speed selected by a participant for a given condition could have considered for another condition by another participant. In order to control the gait speed within L, SS and F conditions and to minimize its influence on gait parameters we could have use a treadmill which allows advantages of long duration trials within a stationary motion capture volume [11] with a controlled walking speed compared with overground walking [12]. On the other hand, although literature also reports a qualitative and quantitative similarity of the treadmill gait compared with freely-performed overground walking [13] several studies comparing kinematic, kinetic and sEMG parameters reported controversial findings [11,12,14-16]. In particular treadmills: i) provide ongoing proprioceptive sensory cueing and modified visual flows with respect to that normal (the subject maintains the same place in space) [15] ; ii) impose systemic regulation on dynamic neuromuscular control [17] implying invariant gait patterns [12]; iii) force the adoption of a "cautious gait" in response to the possible inherent challenges to balance imposed by treadmill walking; iv) induce higher metabolic cost and muscle activation [11], larger step-width and smaller step-width variability [17]. For both the previous considerations and for the fact that we intend to use the TMCf mainly for the analysis of motor behaviors in pathological conditions, we have preferred the natural overground walking.

The temporal profiles of the global muscle co-activation at the three gait speeds, characterized by a double peak in the stance phase, are shown in the Fig. 7.2A. As regard the co-

activation pattern at SS speed, the first co-activation increase coincides with the "weight acceptance" sub-phase, which ranges from 0% to 10% of the gait cycle and represents the duration of the initial double support interval. Within this sub-phase the CNS maximizes the muscle co-activation to increase the whole lower limb stiffness to absorb the load, stabilize the whole locomotor system and ensure the maintenance of progression. The second co-activation increase coincides with the terminal stance sub-phase (30-50% of the gait cycle). This sub-phase is the least stable (single support) since the center of pressure is crossing the ipsilateral toes anteriorly and the center of mass is falling (its vertical coordinate decreases rapidly) [18]. For this reason, the CNS coactivates the ipsilateral lower limb muscles to compensate for the reduced stability. Between the above-mentioned co-activation increases (mid-stance 10-30%) there is a lower amplitude co-activation plateau. In the pre-swing sub-phase (50-60%) the rapid and definitive transfer of the load to the contralateral limb allows the decrease of the global coactivation whose low level remains active within the initial-swing (60-73%) and mid-swing (73-87%) sub-phases. The global co-activation level regrows in the last sub-phase of the gait cycle (terminal-swing) in which the limb is preparing for the contact with the ground. These results reflect the main findings of previous studies that investigated the lower limb muscle co-activation at single joint level [4,19,20]. Indeed, these studies showed hip muscles coactivation in late stance and initial swing sub-phases, knee muscles coactivation in early stance, in push-off and in terminal swing sub-phases, ankle muscles co-activation in early stance and mid-stance sub-phases.

It is worth to note that, beside a similar temporal trends of TMCf curves was observed at three speeds, the global lower limb co-activation is speed-dependent showing differences in amplitude distribution during gait sub-phases among the three gait speeds, particularly between L and both SS and F (Fig. 7.2B). In fact, the representation in polar coordinates shows that, whereas at SS speed the global coactivation is essentially limited to the loading response sub-phase (Fig. 7.2B), at low gait speed the global coactivation is mainly present in the loading response (0-10%), mid-

stance (10-30%) and terminal-stance (30-50%) sub-phases, while at F speed the global coactivation is mainly present in both the loading response and terminal-stance sub-phases.

The findings of this study showed the presence of a high intra-subjects and between subjects, as well as among the three gait speeds, repeatability of TMCf curves, expressed by high values of the coefficient of multiple correlation. The intra-subjects and between subjects repeatability suggests that the co-activation function can be considered robust besides the variability associated to the high muscles number considered as input of the TMCf algorithm, the variability introduced by the measurement system and the inherent physiological variability related to the motor behaviors adopted by the subjects.

In addition to global features of TMCf, both synthetic FWHM and CoA indices show higher values at L speed than at both SS and F speeds. The increased FWHM at L speed and its spreading all over the stance phase (Fig. 7.2B) suggests that the CNS co-activates many muscles to increase the whole lower limb stiffness to compensate for a reduced gait stability at lower speed [Fan et al, 2016]. Although not significant, we found a trend for an increased FWHM also at F compared to SS speed. This may suggest that a low level of global co-activation is required during natural SS speed likely to minimize the energy expenditure and guarantee an effective gait. Indeed, it has been shown that both the energy consumption and muscle activation reach their minimum at SS speed. Interestingly, energy consumption, muscles activation and gait stability all tend to reach an equilibrium point, to ensure a functional gait at SS gait speed [4]. The increased CoA, according to L>SS>F gradient (Fig. 7.2C), as well as its clockwise shift from L to F speed, both indicate that the global co-activation is differently expressed according to sub-phases and gait speed. Further studies should be aimed at investigating in detail how the CNS modulates the global co-activation at progressive increments of gait speed until running. Nevertheless, it is possible to hypothesize that the increase of the global coactivation level in both the loading response and terminal-stance sub-phases at faster speed, is due to an increase of interaction torques between the foot and the ground (Fig. 7.3).

Interestingly, we found that the global co-activation curve was similar to the VF curve in terms of temporal trend (Figs. 7.2A and 7.2B) and cross-correlation results (Fig. 7.4) at all three gait speeds. This finding suggests a very strict spatio-temporal relationship between global force production and global muscles coactivation. VF curves were delayed respect to TMCf curves, because the CNS, through a feedforward mechanism, anticipates the expected perturbation, given by the interaction between foot and ground, and thus stiffens and stabilizes the whole lower limb by activating simultaneously all the lower limb muscles in the loading response (first increase of TMCf and VF curves). Furthermore, the increased muscle co-activation (second increase of the TMCf curve) in the terminal-stance sub-phase determines the second peak on VF curve linked to a downward acceleration and lowering of the center of gravity as body weight falls forward over the forefoot rocker in terminal stance [18]. The global coactivation was positively correlated with the energy consumption and negatively correlated with energy recovery (Table 8.1). The higher the global coactivation, the higher the energy consumption. The less the global co-activation, the higher the energy recovery. These findings suggest that the CNS may either increase the global co-activation level to stabilize the limb during the most unstable (e.g. L speed) or the most demanding (F speed) condition, or decrease the global co-activation level to optimize both the energy consumption and recovery at preferred gait speed (SS speed). This concept is further reinforced by the findings that the global co-activation is positively correlated with some balance-related parameters, i.e. first and second double support and stance durations.

In conclusion, the novelty of this study lies in the fact that our results provide a time-varying characterization, within the gait cycle, of the global lower limb co-activation of twelve muscles at a multi-joint level. Furthermore, the used algorithm does not require an a-priori sorting of the muscles depending on the moment generated at the single joints. The global lower limb coactivation shows a representative temporal profile characterized by two humps within the stance-phase, as well as the ground reaction vertical forces profiles [18]. Furthermore, our findings suggest the applicability of

this method in investigating several aspects, such as motor learning strategies, limb stiffness, gait and postural stability, energy efficiency optimization, also in pathological conditions.

Several factors in the sEMG measurement and pre-processing might influence the linear envelope profiles, and therefore the outcome of co-activation [21]. Particularly, the TMCf profile is strictly dependent on the normalization technique adopted: in our study, the global lower limb muscle coactivation curves were normalized with respect to the peak values across all trials. This choice of normalization procedure is linked to one of the future developments of this study that consists in the global lower limb co-activation analysis during motor tasks in pathologic conditions. Indeed, for patients with motor disorders, other normalization procedures, such as isometric maximum voluntary contraction, can be very long and hardly executable [3].

Furthermore, the analysis of other ranges of gait speeds, until running, could be useful to understand how the CNS modulates the global co-activation at progressive increments of gait speed.

7.4 Bibliography

[1] Hermens, H.J., Freriks, B., Disselhorst-Klug, C., Rau, G., 2000. Development of recommendations for SEMG sensors and sensor placement procedures. Journal of Electromyography and Kinesiology 10 (5), 361-374.
[2] Davis III, R.B., Õunpuu, S., Tyburski, D., Gage, J.R., 1991. A gait analysis data collection and reduction technique. Human Movement Science 10, 575–587.
[3] Burden A. How should we normalize electromyograms obtained from healthy participants? What we have learned from over 25 years of research. J Electromyogr Kinesiol 2010;20(6):1023-35.
[4] Serrao M, Rinaldi M, Ranavolo A, Lacquaniti F, Martino G, Leonardi L, Conte C, Varrecchia T, Draicchio F, Coppola G, Casali C, Pierelli F. Gait Patterns in Patients with Hereditary Spastic Paraparesis. PLOSONE 2016;11(10).
Strazza A, Mengarelli A, Fioretti S, Burattini L, Agostini V, Knaflitz M, Di Nardo F. Surface-EMG analysis for the quantification of thigh muscle dynamic co-contractions during normal gait. Gait & Posture 2017;51:228–33.
[5] Ranavolo A, Donini LM, Mari S, Serrao M, Silvetti A, Iavicoli S, Cava E, Asprino R, Pinto A, Draicchio F. Lower-limb joint coordination pattern in obese subjects. Biomed Res Int. 2013;2013:142323. doi: 10.1155/2013/142323.
[6] Wren TA, Do KP, Rethlefsen SA, Healy B. Cross-correlation as a method for comparing dynamic electromyography signals during gait. J Biomech. 2006;39(14):2714-8.
[7] Nelson-Wong E, Howarth S, Winter DA, Callaghan JP. Application of autocorrelation and cross-correlation analyses in human movement and rehabilitation research. J Orthop Sports Phys Ther. 2009;39(4):287-95.
[8] Cavagna, G.A., Thys, H., Zamboni, A., 1976. The sources of external work in level walking and running. Journal of Physiology 262 (3), 639-657.
[9] Martino G, Ivanenko YP, Serrao M, Ranavolo A, d'Avella A, Draicchio F, Conte C, Casali C, Lacquaniti F. Locomotor patterns in cerebellar ataxia. J Neurophysiol. 2014 Dec 1;112(11):2810-21.
[10] Don, R., Serrao, M., Vinci, P., Ranavolo, A., Cacchio, A., Ioppolo, F., Paoloni, M., Procaccianti, R., Frascarelli, F., De Santis, F., Pierelli, F., Frascarelli, M., Santilli, V., 2007. Foot drop and plantar flexion failure determine different gait strategies in Charcot-Marie-Tooth patients. Clinical Biomechanics 22 (8), 905-916.
[11] Martin JP, Li Q. Overground vs. treadmill walking on biomechanical energy harvesting: An energetics and EMG study. Gait Posture. 2017 Feb;52:124-128.
[12] Hollman JH, Watkins MK, Imhoff AC, Braun CE, Akervik KA, Ness DK. A comparison of variability in spatiotemporal gait parameters between treadmill and overground walking conditions. Gait Posture. 2016 Jan;43:204-9.
[13] Riley PO, Paolini G, Della Croce U, Paylo KW, Kerrigan DC. A kinematic and kinetic comparison of overground and treadmill walking in healthy subjects. Gait Posture 2007;26:17–24.
[14] Row Lazzarini BS, Kataras TJ. Treadmill walking is not equivalent to overground walking for the study of walking smoothness and rhythmicity in older adults. Gait Posture. 2016 May;46:42-6.
[15] Warabi et al., Treadmill walking and overground walking of human subjects compared by recording sole-floor reaction force. Neurosci Res. 2005;53:343–8.
[16] Watt et al. A three-dimensional kinematic and kinetic comparison of overground and treadmill walking in healthy elderly subjects. 2010.
[17] Rosenblatt NJ, Grabiner MD. Measures of frontal plane stability during treadmill and overground walking. Gait Posture. 2010 Mar;31(3):380-4.
[18] Perry J. Gait Analysis–Normal and Pathological Function. Thorofare: Slack Incorporated, 1992.
[19] Peterson DS, Martin PE. Effects of age and walking speed on coactivation and cost of walking in healthy adults. Gait & Posture 2010; 31:355–59.
[20] Rinaldi M, Ranavolo A, Conforto S, Martino G, Draicchio F, Conte C, Varrecchia T, Bini F, Casali C, Pierelli F, Serrao M. Increased lower limb muscle coactivation reduces gait performance and increases metabolic cost in patients with hereditary spastic paraparesis. Clin Biomech 2017;48:63-72.
[21] D'Alessio T, Conforto S. Extraction of the envelope from surface EMG signals. IEEE Eng Med Biol Mag. 2001 Nov-Dec;20(6):55-61.

CHAPTER 8

8. PROGRESSION OF MUSCULAR COACTIVATION AND GAIT VARIABILITY IN CHILDREN WITH DUCHENNE MUSCULAR DYSTROPHY: A 2-YEAR FOLLOW-UP STUDY

In this chapter, text and figures have been taken from or adapted from the article "*Progression of muscular co-activation and gait variability in children with Duchenne Muscular Dystrophy: a 2-year follow-up study" [2019 Submitted, Journal of Electromyography and Kinesiology]*, which was co-authored by me.

Despite Duchenne Muscular Dystrophy being characterized by muscle weakness, no studies have investigated muscle co- activation in patients affected by DMD so far.

In the study *"Progression of muscular co-activation and gait variability in children with Duchenne Muscular Dystrophy: a 2-year follow-up study", submitted on Clinical Biomechanics* (October 2019), we analyzed the activation patterns of lower limb muscles in DMD children through surface electromyography signal (surface EMG) at different times from disease onset during unconstrained gait. Muscular co-activation of agonist-antagonist muscles at the knee and ankle joints was then linked it with motor function.

The purposes of this study were therefore (i) to assess the role of lower limb muscle coactivation in a group of patients with Duchenne Muscular Distrophy taking into account the influence of both SNR and sEMG processing technique; (ii) to evaluate its extent and its relationship with the progression of gait impairment at the 1- and 2-year follow-up evaluations (iii) to compare the obtained data with functional capacity.

This approach may be useful for a better interpretation of the pathologic mechanisms, in terms of muscle behavior, to address rehabilitation treatmen

8.1 Materials and methods

Subjects

Ten male children with DMD were recruited (mean age 5.51 (SD 1.35) years, mean height 1.20 (SD 8.70) m, mean weight 27.16 (SD 8.19) kg). All of them were able to walk without assistance or walking aids on a level surface, and no one underwent surgical interventions at the level of the lower limbs. A preliminary visit performed right after the diagnosis included a first evaluation of the severity of the disease, and a battery of motor tests including the 6-minute walking test (6MWT) [1] and the North Star Ambulatory Assessment (NSAA). Pharmacological treatment was generally planned at the time of the first visit. After the first evaluation, a series of acquisition sessions were programmed: the first of them (identified as T0), happened generally two years after the first visit, so to ensure the effect of the pharmacological treatment. The two subsequent acquisition sessions (identified as T1 and T2) were scheduled with an interval of one year. Gait sessions were recorded at the MarLab – laboratory of robotics and analysis of the movements at the "Ospedale Pediatrico Bambino Gesù" in Palidoro, Rome, at T0, T1, and T2.

Gait analysis

In the three gait analysis sessions, kinematics data were recorded at 200 Hz using a stereo-photogrammetric system (VICON – Nexus motion capture Software) consisting of eight infrared cameras spaced around the walkway. Thirty-five reflective spherical markers were attached on the anatomical landmarks, in accordance with a validated biomechanical model. Anthropometric data were collected for each subject [2].

Surface EMG signals were recorded at 1000 Hz using a Mini Wave sEMG wireless probe system (Cometa System). After skin preparation, bipolar Ag/AgCl surface electrodes (2 cm diameter) were placed over the muscle belly in the direction of the muscle fibres according to the European recommendations for surface electromyography (SENIAM) and the atlas of muscle innervation zones [3] . Electrodes were placed on the following muscles: Rectus femoris (RF); Vastus lateralis (LA); Biceps femoris (BF); Medial Hamstring (HS); Tibialis Anterior (TA); Gastrocnemius (GAS), Soleus (SOL) and Gluteus maximus (GM).

Experimental procedure

The children were asked to walk barefoot at comfortable self-selected speeds along a walkway approximately 8 m long while looking forward. Because we were interested in natural locomotion, only general, qualitative instructions were provided. Before the recording session, the subjects practiced for a few minutes to familiarize themselves with the procedure.

Ten trials per patient were recorded. To avoid muscle fatigue, groups of three trials were separated by 1-minute rest periods.

Data analysis

Kinematic parameters

The data were processed using MATLAB (version 8.3.0.532, MathWorks, Natick, MA, USA) software. Regarding kinematic data, the anatomical angles of the lower limb in the sagittal plane were computed from motion capture data. For each trial, every gait cycle was segmented and defined as the time between two successive foot contacts of the same leg. In this study, foot strike and foot-off events were determined by locating the maximum and minimum excursions of the limb angle, defined as the angle between the vertical axis and the limb segment (from the greater trochanter to the lateral malleolus), projected on the sagittal plane. Since the disease typically affects both lower limbs symmetrically, we focused our analyses on the right dominant leg. Gait

cycle segmentation was used to calculate the following spatiotemporal parameters of gait: gait velocity, gait cadence, step length, stride length, and step width. In addition, the duration of stance phase (expressed as a percentage of the cycle duration) was evaluated.

To account for possible anthropometry variations [5] associated with growth, stride length, step length and stride width were expressed as a percentage of the limb length. The mean (denoted as mean in the following formula) and the standard deviation (denoted as SD in the following formula) were then computed for the step length, stride length and stride width.

Using these the values of mean and standard deviation, the coefficient of variation (CV) was computed, since these parameters are known to be related to stability during gait:

$$CV = \frac{100 * SD}{mean}$$

Thus, the greater is the CV value, the more instable is the gait.

Surface EMG parameters

Segmented portions of raw surface EMG data for each gait cycle were band-pass filtered using a Butterworth filter (20–400 Hz), rectified, and low-pass filtered with a Butterworth filter (cut-off frequency 10 Hz), to obtain the linear envelopes (LE) of each muscle. For each subject and muscle, this was normalized to its peak value across all trials from the same session. From the processed surface EMG signals, the co-activation index was calculated for the pairs of antagonist muscles VL–BF and TA–SOL by using the Vector Coding Technique (VCT) [4]. The advantage of this technique, as compared to amplitude-based indicators of co-activation, is its substantial independence from EMG amplitude. In the case of longitudinal studies, where muscle strength and weakness may play a relevant role, this independence from amplitude makes it possible to observe co-activation with no confounding effects coming from differences in the overall magnitude of muscle activity.

As a matter of fact, Vector Coding Technique is typically used to quantify the coordination among patterns of agonist and antagonist muscle pairs for different signals of equivalent type [4]. This algorithm divides the coordination patterns into 4 classes: In-phase or In-activation (when two signals simultaneously either increase or decrease their respective amplitudes); Anti-phase or Anti-activation (when two muscles act in an opposite way – the first increases and the second decreases its amplitude or vice versa); One-only (when only one muscle is active), and Other-only (when only the other muscle is active) [6].

To identify the co-activation pattern, a 2-D plot is thus constructed, where the horizontal axis corresponds to one surface EMG signal envelope LE_{M1} and the vertical axis corresponds to the other envelope LE_{M2}. The coupling angle (γ) is then defined as the positive direction angle subtended from a vector adjoining two successive time points relative to the right horizontal:

$$\gamma_i = \begin{cases} \arctan\left(\frac{LE_{M2}(i+1) - LE_{M2}(i)}{LE_{M1}(i+1) - LE_{M1}(i)}\right) if \left(LE_{M1}(i+1) - LE_{M1}(i)\right) \geq 0 \\ 180° + \arctan\left(\frac{LE_{M2}(i+1) - LE_{M2}(i)}{LE_{M1}(i+1) - LE_{M1}(i)}\right) if \left(LE_{M1}(i+1) - LE_{M1}(i)\right) < 0 \end{cases}$$

where i is the current time sample and $0° \leq \gamma \leq 360°$.

When coupling angles are 45° and 225°, the two signals are perfectly in-phase (they increase or decrease of the same relative amount sample by sample). On the other hand, at 135° and 315°, a pure anti-phase coordination is present. When the segment adjoining two successive points is parallel to the horizontal (γ=0° or 180°) or vertical axis (γ = 90° or 270°), there is a pure one-only signal phase (one of the muscles increases or decreases its activity with no change on the other). When coupling angles do not relate to vertical, horizontal and diagonal vectors, the patterns are less pure.

For each time sample, muscle activity pattern is thus classified according to the following: One-only activation if $67.5° \leq \gamma i < 112.5°$ or $247.5° \leq \gamma i < 292.5°$; Other-only activation for $0° \leq \gamma i < 22.5°$, $157.5° \leq \gamma i < 202.5°$, or $337.5° \leq \gamma i < 360°$; In-activation if $22.5° \leq \gamma i < 67.5°$ or $202.5° \leq \gamma i < 247.5°$; Anti-activation if $112.5° \leq \gamma i < 157.5°$ or $292.5° \leq \gamma i < 337.5°$.

CI_{VCT} is then calculated as the total number of temporal indexes classified as either In- or Anti-activation relative to the total duration of the multiplied by 100. Complete co-activation corresponds to a $CI_{VCT} = 100\%$.

Statistical analysis

To examine the differences among the co-activation, gait parameters, CV and motor test values at the three evaluation sessions, ANOVA test was performed using MATLAB (version 8.3.0.532, MathWorks, Natick, MA, USA) software. Furthermore, correlation analysis was performed in order to determine the relationship between the co-activation index and the level of functional ability (6MWT), parameters of gait performance and gait stability. Descriptive statistics included means and standard deviation (SD), and significance level was set at $p < 0.05$.

8.2 Results

Changes in gait variables over the 1- and 2-year follow-up evaluations are shown in (Figs. 8.1,8.2). Time had a significant effect on stride width, duration of stance phase, and on coefficients of variability for both stride length and stride width.

Significant differences among the three evaluation sessions were observed on both stride width ($F_{(2,27)} = 8.37$, $p = 0.0019$) and stance phase duration ($F_{(2,27)} = 3.99$, $p = 0.0326$). Pairwise comparison between the sessions identified a significant increase of stride width passing from T0 to T2 ($p = 0.0015$) and a significant decrease of stance phase duration passing from T0 to T1 ($p = 0.0262$).

Analysis of the CV of Stride length at the three evaluation sessions showed significant differences ($F_{(2,27)}$=5.57, p = 0.0106). Pairwise comparison between the sessions identified a significant increase of CV passing from T0 to T2 (p = 0.0330) and from T1 to T2 (p = 0.0102). Furthermore, a significant effect of time on the CV of stride width was observed ($F_{(2,27)}$=7.72, p = 0.0027). Pairwise comparison between the session identified a significant increase of stride width CV values passing from T0 to T2 (T0 vs T1 p = 0.0051; T0 vs T2 (p = 0.0134).

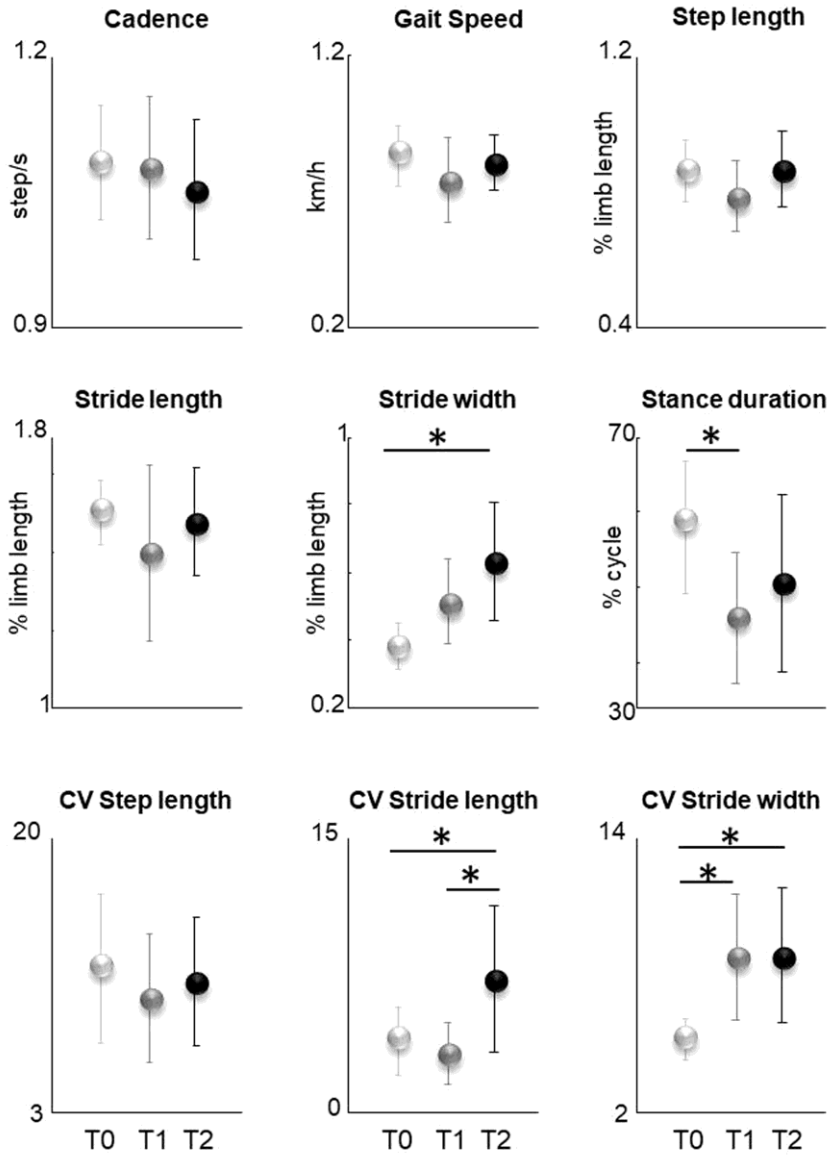

Figure 8.1 (Time-distance parameters and CV values at the baseline T0, at 1-year follow-up T1 and at 2-year follow-up T2./

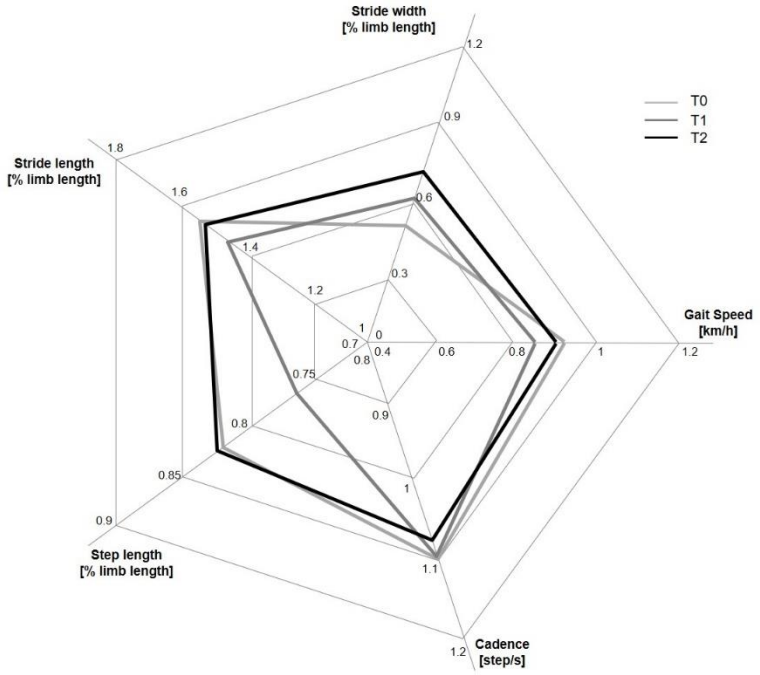

Figure 8.2. Radar plot illustrating the pattern of the time-distance parameters at the baseline T0 (light gray line), at 1-year follow-up T1 (dark gray line), and at 2-year follow-up T2 (black line). Group mean values for each parameter are shown.

Analysis of the CI at the three evaluation sessions, showed significant differences for both the VL–BF ($F_{(2,27)}$=5.44,P=0.012) and the TA–SOL ($F_{(2,27)}$=7.84,P=0.002) pairs of antagonist muscles.

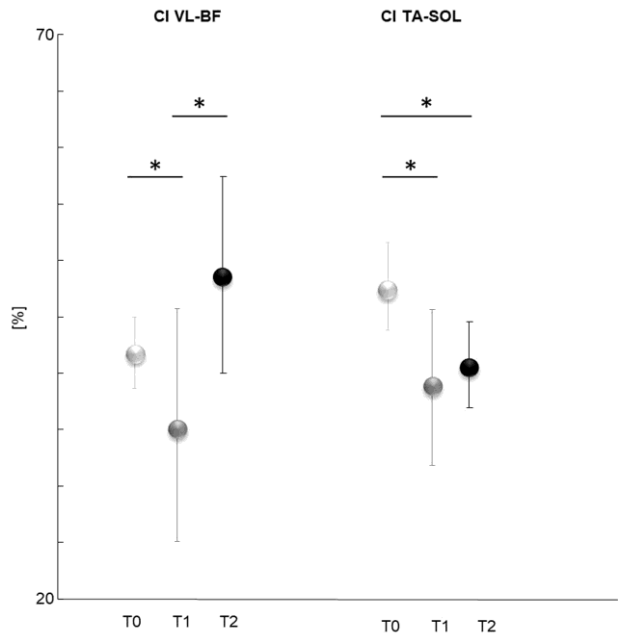

Figure 8.3. CI values at the baseline T0, at 1-year follow-up T1 and at 2-year follow-up T2 for both VL-BF and TA-SOL pairs of antagonist muscles.

In particular, pairwise comparison between the sessions identified a significant decrease of co-activation from T0 to T1 ($p = 0.045$) and an increase of co-activation when passing from T1 to T2 for the pair acting on the knee flexion-extension ($p = 0.009$), and a significant decrease of co-activation passing from T0 to T1 ($p = 0.002$) and from T0 to T2 ($p = 0.044$) for the muscle pair acting on the ankle joint. (Fig. 8.3)

Analysis of the 6MWT distance at the three evaluation sessions showed significant differences ($F_{(2,27)} = 3.56$, $p = 0.045$). In particular, the distance significantly decreased when passing from T1 to T2 (pairwise comparison $p = 0.049$). (Fig. 8.4)

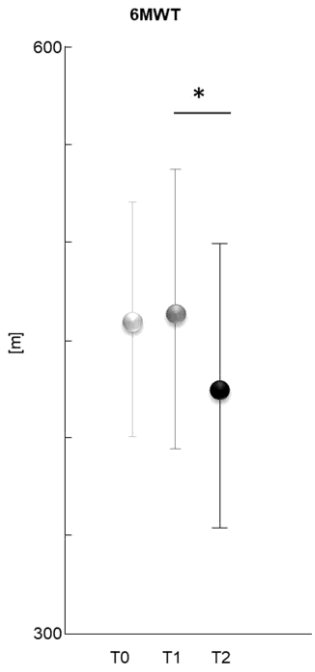

Figure 8.4. 6MWT values at the baseline T0, at 1-year follow-up T1 and at 2-year follow-up T2.

From the correlation analysis, significant negative correlation ($r=-0.382$, $P=0.049$) between CI on VL-BF and 6MWT values was observed. Furthermore, the co-activation of TA-SOL was negatively correlated with the CV of stride width ($r = -0.510$, $p = 0.0077$).

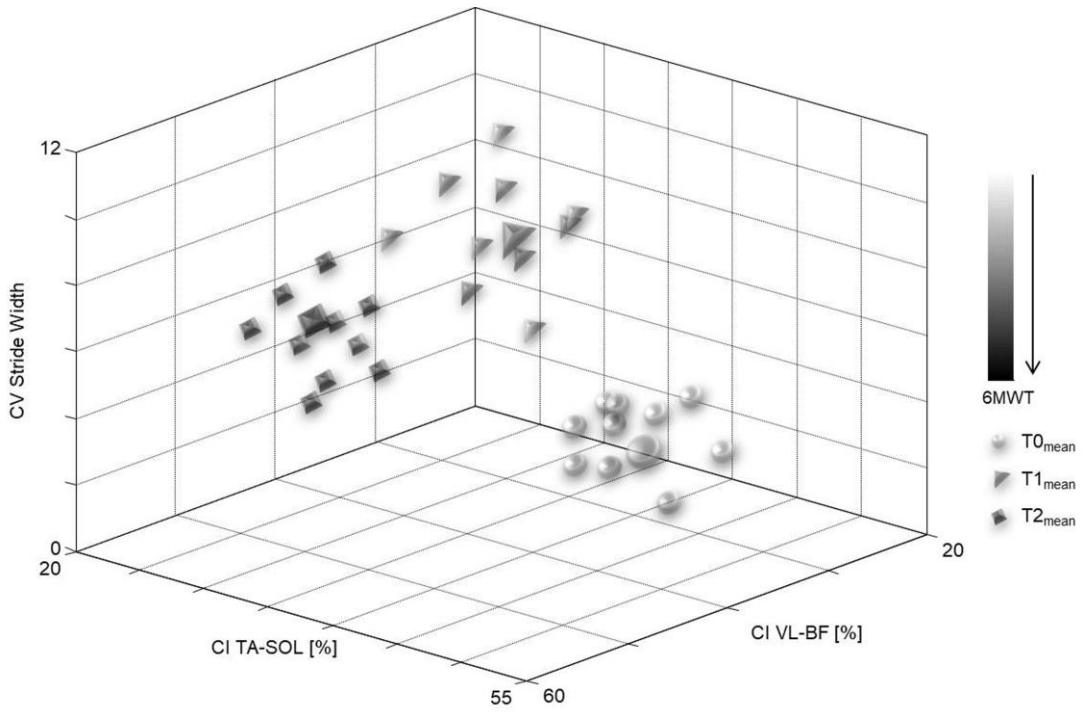

Figure 8.5. CI values for both VL-BF and TA-SOL pairs of antagonist muscles and CV Stride Width values at the baseline T0 (circles), 1-year follow-up T1 (triangles), and 2-year follow-up T2 (squares). Each dot represents a patient with different shades of gray according to the 6MWT values (see bar on the right). Large circle, large triangle and large square represent the mean values among subjects at the baseline T0, 1-year follow-up T1, and 2-year follow-up T2, respectively

8.3 Discussion and Conclusions

Preserving gait autonomy is a priority in the rehabilitation of DMD children. In order to achieve this goal, many authors have contributed in recent years to the advances in the understanding of DMD children gait biomechanics. It is well-known that patients with DMD show a progressive course. The abnormal gait pattern of a child with DMD has been reported to be caused by both primary (e.g muscle weakness) and secondary deficits (e.g. muscle dystrophy), as well as the result of adaptation processes to diminished muscle strength and coordination [7]. Consequently, the patient's walking ability is expected to gradually decline over time.

However, changes in muscle activation during gait of these children related to disease progression during years, have not yet been well established. It has been suggested that muscle weakness has a direct influence on DMD gait [5,7]: regarding the muscles acting at the upper part of the lower

limb, the lower power generation at the hip is explained by weakness of the hip extensors (e.g. Biceps femoris), which might resulting in a pelvic anterior tilt [8], and a more flexed position of the hip. Furthermore, weakness of the hip flexors (e.g. rectus femoris) could contribute to this decrease in power at the hip joint. Regarding the effects at the ankle joint, abnormalities at the muscle groups acting on this joint may be linked to a diminished ability to produce an appropriate dorsiflexion torque at the beginning of stance, when children with DMD either place the foot in plantar flexed position or flat on the ground. However, even though lower limb muscle groups are severely involved in children with DMD [9], most of the results have been described qualitatively up to now, and no specific muscle parameters have been monitored longitudinally, nor they have been directly linked with gait performance parameters.

Time distance parameters and CV

As regard gait parameters, we found a further widening of the base of support at the 2-year follow-up evaluation. A widened base of support reflects the adoption of compensatory mechanisms aimed at maintaining the dynamic balance on the frontal plane by increasing the safety margin between the center of gravity and the edge of the feet [10].

In the present study, we observed a progressive increase in the variability of both stride length and stride width (Figs. 8.1,8.2). It has been discovered that both stride length and stride width variability are linked with locomotion stability [11-13]. The progressive increase in gait variability observed at the 2-year follow-up may thus directly reflect a deterioration of the gait function, which leads to greater instability. Taking this into consideration, gait variability seems to anticipate the future loss of walking autonomy. However, further studies are needed to clarify whether gait variability can be a predictor of the loss of walking autonomy. While we cannot exclude possible confounding factors associated with growth, the normalization of the spatial parameters of gait substantially minimized the direct effect of anthropometry variations on the spatial characteristics of gait.

Co-activation

This study deeply investigated of the function of co-activation in patients with DMD, highlighting the relationship between muscle co-activation during gait and disability, gait performance and postural stability. Similar to spatiotemporal- and kinetic parameters, muscle activity data is also subjective to processing factors [5], which may determine a further variability in longitudinal studies. In this study, the choice of processing parameters, such as the cut-off frequency or the technique for evaluating muscle co-activation, was based on a preliminary study on a smaller sample [14].

During gait, joint stiffness and postural stability [15] are regulated by variations in the forces produced by the simultaneous contraction of antagonistic lower limb muscles.

It has been reported that increased knee and ankle muscle co-activation in pathologic conditions could compensate for the loss of selective muscle control, muscle weakness, abnormal muscle tone and fatigue in patients with central nervous system lesions [16], and this often leads to loss of balance and gait performance.

For instance, in Multiple Sclerosis it has been found that the neuromuscular system simultaneously increases knee and ankle muscle co-activation to ensure stability during forward progression [15]. Furthermore, both in post stroke and hemiplegic patients increased muscle co-activation is a compensation strategy for enhancing postural stability and locomotor performance [17, 18].

Our results revealed changes in lower limb co-activations values in relation to disease progression for both proximal and distal segments in children with DMD. Fig. 3.3 showed a significant decrease in co-activation values after a year, which is confirmed even after two years for distal segments muscles. Despite a decreasing trend from T0 to T1 on co-activation values at the proximal level, a significant increase of co-activation was reported at 2-year follow-up, when patients showed the lowest functional capacity (Figs. 8.3,8.4).

The absence of a common behaviour at T2 for proximal and distal muscles may be associated with a change in activation strategies, as the result of an adaptation to the disease progression, which brings to higher co-activation for the proximal muscles, associated with a lower one of distal ones.

The reduction of co-contraction activities at the distal level might be directly related to the direct effect of the pathology, i.e. the muscle dystrophy that drives the pattern configuration towards the exploitation of the passive characteristics of soft tissues. Moreover, the co-activation of the ankle joint muscle pair was found inversely proportional to the stride width variability. This might indicate that a decreased co-activation over the time at the ankle and knee joints, due to the relevant presence of muscle dystrophy at the distal level, leads to a more unstable gait. The increased co-activation al proximal level may be linked to the decrease in functional capacity. Despite the presence of a large inter-individual variability, this interpretation might be associated with the observed negative correlation between co-activation values at the muscle pair acting at the proximal level, and the gait functional outcomes during the years (Fig. 8.4). We observed a decrease in the 6MWT values from the 1-year follow-up to the 2-year follow-up. Our results are in line with previous studies and this functional decline reflects the progressive nature of degenerative DMD over time [19]. However, while the functional capacity decreases, increase in co-activation at the proximal level at the 2-year follow-up suggests that patients try to maintain an effective gait despite disease progression, by increasing muscle co-activation, especially when the muscular manifestations of the pathology are more evident. Thus, since gait speed remained approximately unchanged over time (Figs 8.1,8.2), increased muscle co-activation at proximal level represents the most important strategy to compensate for a deterioration in both functional ability and increase in gait instability in patients with DMD.

Possible compensatory mechanisms during functional tasks were also highlighted by Peeters 2019 who investigated whether patients with DMD use trunk movement to compensate for reduced arm function when performing seated tasks. In that study, DMD children showed increased ROM in

trunk flexion-extension mainly in the extension direction, and increased muscle activity, thus they lean backwards in order to keep balance, or extend their spine from an initially more slumped posture.

Also in healthy subjects, it has been reported that the CNS co-activates many muscles to increase the whole lower limb stiffness to compensate for a reduced gait stability at lower speed [20, 21]. Conversely, a low level of co-activation is required during natural self-selected speed to likely minimize the energy expenditure and guarantee an effective gait, indeed the co-activation is positively correlated with some balance-related parameters, i.e., first and second double support and stance durations. Furthermore, in older subjects with low postural control ability muscle co-activation was significantly higher than in the elderly with high balance ability. Increased muscle co-activation could thus be a necessary change to compensate for a deterioration in postural control also in the sample observed in this study, in a similar way to what observed in healthy aging [22].

8.4 Bibliography

[1] Mylius CF, Paap D, Takken T. Reference value for the 6-minute walk test in children and adolescents: a systematic review. Expert Rev Respir Med. 2016 Dec;10(12):1335-1352.
[2] Winter DA. Biomechanics of Human Movement, 2nd ed. Wiley and Sons, New York,1979.
[3] Hermens HJ, Freriks B, Disselhorst-Klug C, Rau G. Journal of Electromyography and Kinesiology, Development of recommendations for SEMG sensors and sensor placement procedures, 2000 10(5):361–374.
[4] Yoo HJ, Sim T, Choi A, Park HJ, Yang H, Heo HM, Park KS, Mun JH. Quantifying coordination between agonist and antagonist muscles during a gait. Journal of Mechanical Science and Technology 2016;30(11)5321-28.
[5] Goudriaan M, Van den Hauwe M, Dekeerle J, Verhelst L, Molenaers G, Goemans N, Desloovere K. Gait & Posture. Gait deviations in Duchenne muscular dystrophy-Part 1. A systematic review, 2018,62:247-261.
[6] Chang R, Van Emmerik R, Hamill J. Quantifying rearfoot-forefoot coordination in human walking. J Biomech 2008;41(14):3101-05.
[7] Sutherland DH, Olshen R, Cooper L, Wyatt M, Leach J, Mubarak S, Schultz P. . Developmental Medicine and Child Neurology, The pathomechanics of gait in Duchenne muscular dystrophy 1981, 23: 3–22.
[8] Gaudreault N, Gravel D, Nadeau S, Desjardins P, Brière A. Clinical Orthopaedics and Related Research, A method to evaluate contractures effects during the gait of children with Duchenne dystrophy, 2007, 456: 51–57.
[9] McDonald CM, Abresch RT, Carter GT, Fowler Jr WM, Johnson ER, Kilmer DD, Sigford BJ. Am J Phys Med Rehabil, Profiles of neuromuscular diseases. Duchenne muscular dystrophy. 1995, 74:S70–92.
[10] Serrao M, Pierelli F, Ranavolo A, Draicchio F, Conte C, Don R, Di Fabio R, LeRose M, Padua L, Sandrini G, Casali C. Cerebellum, Gait pattern in inherited cerebellar ataxias, 2012,11:194–211.
[11] Hausdorff JM. Gait & Posture, Stride variability: beyond length and frequency, 2004,20(3):304-305
[12] Serrao M, Chini G, Iosa M, Casali C, Morone G, Conte C, Bini F, Marinozzi F, Coppola G, Pierelli F, Draicchio F, Ranavolo A. Clinical Biomechanics, Harmony as a convergence attractor that minimizes the energy expenditure and variability in physiological gait and the loss of harmony in cerebellar ataxia, 2017(48): 15-23.
[13] Sekiya, Noboru, Nagasaki H, Ito H, Furuna T. Journal of Orthopaedic & Sports Physical Therapy, Optimal walking in terms of variability in step length, 1997, 26(5): 266-272.
[14] Rinaldi M, D'Anna C, Schmid M, Conforto S. Journal of Electromyography and Kinesiology, Assessing the influence of SNR and pre-processing filter bandwidth on the extraction of different muscle co-activation indexes from surface EMG data, 2018, 43:184-192.
[15] Boudarham J, Hameau1 S, Zory R, Hardy A, Bensmail D, Roche N. PlosOne, Coactivation of Lower Limb Muscles during Gait in Patients with Multiple Sclerosis, 2015
[16] Den Otter AR, Geurts AC, Mulder T, Duysens J. Gait & Posture Abnormalities in the temporal patterning of lower extremity muscle activity in hemiparetic gait, 2007, 25:342–52.
[17] Kitatani R, Ohata K, Sato S, Watanabe A, Hashiguchi Y, Yamakami N, Sakuma K, Yamada S. Somatosens Mot Res, Ankle muscle coactivation and its relationship with ankle joint kinematics and kinetics during gait in hemiplegic patients after stroke, 2016, 33(2):79-85.
[18] Lamontagne A, Richards CL, Malouin F. Journal of Electromyography and Kinesiology, Coactivation during gait as an adaptative behavoir after stroke, 2000.
[19] Ropars, J, Lempereur M, Vuillerot C, Tiffreau V, Peudenier S, Cuisset JM, Pereon Y, Leboeuf F, Delporte L, Delpierre Y, Gross R, Brochard S. PloS one, Muscle activation during gait in children with Duchenne muscular dystrophy, 2016
[20] Fan Y, Li Z, Han S, Lv C, Zhang B. Gait & Posture, The influence of gait speed on the stability of walking among the elderly, 2016, 47:31-36.
[21] Varrecchia T, Rinaldi M, Serrao M, Draicchio F, Conte C, Conforto S, Schmid M, Ranavolo A. Journal of Electromyography and Kinesiology, Global lower limb muscle coactivation during walking at different speeds: Relationship between spatio-temporal, kinematic, kinetic, and energetic parameters, 2018, 43:148-157.
[22] Nagai K., Yamada M, Uemura Y, Yamada Y, Ichihashi N, Tsuboyama T. Arch Gerontol Geriatr, Differences in muscle coactivation during postural control between healthy older and young adults, 2011

CHAPTER 9

9. THE EFFECT OF PRE-PROCESSING SETTINGS ON MUSCLE CO-ACTIVATION ASSESSMENT

In this chapter, text and figures have been taken from or adapted from the article "*Assessing the influence of SNR and pre-processing filter bandwidth on the extraction of different muscle co-activation indexes from surface EMG data" [2018, Journal of Electromyography and Kinesiology]*, which was co-authored by me.

The effects of both noise and pre-processing choices for envelope estimation on co-activation indexes were investigated, and results were presented to the conference '6th Congress of the National Group of Bioengineering (GNB) 2018. Further results are published in the Journal of Electromyography and Kinesiology in the paper *"Assessing the influence of SNR and pre-processing filter bandwidth on the extraction of different muscle co-activation indexes from surface EMG data"*, which I drafted (M. Rinaldi et al., 2018).

In this scenario, two elements are object of discussion in the scientific community: i) since an agreed definition of muscle co-activation is missing, the different indicators of muscle co-activation from EMG data may not be totally comparable as they may refer to a different physiological interpretation of the phenomenon; ii) while most co-activation indicators have been introduced and assessed in their specific application cases, to our knowledge a thorough performance comparison between indicators, including their sensitivity to the pre-processing parameters (e.g. cut-off frequency of the low-pass filter for envelope estimation) and to the different signal to noise ratio (SNR) levels, is missing.

Focusing on the latter aspects, SNR strongly affects the performance of algorithms for EMG analysis and activation detection [1]; very variable is also the choice of the lowpass cut-off

frequency used to estimate the amplitude of EMG activity, as it ranges from 3 Hz to 25 Hz [2], and this operator-specific dependence does not guarantee the estimation of stable and repeatable information from the algorithms, unless operator-independent techniques are used [3].

For these reasons, we aim to compare the performance of the most used techniques proposed in literature to assess muscle co-activation [2], according to their respective definition, using a variety of simulated sEMG signals. Specifically: i) we used in-silico sEMG signals generated by the Hogan-Mann model; we used both rectangular and gaussian waveforms to modulate the noise; ii) we added noise to the previous signals with different levels of signal to noise ratio (SNR); iii) we simulated the co-activation by varying the amount of overlapping between the modulating waveforms; iv) we extracted the linear envelopes of each simulated signal by applying low-pass filters with a set of different cut-off frequency values; v) for each technique, we evaluated the performance by comparing the co-activation outcomes on the extracted envelopes with the co-activation outcomes on the reference represented by *ad-hoc* generated modulating waveforms.

9.1 Materials and methods

- **Simulation procedure**

A functional mathematical model of the myoelectric activity recorded from surface electrodes states that the sEMG signal *e(i)* can be expressed as:

$$e(i) = w^{\alpha}(i) \cdot n_1(i)$$

where *e(i)* is the *i-th* sample of the simulated sEMG signal, *w* is a modulating waveform representing muscular activity and n_1 is a realization of random white Gaussian noise process.

The constant α is an exponent relating the muscular activity to the electrical signal and has a value that may vary from 1 [4] to 1.7-2 [5,6]. In this simulation, it is further supposed that α is equal to 1.

In this work the simulated dataset has been built by using two kinds of modulating waveform *w:* a rectangular (R_{wave}) and a gaussian (G_{wave}, standard deviation 50 ms) waveform. For each type of

modulating waveform, the agonist and antagonist muscles have been simulated by assigning fixed values of amplitude to the respective modulating waveforms: these values are 0.5 for agonist and 1 for antagonist (Fig. 9.1).

A further random white Gaussian noise realization n_2, which is statistically independent from n_1, was added to e to simulate typical SNR conditions (5, 10, 15 and 20 dB) [1]. A simulated sEMG signal is then expressed as:

$$sEMG(i) = w(i) \cdot n_1(i) + n_2(i)$$

The linear envelopes (LE) of the simulated signals for each SNR condition and each modulating waveform were extracted, after rectification, by a fourth-order Butterworth low pass filter with four different values of cut-off frequency ($f_{cut\text{-}off}$): 5, 10, 15 and 20 Hz..

The performance of the main techniques used to assess muscle co-activation, which will be described in the next section, was then evaluated on the following signals:

- rectangular (R_{wave}) and gaussian (G_{wave}) modulating waveforms, taken as reference;
- Linear envelopes of sEMG as obtained by R_{wave}, LE_R, for each SNR condition and for each $f_{cut\text{-}off}$;
- Linear envelopes of sEMG as obtained by G_{wave}, LE_G, for each SNR condition and for each $f_{cut\text{-}off}$.

Levels of amplitude were set at 0.5 for the agonist and 1 for the antagonist muscle, respectively. Thus, the co-activation was simulated by pairs of signals mimicking agonist and antagonist activity, with specific amplitudes. For each combination obtained for a triplet of SNR level, $f_{cut\text{-}off}$ and degree of overlapping (25%, 50%, 75%, 100%), fifty independent realizations of a random white Gaussian process for n_1 and fifty independent realizations of the same kind of process for the noise n_2 were generated.

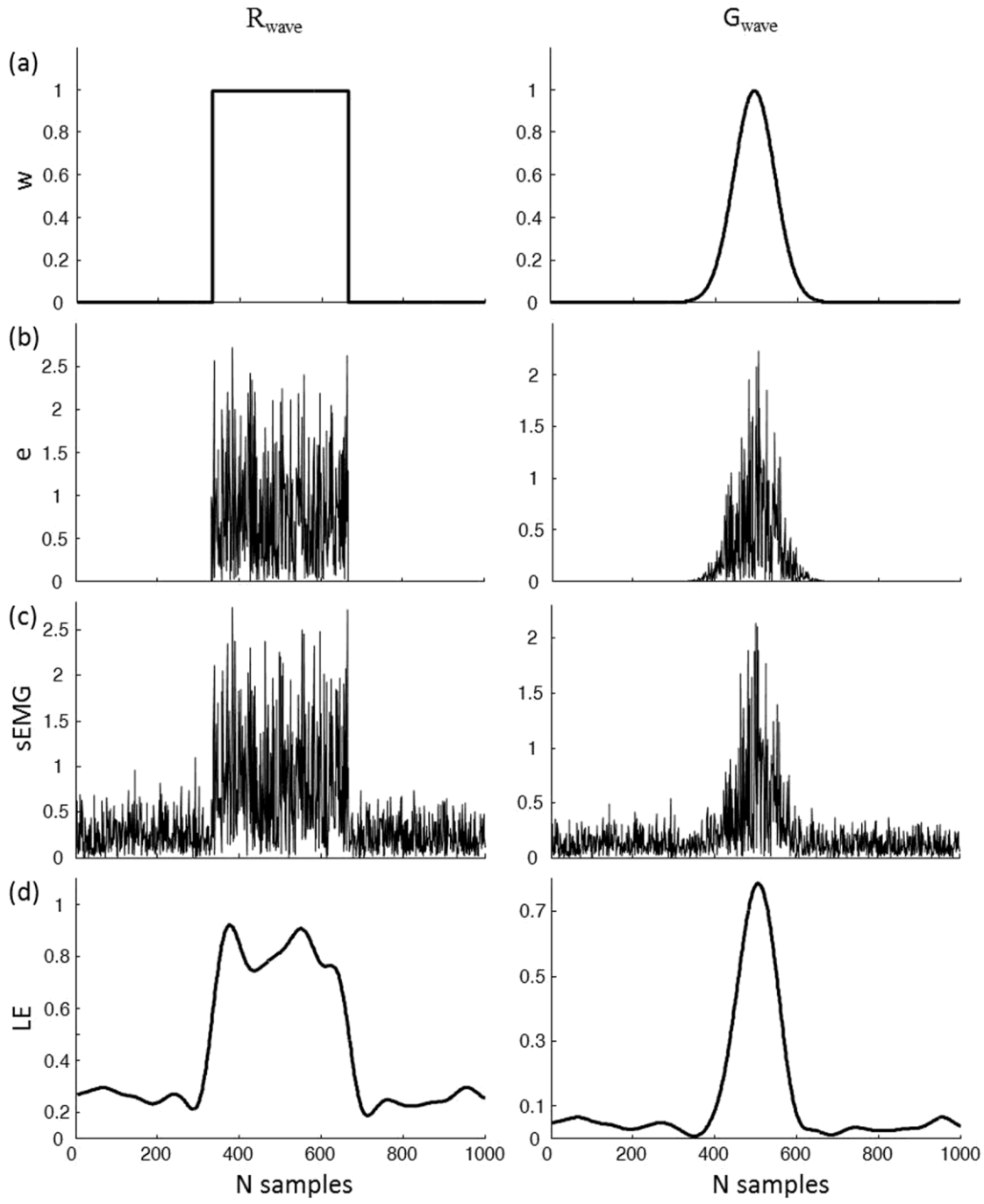

Figure 9.1. (a) Rectangular (R_{wave} at left) and gaussian (G_{wave} at right) modulating functions (w) used in the simulation procedure (amplitude equal to 1). (b) R_{wave} and G_{wave} function modulates the realization of a white Gaussian random process (n_1). The obtained signal simulates the myoelectric activity due to muscle activation (e). The plots present the full wave rectified signals. (c) A second realization of a white Gaussian random process (n_2), uncorrelated with the R_{wave} (left) and G_{wave} (right) obtained at the previous step, simulates additive noise. The plots report sEMG with SNR = 10 dB. (d) Linear envelopes extracted from sEMG with low pass filter (cut-off frequency 10 Hz).

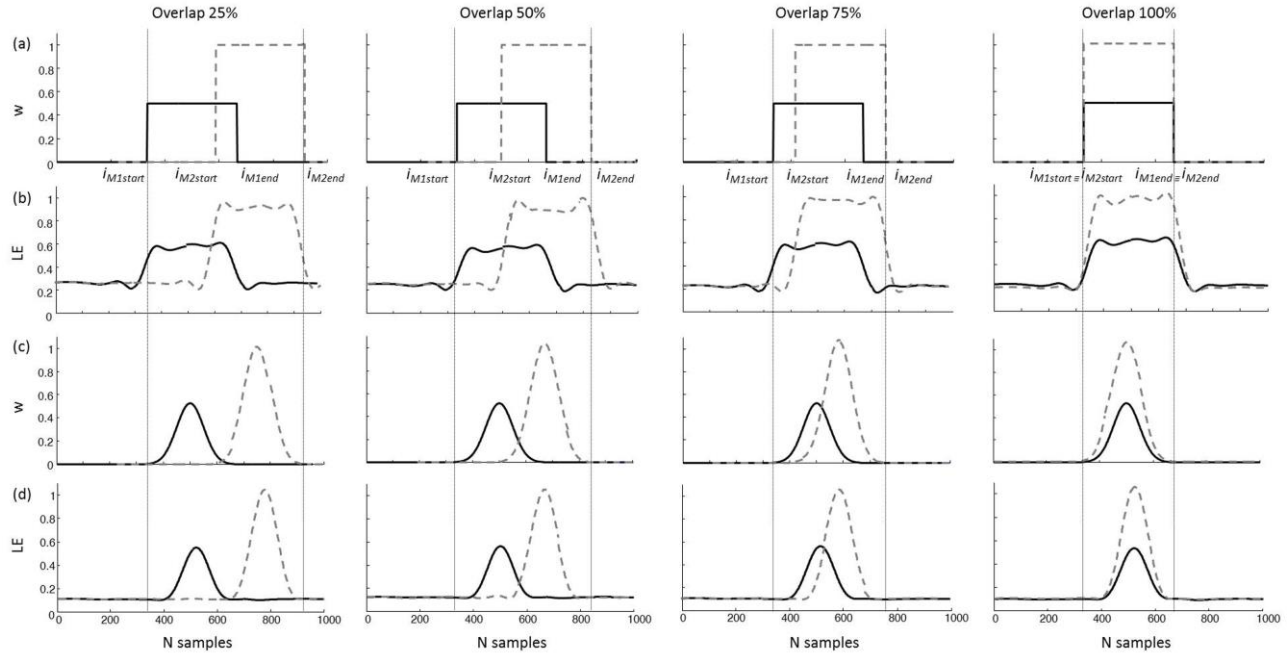

Figure 9.2. (a) R_{wave} (with amplitude equal to 1 and 0.5) with overlaps of 25%, 50%, 75%, and 100%. (b) Examples of linear envelopes (cut-off frequency=10 Hz and SNR=10 dB), obtained from modulating waveforms in (a) and with overlaps of 25%, 50%, 75%, and 100%. (c) Gaussian modulating waveforms G_{wave} (with amplitude equal to 1 and 0.5) with overlaps of 25%, 50%, 75%, and 100%. (d) Examples of linear envelopes (cut-off frequency=10 Hz and SNR=10 dB), obtained from modulating waveforms in (c) and overlapped of 25%, 50%, 75%, and 100%. Vertical lines represent the time support (between $i_{M1start}$ and i_{M2end}) considered for the co-activation analysis. The instants when the first modulating waveform returns to zero (i_{M1end}) and when the second modulating waveform becomes higher than zero ($i_{M2start}$) are also indicated.

The proposed model has been chosen for two reasons: the simplicity in its implementation, which makes the dataset generation easier, and the independence from frequency signature that doesn't affect the co-activation indexes; despite being rather old, it is still popular in the scientific community as an effective yet simple method to be used when comparing different estimation methods [7,8]. The physiological parameters embedded in the most recent models could be useful to study how muscle anatomy and geometry, motor unit distribution and volume conductor affect the muscle co-activation.

- **Techniques to assess muscles co-activation**

In the following the six computational techniques under comparison are grouped into three main categories: agonist-antagonist, multi-muscle, vector coding.

Agonist–antagonist approach

The co-activation algorithms proposed by Kellis et al, 2003, and by Falconer et al, 1985, Unnithan et al, 1996, Rudolph et al, 2000 [9-12] are based on an agonist–antagonist approach, and require (except for Rudolph) an a-priori sorting of the muscles depending on the generated moment. In physiological movements, agonist and antagonist muscles contract in a non-simultaneous way. Indeed, when a muscle group (agonist) contracts to generate a moment and rotate a body segment around a joint, the antagonist muscle group remains inactive in such a way that it does not cause braking action through the production of an opposite force moment. In the following we will denote the two muscles as M_1 and M_2, and the corresponding linear envelopes LE_{M1} and LE_{M2} as lasting N samples. All the co-activation indexes introduced by these techniques assume values between 0 and 100 (the lower the index value, the lower the level of muscle co-activation, except for Kellis). The time support used to calculate these indexes starts when the first modulating waveform becomes higher than zero ($i_{M1start}$) and ends when the second one returns to zero (i_{M2end}). i_{M1end} and $i_{M2start}$ are referred to the instant when the first modulating waveform returns to zero and the instant when the second one becomes higher than zero, respectively.

A) Kellis method

The approach is based on the identification of the inter-relationships between antagonist muscles during movement: if M_1 is a stabilizer/antagonist and M_2 provides the main force for the movement, the co-activation index CI_K provides a relative measure of the M_1 contribution to the total activation during the task, and it is calculated as follows:

$$CI_K = \frac{\sum_{i=i_{M1start}}^{i_{M2end}} LE_{M1}(i)}{\sum_{i=i_{M1start}}^{i_{M2end}} (LE_{M1}(i) + LE_{M2}(i))} \cdot 100$$

Low CI_K values indicate low activation of the stabilizer/antagonist, values close to 50 indicate the same activation of agonists and antagonists, and values in the range 50-100 indicate an inversion of the behaviour. For this index, maximum co-activation corresponds to having an index of 50.

B) Falconer and Winter method

The co-activation index calculated by Falconer and Winter (CI_{FW}) is expressed as:

$$CI_{FW} = \frac{2I_{ant}}{I_{Total}} \cdot 100$$

Where

$$I_{Total} = \sum_{i=i_{M1start}}^{i_{M2end}} (LE_{M1}(i) + LE_{M2}(i))$$

and I_{ant} is the area of total antagonistic activity:

$$I_{ant} = \sum_{i=i_{M1start}}^{i_{M2start}} LE_{M2}(i) + \sum_{i=i_{M2start}}^{i_{M2end}} LE_{M1}(i)$$

where in our simulation the vectors **u** = [$i_{M1start}$:$i_{M2start}$] and **v** = [$i_{M2start}$:i_{M2end}] correspond to the vector indexes where $LE_{M2}(\mathbf{u}) < LE_{M1}(\mathbf{u})$ and $LE_{M1}(\mathbf{v}) < LE_{M2}(\mathbf{v})$, respectively. In this case, maximum co-activation corresponds to having $CI_{FW} = 100$.

C) Unnithan method

The co-activation index CI_U is calculated by dividing the area overlapped by the linear envelopes of the agonist and antagonist muscles by the number of data points.

$$CI_U = \frac{1}{(i_{M2end} - i_{M1start} + 1)} \left(\sum_{i=i_{M1start}}^{i_{M2end}} \min[LE_{M1}(i), LE_{M2}(i)] \right) \cdot 100$$

This index will be maximum if linear envelopes of each muscle have always the same value, i.e. maximum co-activation. In this case, maximum co-activation corresponds to having $CI_U = 100$.

D) Rudolph method

This method provides a time-dependent co-activation function *C(i)*:

$$C(i) = \frac{min\{LE_{M1}(i), LE_{M2}(i)\}}{max\{[LE_{M1}(i), LE_{M2}(i)\}} \cdot (LE_{M1}(i) + LE_{M2}(i))$$

with i ranging from $i_{M1start}$ to i_{M2end}. The mean value of *C(i)* over this activation range represents a summary co-activation index. Also in this case, the index is maximum when the minimum corresponds to the maximum for each sample, i.e. complete co-activation. The algorithm proposed by Rudolph and colleagues provides co-activation values ranging between 0 and 200; in order to obtain co-activation values within the range 0-100, as seen for the other methods, Don and colleagues slightly modified the equation by Rudolph et al, 2000, by replacing the second factor, consisting of the sum of the two samples, with the mean:

$$C(i) = \frac{min\{LE_{M1}(i), LE_{M2}(i)\}}{max\{LE_{M1}(i), LE_{M2}(i)\}} \cdot \left(\frac{LE_{M1}(i) + LE_{M2}(i)}{2}\right)$$

with i ranging from $i_{M1start}$ to i_{M2end}. Thus, the summary co-activation index (CI_{RU}) can be expressed as:

$$CI_{RU} = \frac{\sum_i C(i)}{(i_{M2end} - i_{M1start} + 1)} \cdot 100$$

<u>Time-varying Multi-muscle approach</u>

The Time-varying Multi-muscle Co-activation function *(TMCf)* extends the analysis to the simultaneous activity on multiple muscles or muscle groups and provides an index assuming values between 0 and 100 [13]:

$$TMCf(d(i), i) = C(d(i)) \cdot m(i) \cdot cc(i)$$

Where i ranges from $i_{M1start}$ to i_{M2end} and

$$C\big(d(i)\big) = \left(1 - \frac{1}{1 + e^{-12(d(i)-0.5)}}\right)$$

is a sigmoid weight reduction coefficient, ranging between 0 and 1, that takes into account, within the exponential function, the mean of the differences between each pair of muscles:

$$d(i) = \left(\frac{\sum_{k=1}^{M-1} \sum_{j=k+1}^{M} \left| LE_k(i) - LE_j(i) \right|}{(i_{M2end} - i_{M1start} + 1) \cdot \frac{M!}{2!\,(M-2)!}} \right)$$

Where M is the number of muscles (M = 2 in this work) and M!/2!(M-2)! is the total number of possible differences between each pair of muscles.

The *TMCf (d(i),i)* has the following properties: inverse relationship with the mean of the differences *d(i*), values close to the mean activation of the *m(i)* muscle sample values considered when *d(i)* is close to 0, and values close to 0 when *d(i)* is close to 1. In particular, the smaller the differences in muscle sample activation, the closer the *d(i)* values are to 0 and the closer the sigmoid-coefficient values are to 1, leaving the *TMCf (d(i),i)* value close to the value of its mean. Inversely, the greater the differences in muscle activations, the more *d(i)* increases and the more the sigmoid coefficient *C(d(i)* decreases, thereby reducing the *TMCf (d(i),i)* values

$$m(i) = \left(\frac{\sum_{k=1}^{M} LE_k(i)}{M} \right)$$

m(i) is a weighting factor that takes into account the mean activation behaviour of the muscles under analysis.

$$cc(i) = \frac{\left(\frac{\sum_{k=1}^{M} LE_k(i)}{M} \right)}{\max\limits_{k=1,\dots M} LE_k(i)}$$

while *cc(i)* is a correction coefficient introduced to adjust *TMCf (d(i),i)* in the trivial case of two muscles. The overall co-activation index (CI_{RA}) is then obtained by calculating the mean value along the time support of the activation:

$$CI_{RA} = \frac{\sum_{i=i_{M1start}}^{i_{M2end}} TMCf(i)}{(i_{M2end} - i_{M1start} + 1)} \cdot 100$$

Vector Coding approach

An approach based on a Vector Coding Technique (VCT) is typically used to quantify the coordination among patterns of agonist and antagonist muscles for different signals of equivalent type [14]. The results divide the coordination patterns into 4 classes: In-phase or In-activation (when two signals simultaneously either increase or decrease their respective amplitudes); Anti-phase or Anti-activation (when two muscles act in an antagonist way – the first increases and the second decreases its amplitude or vice versa); One-only (when only one muscle is active), and Other-only (when only the other muscle is active) [15].

To identify the co-activation pattern, a 2-D plot is constructed where the horizontal axis corresponds to one sEMG signal envelope LE_{M1} and the vertical axis corresponds to the other sEMG signal envelope LE_{M2} overlapped with the previous one with a certain percentage of overlap. The coupling angle (γ) is then defined as the positive direction angle subtended from a vector adjoining two successive time points relative to the right horizontal [29]:

$$\gamma_i = \begin{cases} \arctan\left(\frac{LE_{M2}(i+1) - LE_{M2}(i)}{LE_{M1}(i+1) - LE_{M1}(i)}\right) if \left(LE_{M1}(i+1) - LE_{M1}(i)\right) \geq 0 \\ 180° + \arctan\left(\frac{LE_{M2}(i+1) - LE_{M2}(i)}{LE_{M1}(i+1) - LE_{M1}(i)}\right) if \left(LE_{M1}(i+1) - LE_{M1}(i)\right) < 0 \end{cases}$$

where i ranges from $i_{M1start}$ to i_{M2end}-1 and $0° \leq \gamma \leq 360°$.

When coupling angles are 45° and 225°, the couple of the signals is in-phase. In-phase couples rotate in the same direction. On the other hand, at 135° and 315°, the coordination is anti-phase. Anti-phase couples rotate in opposite directions. When the segment adjoining two successive points is parallel to the horizontal axis ($\gamma = 0°$ or 180°), there is a one-only signal phase. When the segment adjoining two successive points is parallel to the vertical axis ($\gamma = 90°$ or 270°) indicate the other-

only signal phase. When coupling angles do not relate to vertical, horizontal and diagonal vectors, the patterns are less pure (Fig. 9.3).

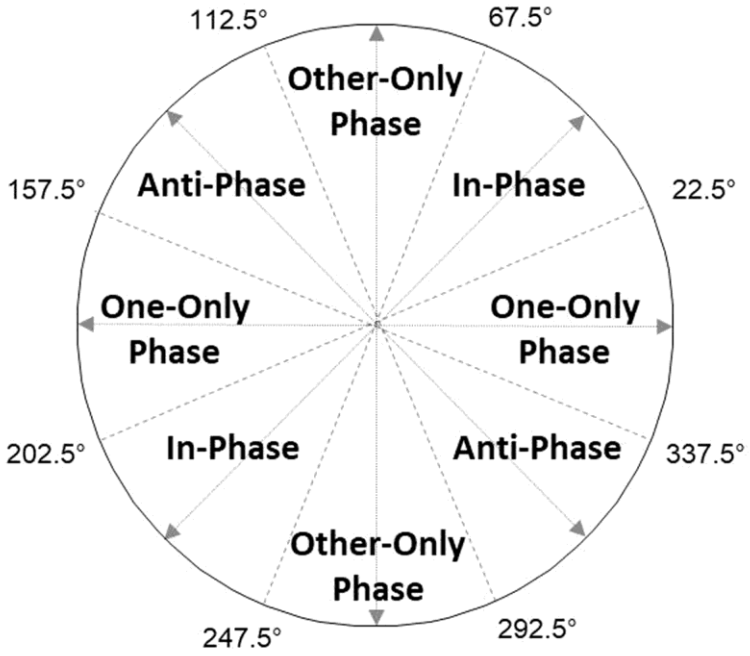

Figure 9.3. Definition of muscle activity patterns depending on the range of coupling angle.

Muscle activity pattern is then classified according to the following: One-only activation if $67.5 \leq \gamma_i < 112.5$ or $247.5 \leq \gamma_i < 292.5$; Other-only activation for $0 \leq \gamma_i < 22.5$, $157.5 \leq \gamma_i < 202.5$, or $337.5 \leq \gamma_i < 360$; In-activation if $22.5 \leq \gamma_i < 67.5$ or $202.5 \leq \gamma_i < 247.5$; Anti-activation if $112.5 \leq \gamma_i < 157.5$ or $292.5 \leq \gamma_i < 337.5$ (Fig. 9.4).

CI_{VCT} is then calculated as the total number of temporal instants classified as either In- or Anti-activation relative to the total duration of the activation (in the studied case, it is between $i_{M1start}$ and i_{M2end}) multiplied by 100. Complete co-activation corresponds to a $CI_{VCT} = 100$.

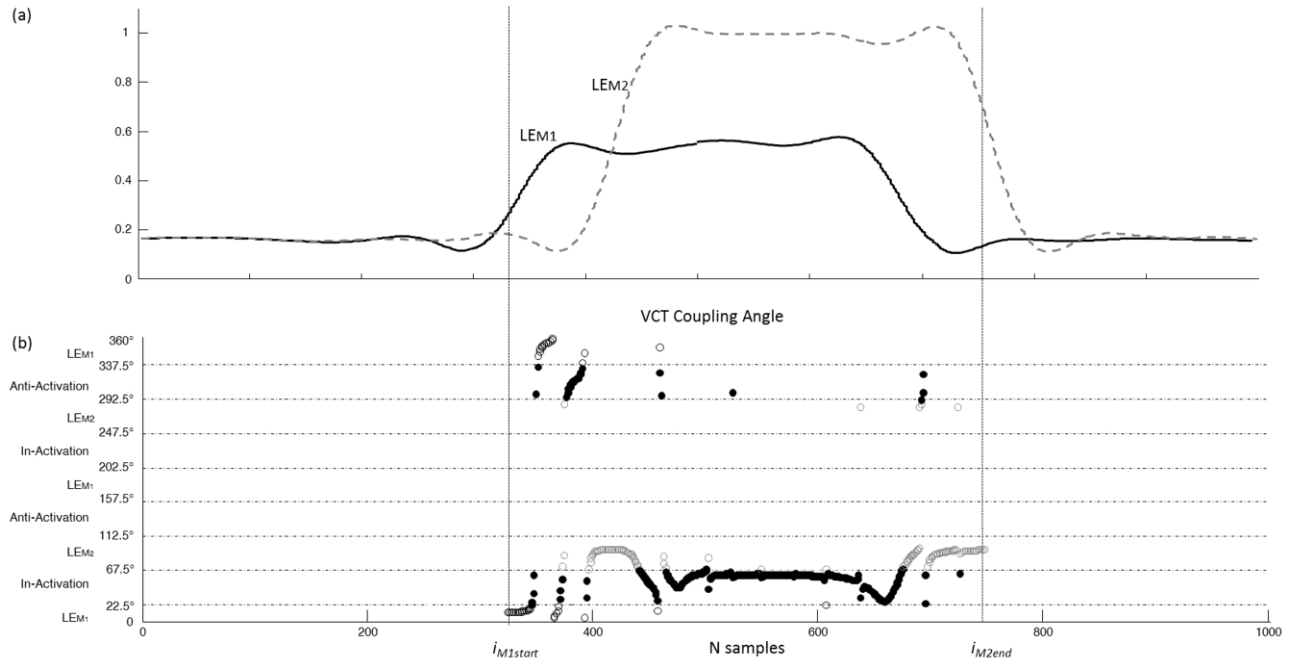

Figure 9.4. (a) Examples of linear envelopes (cut-off frequency=10 Hz and SNR=10 dB), obtained from R_{wave} overlapped for the 75% of their duration. (b) The analysis of co-activation on the signals in (a) by using VCT. Vertical lines represent the time support (between $i_{M1start}$ and i_{M2end}) considered for the co-activation analysis. Three different colors in the figure represent the result of: empty black circles for one-only activation, empty light gray circles for other-only activation, full black circles for co-activation. The Horizontal axis in the figure represents the changes of LE_{M1} and LE_{M2}. The vertical axis represents the result of the VCT method to analyze by the changes of coupling angle.

- **Algorithms performance**

The performance of each algorithm (CI_{FW}, CI_{U}, CI_{RU}, CI_{K}, CI_{RA}, CI_{VCT}) was evaluated on a testing set of fifty simulated time series for each test case defined by the triplet of factors: SNR, overlapping percentage, $f_{cut\text{-}off}$.

The estimated co-activation values are expressed, for each test case, as the mean value of the co-activation indexes calculated over the fifty test signals. The co-activation indexes obtained on the modulating waveforms were considered as reference.

The following aspects were thus analysed:

- the sensitivity of the different techniques with respect to the different SNR conditions;

- the influence of the low pass cut-off frequency on co-activation estimation;

- the performance with respect to different overlapping between the two signals;
- the influence of the modulating waveform (i.e. rectangular or gaussian).

To investigate the ability of each technique to be sensitive to the amount of co-activation, indirectly expressed in terms of amount of overlapping, we linearly fitted the data across the different values of overlapping, and calculated the slope (*s*) of the fitting line obtained by using the value of CI as predictor of the amount of coactivation, after verifying that the linear model well approximated the data ($R > 0.995$). A value of *s* close to 1 may be considered as a good predictor.

- **Statistical analysis**

For each algorithm, to examine the differences between the co-activation value and the reference, a one-sample t-test for each level of overlap, SNR and $f_{cut\text{-}off}$ was performed using MATLAB (version 8.3.0.532, MathWorks, Natick, MA, USA) software. Descriptive statistics included means ± SD, and significance level was set at $p < 0.05$.

9.2 Results

The results of each algorithm for both rectangular and gaussian modulating waveforms are shown in Fig. 9.5 and Fig. 9.6, respectively.

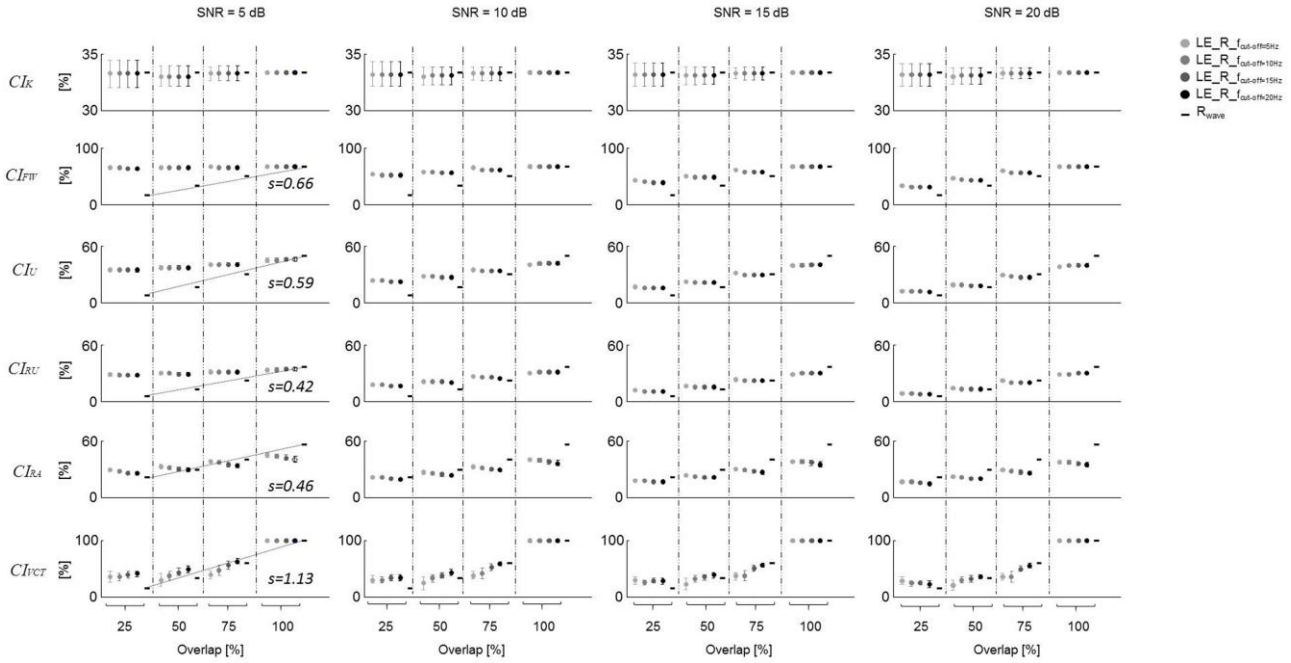

Figure 9.5. CI values (±SD) obtained, for each algorithm, by averaging the simulation results of fifty time series of linear envelopes extracted from sEMG generated by utilizing fifty independent realizations of a white Gaussian random process for n_1, fifty independent realizations of the same kind of process for the noise n_2 (SNR equal to 5, 10, 15, 20 dB), and a rectangular modulating waveform (R_{wave}). Every dot represents CI values obtained for each low pass frequency (5, 10, 15, 20 Hz) used to extract the liner envelopes of the simulated sEMG signals at every level of overlap (dashed vertical lines). Black horizontal dashes are the results of each algorithm obtained on the rectangular modulating waveforms (i.e. the reference). For each algorithm, the fitting lines with the values of the slope (s) were also reported.

- **Performance evaluation**

Rectangular modulating waveform

From the analysis of Kellis method, significant differences between algorithm performances and the reference were observed only for overlap 50% for each $f_{cut\text{-}off}$, independently from SNR ($p<0.05$) (Fig. 9.5). As suggested by the definition in the section 2.2.1, this method gives information only about the activation of one signal (a priori identified as the antagonist signal) compared to the total activation. Thus, we believe that CI_K is not directly linked to an effective estimation of the co-activation level between two signals, defined as the simultaneous activity of agonist and antagonist muscles. This independence is also visible from the almost flat regression line with the amount of overlapping. For this reason, Kellis method will not be examined further.

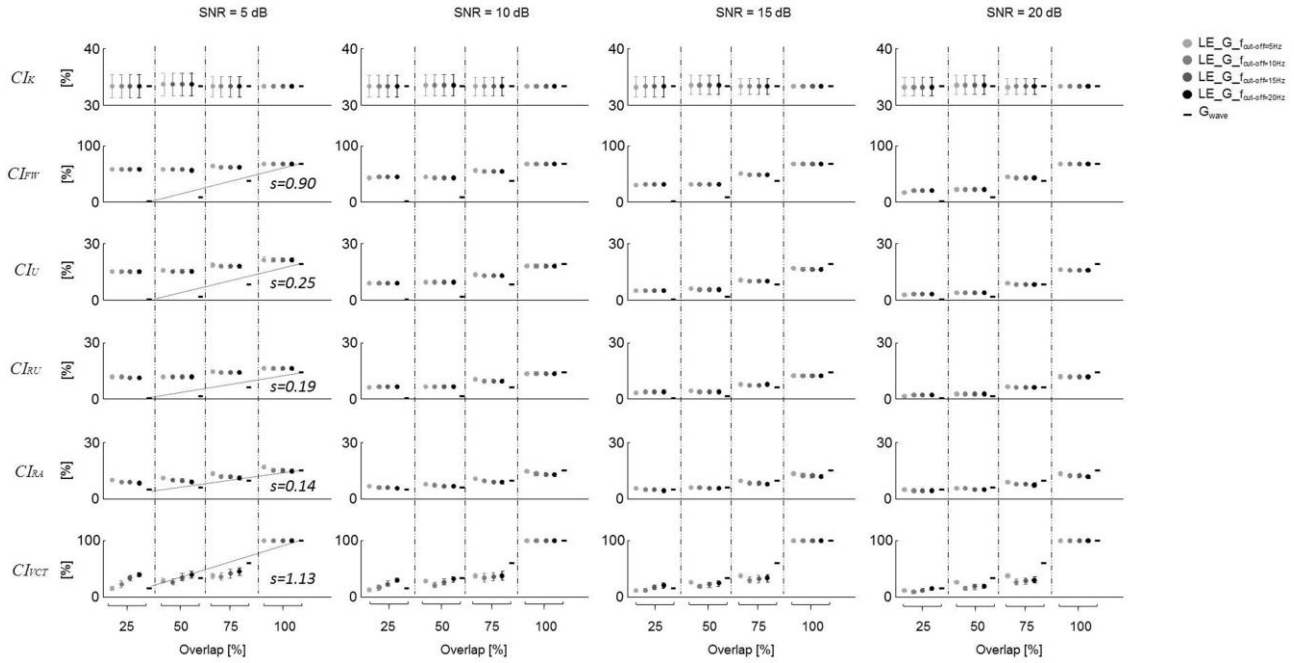

Figure 9.6. CI values (±SD) obtained, for each algorithm, by averaging the simulation results of fifty time series of linear envelopes extracted from sEMG(i) generated by utilizing fifty independent realizations of a white Gaussian random process for n_1, fifty independent realizations of the same kind of process for the noise n_2 (SNR equal to 5, 10, 15, 20 dB), and a gaussian modulating waveform (G_{wave}). Every dot represents CI values obtained for each low pass frequency (5, 10, 15, 20 Hz) used to extract the liner envelopes of the simulated sEMG signals at every level of overlap (dashed vertical lines). Black horizontal dashes are the results of each algorithm obtained on the gaussian modulating waveforms (i.e. the reference). For each algorithm, the fitting lines with the values of the slope (s) were also reported.

As regards to CI_{FW} and CI_{VCT}, the t-test shows significant differences from the reference value for each $f_{cut\text{-}off}$ and for each overlap ($p < 0.001$) except for overlap 100% ($p > 0.05$) (Fig. 9.5). Furthermore, performances of these methods seem to be generally better for high levels of $f_{cut\text{-}off}$.

For each SNR and level of overlap, CI_U, CI_{RU} and CI_{RA} show significant differences from the reference for each $f_{cut\text{-}off}$ ($p < 0.001$) (Fig. 9.5). Furthermore, an improvement in the algorithm performance with respect to the R_{wave} reference can be observed for high levels of SNR on both CI_{RU} and CI_U, while CI_{RA} seems to be less sensitive to the SNR level.

The analysis of the fitting line slope on the R_{wave} reference performance suggests that both CI_{FW} and CI_{VCT} are more sensitive to the level of overlap than the others, showing higher values of *s* (Fig. 9.5).

Gaussian modulating waveform

Results obtained with gaussian modulating waveform are similar to those obtained with the rectangular modulating waveform (Fig. 9.6). As observed for the R_{wave} reference, both CI_{FW} and CI_{VCT} are highly sensitive to the amount of co-activation, indirectly expressed in terms of amount of overlapping, showing high values of *s*. Nevertheless, for G_{wave} reference a decrease in *s* values, and thus a worsening of the ability to be sensitive to the amount of co-activation, was observed for the other indexes CI_U, CI_{RU} and CI_{RA}.

9.3 Discussion and Conclusion

Signals recorded by means of surface electromyography contain useful information for a better understanding of the strategies underlying human movement. In particular, a practical contribution to those studies that investigate motor control mechanisms leading to the contemporary activation of muscular groups may be provided by a reliable estimation of the level of muscle co-activation because it has quantitative effects on body stability, muscles, and joints in human movements [16,17]. This information could, in fact, represent an assessment of the simultaneous activity of agonist and antagonist muscles crossing the same joint [18] obtained without using invasive measurements.

Essentially, the Central Nervous System (CNS) exploits muscle co-activation as a motor control mechanism to modulate joint stiffness and postural stability, to optimize energy efficiency, to enhance movement accuracy so allowing adaptation to environmental demands [19]. Thus, since muscle co-activation is widely used in orthopedics, neurology, ergonomics and several other clinical fields [13,20] to understand the strategy exerted by the CNS in controlling and modulating the neuromuscular output, it is important to correctly process myoelectric signals in order to extract this information by means of algorithms that are as robust and as objective as possible.

The results obtained in this study demonstrated some practical elements: first, data recording conditions, and the relative amount of muscular activation with respect to the background noise (as simulated by different levels of SNR) play a relevant role in the ability of the indexes introduced by the studied techniques to follow muscular co-activation; then, operator choices for pre-processing (namely, the choice of the cut-off frequency for envelope estimation) seem to be relevant for most of the techniques analyzed in this study (Falconer and Winter, Unnithan, Rudolph, Ranavolo and Vector Coding methods); a rather minor effect is associated with the shape of the muscular activation, as differences between the two types of modulating functions are in general negligible. Some techniques (Unnithan, Rudolph and Ranavolo methods), however, showed a worse sensitivity to the amount of co-activation, when passing from rectangular to gaussian modulation, as shown by the decrease of s, which represents a reduction on the coactivation ability to track variations in terms of overlapping.

Performances obtained from Kellis method seem to be independent from both SNR and cut-off frequency for both rectangular and gaussian modulating waveforms (Figs. 9.5, 9.6). Nevertheless, this technique showed the highest values of variability across the realizations. Furthermore, it is based on the anatomic and functional role of the two muscles, taking into consideration that one muscle is generally considered as the stabilizer whereas the other provides the main force for movement. In this way, the co-activation index provides a relative measure of the stabilizer muscle contribution to the total activation during the task, without directly providing an effective estimation of the simultaneous activity of agonist and antagonist muscles.

Regarding Falconer and Winter method, performances are influenced by the values of both cut-off frequency and SNR. Furthermore, this method has a pretty good sensitivity to the amount of overlap, both for rectangular and gaussian modulating waveforms (Figs. 9.5 and 9.6).

The techniques proposed by Unnithan and Rudolph are moderately influenced by the value of the cut-off frequency. Furthermore, these methods seem to improve their performance for high levels of SNR, independently from the type of modulating waveform (Figs. 9.5, 9.6).

Given its independence from SNR, the performance of the method proposed by Ranavolo is instead influenced by the value of the cut-off frequency: better performance for low levels of cut-off frequency are observed both for rectangular and gaussian modulating waveforms (Figs. 9.5, 9.6). A possible interpretation of this result can be found in the mathematical definition of the algorithm: the construction of the co-activation curve, as defined in the section 2.2.2, is strongly dependent on the level of smoothness applied on the signals used to estimate the co-activation.

The sensitivity obtained with Unnithan, Rudolph and Ranavolo methods resulted lower with the gaussian modulating waveform than with the rectangular one (Figs. 9.5, 9.6). Thus, the use of a rectangular modulating waveforms improves the ability of these techniques to be sensitive to the amount of co-activation, indirectly expressed in terms of amount of overlapping.

The Vector Coding Technique is influenced by the values of both cut-off frequency and SNR, and it achieves better performance for cut-off frequencies at least equal to 10 Hz, independently from the type of modulating waveform. Furthermore, this method is the most sensitive to the level of overlap, as suggested by the value of the fitting line slope *(s)* for both modulating waveforms (Figs. 9.5, 9.6). Since with this method it is possible to temporally separate the coordination of two muscles into In- and Anti-activation phases, the relative interactions between the two muscles can be continuously monitored over time.

The relevance of the analysis of muscle co-activation to several fields is well known, thus it is important to correctly process myoelectric signals in order to extract this parameter by avoiding estimation bias. In this study, the obtained performance of some popular techniques used to assess muscle co-activation was thus evaluated by means of simulated sEMG signals generated with varying SNR levels and different modulating functions, and processed with varying values of low-

pass filtering. The sensitivity of each technique to capture variations in co-activation was tested by using different levels of simultaneous action of the muscles. The analysis of the results shows that the performance of the methodologies used to assess muscle co-activation are influenced by the choice of the low pass cut-off frequency, as well as by the level of signal to noise ratio.

In particular, for low values of SNR, Ranavolo and Vector Coding are to be preferred and the Vector Coding Technique shows the highest performance when the SNR is higher. For the vector coding technique, it is to be highlighted that its performance improves with higher cut-off frequencies. These results may be used to choose the co-activation index that may better represent the extent and amount of co-activation based on the recording conditions (SNR level), and processing needs (cut-off frequencies).

9.4 Bibliography

[1] Bonato P, D'Alessio T, Knaflitz M. A statistical method for the measurement of muscle activation intervals from surface myoelectric signal during gait. IEEE Trans Biomed Eng. 1998;45(3):287-99.

[2] Rosa MC, Marques A, Demain S, Metcalf CD, Rodrigues J. Methodologies to assess muscle co-contraction during gait in people with neurological impairment – a systematic literature review. J Electromyogr Kinesiol 2014;24(2):179-91.

[3] D'Alessio T, Conforto S. Extraction of the envelope from surface EMG signals. IEEE Eng Med Biol 2001;20(6):55-61.

[4] Gottlieb GL, Agarwal G. Dynamic relationship between isometric muscle tension and the electromyogram in man. J. Appl. Physiol 1971;30:345-51.

[5] Hogan N, Mann RW. Myoelectric signal processing: Optimal estimation applied to electromyography. Part I: Derivation of the optimal myoprocessor. IEEE Tran: Biomed. Eng 1980(27):382-95.

[6] Hogan N, Mann RW. Myoelectric signal processing: Optimal estimation applied to electromyography. Part II: Experimental demonstration of optimal myoprocessor performances. IEEE Trans. Biomed. Eng 1980(27):396-410.

[7] Hayashi, H, Furui, A, Kurita, Y, Tsuji, TA. Variance Distribution Model of Surface EMG Signals Based on Inverse Gamma Distribution. IEEE Transactions on Biomedical Engineering 2017;64: 2672-2681.

[8] Xu, Y, McClelland, VM, Cvetkovic, Z, Mills, KR. Corticomuscular Coherence with Time Lag with Application to Delay Estimation. IEEE Transactions on Biomedical Engineering 2017;64:588-600.

[9] Kellis E, Arabatzi F, Papadopoulos C. Muscle co-activation around the knee in drop jumping using the co-contraction index. J Electromyogr Kinesiol 2003 Jun;13(3):229-38.

[10] Falconer FK., Winter D. Quantitative Assessment of Cocontraction at the Ankle Joint During Walking. Electromyography and Clinical Neurophysiology 1985;25 (2–3): 135–49.

[11] Unnithan VB, Dowling JJ, Frost G, Volpe Ayub B, Bar-Or O. Cocontraction and phasic activity during GAIT in children with cerebral palsy. Electromyogr Clin Neurophysiol 1996;36(8):487–94.

[12] Rudolph KS, Axe MJ, Snyder-Mackler L. Dynamic stability after ACL injury: who can hop? Knee Surg Sports Traumatol Arthrosc 2000;8(5):262-69.

[13] Ranavolo A, Mari S, Conte C, Serrao M, Silvetti A, Iavicoli S, Draicchio F. A new muscle co-activation index for biomechanical load evaluation in work activities. Ergonomics. 2015;58(6):966-79.

[14] Yoo HJ, Sim T, Choi A, Park HJ, Yang H, Heo HM, Park KS, Mun JH. Quantifying coordination between agonist and antagonist muscles during a gait. Journal of Mechanical Science and Technology 2016;30(11)5321-28.

[15] Chang R, Van Emmerik R, Hamill J. Quantifying rearfoot-forefoot coordination in human walking. J Biomech 2008;41(14):3101-05.

[16] Hug F. Can muscle coordination be precisely studied by surface electromyography?. Journal of Electromyography and Kinesiology 2011;21(1):1-12.

[17] Arias P, Espinosa N, Robles-García V, Cao R,Cudeiro J. Antagonist muscle co-activation during straight walking and its relation to kinematics: Insight from young, elderly and parkinson's disease, Brain Research 2012;1455:124-131.

[18] Busse ME, Wiles CM, van Deursen RWM. Muscle co-activation in neurological conditions. Phys Ther Rev 2005;7(4):247–53.

[19] Simmons RW, Richardson C. Peripheral regulation of stiffness during arm movements by coactivation of the antagonist muscles. Brain Res. 1988;473(1):134-40.

[20] Le P, Best TM, Khan SN, Mendel E, Marras WS. A review of methods to assess coactivation in the spine. J Electromyogr Kinesiol 2017;32:51-60.

CHAPTER 10

10. THE EFFECT OF NON-NEGATIVE MATRIX FACTORIZATION INITIALIZATION ON THE ACCURATE IDENTIFICATION OF MUSCLE SYNERGIES

In this chapter, text and figures have been taken from or adapted from the Conference paper "*The effect of Non-Negative Matrix Factorization initialization on the accurate identification of muscle synergies with correlated activation signals" [2018, MeMea]*, which was co-authored by me.

The theory of modular motor control hypothesizes that muscle coordination during different motor tasks can be represented by the modulation of the activity of a limited set of motor modules, called muscle synergies [1-3]. In the synchronous synergies model, muscle coordination can be divided into a spatial component W, representing the contribution of each muscle on each synergy, and a series of temporal coefficients C, that are representative of the temporal activation profile of each motor module.

The analysis of the spatio-temporal structure of muscle synergies has been widely used as a tool for the assessment of several features of muscle activity in the presence of different pathologies such as stroke. Given this, the correct identification of one or both components of this modular structure can help with the definition of synergy-based synthetic parameters for the quantitative description of the motor performances in patients.

The correct identification of the modular structures (i.e. W and C) requires a series of necessary steps starting from the raw measured multi-muscle myoelectric signal, such as filtering, envelope extraction, amplitude and time scale normalization and decomposition. Up to now, a number of studies performing muscle synergy analysis have taken subjective and different methodological

choices leading to substantially different interpretations of the obtained results. In these regards, a complete understanding of how different choices in the processing steps influence those results is crucial for allowing the quantitative assessment of motor control strategies through muscle synergy analysis.

Among the previously described processing steps for muscle synergy analysis, this study focuses on the limitation of the decomposition algorithm and its specific settings. Different methods of extracting muscle synergies from pre-processed sEMG data are compared in [4]. Among the various dimensionality reduction algorithms typically used for this purpose, Non-Negative Matrix Factorization (NNMF) is the most used, due to its low computational complexity and to its reliability [4,5]. This algorithm works by factorizing the original matrix D containing the sEMG envelopes into the two matrices, W, containing the spatial component of each synergy, and C, containing their temporal activation coefficients. NNMF works exploiting the statistical independence of data; in muscle synergy analysis, however, a high degree of correlation among activation coefficients may be present, in particular when dealing with post-stroke patients [6-7]. The presence of a correlated structure in the control scheme detrimentally affects the results of NNMF factorization, leading to the impossibility of accurately identifying the spatial structure of the underlying motor modules.

The traditional NNMF implementation randomly initializes the two matrices W and C from a uniform distribution between 0 and 1; however, it has been shown that other initialization strategies, based on the structure of the original data, can significantly improve the performances of the algorithm, without the definition of different update rules [6]. Among these studies, Singular Value Decomposition (SVD) has been proved to be a reliable initialization choice for NNMF [7]. In addition, several studies have hypothesized that the implementation of several sparsity constraints into the NNMF update rules can lead to a better identification of the W component, suggesting the idea that a sparse initialization can improve the factorization performance.

The aim of the study "*The effect of Non-Negative Matrix Factorization initialization on the accurate identification of muscle synergies with correlated activation signals*" presented at MeMea 2018, has been the comparison of three different initialization choices for NNMF (random uniform, SVD-based and sparse) when extracting muscle synergies from experimental surface electromyography data. To test the behavior of the algorithm in the presence of different levels of correlation, the temporal component of the motor coordination has been artificially corrupted, in order to simulate extremely challenging conditions for the identification of the correct W matrix, as it commonly happens in the factorization of EMG data from pathological subjects [8].

10.1 Materials and methods

Muscle synergy model

Among the different mathematical models for modular motor control [9], in this study we refer to the synchronous muscle synergy model (i.e. fixed spatial structures W) defined by the following equation:

Let D be a matrix containing sEMG envelope data, each row of this matrix is a specific degree of freedom (DOF) (i.e. the envelope of each muscle), while each column represents the value of these DOFs in a specific sample in time.

The synchronous model of synergies considers that those ratios of signals, characterizing different DOF, remain constant over time. This kind of interpretation is applied in the muscle space; in this description, different muscles are assumed to be activated simultaneously without muscle-specific time delays. The mathematical definition for this model is:

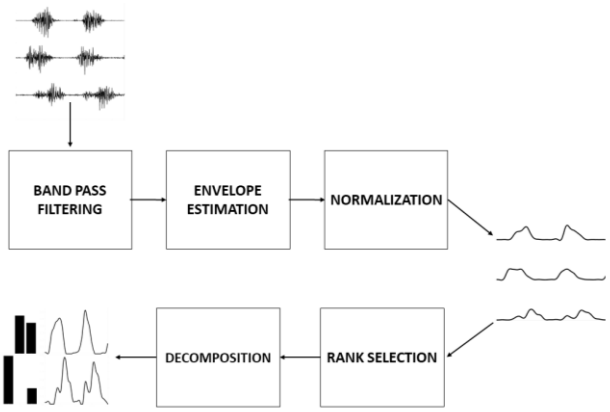

Figure 10.1 – Block diagram for the processing steps needed for muscle synergy extraction from raw sEMG data.

$$d(t) = \sum_{n=1}^{N} [W_n C_n(t)] + \varepsilon(t)$$

In this model, the vector d(t) is a column of the matrix D. The column vector W_n corresponds to the time-invariant muscle groups, that are the spatial components of the model, while the C_n are the timing coefficients corresponding to each group. The error associated with this approximation is ε. The number N is the rank of the model, which corresponds to the number of muscle synergies to be used for the description of the movement. This model is often expressed in a matrix form

$$D = WC + \varepsilon$$

where each letter corresponds to the matrix containing the D, W and C coefficients. This relationship is the one used in the most common algorithms for the extraction of synchronous synergies. It should be noted that both the mathematical expressions have the very same meaning.

Processing steps for muscle synergy extraction

The block diagram relative to the processing chain for muscle synergy identification is reported in Fig 10.1. Band-pass filtering is needed for artifact rejection, prior to any analysis on the experimental

data. Envelope is typically extracted by rectification and low pass filtering, although different choices for the time constant have been used in literature .

Non-Negative Matrix Factorization

NNMF is an iterative algorithm that aims at factorizing a non-negative matrix D into two matrices W (containing the synergy vectors) and C (containing the temporal activation coefficients) such that D ≈ WC. The algorithm works via the implementation of the following multiplicative rules:

$$W_{ik} \leftarrow W_{ik} \frac{(DC^T)_{ik}}{(WCC^T)_{ik}} \quad C_{kj} \leftarrow C_{kj} \frac{(W^T D)_{kj}}{(WW^T C)_{kj}}$$

Updating the matrices with these rules ensures the non-increasing trend of the Frobenius norm of the error matrix D – WC at each iteration of the algorithm.

Initialization techniques

The typical initialization technique for NNMF has been implemented by extracting each element of the W matrix from a random uniform distribution between 0 and 1 (RAND), while the SVD based initialization has been achieved according to the procedure described in [7] (SVD). Sparse initialization (SPARSE) has been implemented by first initializing the W matrix with random uniform values in the range [0 0.05], and then changing the weight of one element for each synergy to a random value in the range [0.7 0.8], so to maximize the sparseness for each synergy vector. For all the three initialization techniques for W, C has been initialized according to the RAND procedure.

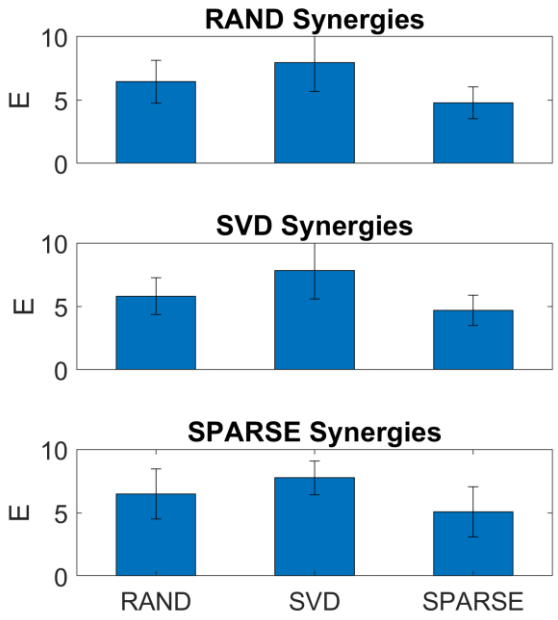

Figure 10.2 – Mean E values for the identification of modules obtained by the extraction with the three different initialization choices. The three bar plots represent the three sets of modules obtained by decomposing the original data with RAND, SVD and SPARSE initialization.

Experimental data

For the assessment of the differences between the three initialization techniques sEMG data coming from the healthy population (11 subjects). Briefly, the subjects executed a 2min unconstrained pedaling task at 60 rpm on a cycle ergometer, while EMG data were recorded from the following eight lower limb muscles: *Gluteus maximus* (Gmax), *Biceps Femoris long head* (BF), *Gastrocnemius Medialis* (GAM), *Soleus* (SOL), *Rectus Femoris* (RF), *Vastus Lateralis* (VL), *Vastus Medialis* (VM) and *Tibialis Anterior* (TA). Details regarding the EMG pre-processing and synchronization with the pedal angle can be found in [10].

The three initialization techniques have been implemented to seed NNMF update rules for the extraction of 4 synergies from all subjects, defining three sets of factors $W_{true/INIT}$ and $C_{true/INIT}$ (where INIT can indicate RAND, SVD and SPARSE). Subsequently, the maxima of the coefficients C_{true} have been aligned in order to maximize the correlation between the activation profiles and obtaining a new matrix C_{corr}. A corrupted data matrix has been defined as $D_{corr} = W_{true}C_{corr}$ for each

initialization technique used for the definition of the synergy vectors W_{true}. Each matrix D_{corr} has then been decomposed with all the three initializations, obtaining the estimated modules W_{RAND}, W_{SVD} and W_{SPARSE}. The estimation procedure has been replicated 100 times for each simulated D_{corr}.

Performance assessment

An error measure E for the estimation of the W matrix has been defined as

$$E = \sqrt{\left(100\frac{mean(Wtrue - W)}{range(W_{true})}\right)^2 + \left(100\frac{std(Wtrue - W)}{range(W_{true})}\right)^2}$$

This quantity represents the root mean squared error of the identification of the W vectors, expressed in percentage of the range of variation of each synergy vector. E values have been evaluated for each column of W (i.e. for each single synergy vector), and then a mean indicator across the four modules has been taken as representative of the estimation performance. Values for this parameter underwent statistical analysis, using a one-way ANOVA test with the estimation algorithm (RAND, SVD or SPARSE) as factor.

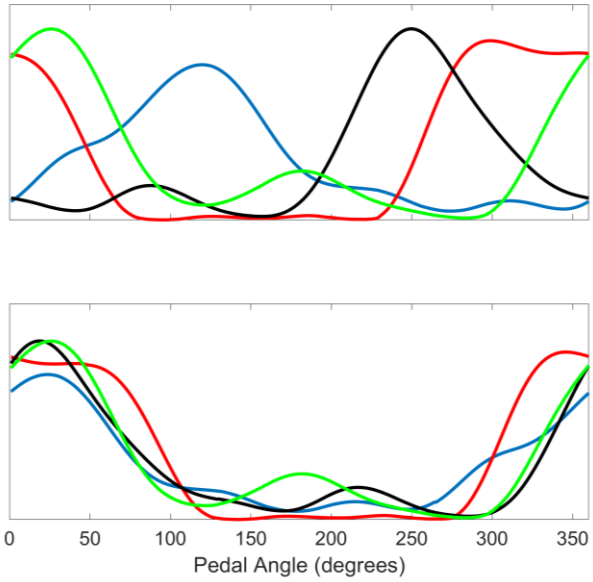

Figure 10.3 – The four original (top) and correlated (bottom) mean activation profiles for a subject.

10.2 Results

The artificial synchronization of the C coefficients has yielded a correlation value for the temporal component of the synergies of 0.86±cc. The mean correlated activation profiles are shown in Fig. 10.3. Values of the quality factor obtained in our simulations are reported in Fig. 10.2. SPARSE initialization has been able to reach better estimation quality than RAND and SVD in the identification of all the three set of motor modules. ANOVA test confirmed a significant effect of the initialization on the estimation error; post-hoc analysis has shown a significant reduction of the error when SPARSE initialization is used (p values).

An example of the modules extracted by the three methods is shown in Fig. 10.4. It can be seen how SVD and RAND initialization sometimes identify non-existent muscle weightings that can lead to a misinterpretation of the muscle synergy spatial composition.

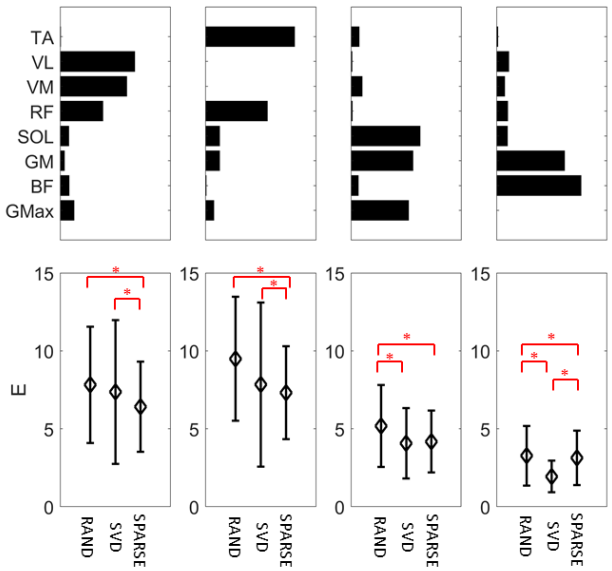

Figure 10.4 – An example of the W_{true} and the relative identification errors given by the three initialization techniques. Statistical significance has been highlighted ($p<0.05$, Wilcoxon Rank-Sum test).

10.3 Discussion and Conclusions

The aim of this work has been the assessment of the effect of different initialization techniques on the extraction of muscle synergies in extremely challenging conditions. The artificial manipulation of the activation coefficients has been inserted to simulate the pathological condition in which the CNS is not able to control independently all the motor modules [8].

Our results suggest that the choice of a sparse structure in the initialization data for NNMF can improve the quality of the identification of the motor modules underlying the control schemes of the subject, even when the different synergies are activated simultaneously. SVD initialization has shown worse performance than the other two methods; however, the presented results refer to the mean error of the identification of all the four motor modules, so that a more detailed analysis of the quality in the identification of each single module is needed. In general, from the example in Fig. 10.4, it can be hypothesized that SPARSE has the advantage of being able to estimate small weights better than RAND; SVD has the same performance of SPARSE in the identification of three modules, while for W_4, it overestimates all the smallest weights. This last result is a possible explanation for the higher error values yielded by SVD initialization, and a more thorough analysis of the mathematical reason for this behavior can be useful for the understanding on the differences between SVD and SPARSE initialization techniques.

In this study, the activation coefficients have been characterized by a single level of correlation; the analysis of how the three techniques behave in correspondence of different levels of correlation is needed in order to completely characterize the effects of different initialization strategies for NNMF, in solving the problem of muscle synergy extraction. In addition, the level of correlation that has been reached by synchronizing the peak activation of the C profiles can be not high enough for testing NNMF behavior in pathological conditions; it is reasonable to hypothesize that if the CNS is not able to control independently the four modules, correlation values in the activation coefficients are higher than 0.86.

In this work, we focused on the identification of the spatial structure of the modular control schemes, and we evaluated the performance in the identification of just the W matrix; although it is not ensured that a correct identification of W implies a correct identification of C, the presented results are valid when a synchronous model for muscle synergy is used, in which the fixed component of the control strategies is represented by the W vectors. Other studies [11] suggest that the fixed characteristics are contained in the C coefficients; when the focus is on the identification of the temporal component of the muscle synergies, it is possible that other initialization techniques, different from SVD or SPARSE, lead to a better identification of highly correlated structures.

The choice of the rank of the NNMF approximation (i.e. the number of synergies to be extracted) has been made based on the previous results of the analyses carried on with the same experimental data [8]; the definition of a robust criterion for the selection of the correct number of synergies is still an open issue, and it is not clear whether the choice of different initialization techniques can help with its solution.

In conclusion, these results show how muscle synergy analysis results are strongly dependent on the initialization choices for NNMF; because of this, the complete characterization of how different processing choices can affect the structure of the extracted muscle synergies is crucial for a correct interpretation of synergy-based results in the clinical environment.

10.4 Bibliography

[1] Bernstein NA. 1967. The Coordination and Regulation of Movements. Pergamon Press.

[2] Saltiel P, et al. 2001. Muscle synergies encoded within the spinal cord: evidence from focal intraspinal NMDA iontophoresis in the frog. Journal of Neurophysiology, 85(2), p. 605-19

[3] D'Avella A, Saltiel P, Bizzi E. 2003. Combinations of muscle synergies in the construction of a natural motor behavior. Nature Neuroscience, p. 6(3): p. 300-8.

[4] Tresch MC, Cheung V, d'Avella A. 2006. Matrix Factorization Algorithms for the Identification of Muscle Synergies: Evaluation on Simulated and Experimental Data Sets. Journal of Neurophysiology: 95:2199-2212.

[5] Lee DD, Seung HS. 2001. Algorithms for non-negative matrix factorization. Neural Information Processing Systems, 13, p. 556-562.

[6] Janecek, A., & Tan, Y. (2011). Using population based algorithms for initializing nonnegative matrix factorization. Advances in swarm intelligence, 307-316.

[7] Boutsidis, C., Gallopoulos, E. (2008). SVD Based initialization: A head start for nonnegative matrix factorization. Journal of Pattern Recong., 41, 1350-1362.

[8] Ambrosini, E., De Marchis, C., Pedrocchi, A., Ferrigno, G., Monticone, M., Schmid, M., D'Alessio, T., Conforto, S., Ferrante, S. (2016). Neuro-Mechanics of Recumbent Leg Cycling in Post-Acute Stroke Patients. Annals of Biomedical Engineering, 44(11), 3238–3251.

[9] Chiovetto, E., D'Avella A. Giese, M. A. (2016). A unifying framework for the identification of motor primitives

[10] De Marchis, C., Schmid, M., Bibbo, D., Bernabucci, I., & Conforto, S. (2013). Inter-individual variability of forces and modular muscle coordination in cycling: A study on untrained subjects. Human movement science, 32(6), 1480-1494.

[11] Ivanenko YP, Poppele RE e Lacquaniti F. 2004. Five basic muscle activation patterns account for muscle activity during human locomotion. Journal of Physiology, 556 (Pt 1), p. 267-82.

CHAPTER 11

11. GENERAL DISCUSSION AND CONCLUSIONS

Gait analysis allows us to obtain important information of the status of health of an individual and his quality of life: Among the different aspects which are the object of debate in the scientific community on gait analysis in pathologic conditions, two questions were deepened within this PhD:

- The assessement of gait patterns in patients with several neurological gait disorders and lower limb amputations. Some specific biomechanical features, that may not emerge because they are hidden within the global walking strategy, were highlighted by subgroups or cluster analysis.
- The assessements of the role of muscle coactivation mechanisms during walking in pathologic conditions and its relstionship with gait performance. The influence of several factors in the sEMG measurement and pre-processing on the linear envelope profiles extraction, and therefore on the outcome of muscle co-activation were taken into account.

The analyses carried out within this PhD have been designed to shed light on these two points, and the results obtained and presented in this dissertation extend the knowledge about them, and will be summarized in the following.

Gait features in pathologic conditions

Patients with degenerative diseases such as cerebellar ataxia (CA), spastic paraplegia (SP), Parkinson's disease (PD) and Duchenne Muscular Dystrophy (DMD) often present a progressive gait function decline that inexorably impacts their autonomy, risk of falls, and quality of life [1,2]. For this reason, and considering the associated social and economic costs, one of the most important areas of intervention in neurorehabilitation should be the treatment of gait abnormalities. Consequently, evaluating gait to quantify and typify specific gait impairments in these conditions is

crucial when focusing on the specific factors in rehabilitation and thus for designing treatments tailored to individual needs. This need is further reinforced by the knowledge that gait outcomes are correlated with longevity [3], cognitive decline [4], and adverse events [5]. A deeper characterization of walking impairment in such different diseases might shed light on the nature of both the primary specific gait disorder and its ompensatory mechanisms. In addition, such deeper understanding might represent a reasonable prerequisite for establishing better-focused rehabilitation strategies.

As regard HSP patients, several previous studies highlighted the clinical variability and heterogeneity of the pathology [6-8] As concerns the time-distance parameters, the results revealed a decrease of walking speed, stride length and step height, and an increase in stance duration that are related to the severity of the pathology. These modifications are mainly a consequence of the development of spasticity but in part also depend on a cautious compensatory strategy in order to achieve greater stability [7,9]. The analysis of limb joint kinematics revealed that HPS patients differ from controls in the amplitude of the RoMs. In particular, the knee kinematics provides the most significant information in order to characterize gait patterns in HSP. Higher leg stiffness was also associated with a reduced swing phase dorsiflexion and a smaller toe clearance [8,10]. This can be attributed to a lack of muscle strength and potentially higher passive stiffness in the knee extensors as a result of changes to the connective tissue as the HSP progresses [8].

In addition to general biomechanical characteristics of gait, one would expect some differential characteristics in distinct subgroups of patients according to clinical involvement of the pyramidal tract, given that patients with hereditary spastic paraparesis exhibit different degrees of severity both within and between families. Thus, some specific biomechanical features may not emerge because they are hidden within their global walking strategy.

When subgrouping patients according to the hip, knee and ankle joint kinematic behavior, three clear gait patterns emerged. The gait pattern of subgroup one was characterized by reduced RoMs at

hip, knee and ankle joints. Patients of this subgroup were the most severely affected (highest SPRS score), and walked at the slowest speed. The gait pattern of subgroup three was characterized by increased hip joint RoM and knee and ankle joint RoMs close to control values. These patients were themost mildly affected (lowest SPRS score) and showed the highest walking speed. Patients of subgroup two had characteristics between those of subgroups one and three, in terms of disease severity and gait speed, and showed hip joint RoM close to controls but decreased knee and ankle joint RoMs.

A comprehensive evaluation of HSP should take into account the segmental changes in the spinal cord as well as in muscle properties [11], and to achieve adequate treatment it is crucial to address the mechanisms underlying the impaired function. Indeed, in deciding the preferable relaxation procedure for any one patient, an assessment of the degree and the distribution of spasticity is important [12]. Differences in widening of the spinal segmental output between the groups suggest that the more severe the disease, the wider the map, and the less selective the muscle recruitment is, according to a distal-proximal gradient along the spinal cord. For instance, rehabilitative treatments can be focused on improving muscle selectivity recruitment by enhancing segmental afferent input and descending motor control, promoting reciprocal and segmental inhibition. The current treatments based on physical therapy, intramuscular injections of botulinum toxins, intrathecal baclofen therapy [13], functional electrical stimulation [8], hydrotherapy or using the body weight support as a tool to decrease or differentially activate groups of muscles [14,15], should consider the progression of muscle impairments at spinal segmental level to improve the selective muscular recruitment and reduce spasticity [17].

On the whole, the results suggest that the development of spasticity due to the degeneration of the corticospinal tract in patients with HSP is related to a EMG widening during locomotion, spreading from distal to proximal spinal segments [18-20].

The progression of gait impairment in a group of patients with primary degenerative cerebellar ataxias over a period of 4 years revealed decreased step length and hip, knee, and ankle joint RoM and increased trunk rotation RoM and stride-to-stride and step length variability. It is likely that ataxic patients increasingly shorten their step length as the disease progresses as a balance-related mechanism aimed at reducing duration in the most unstable configuration (single support) and in an attempt to maintain an effective gait. [21-27]. The progressive increase in gait variability observed at the 4-year follow-up may directly reflect gait function deterioration, leading to greater instability and an increased risk of falls. Interestingly, the increase in trunk rotation may represent another compensatory mechanism aimed at maintaining an adequate gait speed. This finding further reinforces the notion that trunk plays a compensatory role in maintaining an effective gait.

In conclusion, patients try to maintain an effective gait by adopting different compensatory mechanisms during the course of the disease in spite of disease progression.

As regard Parkinson disease, previous studies have disclosed abnormalities in cadence, stance duration, swing duration, double support duration, leg length, step length, velocity, hip, knee and ankle ROMs. Such abnormal gait parameters seem to correlate with the clinical outcomes of UPDRS score, H-Y stage and milliequivalents of levodopa taken. Importantly, gait parameters can either normalize or improve after several rehabilitative treatment strategies including physiotherapy, assistive equipment, sensory cueing, treadmill training, physical activity, home base exercises.

ANNs, that recently have been used as diagnostic tool in several clinical conditions, could be used with gait analysis to identify the severity of gait deficit in PD. Indeed, a diagnostic algorithm based on ANNs technique is able to automatically classify the gait deficit according to the disease progression.

As regard patients affected by Duchenne Muscular Dystrophy, we observed a progressive increase in the variability of both stride length and stride width. It has been discovered that both

stride length and stride width variability are linked with locomotion stability [25]. The progressive increase in gait variability observed at the 2-year follow-up may thus directly reflect a deterioration of the gait function, which leads to greater instability. Taking this into consideration, gait variability seems to anticipate the future loss of walking autonomy.

A non-hierarchical cluster analysis was helpful to better identify specific gait patterns in patients with CA, HSP and PD compared to each other and to healthy subjects. The specific gait pattern formed by the increased step width, reduced ankle joint RoM, and increased gait variability [25], can differentiate patients with CA from healthy subjects and patients with other degenerative neurological diseases. These abnormal parameters may be considered as sensitive tools for evaluating the effect of pharmacological and rehabilitative treatments. For instance, specific rehabilitative treatment may be aimed at improving the most relevant gait parameters (i.e. step width and gait variability) or for developing mechanical or elastic devices or footwear specifically designed to reduce gait variability or increase the ankle joint stability.

Common and specific gait patterns in people with amputation, either regardless of, or according to their level of amputation and the type of prosthetic component were also identified.
In general, regardless of the level of amputation and type of prosthesis, subjects with TTA and with TFA showed a common gait pattern characterized by a symmetric increase of step length, step width, double support duration, pelvic obliquity, trunk lateral bending, and trunk rotation range of motions with increased pelvis and trunk ante-flexed (flexed in a forward direction) posture. Almost all these gait deficits reflect compensatory mechanisms adopted by people with amputation presumably to increase their stability in the frontal plane (increased step width), to maintain the most stable configuration (increased double support duration), to assist the lift of the affected limb (increased trunk lateral bending), while increasing the time of the stance and the force production during weight acceptance in the unaffected limb. Conversely, the reduced ankle joint range of

motion in the prosthetic limb, which is the common prosthetic joint in both subjects with TTA and with TFA, is directly linked to the use of the prosthesis.

The subjects with TFA seem to be unable to control the prosthetic limb during the heel strike, likely caused by a reduced deceleration of the prosthetic limb from the late swing to the initial contact. As a final result, this specific gait pattern makes the subjects with TFA unable to recover energy during the stance phase [28,29].

In conclusion, in spite of common gait characteristics in subjects with lower limb prostheses, both the anatomical level of amputation and type of prostheses determine a specific gait pattern that should be taken into account when developing new and ergonomic prosthetic devices and when planning the rehabilitation programs aimed at improving the physiology of gait and reducing the gait asymmetries.

Muscular caharacterization in pathologic conditions

Muscle coactivation is the mechanism that regulates the simultaneous activity of antagonist muscles around the same joint. During walking, muscle joint coactivation varies within the gait cycle according to the functional role of the lower limb joints. Our results show that muscle coactivation in healthy subjects is speed dependent and positively correlated with both energy consumption and balance-related gait parameters.

It is noteworthy that although a similar temporal trend of muscle coactivation curves was observed at several gait speeds, the global lower limb coactivation is speed-dependent, showing differences in amplitude distribution during gait subphases among the three gait speeds investigated, particularly between low (L) and both self-selected (SS) and fast (F). In fact, whereas at SS speed the global coactivation is essentially limited to the loading-response subphas, at L gait speed, the global coactivation is mainly present in the loading-response (0–10%), midstance (10–30%), and terminal- stance (30–50%) subphases, while, at F speed, the global coactivation is mainly present in both the loading-response and terminal- stance subphases.

Our findings agree well with previous evidences showing that the major muscle groups are active at the beginning and the end of the stance and the swing phases of the cycle [30], which reflect deceleration and acceleration of the lower limb, during body weight shift from one foot to the other. Conversely, during the mid-stance and midswing subphases, most muscles are relatively quiescent. Such a temporal profile of the global coactivation has a functional link with both the energy consumption and recovery. Indeed, the global coactivation was positively correlated with the energy consumption and negatively correlated with energy recovery. The higher the global coactivation, the higher the energy consumption. The less the global coactivation, the higher the energy recovery. These findings suggest that the lower limb coactivation behavior could be a useful measure of the motor control strategy, limb stiffness, postural stability, energy efficiency optimization, and several aspects in pathological conditions.

The investigation of the lower limb muscle coactivation in patients with HSP shows taht the knee and ankle joint muscle coactivation is higher in HSP patients compared with controls, in both the entire gait cycle and subphases of gait; both knee and ankle coactivation patterns are positively correlated with knee and ankle joints spasticity; both knee and ankle coactivation patterns are positively correlated with energy consumption and negatively correlated with energy recovery.
In patients with HSP, the abnormal coactivation pattern may reflect both or either abnormal descending motor commands and/or plastic rearrangement of the spinal circuitries [31] which, in turn, lead to a lack of selectivity of the descending motor drives to motoneuronal pools. In addition, these abnormalities influence the mechanisms of both energetic consumption and recovery during walking.

It has been suggested that muscle weakness has a direct influence on DMD gait [32,33]. Our results revealed changes in lower limb co-activations values in relation to disease progression for both proximal and distal segments in children with DMD. A significant decrease in co-activation values after a year (T1) was observed, which is confirmed even after two years (T2) for distal

segments muscles. Despite a decreasing trend from T0 to T1 on co-activation values at the proximal level, a significant increase of co-activation was reported at 2-year follow-up, when patients showed the lowest functional capacity. A negative correlation between co-activation values at the muscle pair acting at the proximal level, and the gait functional outcomes during the years was observed.

Our results are in line with previous studies and this functional decline reflects the progressive nature of degenerative DMD over time [34]. However, while the functional capacity decreases, increase in co-activation at the proximal level at the 2-year follow-up suggests that patients try to maintain an effective gait despite disease progression, by increasing muscle co-activation, especially when the muscular manifestations of the pathology are more evident. Thus, since gait speed remained approximately unchanged over time, increased muscle co-activation at proximal level represents the most important strategy to compensate for a deterioration in both functional ability and increase in gait instability in patients with DMD.

Several factors in the sEMG measurement and pre-processing might influence the linear envelope profiles, and therefore the outcome of co-activation [35].

The relevance of the analysis of muscle co-activation to several fields is well known, thus it is important to correctly process myoelectric signals in order to extract this parameter by avoiding estimation bias. The obtained performance of some popular techniques used to assess muscle co-activation was evaluated by means of simulated sEMG signals generated with varying SNR levels and different modulating functions, and processed with varying values of low-pass filtering. The sensitivity of each technique to capture variations in co-activation was tested by using different levels of simultaneous action of the muscles. The analysis of the results shows that the performance of the methodologies used to assess muscle co-activation are influenced by the choice of the low pass cut-off frequency, as well as by the level of signal to noise ratio.

In particular, for low values of SNR, methods proposed by Ranavolo [36] and Vector Coding Technique [37] are to be preferred and the Vector Coding Technique shows the highest

performance when the SNR is higher. For the vector coding technique, it is to be highlighted that its performance improves with higher cut-off frequencies. These results may be used to choose the co-activation index that may better represent the extent and amount of co-activation based on the recording conditions (SNR level), and processing needs (cut-off frequencies).

I believe that the results obtained in this PhD project may provide important support to extend the knowledge about functional assessement in clinical and neurophysiological fields.

In particular, these results suggested that both the characteristics of the pathology and the technique used for data elaboration are two important aspects to be considered in the design of tools for training and rehabilitation.

Bibliography

[1] Bodranghien, F., Bastian, A., Casali, C., Hallett, M., Louis, E. D., Manto, M., et al. (2016). Consensus paper: Revisiting the symptoms and signs of cerebellar syndrome. Cerebellum, 15, 369–391.

[2] Martinez-Martin, P., Rodriguez-Blazquez, C., Forjaz, M. J., & Kurtis, M. M. (2015). Impact of pharmacotherapy on quality of life in patients with Parkinson's disease.CNS Drugs, 29, 397–413

[3] Studenski, S., Perera, S., Patel, K., Rosano, C., Faulkner, K., Inzitari, M., et al. (2011). Gait speed and survival in older adults. JAMA, 305, 50–58.

[4] Verghese, J., Wang, C., Lipton, R. B., Holtzer, R., & Xue, X. (2007). Quantitative gait dysfunction and risk of cognitive decline and dementia. Journal of Neurology, Neurosurgery and Psychiatry, 78, 929–935.

[5] Abellan van Kan, G., Rolland, Y., Andrieu, S., Bauer, J., Beauchet, O., Bonnefoy, M., et al. (2009). Gait speed at usual pace as a predictor of adverse outcomes in community-dwelling older people an International Academy on Nutrition and Aging (IANA) Task Force [Review]. The Journal of Nutrition, Health & Aging, 13, 881–889.

[6] Fink JK. Hereditary spastic paraplegia: clinical principles and genetic advances. Semin Neurol 2014;34:293–305. https://doi.org/10.1055/s-0034-1386767.

[7] Klebe S, Stolze H, Kopper F, Lorenz D, Wenzelburger R, Volkmann J, et al. Gait analysis of sporadic and hereditary spastic paraplegia. J Neurol 2004; 251:571–8. https://doi.org/10.1007/s00415-004-0366-7.

[8] Marsden J, Stevenson V, McFadden C, Swain I, Taylor P. The effects of functional electrical stimulation on walking in hereditary and spontaneous spastic paraparesis. Neuromodulation 2013;16:256–60; discussion 260.

[9] Cimolin V, Piccinini L, D'Angelo MG, Turconi AC, Berti M, Crivellini M, et al. Are patients with hereditary spastic paraplegia different from patients with spastic diplegia during walking? Gait evaluation using 3D gait analysis. Funct Neurol 2007;22:23–8

[10] Piccinini L, Cimolin V, D'Angelo MG, Turconi AC, Crivellini M, Galli M. 3D gait analysis in patients with hereditary spastic paraparesis and spastic diplegia: a kinematic, kinetic and EMG comparison. Eur J Paediatr Neurol 2011;15:138–45. https://doi.org/10.1016/j.ejpn.2010.07.009

[11] Rösche J. Treatment of spasticity. Spinal Cord 2002;40:261–2. https://doi.org/ 10.1038/sj.sc.3101313.

[12] Levine MG, Kabat H. SPASTICITY—its nature and treatment. Calif Med 1954;80:306–10.

[13] Dan B, Bouillot E, Bengoetxea A, Cheron G. Effect of intrathecal baclofen on gait control in human hereditary spastic paraparesis. Neurosci Lett 2000;280:175–8.

[14] Sylos-Labini F, Lacquaniti F, Ivanenko YP. Human locomotion under reduced gravity conditions: biomechanical and neurophysiological considerations. Biomed Res Int 2014;2014:547242. https://doi.org/10.1155/2014/547242.

[15] Cappellini G, Ivanenko YP, Martino G, MacLellan MJ, Sacco A, Morelli D, et al. Immature spinal locomotor output in children with cerebral palsy. Front Physiol 2016;7. http://doi.org/10.3389/fphys.2016.00478.

[16] Yokoyama H, Ogawa T, Shinya M, Kawashima N, Nakazawa K. Speed dependency in a-motoneuron activity and locomotor modules in human locomotion: indirect evidence for phylogenetically conserved spinal circuits. Proc Biol Sci 2017;284. http://doi.org/10.1098/rspb.2017.0290.

[17] Capogrosso M, Milekovic T, Borton D, Wagner F, Moraud EM, Mignardot J-B, et al. Abrain-spine interface alleviating gait deficits after spinal cord injury in primates. Nature 2016;539:284–8. https://doi.org/10.1038/nature20118.

[18] Ivanenko YP, Poppele RE, Lacquaniti F. Spinal cord maps of spatiotemporal alphamotoneuron activation in humans walking at different speeds. J Neurophysiol 2006;95:602–18. https://doi.org/10.1152/jn.00767.2005.

[19] Kendall FP. Muscles: testing and function with posture and pain. Lippincott Williams & Wilkins; 2005

[20] Dietz V, Sinkjaer T. Spastic movement disorder: impaired reflex function and altered muscle mechanics. Lancet Neurol 2007;6:725–33. https://doi.org/ 10.1016/S1474-4422(07)70193-X.

[21] Conte C, Pierelli F, Casali C, Ranavolo A, Draicchio F, Martino G, et al. Upper body kinematics in patients with cerebellar ataxia. Cerebellum. 2014;13(6):689–97.

[22] Schwab A, Meijaard J. A review on bicycle dynamics and rider control. Veh Syst Dyn. 2013;51(7):1059–90.

[23] Cain SM, Ashton-Miller JA, Perkins NC. On the skill of balancing while riding a bicycle. PLoS One. 2016;11(2):e0149340

[24] Serrao M, Pierelli F, Ranavolo A, Draicchio F, Conte C, Don R, et al. Gait pattern in inherited cerebellar ataxias. Cerebellum. 2012;11:194–211.

[25] Hausdorff JM. Stride variability: beyond length and frequency. Gait Posture. 2004;20(3):304. author reply 305
[26] Schniepp R,Wuehr M, Neuhaeusser M, Kamenova M, Dimitriadis K, Klopstock T, et al. Locomotion speed determines gait variability in cerebellar ataxia and vestibular failure. MovDisord. 2012;27: 125–31.
[27] Wuehr M, Schniepp R, Schlick C, Huth S, Pradhan C, Dieterich M, et al. Sensory loss and walking speed related factors for gait alterations in patients with peripheral neuropathy. Gait Posture. 2013; doi:10.1016/j.gaitpost.2013.11.013.
[28] Ivanenko YP, Dominici N, Daprati E, Nico D, Cappellini G, Lacquaniti F.Locomotor body scheme. Hum Mov Sci. 2011 Apr;30(2):341-51. doi:10.1016/j.humov.2010.04.001. Epub 2010 Jun 17. Review. PubMed PMID: 21453667.
[29] Assessment of gait stability, harmony, and symmetry in subjects with lower-limb amputation evaluated by trunk accelerations.
[30] Perry, J., 1992. Gait analysis-normal and pathological function. Slack Incorporated, Thorofare.
[31] Nardone A, Galante M, Lucas B, Schieppati M. Stance control is not affected byparesis and reflex hyperexcitability: the case of spastic patients. J Neurol Neurosurg Psychiatry 2001;70:635–43
[32] Goudriaan M, Van den Hauwe M, Dekeerle J, Verhelst L, Molenaers G, Goemans N, Desloovere K. Gait & Posture. Gait deviations in Duchenne muscular dystrophy-Part 1. A systematic review, 2018,62:247-261.
[33] Sutherland DH, Olshen R, Cooper L, Wyatt M, Leach J, Mubarak S, Schultz P. . Developmental Medicine and Child Neurology, The pathomechanics of gait in Duchenne muscular dystrophy 1981, 23: 3–22.
[34] Ropars, J, Lempereur M, Vuillerot C, Tiffreau V, Peudenier S, Cuisset JM, Pereon Y, Leboeuf F, Delporte L, Delpierre Y, Gross R, Brochard S. PloS one, Muscle activation during gait in children with Duchenne muscular dystrophy, 2016.
[35] D'Alessio, T., Conforto, S., 2001. Extraction of the envelope from surface EMG signals. IEEE Eng Med Biol 20 (6), 55–61
[36] Ranavolo, A., Mari, S., Conte, C., Serrao, M., Silvetti, A., Iavicoli, S., Draicchio, F., 2015. A
new muscle co-activation index for biomechanical load evaluation in work activities. Ergonomics 58 (6), 966–979. Rosa, M.C., Marques, A., Demain, S., Metcalf
[37] Yoo, H.J., Sim, T., Choi, A., Park, H.J., Yang, H., Heo, H.M., Park, K.S., Mun, J.H., 2016. Quantifying coordination between agonist and antagonist muscles during a gait. Journal of Mechanical Science and Technology 30 (11), 5321–5328.

12. APPENDIX

In the present appendix, other research activities carried out durind my PHD are summarized.

Three-dimensional motion analysis tecqnique was used to characterize both work activities and sport. The main results were collected in the following works.

Characterization of lifting activities and works with repeated movements of the upper limbs :

1. International Journal of Industrial Ergonomics, "Surface electromyography for risk assessment in work activities designed using the "revised NIOSH lifting equation", A. Ranavolo, T. Varrecchia, S. Iavicoli, A. Marchesi, **M. Rinaldi**, M. Serrao, S. Conforto, M. Cesarelli, F. Draicchio, 2018.
2. International Journal of Industrial Ergonomics, "Lifting activity assessment using surface electromyographic features and neural networks", T. Varrecchia, C. De Marchis, **M. Rinaldi**, F. Draicchio, M. Serrao, M. Schmid, S. Conforto, A. Ranavolo, 2018.
3. Industrial Health, "Mechanical lifting energy consumption in work activities designed by means of the "revised NIOSH lifting equation", A. Ranavolo, T. Varrecchia, **M. Rinaldi**, A. Silvetti, M. Serrao, S. Conforto, F. Draicchio, 2017.
4. International Conference on Applied Human Factors and Ergonomics. AHFE 2017, 17-21 July 2017, California, USA and Chapter of Advances in Social & Occupational Ergonomics, "Comparison of two post office workstation layouts by means of an optoelectronic motion analysis system" A. Silvetti, A. Ranavolo, T. Varrecchia, **M. Rinaldi**, G. Chini, A. Marchesi, F. Draicchio.
5. Congresso Nazionale SIE 2016, 16-18 November 2016, Naples, Italy, "Analisi Cinematica di una postazione di interfaccia cliente/operatore" A. Silvetti, A. Ranavolo, T. Varrecchia, **M. Rinaldi**, G. Chini, A. Marchesi, F. Draicchio.

1. European Journal of Sport Science: “Biomechanical characterization of the Junzuki karate punch: indexes of performance”; **Martina Rinaldi**, Yasmen Nasr, Ghada Atef, Fabiano Bini, Tiwana Varrecchia, Carmela Conte, Giorgia Chini, Alberto Ranavolo, Francesco Draicchio, Francesco Pierelli, Mokhtar Amin, Franco Marinozzi, Mariano Serrao.